2016

The Regulation of Alternative Pre-mRNA Splicing in Photoreceptor Cells.

Daniel P. Murphy

The Regulation of Alternative Pre-mRNA Splicing in Photoreceptor Cells.

Daniel P. Murphy

Dissertation submitted to the
School of Medicine
at West Virginia University
in partial fulfillment of the requirements
for the degree of

Doctor of Philosophy
in
Biochemistry and Molecular Biology

Peter Stoilov, Ph.D., Chair
Visvanathan Ramamurthy, Ph.D.
Lisa Salati, Ph.D.
J. Michael Ruppert, M.D., Ph.D.
Peter Mathers, Ph.D.

Graduate Program in Biochemistry
West Virginia University School of Medicine
Morgantown, West Virginia
2016

Keywords: RNA splicing, Retina, Photoreceptor, Musashi, BBS8, Primary Cilia, Exon 2A

Abstract

The Regulation of Alternative Pre-mRNA Splicing in Photoreceptor Cells.

Alternative pre-mRNA splicing provides an important mechanism for generating the diverse array of proteins required to generate complex tissue and cell types from a limited genome. Therefore, the proper regulation of alternative splicing is vital to shape cellular identity and function. As consequence, defects in alternative splicing are associated with disease phenotypes that can range from systemic syndromes to the dysfunction of single cell types. For example, heterozygous mutations in ubiquitously expressed components of the spliceosome lead to photoreceptor specific cell death. This suggests that the topography of alternative splicing in photoreceptors cells may be unique, a notion which is supported by reports of photoreceptor specific splicing events. However, the mechanisms mediating photoreceptor specific splicing, and the reason why photoreceptors are uniquely sensitive to perturbations in the splicing machinery, remain unknown.

In this work, I characterize the alternative splicing program of photoreceptor cells using exon 2A of the *BBS8* gene as a model. The photoreceptor specific exon 2A was recently discovered through a mutation in the 3' splice site that was linked with non-syndromic retinitis pigmentosa (RP). Skipping of this exon in photoreceptor cells was thought to limit the phenotype of the mutation to RP, rather than the systemic disease Bardet-Biedl syndrome (BBS). I show that the IVS1-2A>G mutation in *BBS8* leads to missplicing of exon 2A, producing a shift in the reading frame predicted to eliminate the BBS8 protein specifically in photoreceptor cells. I also show that in the absence of splicing elements within the exon, the splicing of exon 2A is directed entirely by sequences located within the adjacent introns.

To gain a more expansive view of the photoreceptor splicing program, I utilize mouse models to isolate the gene expression and alternative splicing profile of photoreceptor cells by RNA sequencing. Bioinformatics analysis indicates that while photoreceptors share a general splicing pattern with other neurons, they exhibit a distinct program that affects a broad set of genes. Cell type specific splicing in photoreceptors appears to be regulated by a combinatorial mechanism which involves activation by the Musashi proteins in the absence of many typical neuronal splicing regulators. This program controls a subset of exons, including BBS8 exon 2A, which are spliced in a "switch-like" manner to produce photoreceptor specific protein isoforms. These splicing events share a temporal inclusion pattern which precedes the development of the light sensing outer segment. Remarkably, multiple switch-like exons are located within genes that are necessary for the biogenesis and maintenance of primary cilia. This suggests that alternative splicing may modulate protein function to allow for development and maintenance of the unique structure of photoreceptor cells.

This work provides a foundation on which to characterize the regulation of alternative splicing in photoreceptor cells, and identifies multiple splicing events which may impact the function of the photoreceptor outer segment.

Acknowledgements

There are many people who have made it possible for me to complete this work, the first and foremost of whom is my advisor, Dr. Peter Stoilov. When I began here at WVU I had very little laboratory experience and no idea of how to design experiments. Dr. Stoilov patiently helped me every step of the way, while providing a great example of the hard work and dedication it takes to build a career as a scientist. Similarly, Dr. Ramamurthy and Dr. Salati, have been invaluable as mentors in all aspects of science and life as a graduate student. Those faculty and students in our weekly lab meetings have also been instrumental in providing advice and feedback. Among my fellow biochemistry graduate students I must acknowledge Holly and Travis Cyphert, Amanda Suchanek, Kimberly Alonge, and Zach Wright, for their friendship and support. The same goes for my core group of beer snobs and homebrew buddies, Steve Markwell, Jacob Kaiser, Chris Bostick and Lindsay Lueptow. Our weekend trips to the Apothecary helped to keep me sane. All those mentioned above, and many others (you know who you are), made it possible for me to feel at home despite moving over 500 miles from my family.

I would not be here without the love and support of my family. I must thank my parents especially for making the long trip out to Morgantown so many times, their visits were a source of repose that kept me going through stressful times. Likewise, my siblings, Colleen, Erin, Joe, and brother-in-law Kris have been a continual source of support and friendship that I could not have done without. A special thanks to Joe for coming to WV and putting up with sharing an apartment with me. The past six years have been a whirlwind of stress, uncertainty, personal growth, and joy. I can't thank you all enough.

Table of Contents

List of Tables

Chapter 2.

List of Figures

List of Abbreviations.

RP-Retinitis Pigmentosa

BBS- Bardet-Biedl Syndrome

SS-Splice Site

snRNP- Small Nuclear Ribonucleoprotein Particle

snRNA- Small Nuclear Ribonucleic Acid

U2AF- U2 Associated Factor

SR- Serine Arginine (family of splicing factors)

hnRNPs- Heterogeneous Nuclear Ribonucleoprotein (Family of splicing factors)

Nova- Neuro-Oncological Ventral Antigen

RbFox- RNA Binding Protein Feminizing locus On X-1 Homolog

NMD- Nonsense-Mediated Decay

ELAVL- Embryonic Lethal Abnormal Vision-Like

PTBP- Polypyrimidine Tract Binding Protein

NSR100- Neural-Specific SR-Related Protein of 100kDa

ONL- Outer Nuclear Layer

INL- Inner Nuclear Layer

GCL- Ganglion Cell Layer

RPE- Retinal Pigmented Epithelium

RPC-Retinal Progenitor Cell

OS- Outer Segment

IS- Inner Segment

IFT- Intraflagellar Transport

CC- Connecting Cilium

adRP- Autosomal Dominant Retinitis Pigmentosa

PRPF- pre-mRNA processing factor

Arl6- ADP Ribosylation Factor-Like 6

Chapter 1. Literature Review

I. Introduction

Alternative splicing of pre-mRNA transcripts is a major mechanism for increasing protein diversity and generating tissue complexity[1]. Accurate regulation of the spliceosome requires the spatiotemporal coordination of numerous protein and RNA interactions, guided by short sequence elements that are widespread across the genome[2]. As such, genetic mutations that disrupt alternative splicing often lead to disease[3,4]. For instance, RP is caused by genetic mutations in a wide variety of genes, including multiple components of the spliceosome[5–7]. A recent study identified a link between RP and disrupted splicing of a photoreceptor specific exon inclusion event[8]. This photoreceptor specific splicing event provides a unique tool to uncover how mutations in ubiquitously expressed genes can lead to cell type specific phenotypes. The goal of this review is to discuss the regulation of alternative splicing in the context of the distinct structure, and function, of the photoreceptor cell.

II. Mechanism of pre-mRNA Splicing

Analysis of high-throughput sequencing data indicates that over 95% of human multiexon genes undergo alternative splicing[9,10]. Eukaryotic splicing involves the joining of exons and removal of intronic sequences in pre-mRNA to produce mature mRNA transcripts. The exon/intron borders are marked by short and highly degenerate sequence elements, such as the 5' GU and 3' AG splice sites located at either end of an intron, hereafter referred to as the 5' and 3' SS (splice site)[2]. Other consensus elements include an adenosine residue known as the branch point, which is followed by a series of pyrimidines known as the polypyrimidine tract. These elements are found near the 3' SS, approximately 15-50 nucleotides from the intron/exon border (see Figure 1A)[2,11,12]. These sequences are recognized by the core spliceosome, a macromolecule comprising multiple small nuclear ribonucleoprotein particles (snRNPs), which are composed of a small nuclear RNA (snRNA) and a host of associated proteins[11,12].

Spliceosome formation is driven by base pairing interactions between the mRNA and the non-coding RNA components of snRNPs, which position the RNA for catalysis (see Figure 1 B). In spliceosome formation, the U1 and U2/U2AF (U2 Associated Factor) snRNPs recognize the 5' and 3' SS, respectively. The intron definition complex is formed through an interaction between the U1 and U2 snRNPs, which brings the 5' SS, branch point, and 3' SS together by looping out the intron. This complex then recruits the pre-assembled tri-snRNP composed of U4/U6 and U5[2,11,12]. Next, the complex undergoes a series of rearrangements resulting in the loss of the U1 and U4 snRNPs and the formation of the catalytic complex. This structure positions the branch point adenosine and the 3' SS to allow the RNA to catalyze two transesterification reactions which remove the intron and ligate the exons together[2,13,14].

While the steps of assembly and catalysis are well conserved from yeast to humans, the exons of multicellular eukaryotes are often surrounded by large introns. As such, rather than intron definition, higher eukaryotes form the exon definition complex, in which the U2 snRNP from the upstream intron interacts with the U1 sn RNP of the downstream intron[11].

2.1: Regulation of alternative splicing

The information provided by the sequence elements discussed above is not sufficient for the spliceosome to accurately identify eukaryotic exons. Large introns often contain multiple motifs that match the splice site consensus sequences, and the snRNP interactions with the mRNA are fairly weak[11,12]. Therefore, precise alternative splicing requires additional sequence elements located within introns and exons to correctly define these boundaries. These elements are recognized by splicing regulatory factors, which can stabilize or inhibit the binding of the spliceosome. The two largest families of such regulatory factors are the serine arginine (SR) rich proteins, which mainly promote exon inclusion, and the heterogeneous nuclear ribonucleoproteins, (hnRNPs) which generally suppress exon inclusion (see Figure 1C)[15,16].

Exon definition by the spliceosome depends upon a combination of 1) how well the splice sites match the consensus sequence, 2) the presence of regulatory sequence elements, and 3) the expression of splicing factors that recognize those elements. Interestingly, multiple splicing factors have been shown to direct splicing in a position-dependent manner. For example, Nova (neuro-oncological ventral antigen) and Rbfox (RNA binding protein feminizing locus on X homolog) proteins enhance exon inclusion when bound to the downstream intron; however they promote exon skipping when bound to the upstream intron or the exon itself[17]. The combinatorial control of exon recognition allows for certain exons to be included or excluded only in cells that express specific splicing factors. Moreover, the splicing of a transcript can be altered in complex ways, beyond simple inclusion or skipping of a cassette exon as in Figure 1 D. For instance, inclusion of two adjacent exons can be mutually exclusive, or a single exon can be resized with alternate 5' and 3' splice sites. Splicing can also result in the use of

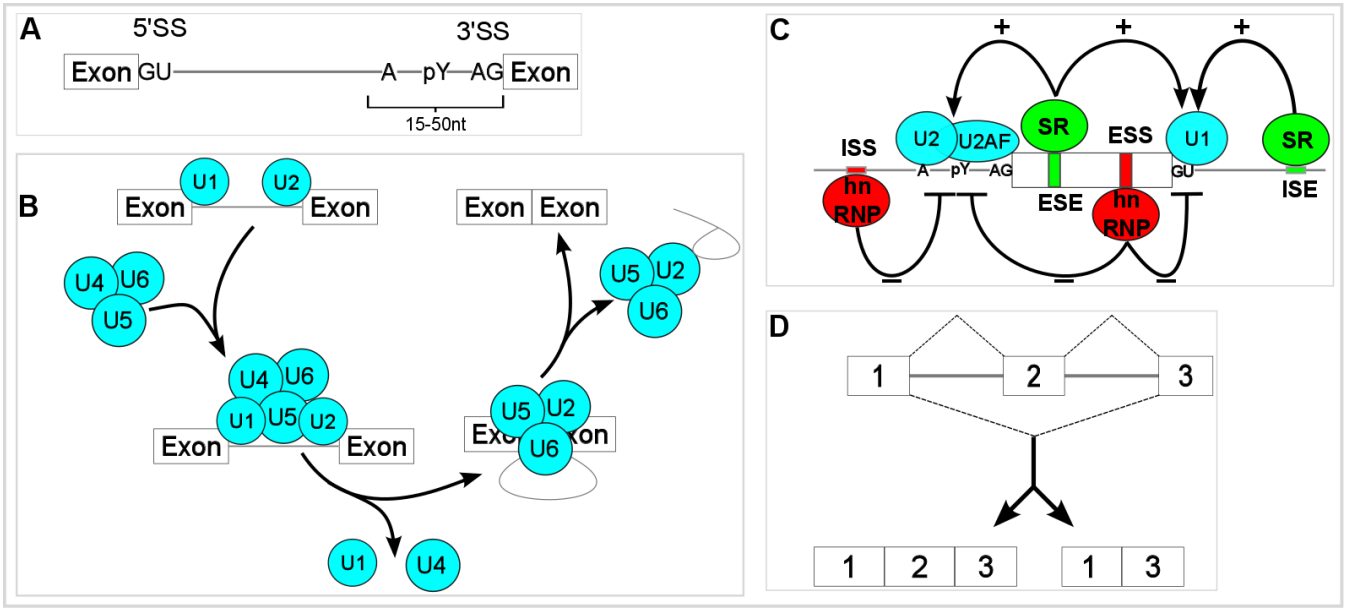

Figure 1 The spliceosome recognizes consensus splice sites, and splicing factors aid in exon definition. A) Cartoon showing approximate locations of the consensus splice sites which mark the boundaries of an intron; SS, splice site. **B)** Cartoon showing the process of intron definition by the spliceosome. See text for details. All snRNPs are shown in teal. **C)** SR proteins, in green, and hnRNPs in red, bind to regulatory elements, also in green/red, within the exon (white box) or intron (grey line) to regulate spliceosome formation; ISE, intronic splicing enhancer; ISS, intronic splicing silencer; ESE, exonic splicing enhancer; ESS, exonic splicing silencer. **D)** Schematic of alternative exon splicing, showing two isoforms which result from inclusion or skipping of exon 2.

alternative promotors, poly-adenylation sites and even retained introns. These mechanisms can achieve a wide variation in transcript isoforms and thus generate increased protein diversity[1,2]. In addition to altering protein structure and function, alternative splicing can be used to regulate gene expression. Splicing variations can alter transcript localization and translation, or they can signal for degradation when coupled with nonsense-mediated decay (NMD)[18,19]. Consequently, the temporal and spatial restriction of splicing factor expression is vital to develop and maintain tissue specificity[2,13,18].

2.2: Alternative splicing in the brain

Alternative splicing is especially important in complex tissues. From an evolutionary perspective, levels of alternative splicing are highest in primates and decrease with further evolutionary distance from humans[20]. Within species, multiple studies have demonstrated that the frequency of alternative splicing events is very high in neuronal tissues, such as the retina and brain[9,20,21]. These observations are supported by the presence of multiple RNA-binding proteins expressed specifically in neurons[22]. For instance, members of the ElavL (embryonic lethal abnormal vision-like) and Nova families, as well as RBFOX3 (aka NEUN), PTBP2 (Polypyrimidine tract-binding protein 2), and NSR100 (neural-specific SR-related protein of 100kDa, aka Srrm4), are all neuron specific. The importance of these splicing factors in neuronal development and function is highlighted by the finding that loss-of-function of these proteins results in a variety of severe neurological phenotypes in mice[17,22–24]. Dysregulation of alternative splicing associated with nsr100 and Rbfox proteins in neurons has also been linked with cognitive impairment, including autism spectrum disorder[25,26].

Unraveling the impact of splice sites, splicing factors, and alternative transcripts on cellular function can be challenging. Complex interactions can arise due to regulation of one splicing factor by another, as well as changes in expression or subcellular localization of splicing factors during development.

III. Structure and Function of the Retina

The vertebrate retina is an extension of the central nervous system and thus shares anatomical and functional characteristics with neurons. Moreover, with fewer cell types and a comparatively straightforward structure, the retina is an ideal model to study neuronal alternative splicing and gene expression profiles[27,28]. Anatomically, the vertebrate retina is structured as a layered arrangement of six main cell types: photoreceptor, bipolar, amacrine, horizontal, and ganglion cells, as well as Müller glia. Each cell type can be further classified into a number of subtypes, bringing the total number of cell types closer to 60[29].

The neural retina forms three layers of cell bodies, the outer nuclear layer (ONL), inner nuclear layer (INL), and ganglion cell layer (GCL), separated by two synaptic layers (see Figure 2A). The light sensing photoreceptor cells are located at the back of the retina, within the ONL and adjacent to the pigmented epithelial cells (RPE). Light activation of photoreceptor cells signals second order neurons in the INL, composed of bipolar, amacrine and horizontal cells. The neurons of the INL synapse with ganglion cells, which connect the retina to the brain via the optic nerve. At the far back of the retina is a single layer of epithelial cells known as the RPE. These cells serve several important functions, including phagocytosis of the photoreceptor outer segment, absorption of scattered light, and recycling of the chromophore retinal[30].

3.1: Retinal development

During embryonic development, the optic vesicles that form each eye are derived from the ventral forebrain. Patterning of the eye and neural retina is achieved through coordination of signaling pathways and expression of distinct transcription factors[31]. All six retinal cell types are derived from multipotent retinal progenitor cells (RPCs). Current models of fate determination favor a mechanism in which the RPCs progress through a series of competency states, each characterized by the probability that an individual RPC will progress to a specific cell fate[32]. This

is shown through the overlap in the developmental timelines of each cell, which appear to be conserved in vertebrates[33]. Generally, ganglion cells are the first to be 'born', followed closely by cone photoreceptor cells, horizontal cells, and amacrine cells. These are followed by rod photoreceptor cells, then bipolar cells, and finally Müller glial cells[32].

3.2: Photoreceptor cells

Vertebrates have two main types of photoreceptors involved in vision: rods, which are specialized to detect low-intensity light but cannot sense color, and cones, which are color sensing but require higher light intensity than rods[30]. Both rod and cone photoreceptors are highly specialized cells with a polarized structure, segmented into an outer and an inner segment (see Figure 2B)[34]. The light-sensing structure of the photoreceptor is the outer segment (OS), which is a modified cilia filled with flattened, disc-like membranes that are densely packed with light-sensing pigments. The OS joins the inner segment (IS), which comprises the cell body, through a narrow strip called the connecting cilium (CC) (see Figure 2C). The IS is the center for metabolism and biosynthesis in the photoreceptor. Accordingly, all OS proteins must be transported from the IS through the CC[35]. This leads to extremely high

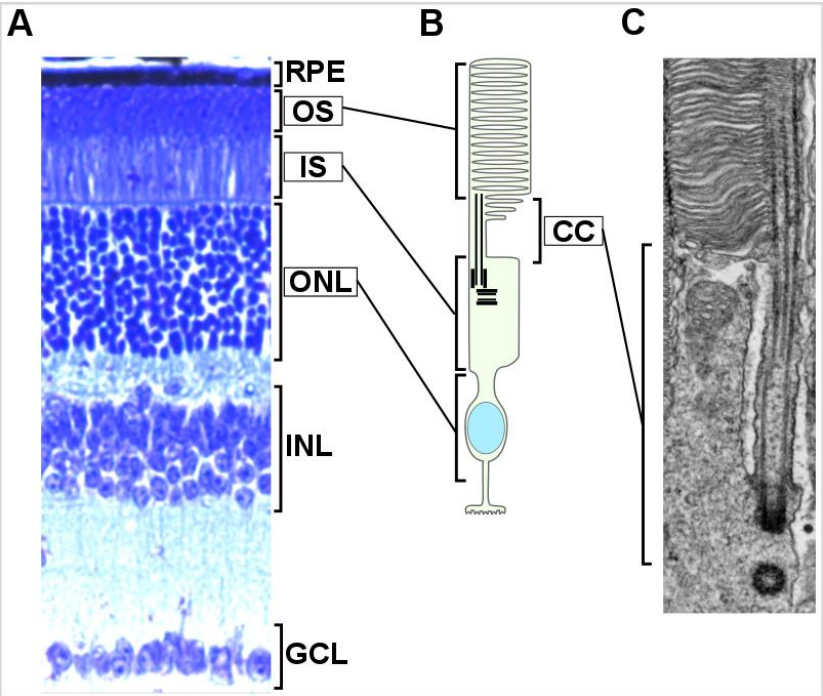

Figure 2. Morphology of the murine retina and rod photoreceptor. A) Section of mouse retina stained with toluidine blue, cell layers and photoreceptor segments are labeled. **B)** Cartoon of rod photoreceptor cell with morphology indicated from **A. C)** Electron micrograph image of mouse rod photoreceptor showing connecting cilium. RPE, retinal pigmented epithelium. OS, outer segment. IS, inner segment. ONL, outer nuclear layer, INL, inner nuclear layer, GCL, ganglion cell layer, CC, connecting cilium.

demand for protein transport to the rod OS as the distal end is regularly shed and phagocytosed by the RPE. As a consequence, perturbations to the CC structure or trafficking can result in impaired biogenesis and maintenance of the OS, often leading to photoreceptor cell death[36,37].

3.3: The Connecting Cilium

Interestingly, the genes involved in biogenesis and maintenance of the photoreceptor primary cilia are ubiquitously expressed in ciliated cell types. Accordingly, the CC of photoreceptor cells form through ciliogenesis much as the primary cilia of other cell types. Ciliogenesis starts when the mother centriole of the basal body anchors to a ciliary vesicle. An array of nine microtubule doublets extends from the mother centriole to form the axoneme. Once the ciliary vesicle fuses with the plasma membrane, the axoneme extends into the extracellular space[38,39]. The formation and maintenance of cilia are highly dependent upon bidirectional protein trafficking termed intraflagellar transport (IFT). IFT is mediated by the protein complexes IFT-A and IFT-B, which associate with molecular motors for retrograde and anterograde transport, respectively[39]. Additional protein complexes such as the BBSome, discussed below, are also required for protein transport in cilia and photoreceptors.

Structurally, the CC of a photoreceptor is very similar to the transition zone of motile cilia[40]. While it is roughly 10 times the length of a typical transition zone, the CC contains the majority of ciliary transition zone components[41]. As a diffusion barrier, the base of the CC is often compared to the nuclear pore. A pinwheel-like arrangement of transition fibers arises from the basal body and acts as a sieve, preventing diffusion of vesicles. Lateral diffusion of membrane proteins is similarly obstructed by a ring of septin proteins, just above the transition fibers. Within the CC itself are champagne glass-shaped structures known as Y-links, which connect the axoneme to the ciliary membrane[36,39,41]. A variety of multiprotein complexes exist within the CC where they are thought to act as a “ciliary gate” regulating protein trafficking in and out of the transition zone[36,39,42,43].

Mutations in IFT components or transition zone proteins can lead to the disruption of ciliary biogenesis and maintenance, causing a variety of syndromes known as ciliopathies[36,38,44]. These syndromes include BBS, Ushers syndrome, Alstrom syndrome, Jeune syndrome, and Senior-Loken syndrome[37,45]. Degeneration of photoreceptor cells in the retina is a hallmark of many ciliopathies, highlighting the importance of the CC in the function of photoreceptor cells.

IV. Retinitis Pigmentosa and pre-mRNA splicing

While RP is often associated with systemic syndromes, most cases of RP are non-syndromic, and symptoms are limited to the loss of photoreceptors in the retina. The death of the rod photoreceptors in RP results in night blindness and progressive loss of vision that can eventually lead to complete blindness. Symptoms generally appear in early teenage years and worsen over time, with severe loss of vision by middle age[6]. Approximately 1 in 4000 individuals is affected with RP in the United States[46,47]. Genetically, RP is extremely heterogeneous, and can be passed down through all modes of inheritance[5,7,47]. Currently, over 60 genes and hundreds of genetic loci have been linked to nonsyndromic RP[7,48]. Of these, 20 are linked with autosomal dominant forms (adRP). Accordingly, development of therapy is hampered by difficulty in diagnosing causative mutations. Strangely, while many of mutations are found in photoreceptor specific genes that are required for phototransduction, other mutations are in ubiquitously expressed genes[47,49].

A notable example of this are mutations in 7 genes identified to cause adRP, which encode ubiquitously expressed pre-mRNA processing factors, such as pre-mRNA processing factor (PRPF) 3, 4, 6, 8, and 31, RP9, and SNRNP200. Excluding RP9, these factors are required for the proper activity of the U4/U6.U5 tri-snRNP, a core component of the spliceosome (see Figure 1B)[6,7,47,50]. Additional genes encode ubiquitously expressed enzymes such as IMPDH and hexokinase[51].

These observations have prompted a question that has yet to be answered: How do mutations in essential housekeeping proteins lead to a phenotype restricted to the retina? In the context of splicing, various ideas have been proposed[47,49,50] For example, the haploinsufficiency model is based on the notion that photoreceptors require high levels of pre-mRNA processing due to factors like high protein turnover. In this model, cell death results from a reduction in spliceosomal components below a certain threshold. Prolonged suboptimal splicing conditions eventually lead to photoreceptor degeneration, while other cell types have a lower demand and remain viable. Support for this model comes from observations that photoreceptor cells are highly metabolically active and that the murine retina expresses high levels of PRPF 3,8, and 31 compared to other tissues[52]. In addition, multiple adRP-associated mutations were found to impair assembly of the U4/U6.U5 tri-SNRP[53–55]. Another potential mechanism is based on a decrease in spliceosomal fidelity, leading to production of misspliced transcripts that are specifically toxic to photoreceptor cells. Evidence for this hypothesis comes from adRP-linked mutations in *SNRNP200* that lead to an increase in misspliced products, rather than decreased spliceosomal assembly or activity[56,57]. Finally, a previously unidentified splicing factor, or factors, that is unique to photoreceptors could exacerbate the phenotype of the spliceosomal mutations. It may be that all of these concepts play a role in development of autosomal dominant RP. Regardless, there remain unknown elements affecting alternative splicing in photoreceptors, which will require further investigation. The reports of photoreceptor cell-specific splicing events, discussed below, highlight this notion.

4.1: Photoreceptor specific splicing of BBS8 Exon 2a

The key to distinguishing the splicing machinery in photoreceptors from other cell types lies in the characterization of photoreceptor specific splicing events. Recently, a mutation in the 3’ splice site of BBS8 exon 2a was found to cause non-syndromic autosomal recessive RP (see Figure 3A). Laser capture microdissection of retinal tissue suggests that this exon is expressed

specifically in photoreceptors (see Figure 3B)[58]. BBS8 encodes one component of a highly conserved octomeric protein complex called the BBSome, which is thought to act as an adapter protein that moves from the base to the tip of cilia in association with IFT complexes[59–61]. Recent evidence supports a role for the BBSome in removal of membrane signaling components from the ciliary tip through retrograde transport[62,63]. Abrogated function of the BBSome is associated with BBS. This ciliopathy is characterized by obesity, polydactyly, renal abnormalities, and RP[37,64]. The mutation of the 3' SS of BBS8 exon 2a is thought to cause skipping of the exon specifically in photoreceptors, resulting in the phenotype of non-syndromic RP rather than systemic BBS[58]. However, the impact of the 10 amino acids encoded by exon 2a on the function of BBS8 protein in photoreceptors remains unclear. Regardless, this splicing event presents a unique tool with which to uncover the sequence elements and splicing factors responsible for photoreceptor specific exon inclusion.

V. Conclusions

The connections between pre-mRNA splicing and ciliary dysfunction as observed in RP remain unclear. The photoreceptor specific exon 2a of the BBS8 gene offers an elegant system to study these questions. Further, the existence of a mechanism limiting exon 2a inclusion to photoreceptor cells hints that there may be additional transcripts which are under the same regulation. In support of this, a previous report identified a photoreceptor specific isoform of the Basignin gene, which is required for retinal development in mice[65,66]. More recently, a retina specific isoform of Arl6 (ADP Ribosylation Factor-Like 6) was shown to be required for vision in zebrafish and normal IS morphology in mice[67,68]. Interestingly, Arl6 is necessary for membrane targeting of the BBSome through direct interaction with BBS1, and loss of Arl6 leads to BBS[69–71].

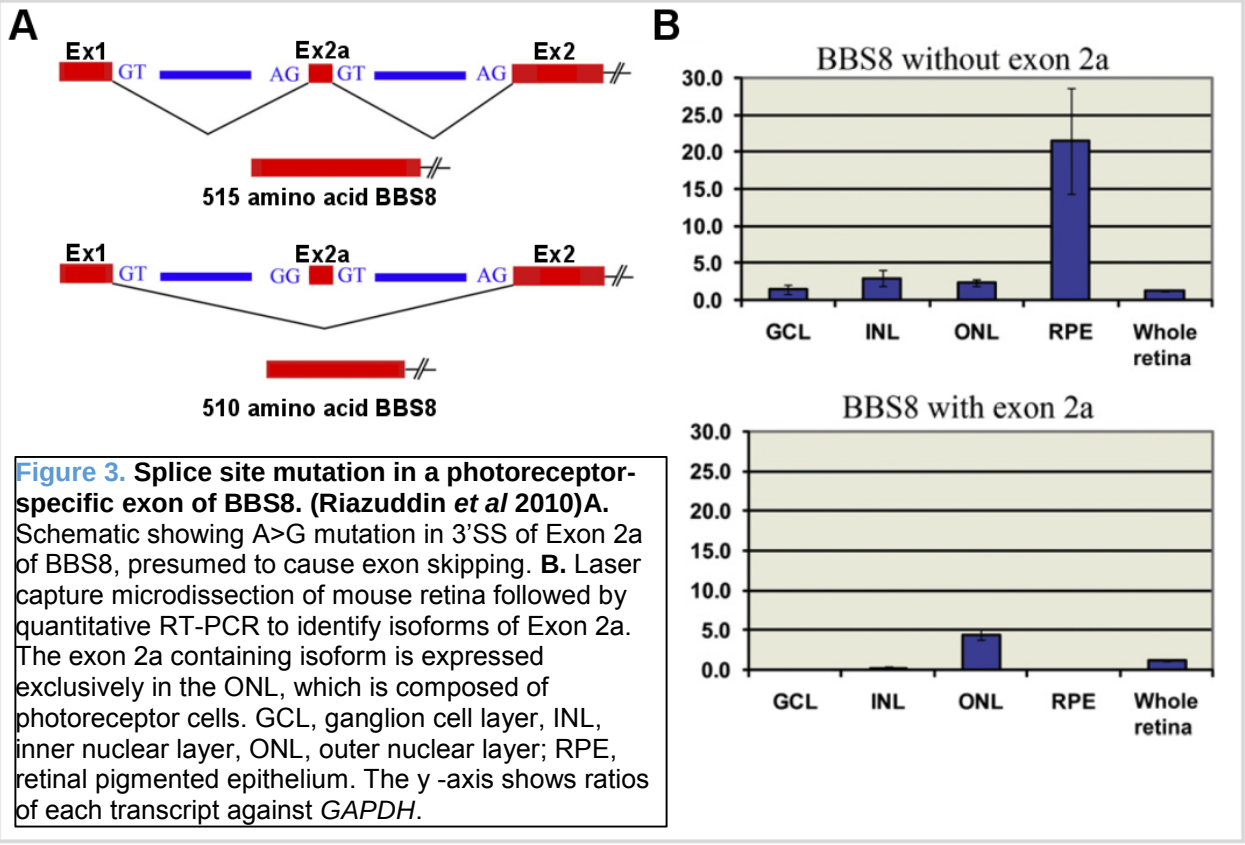

Figure 3. Splice site mutation in a photoreceptor-specific exon of BBS8. (Riazuddin *et al* 2010)A. Schematic showing A>G mutation in 3'SS of Exon 2a of BBS8, presumed to cause exon skipping. **B.** Laser capture microdissection of mouse retina followed by quantitative RT-PCR to identify isoforms of Exon 2a. The exon 2a containing isoform is expressed exclusively in the ONL, which is composed of photoreceptor cells. GCL, ganglion cell layer, INL, inner nuclear layer, ONL, outer nuclear layer; RPE, retinal pigmented epithelium. The y -axis shows ratios of each transcript against *GAPDH*.

5.1: Purpose

These data suggest that photoreceptors exhibit a distinct splicing program, which is necessary to shape their development and function through the production of photoreceptor specific protein isoforms. The purpose of this project was to investigate the regulation of the photoreceptor alternative splicing program. Using the aforementioned splicing events as models, we can begin to characterize the unique features which regulate alternative splicing in photoreceptor cells. This knowledge will be invaluable in uncovering novel disease genes and linking disease phenotypes to causal mutations. It can also lead to identification of the molecular mechanisms that mediate the susceptibility of photoreceptor cells to defects in alternative splicing. Finally, many questions remain about the regulation of protein trafficking across the photoreceptor connecting cilium. Analysis of photoreceptor specific protein isoforms such as BBS8 may reveal an important role for alternative splicing in this context.

5.2: References

1. Nilsen, T. W. & Graveley, B. R. Expansion of the eukaryotic proteome by alternative splicing. *Nature* **463,** 457–463 (2010).
2. Black, D. L. Mechanisms of Alternative Pre-Messenger Rna Splicing. *Annu. Rev. Biochem.* **72,** 291–336 (2003).
3. Garcia-Blanco, M. A. Alternative splicing: therapeutic target and tool. *Prog. Mol. Subcell. Biol.* **44,** 47–64 (2006).
4. Ward, A. J. & Cooper, T. A. The Pathobiology of Splicing. *J. Pathol.* **220,** 152–163 (2010).
5. Daiger, S. P., Sullivan, L. S. & Bowne, S. J. 'Genes and Mutations Causing Retinitis Pigmentosa'. *Clin. Genet.* n/a–n/a (2013). doi:10.1111/cge.12203
6. Ferrari, S. *et al.* Retinitis Pigmentosa: Genes and Disease Mechanisms. *Curr. Genomics* **12,** 238–249 (2011).
7. Daiger, S. P., Bowne, S. J. & Sullivan, L. S. Genes and Mutations Causing Autosomal Dominant Retinitis Pigmentosa. *Cold Spring Harb. Perspect. Med.* a017129 (2014). doi:10.1101/cshperspect.a017129
8. Riazuddin, S. A. *et al.* A Splice-Site Mutation in a Retina-Specific Exon of BBS8 Causes Nonsyndromic Retinitis Pigmentosa. *Am. J. Hum. Genet.* **86,** 805–812 (2010).
9. Pan, Q., Shai, O., Lee, L. J., Frey, B. J. & Blencowe, B. J. Deep surveying of alternative splicing complexity in the human transcriptome by high-throughput sequencing. *Nat. Genet.* **40,** 1413–1415 (2008).
10. Wang, E. T. *et al.* Alternative isoform regulation in human tissue transcriptomes. *Nature* **456,** 470–476 (2008).
11. Matera, A. G. & Wang, Z. A day in the life of the spliceosome. *Nat. Rev. Mol. Cell Biol.* **15,** 108–121 (2014).
12. Will, C. L. & Lührmann, R. Spliceosome Structure and Function. *Cold Spring Harb. Perspect. Biol.* **3,** (2011).

13. Chen, M. & Manley, J. L. Mechanisms of alternative splicing regulation: insights from molecular and genomics approaches. *Nat. Rev. Mol. Cell Biol.* **10,** 741–754 (2009).
14. Fica, S. M. *et al.* RNA catalyses nuclear pre-mRNA splicing. *Nature* **503,** 229–234 (2013).
15. Kornblihtt, A. R. *et al.* Alternative splicing: a pivotal step between eukaryotic transcription and translation. *Nat. Rev. Mol. Cell Biol.* **14,** 153–165 (2013).
16. Wahl, M. C., Will, C. L. & Lührmann, R. The Spliceosome: Design Principles of a Dynamic RNP Machine. *Cell* **136,** 701–718 (2009).
17. Raj, B. & Blencowe, B. J. Alternative Splicing in the Mammalian Nervous System: Recent Insights into Mechanisms and Functional Roles. *Neuron* **87,** 14–27 (2015).
18. Zheng, S. & Black, D. L. Alternative Pre-mRNA Splicing in Neurons, Growing Up and Extending Its Reach. *Trends Genet. TIG* **29,** 442–448 (2013).
19. Yap, K. & Makeyev, E. V. Regulation of gene expression in mammalian nervous system through alternative pre-mRNA splicing coupled with RNA quality control mechanisms. *Mol. Cell. Neurosci.* **56,** 420–428 (2013).
20. Barbosa-Morais, N. L. *et al.* The evolutionary landscape of alternative splicing in vertebrate species. *Science* **338,** 1587–1593 (2012).
21. Merkin, J., Russell, C., Chen, P. & Burge, C. B. Evolutionary Dynamics of Gene and Isoform Regulation in Mammalian Tissues. *Science* **338,** 1593–1599 (2012).
22. Darnell, R. B. RNA protein interaction in neurons. *Annu. Rev. Neurosci.* **36,** 243–270 (2013).
23. Quesnel-Vallières, M., Irimia, M., Cordes, S. P. & Blencowe, B. J. Essential roles for the splicing regulator nSR100/SRRM4 during nervous system development. *Genes Dev.* **29,** 746–759 (2015).
24. Licatalosi, D. D. *et al.* Ptbp2 represses adult-specific splicing to regulate the generation of neuronal precursors in the embryonic brain. *Genes Dev.* **26,** 1626–1642 (2012).
25. Irimia, M. *et al.* A Highly Conserved Program of Neuronal Microexons Is Misregulated in Autistic Brains. *Cell* **159,** 1511–1523 (2014).

26. Weyn-Vanhentenryck, S. M. *et al.* HITS-CLIP and integrative modeling define the Rbfox splicing-regulatory network linked to brain development and autism. *Cell Rep.* **6,** 1139–1152 (2014).
27. Nowak, J. Z. The retina as a model neural tissue: comparative studies on retinal and brain aminergic mechanisms. *Pol. J. Pharmacol. Pharm.* **39,** 451–482 (1987).
28. London, A., Benhar, I. & Schwartz, M. The retina as a window to the brain—from eye research to CNS disorders. *Nat. Rev. Neurol.* **9,** 44–53 (2013).
29. Masland, R. H. Cell Populations of the Retina: The Proctor Lecture. *Invest. Ophthalmol. Vis. Sci.* **52,** 4581–4591 (2011).
30. *Webvision: The Organization of the Retina and Visual System*. (University of Utah Health Sciences Center, 1995). at <http://www.ncbi.nlm.nih.gov/books/NBK11530/>
31. Gregory-Evans, C. Y., Wallace, V. A. & Gregory-Evans, K. Gene networks: Dissecting pathways in retinal development and disease. *Prog. Retin. Eye Res.* **33,** 40–66 (2013).
32. Cepko, C. Intrinsically different retinal progenitor cells produce specific types of progeny. *Nat. Rev. Neurosci.* **15,** 615–627 (2014).
33. Photoreceptor cell fate specification in vertebrates | Development. at <http://dev.biologists.org/content/142/19/3263.long>
34. Pearring, J. N., Salinas, R. Y., Baker, S. A. & Arshavsky, V. Y. Protein sorting, targeting and trafficking in photoreceptor cells. *Prog. Retin. Eye Res.* doi:10.1016/j.preteyeres.2013.03.002
35. Sung, C.-H. & Chuang, J.-Z. The cell biology of vision. *J. Cell Biol.* **190,** 953–963 (2010).
36. Madhivanan, K. & Aguilar, R. C. Ciliopathies: The Trafficking Connection. *Traffic* **15,** 1031–1056 (2014).
37. Mockel, A. *et al.* Retinal dystrophy in Bardet–Biedl syndrome and related syndromic ciliopathies. *Prog. Retin. Eye Res.* **30,** 258–274 (2011).

38. Sedmak, T. & Wolfrum, U. Intraflagellar transport proteins in ciliogenesis of photoreceptor cells. *Biol. Cell Auspices Eur. Cell Biol. Organ.* **103,** 449–466 (2011).
39. Khanna, H. Photoreceptor Sensory Cilium: Traversing the Ciliary Gate. *Cells* **4,** 674–686 (2015).
40. Falk, N., Lösl, M., Schröder, N. & Gießl, A. Specialized Cilia in Mammalian Sensory Systems. *Cells* **4,** 500–519 (2015).
41. Chuang, J.-Z., Hsu, Y.-C. & Sung, C.-H. Ultrastructural visualization of trans-ciliary rhodopsin cargoes in mammalian rods. *Cilia* **4,** (2015).
42. Chih, B. *et al.* A ciliopathy complex at the transition zone protects the cilia as a privileged membrane domain. *Nat. Cell Biol.* **14,** 61–72 (2012).
43. Barker, A. R., Renzaglia, K. S., Fry, K. & Dawe, H. R. Bioinformatic analysis of ciliary transition zone proteins reveals insights into the evolution of ciliopathy networks. *BMC Genomics* **15,** 531 (2014).
44. Wheway, G., Parry, D. A. & Johnson, C. A. The role of primary cilia in the development and disease of the retina. *Organogenesis* **10,** 69–85 (2014).
45. Taub, D. G. & Liu, Q. The Role of Intraflagellar Transport in the Photoreceptor Sensory Cilium. *Adv. Exp. Med. Biol.* **854,** 627–633 (2016).
46. Ayuso, C. & Millan, J. M. Retinitis pigmentosa and allied conditions today: a paradigm of translational research. *Genome Med.* **2,** 34 (2010).
47. Berger, W., Kloeckener-Gruissem, B. & Neidhardt, J. The molecular basis of human retinal and vitreoretinal diseases. *Prog. Retin. Eye Res.* **29,** 335–375 (2010).
48. RetNet: Disease Table. at <https://sph.uth.edu/retnet/disease.htm>
49. Mordes, D. *et al.* Pre-mRNA splicing and retinitis pigmentosa. *Mol. Vis.* **12,** 1259–1271 (2006).
50. Liu, M. M. & Zack, D. J. Alternative splicing and retinal degeneration. *Clin. Genet.* n/a–n/a (2013). doi:10.1111/cge.12181

51. Daiger, S. P., Bowne, S. J. & Sullivan, L. S. Genes and Mutations Causing Autosomal Dominant Retinitis Pigmentosa. *Cold Spring Harb. Perspect. Med.* **5,** a017129 (2015).
52. Cao, H. *et al.* Temporal and tissue specific regulation of RP-associated splicing factor genes PRPF3, PRPF31 and PRPC8--implications in the pathogenesis of RP. *PloS One* **6,** e15860 (2011).
53. Gonzalez-Santos, J. M., Cao, H., Duan, R. C. & Hu, J. Mutation in the splicing factor Hprp3p linked to retinitis pigmentosa impairs interactions within the U4/U6 snRNP complex. *Hum. Mol. Genet.* **17,** 225–239 (2008).
54. Linder, B. *et al.* Identification of a PRPF4 loss-of-function variant that abrogates U4/U6.U5 tri-snRNP integration and is associated with retinitis pigmentosa. *PloS One* **9,** e111754 (2014).
55. Huranová, M., Hnilicová, J., Fleischer, B., Cvacková, Z. & Stanek, D. A mutation linked to retinitis pigmentosa in HPRP31 causes protein instability and impairs its interactions with spliceosomal snRNPs. *Hum. Mol. Genet.* **18,** 2014–2023 (2009).
56. Cvačková, Z., Matějů, D. & Staněk, D. Retinitis pigmentosa mutations of SNRNP200 enhance cryptic splice-site recognition. *Hum. Mutat.* **35,** 308–317 (2014).
57. Zhao, C. *et al.* Autosomal-Dominant Retinitis Pigmentosa Caused by a Mutation in SNRNP200, a Gene Required for Unwinding of U4/U6 snRNAs. *Am. J. Hum. Genet.* **85,** 617–627 (2009).
58. Riazuddin, S. A. *et al.* A splice-site mutation in a retina-specific exon of BBS8 causes nonsyndromic retinitis pigmentosa. *Am. J. Hum. Genet.* **86,** 805–812 (2010).
59. Nachury, M. V. How do cilia organize signalling cascades? *Philos. Trans. R. Soc. B Biol. Sci.* **369,** (2014).
60. Ou, G., E. Blacque, O., Snow, J. J., Leroux, M. R. & Scholey, J. M. Functional coordination of intraflagellar transport motors. *Nature* **436,** 583–587 (2005).

61. Lechtreck, K.-F. *et al.* The Chlamydomonas reinhardtii BBSome is an IFT cargo required for export of specific signaling proteins from flagella. *J. Cell Biol.* **187,** 1117–1132 (2009).
62. Eguether, T. *et al.* IFT27 Links the BBSome to IFT for Maintenance of the Ciliary Signaling Compartment. *Dev. Cell* **31,** 279–290 (2014).
63. Liew, G. M. *et al.* The Intraflagellar Transport Protein IFT27 Promotes BBSome Exit from Cilia through the GTPase ARL6/BBS3. *Dev. Cell* **31,** 265–278 (2014).
64. Zaghloul, N. A. & Katsanis, N. Mechanistic insights into Bardet-Biedl syndrome, a model ciliopathy. *J. Clin. Invest.* **119,** 428–437 (2009).
65. Ochrietor, J. D. *et al.* Retina-specific expression of 5A11/Basigin-2, a member of the immunoglobulin gene superfamily. *Invest. Ophthalmol. Vis. Sci.* **44,** 4086–4096 (2003).
66. Clamp, M. F., Ochrietor, J. D., Moroz, T. P. & Linser, P. J. Developmental analyses of 5A11/Basigin, 5A11/Basigin-2 and their putative binding partner MCT1 in the mouse eye. *Exp. Eye Res.* **78,** 777–789 (2004).
67. Pretorius, P. R. *et al.* Identification and Functional Analysis of the Vision-Specific BBS3 (ARL6) Long Isoform. *PLoS Genet.* **6,** (2010).
68. Pretorius, P. R., Aldahmesh, M. A., Alkuraya, F. S., Sheffield, V. C. & Slusarski, D. C. Functional analysis of BBS3 A89V that results in non-syndromic retinal degeneration. *Hum. Mol. Genet.* **20,** 1625–1632 (2011).
69. Chiang, A. P. *et al.* Comparative genomic analysis identifies an ADP-ribosylation factor-like gene as the cause of Bardet-Biedl syndrome (BBS3). *Am. J. Hum. Genet.* **75,** 475–484 (2004).
70. Mourão, A., Nager, A. R., Nachury, M. V. & Lorentzen, E. Structural Basis for Membrane Targeting of the BBSome by ARL6. *Nat. Struct. Mol. Biol.* **21,** 1035–1041 (2014).
71. Jin, H. *et al.* The Conserved Bardet-Biedl Syndrome Proteins Assemble a Coat that Traffics Membrane Proteins to Cilia. *Cell* **141,** 1208–1219 (2010).

REPRINTED WITH PERMISSION FROM SPRINGER PUBLISHING

Chapter 2: Book chapter. Methods in Molecular Biology- Spliceosomal Pre-mRNA Splicing. 2014.

Medium throughput analysis of alternative splicing by fluorescently labeled RT-PCR

Ryan Percifield, Daniel Murphy, Peter Stoilov*

West Virginia University, Department of Biochemistry

1 Medical Center Dr, P.O. Box 9142

Morgantown, WV 26506

phone: 304 293 6334

fax: 304 293 6846

e-mail: pstoilov@hsc.wvu.edu

Author Contributions

RP: experimental design, data acquisition, data analysis and interpretation, drafting and revising the article.

DM: experimental design, data acquisition, data analysis and interpretation.

PS: conception, experimental design, data acquisition, data analysis and interpretation, drafting and revising the article.

Summary

Reverse transcription-PCR (RT-PCR) is a core technique for detecting and quantifying alternative pre-mRNA splicing. RT-PCR is multistep process involving RNA isolation, reverse transcription, and PCR that is often performed using radiolabeled primers. As a result RT-PCR analysis of alternative splicing is a laborious technique that quickly becomes prohibitively expensive when applied to large numbers of samples. Here, we describe a RT-PCR approach for detecting alternative splicing in multi-well plates that can be applied to effortlessly quantify exon inclusion levels in large number of samples. The procedures outlined here can also be automated on standard liquid handling equipment to produce medium throughput assay capable of handling thousands of samples per day.

Keywords: alternative splicing, RNA isolation, 96-well plate format, RT-PCR, fluorescent primers, capillary electrophoresis

1. Introduction

Pre-mRNA splicing has emerged as major mechanism for regulation of gene expression and protein function (1). In higher eukaryotes alternative splicing generates astonishing protein diversity from a relatively limited number of gene (2; 3). Perturbations in constitutive and alternative pre-mRNA splicing are a frequently cause of disease. Estimated 15% of disease causing mutations disrupting canonical splice sites and another 20 to 30% disrupting splicing regulatory sequences located within the exons (4; 5). As a result there has been a significant interest in developing increased throughput approaches to screen for chemical and genetic modulators of alternative splicing. In the past *in vivo* luciferase and fluorescent protein reporters have successfully been used in high throughput screens to identify modulators of alternative splicing (6–9). However these approaches suffer from significant false discovery rates and

require secondary validations assays to reliably identify the positive hits. Reverse transcription/PCR (RT-PCR) is the method of choice for such secondary assays. However, the throughput of RT-PCR has been limited due to the relatively high cost of the necessary consumables and reagents. Here we describe a medium throughput procedure for RNA isolation and RT-PCR in multi-well plates that uses low cost consumables. The protocol outlined below can be applied effortlessly in most laboratories to processed 192 to 384 samples per day. This throughput is sufficient to directly screen targeted compound and siRNA libraries such as the InhibitorSelect and ON-TARGETplus collections offered by EMD biosciences and Dharmacon. Furthermore, all steps of the protocol can be fully automated using standard liquid handling equipment to create a medium throughput assay capable of handling thousands of samples per day in 96 and 384 well formats.

2. Materials

2.1. Prepare all solutions with ultrapure (18mΩ) nuclease free water and store them as indicated in the instructions. As some waste products produced during these protocols can be harmful to the environment, please refer to your local regulations and procedures when disposing of waste.RNA Extraction Components

1. A centrifuge with deep swing-out buckets capable of spinning 2 deep-well plates in each adapter at a speed of 1500G.
2. Low volume spectrophotometer: NanoDrop (Thermo Scientific) or equivalent.
3. 96-well tissue culture plates
4. Nuclease free liquid troughs

5. 96-well, 400µl, 0.45µm hydrophilic PVDF filter plates (Seahorse Biosciences part # 200943-100, *see* **Note 1**).
6. 96-well 1ml deep-well plates
7. 96-well nuclease free PCR plates
8. Aluminum plate sealing film
9. DNase I, RNase free.
10. RNA Lysis Buffer: 6M Lithium chloride, 5% Triton X-100, 5% DGME (Di-ethylene glycol mono-ethyl ether), 10mM EDTA pH 8.0, 100mM Tris-HCl pH 8.8. Filter through 0.45µM filter and store at room temperature. Just before use add 2% β-mercaptoethanol.
11. RNA Wash Solution I: 5M Lithium chloride, 55% Ethanol. Filter and store at room temperature (*see* **Note 2**).
12. RNA Wash Solution II: 30mM Tris-HCl pH 7.6, 70% Ethanol. Filter and store at room temperature.
13. Phosphate Buffered Saline (PBS)

2.2. cDNA Synthesis Components

14. 96-well nuclease free PCR plate
15. Plate sealing film
16. Ultrapure water
17. dNTP mix, 10mM each
18. Primer mix: 10µM Anchored oligo dT ($dT_{24}VN$) and 50µM random hexamers
19. 10X Reverse transcriptase buffer: 500 mM Tris-HCl (pH 8.3), 750 mM KC1, 30 mM $MgCl_2$.
20. RNase H(-) reverse transcriptase (*see* **Note 2)**

2.3. PCR Components

1. 96-well nuclease free PCR plate
2. Plate sealing film
3. Ultrapure water
4. dNTP mix, 10mM each
5. Forward and reverse PCR primer mix, 10μM each. One of the primers needs to be fluorescently labeled (see Note 3).
6. 10X Taq buffer 500 mM KCl, 100 mM Tris HCl (pH 9.0 at 25°C), 15 mM MgCl2, and 1% Triton X-100
7. Taq polymerase at 15 units/μl (see Note 2)

2.4. Acrylamide Gel Electrophoresis Components

1. Vertical gel electrophoresis apparatus (Labrepco model V16 or equivalent)
2. High voltage power supply
3. PCR tube strips and caps (8- or 12-tube)
4. Sigmacote (Sigma Aldrich)or equivalent siliconizing reagent.
5. 10% weight/volume Ammonium Persulfate (APS) solution in water.
6. Tetramethylenediamine (TEMED).
7. 1X Tris-Borate EDTA Buffer (TBE): 89mM Tris, 89mM Boric acid, 2mM EDTA. The buffer can be made as a 5X stock solution and diluted before use.
8. Acrylamide gel solution: 4% Acrylamide/Bis-acrylamide (19:1 crosslink ratio), 1xTBE, 7.5M Urea. Filter solution through 0.45μM buffer and store in a dark bottle at 4°C.
9. Clear formamide loading buffer: Deionized formamide, 2 mM EDTA
10. Formamide loading buffer with tracking dyes: Deionized formamide, 2 mM EDTA 0.25% (w/v) bromophenol blue, and 0.25% (w/v) xylene cyanol FF.

11. Fluorescently labeled size standards: Life technologies/ABI GeneScan 1000 Rox or GeneScan 1200 LIZ. Alternatively custom size standards can be prepared by a simple PCR amplification with a ROX labeled primer (10).

2.5. Capillary Electrophoresis Components

1. ABI capillary sequencer. Access to this equipment is typically available as part of sequencing core facility or commercial service.
2. 96-well half skirt PCR plate compatible with ABI sequencers (*see* **Note 4**).
3. Clear formamide loading buffer: Deionized formamide, 2 mM EDTA 0.25% (w/v)
4. Fluorescently labeled size standard

3. Methods

This protocol involves procedures for RNA isolation, cDNA synthesis, PCR and capillary electrophoresis that are carried out in 96 well plates. The RNA isolation procedure is adapted from Bair et al and uses high concentrations of LiCl, which has long been known to efficiently strip the proteins from the RNA (11; 12). The RNA is then bound to solid support, and after washing away the contaminants is eluted in water. In our hands PVDF membranes proved superior to silica or glass fiber support that is typically used in nucleic acid purification procedures. In particular the PVDF membranes unlike glass-fiber filters did not bind the detergents used to lyse the cells and produced RNA free of contaminants (Figure 1).

cDNA synthesis and PCR amplification procedures follow standard protocols. A key feature of the approach described here is the use of fluorescently labeled primer in the PCR amplification. The fluorescent label allows the amplification products to be subsequently quantified by capillary electrophoresis. Substituting standard gel electrophoresis procedures for automated capillary electrophoresis significantly decreases the labor involved and increases the

throughput of the assay. Although we also describe the gel electrophoresis procedures, we recommend using it only on a limited subset of samples as a quality control and troubleshooting tool.

3.1. RNA isolation from adherent cells in 96-well plates

Just prior to beginning the extraction procedure add 20µl per *ml* β-mercaptoethanol to the RNA Lysis Buffer (*see* **Note 5**).

1. Grow the cells in 96 well tissue culture plates.
2. Before lysing the cells stack a 96 well PVDF filter plate on top of a deep well plate.

Steps 3 through 6 describe the lysis procedure for adherent cells. If working with suspension cultures or very loosely adherent cells skip to step #7.

3. If working with adherent cells invert the tissue culture plate and shake off the media. Tap the plate on a stack of paper towels to remove the excess liquid.
4. Wash cells once with 200µl of PBS. If the cells are adhering loosely to the plate, skip this step as it can result in washing the cells away.
5. Add 200µl RNA Lysis Buffer to each well (*see* **Note 6**).
6. Using a multi-channel pipette transfer the lysates into the filter plate. Proceed to step #11 of the protocol.
7. If working with suspension cells resuspend the cells in the culture media by pipetting up and down and transfer the suspension to the filter plate.
8. Spin the plate at 1500g for 3 minutes to remove the media.
9. Discard the liquid accumulated in the deep well plate, tap the plate face down on stack of paper towels to remove excess liquid and reuse the plate.
10. Add 200µl of lysis buffer to each well and incubate for 3 minutes at room temperature.
11. Spin the plate at 1500g for 3 minutes.

12. Add 200µl RNA Wash Solution I and spin at 1500g for 3 minutes.

13. Discard the liquid accumulated in the deep well plate as in step #9

14. Add 200µl RNA Wash Solution II and spin at 1500g for 3 minutes.

15. Add 20µl of DNase solution (0.1U/ul in 1X DNase buffer) to the membrane, seal the plate and incubate at 37ºC for 20 minutes.

16. Add 200µl RNA Lysis Buffer and incubate at room temperature for 2 minutes.

17. Spin at 1500g for 2 minutes.

18. Discard the liquid accumulated in the deep well plate as in step #9.

19. Add 200µl RNA Wash Solution I and spin at 1500g for 2 minutes.

20. Add 200µl RNA Wash Solution II and spin at 1500g for 2 minutes.

21. Discard the liquid accumulated in the deep well plate as in step #9.

22. Repeat Step 13, this time extending the spin to 5 min.

23. Transfer the filter plate to a full-skirt PCR plate.

24. Add 16µl-25ul of water to the membrane, incubate for 5 minutes at room temperature and spin at 1500g for 5. The filter plate retention volume is typically 1ul per well resulting in RNA solution volume of 15µl-24µl. If all RNA is going to be used for cDNA synthesis, step 20 can be omitted. In this case the RNA can be eluted using 16µl of water into a plate containing 5µl of reverse transcription master mix to perform the first strand synthesis (see below).

25. Check the RNA quality in a subset of wells by agarose gel electrophoresis of 5µl of the sample (*see* **Note 7**). If necessary determine the RNA concentration using a NanoDrop spectrophotometer. At this point the plates can be sealed using aluminum sealing film and stored at -80°C, or used for first strand DNA synthesis.

3.2. First strand cDNA synthesis

1. For each 96 well plate prepare a reverse transcription master mix containing 220µl 10X reverse transcriptase buffer, 110µl 10mM dNTPs, 110µl oligo dT/random hexamer mix, 55µl of reverse transcriptase, and 55µl of water.

2. Dispense 5µl of the master mix in each well of a 96 well PCR plate.

3. Add 15µl of RNA solution to each well of the plate containing the reverse transcription mix. Alternatively use the plate containing the reverse transcription mix to catch the RNA eluted with 16 µl of water in step19 of the RNA isolation procedure above.

4. Spin down the plate briefly to collect any drops and purge air bubbles trapped at the bottom of the wells.

5. Cover the plate with sealing film and run in a thermal cycler under the following conditions: step 1 - 25°C for 5 minutes, step 2 - 43°C for 40 minutes, step 3 - 75°C for 15 minutes, followed by a 10°C hold until ready to remove the plate.

6. Remove the plate from the thermal cycler.

7. Dilute the reactions with 20 µl of water, reseal the plate and store at -20°C until needed.

3.3. PCR Primer design

PCR primers for measuring exon inclusion levels can be designed using primer3. The primers are placed in the constitutive exons that flank the alternatively spliced region and should have melting temperatures of approximately 60°C. Typically the primers will be located in the exons immediately adjacent to the alternatively spliced region (Figure 2A). In cases where the size or nucleotide composition of the constitutive exons place constrains on the primer design, the primers can be moved further away (Figure 2B). This placement will produce PCR products of

different size corresponding to the exon included and exon skipped mRNA isoforms. Optimally the primers should be designed so that the shortest (skipped) product should be between 150 and 250nt. The longest PCR product should not exceed 800nt in size. This size limit is dictated by the lower amplification efficiency of large fragments which leads to under representation of the product derived from the exon included isoform and inaccurate quantification of the exon inclusion rates. The inclusion rate of such large alternative exons can be assessed using a set of three primers that includes a shared forward primer and two reverse primers placed in the downstream exons (Figure 2C). The same approach using a shared forward primer and two reverse primers can also be used to detect mutually exclusive exons, which typically have the same size, or alternative 3' terminal exons (Figure 2D).

One of the primers in the set is synthesized with fluorescent tag at the 5' end. In the cases where a set of three primers is used the label should be placed on the shared primer. The fluorescent tag needs to be compatible with the capillary electrophoresis equipment that will be used to separate and quantify the PCR products. The tag also needs to be different from the fluorescent label of the size standard. ABI capillary sequencers can use both ROX or LIZ labeled size standards. We recommend using FAM or HEX to label the primers. Bot tags are compatible with the ABI equipment (Table 1) and are commonly available as an inexpensive 5' modification option from a number of oligonucleotide synthesis service companies.

3.4. PCR amplification

1. For each 96 well plate prepare a PCR master mix containing 165µl 10X Taq PCR buffer 33µl dNTPs, 33µl 10µM Primer mix, 17µl of Taq DNA polymerase, and 1182µl of water.

2. Dispense 13µl of the master mix in each well of a 96 well PCR plate.

3. Transfer 2µl of the first strand synthesis reactions to the plate containing the PCR mix. Spin down the plate briefly to collect any drops and purge air bubbles trapped at the bottom of the wells.

4. Cover the plate with sealing film and amplify the templates using the following conditions:

   Initial denaturation: 94°C for 4 minutes

   20 to 35 amplification cycles: 94°C for 30 seconds; 60°C for 30 seconds; 72°C for 60 seconds (*see* **Note 8**).

   Final extension: 72°C for 5 minutes

   Hold at 10°C until ready to remove the plate.

3.5. Electrophoresis and Quantification of exon inclusion

The PCR amplicons can be visualized and quantified either by gel or capillary electrophoresis. Gel electrophoresis is significantly more laborious. However it is indispensable as a tool to control the quality of the samples and troubleshoot problems. In particular we recommend analyzing 12 to 16 samples by gel electrophoresis to ensure that the PCR reactions did not fail and to estimate if a dilution of the samples may be necessary prior to submitting the full sample set for capillary electrophoresis. The fluorescently labeled PCR amplicons separated by gel electrophoresis can be imaged directly on a Typhoon Phorsphorimager (GE) and quantified either by the ImageQuant software that accompanies the instrument or by the freely available ImageJ software (Figure 3).

Capillary electrophoresis instruments offer single nucleotide resolution over a wider range of fragment sizes, increased sensitivity, and significantly higher throughput compared to gel electrophoresis.

3.5.1. Fragment Analysis By Gel Electrophoresis

Acrylamide gel electrophoresis

1. Clean the sides of each glass plate with absolute ethanol and then dry with paper towels (*see* **Note 9**).

2. If the glass plates have not been siliconized before, apply Sigmacote (*see* **Note 10**) to the ethanol cleaned sides and spread/dry with a paper towel. Clean again the plates with ethanol as described in step #1.

3. Place the spacers on the larger of the two glass plates (two side spacers with the foam dam toward the top and the bottom spacer across the bottom edge) then take the smaller of the two plates and place it on top with the cleaned side facing the other plate, thus making a plate-spacer-plate sandwich.

4. Clip the sandwich together with paper clips and set aside.

5. Assemble as many gels as needed as described above.

6. In a clean flask mix acrylamide solution (25ml/gel) with 1/100 volume 10% APS (250µl/gel) and 1/1000 volume TEMED (25µl/gel).

7. Holding the plate sandwich at approximately 15-20 degrees from horizontal, pour the gel solution in a steady stream along one of the side spacers allowing it to flow smoothly between the two glass plates while ensuring that no air bubbles are formed. Once filled to the top, place the gel horizontally to insert the comb. Leave the gel in this position until the gel polymerizes (approximately 20-30 minutes).

8. After the gel has solidified remove the clips, the bottom gel spacer, and the well comb.

9. Place the sandwich into the running apparatus with the larger glass plate facing out. Use two clips on each side of the gel to clip the sandwich to the gel.

10. Immediately rinse the wells using an 18 gauge needle on a 50 ml syringe filled with 1xTBE running buffer.

11. Fill the upper and lower reservoirs with 1X TBE buffer ensuring that the gel is covered and that there is no air trapped at the bottom.

12. Apply a piece of clear adhesive tape such as Scotch tape, to the outside glass plate directly under the wells. On the tape, use a Sharpie pen to label each well with a number that corresponds to the sample that will be loaded into the well (*see* **Note 11**).

13. Attach the cover of the gel apparatus and pre-run the gel for 30 to 50 minutes at 450 volts. While the gel is preheating prepare the PCR amplicons for loading as described below.

14. Prepare a loading buffer mix containing 10µl clear formamide loading buffer and 0.3µl fluorescent size standard for each sample to be loaded on the gel.

15. Depending on the number of samples being analyzed place one or more PCR tube strips on a PCR tube rack.

16. Dispense 10µl of the loading buffer mix to each tube.

17. Transfer 2 µl of the PCR amplicon to each of the tubes containing the loading buffer mix.

18. Seal the tubes and incubate in a thermal cycler at 95°C for 5 minutes to denature the samples. Place the tubes on ice.

19. Turn off the gel power supply. Rinse again the wells as described in step #11 to remove accumulated urea. Failing to remove the urea will interfere with loading the samples and distort the bands.

20. Load 10 µl of the denatured samples in each well.

21. Optionally load 1-2µl of the gel loading buffer containing tracking dyes to and empty well at least one lane apart from the nearest sample (*see* **Note 12**).

22. Run the gel at 450 volts for 55 minutes or until the bromophenol blue dye moves out of the gel then turn off the power supply.

23. Remove the gel sandwich from the electrophoresis apparatus.

24. Remove the side spacers and the adhesive tape. Do not disassemble the gel sandwich!

25. Clean the plates with deionized water to remove any dried acrylamide or urea attached to the outside of the plates.

26. Clean and dry the plates with ethanol soaked paper towels to remove any remaining dirt and dry the plates (*see* **Note 9**).

Phosphorimager **Visualization**

1. Clean and dry the surface of the phosphorimager with ethanol soaked paper towels (*see* **Note 9**).

2. Place the gel sandwich(es) on the phosphorimager glass plate.

3. In the Typhoon control software select the scan area, then close the imager lid.

4. In the Typhoon control software set the phosphorimager to fluorescence mode.

5. Select the appropriate combinations of excitation lasers and band pass emission filters depending on labels present in the samples and the size standards. The settings for the most common labels are listed on Table 1.

6. Set the focal plane to +3 mm (this adjusts the focal point to 3 mm above the surface of the phosphorimager to account for the width of the glass plate of the gel).

7. Choose the appropriate orientation for your output image.

8. Scan the gel. While scanning make sure that there are no saturated pixels (marked in red on the preview window). If there are saturated pixels, rescan the gel after lowering the photomultiplier (PMT) voltage for the appropriate channel.

3.5.2. Fragment analysis by capillary electrophoresis

1. Dilute the PCR amplicons with water. The dilution factor depends on the signal strength and can vary from two to hundred fold. The approximate dilution factor can be determined from the the gel electrophoresis analysis. We recommend running a pilot experiment to determine the relationship between the signal strengths detected by the phosphorimager and capillary electrophoresis equipment.
2. Prepare loading buffer mix containing 1ml clear formamide loading buffer and 30µl for each 96 well plate.
3. Dispense 10 µl of the loading buffer mix in each well of a half skirt 96 well PCR plate.
4. Transfer 2 µl of the diluted PCR amplicons to the plate containing the loading buffer mix.
5. Seal the plate and incubate in a thermal cycler at 95°C for 5 minutes to denature the samples.

6. Place the plates on ice and bring them to the facility operating the ABI capillary electrophoresis equipment to perform fragment analysis. The denatured plates can be stored frozen at -20°C for several days.
7. The electrophoretograms generated by the capillary electrophoresis equipment can be analyzed using the PeakScanner software to determine the peak sizes and intensities. Follow the PeakScanner manual for detailed procedures (*see* **Note 13**).
8. Export the peak size and area data from PeakScanner as comma or tab delimited text file.
9. Import the peak data in spreadsheet software (Microsoft Office Excel; Libre Office Calc) and calculate the relative exon inclusion levels.
10. The relative exon inclusion rate is calculated as the amount of the bands that contain the exon normalized to the total amount of DNA in all bands (*see* **Note 14**).

4. Notes

1. In the United States hydrophilic PVDF plates from Seahorse Biosciences (part # 200943-100) are sold by Phenix Research Products (catalog # MPF-011) and ISC Bioexpress (catalog # T-3180-7). We have not tested the performance of hydrophilic PVDF plates from other manufacturers in this protocol.
2. Dissolving LiCl in water is extremely exothermic reaction. Allow the solution to cool before adding the remaining components.
3. Taq polymerase and RNase H(-) MMLV reverse transcriptase can be obtained from a number of vendors. Enzyme costs can be substantially reduced by expressing and purifying recombinant enzymes in E.coli following published protocols (13; 14). We use 6xHis-tagged MMLV clone containing the following mutations: (i) D524N – to eliminate the RNase H activity ; (ii) Q84A – to improve processivity ; (iii) Δ1-23 - deletion of the first 23 amino acids to improve solubility (13; 15; 16).

4. ABI sequencer compatible plates can be obtained from a number of manufacturers.

5. For example, one 96-well plate will require 38.4 ml of RNA Lysis Buffer (19.2 ml at step #2 and another 19.2 ml at step #9). So, it is practical to make up 40 ml total to ensure extra for ease of pipetting from the liquid troughs. After adding 40 ml of the RNA Lysis Buffer to an RNase free conical tube, a total of 800µl of β-mercaptoethanol is added and thoroughly mixed.

6. High numbers of cells, for example plates that contain densely seeded HEK 293 cells, may not lyse efficiently in 200µl of lysis buffer and subsequently clog the filter plate. In such cases increase the volume of the lysis buffer to 300µl and apply only 100µl to the filter plate in step #6 of the RNA extraction protocol.

7. RNA concentrations are typically 30-50ng/µl (0.9-1.5ug total) for 90% confluent well of HEK293 cells (50,000 cells); 10-20ng/µl (250-500ng total) for 90% confluent fibroblasts or MDA-MB-231 cells. 260/280 ratio is typically 1.9 to 2.0.

8. The number of cycles depends on the copy number of the template and the number of cells in the starting material. We recommend determining it experimentally for each template. Moderately expressed transcripts are easily detectable at 25 to 30 cycles.

9. It is critical that all surfaces are clean and free of dust as dirt and dust particles are often highly fluorescent and will interfere with the fluorescent imaging.

10. Rainex is a suitable, less expensive alternative. It is sufficient to siliconize the plates once every six to twelve months depending on the frequency of use.

11. Because the amplicon/formamide mix that will be loaded into each well is clear it is easy to lose track of which well has which sample and it is very difficult to determine if a sample was loaded into a well. By numbering the wells one can keep track of the wells that have been loaded to prevent a well from being accidentally skipped or being loaded with two samples.

12. Both bromophenol blue and xylene cyanol FF are strongly fluorescent and may interfere with the signal if placed two close to the samples.

13. PeakScanner is available after registration as a free download from Life Technologies.

14. The electrophoretograms may contain bands arising from nonspecific amplification. The areas of these bands should not be included when calculating the relative exon inclusion levels.

15. The HEX label can also be detected on the G5 set although this is not supported by ABI.

References

1. Nilsen TW, Graveley BR. Expansion of the eukaryotic proteome by alternative splicing. Nature 2010 Jan;463(7280):457–463.
2. Wang ET, Sandberg R, Luo S, Khrebtukova I, Zhang L, Mayr C, Kingsmore SF, Schroth GP, BURGE CB. Alternative isoform regulation in human tissue transcriptomes. Nature 2008 Nov;456(7221):470–476.
3. Pan Q, Shai O, Lee LJ, Frey BJ, Blencowe BJ. Deep surveying of alternative splicing complexity in the human transcriptome by high-throughput sequencing. Nat Genet 2008 Nov;40(12):1413–1415.
4. Krawczak M, Thomas NST, Hundrieser B, Mort M, Wittig M, Hampe J, Cooper DN. Single base-pair substitutions in exon–intron junctions of human genes: nature, distribution, and consequences for mRNA splicing. Human Mutation 2007;28(2):150–158.
5. Sterne-Weiler T, Howard J, Mort M, Cooper DN, Sanford JR. Loss of exon identity is a common mechanism of human inherited disease. Genome Research 2011 Jul;21(10):1563–1571.
6. Levinson N, Hinman R, Patil A, Stephenson CRJ, Werner S, Woo GHC, Xiao J, Wipf P, Lynch KW. Use of transcriptional synergy to augment sensitivity of a splicing reporter assay. RNA 2006 May;12(5):925–930.
7. Younis I, Berg M, Kaida D, Dittmar K, Wang C, Dreyfuss G. Rapid-Response Splicing Reporter Screens Identify Differential Regulators of Constitutive and Alternative Splicing. Mol. Cell. Biol. 2010 Apr;30(7):1718–1728.
8. Stoilov P, Lin C-H, Damoiseaux R, Nikolic J, Black DL. A high-throughput screening strategy identifies cardiotonic steroids as alternative splicing modulators. Proc Natl Acad Sci U S A 2008 Aug;105(32):11218–23.
9. Newman EA, Muh SJ, Hovhannisyan RH, Warzecha CC, Jones RB, McKeehan WL, Carstens RP. Identification of RNA-binding proteins that regulate FGFR2 splicing through

the use of sensitive and specific dual color fluorescence minigene assays. RNA 2006 Jun;12(6):1129–41.

10. DeWoody JA, Schupp J, Kenefic L, Busch J, Murfitt L, Keim P. Universal method for producing ROX-labeled size standards suitable for automated genotyping. BioTechniques 2004 Sep;37(3):348, 350, 352.
11. El-Baradi TTAL, Raué HA, De Regt VCHF, Planta RJ. Stepwise dissociation of yeast 60S ribosomal subunits by LiCl and identification of L25 as a primary 26S rRNA binding protein. European Journal of Biochemistry 1984;144(2):393–400.
12. Bair RJ, Heath EM, Meehan H, Paulsen KE, Wages JM. Compositions and methods for using a solid support to purify RNA. 2004 Jan 29; US Patent number 7148343
13. Liu S, Goff SP, Gao G. Gln84 of moloney murine leukemia virus reverse transcriptase regulates the incorporation rates of ribonucleotides and deoxyribonucleotides. FEBS Letters 2006;580(5):1497–1501.
14. Lawyer FC, Stoffel S, Saiki RK, Chang SY, Landre PA, Abramson RD, Gelfand DH. High-level expression, purification, and enzymatic characterization of full-length Thermus aquaticus DNA polymerase and a truncated form deficient in 5’ to 3’ exonuclease activity. Genome Res. 1993 May;2(4):275–287.
15. Blain S, Goff S. Nuclease activities of Moloney murine leukemia virus reverse transcriptase. Mutants with altered substrate specificities. J. Biol. Chem. 1993 Nov;268(31):23585–23592.
16. Das D, Georgiadis MM. A directed approach to improving the solubility of Moloney murine leukemia virus reverse transcriptase. Protein Sci. 2001;10(10):1936–1941.

Tables.

Table 1. Typhoon phosphorimager excitation/emission combinations and ABI capillary electrophoresis filter sets for detecting commonly used fluorescent labels.

Label	**Typhoon Excitation laser**	**Typhoon Emission filter**	**ABI dye filter set**
FAM	480nm (Blue laser)	520nm band pass 40	A, D, F, G5, C, S
	532nm (Green laser)	526nm short pass	
HEX	532nm (Green laser)	555nm band pass 20	D (*see* **Note 15**)
ROX	532nm (Green laser)	610nm band pass 30	A,D,F
LIZ	633nm (Red laser)	670nm band pass 30	G5, S

Figures.

Figure 1. Agarose gel electrophoresis of RNA extracted from cells grown in 96 well plates. The first lane contains the size standard. The positions of the 18S and 26S ribosomal RNAs are indicated on the side.

Figure 2. Primer placement for detecting alternatively splicing events. Each panel shows a stylized gene structure (top) and the expected PCR products (bottom). The start indicates the label position in the primers and the PCR products. Primers are typically placed in the constitutive exons flanking the alternatively spliced regions (A and B). A combination of a shared forward primer and two reverse primers can be used to detect large cassettes (more than 700bp), mutually exclusive or alternative 3' exons (C and D).

Figure 3. Gel electrophoresis of alternatively spliced products imaged on typhoon phosphorimager. The PCR amplicons derived from three alternative isoforms are labeled by FAM (green bands indicated by arrows). The custom size standard (75nt-800nt) is labeled with ROX (red bands).

Figure 1

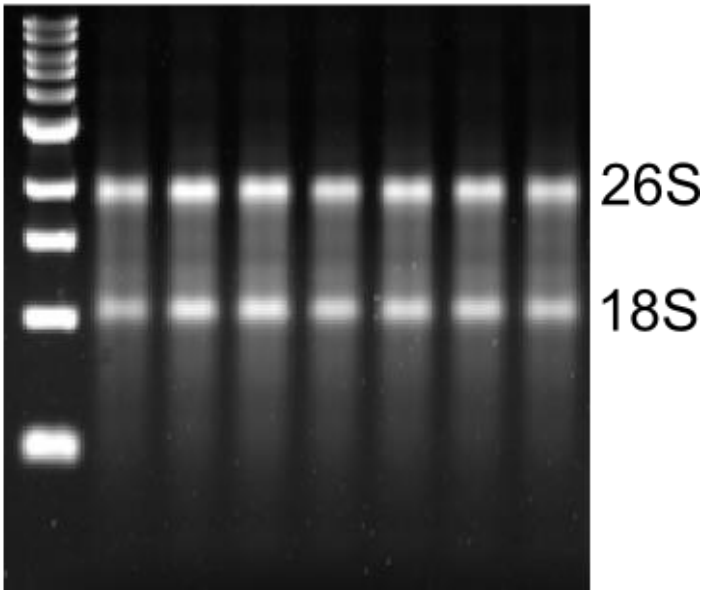

Figure 2

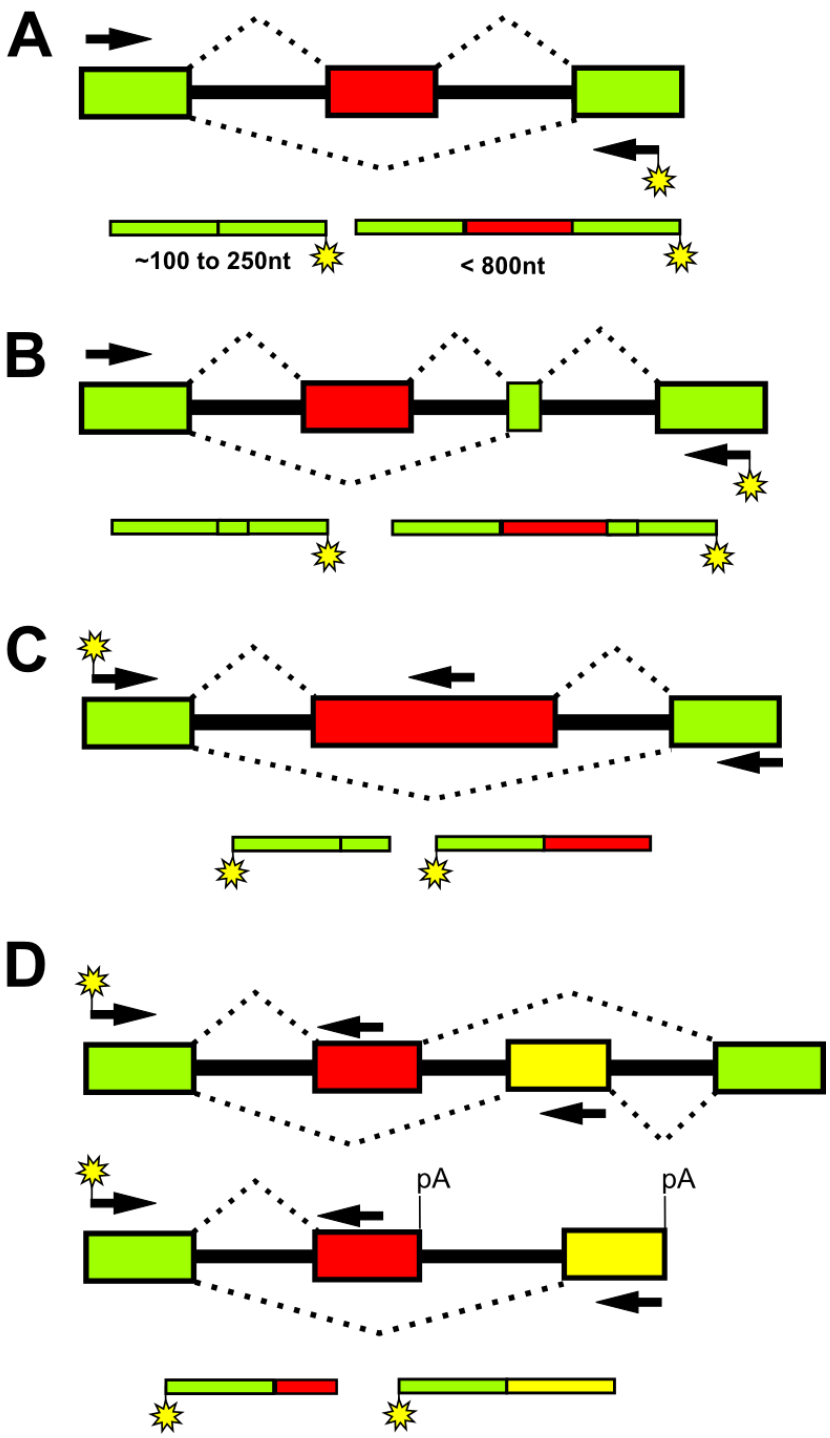

Figure 3

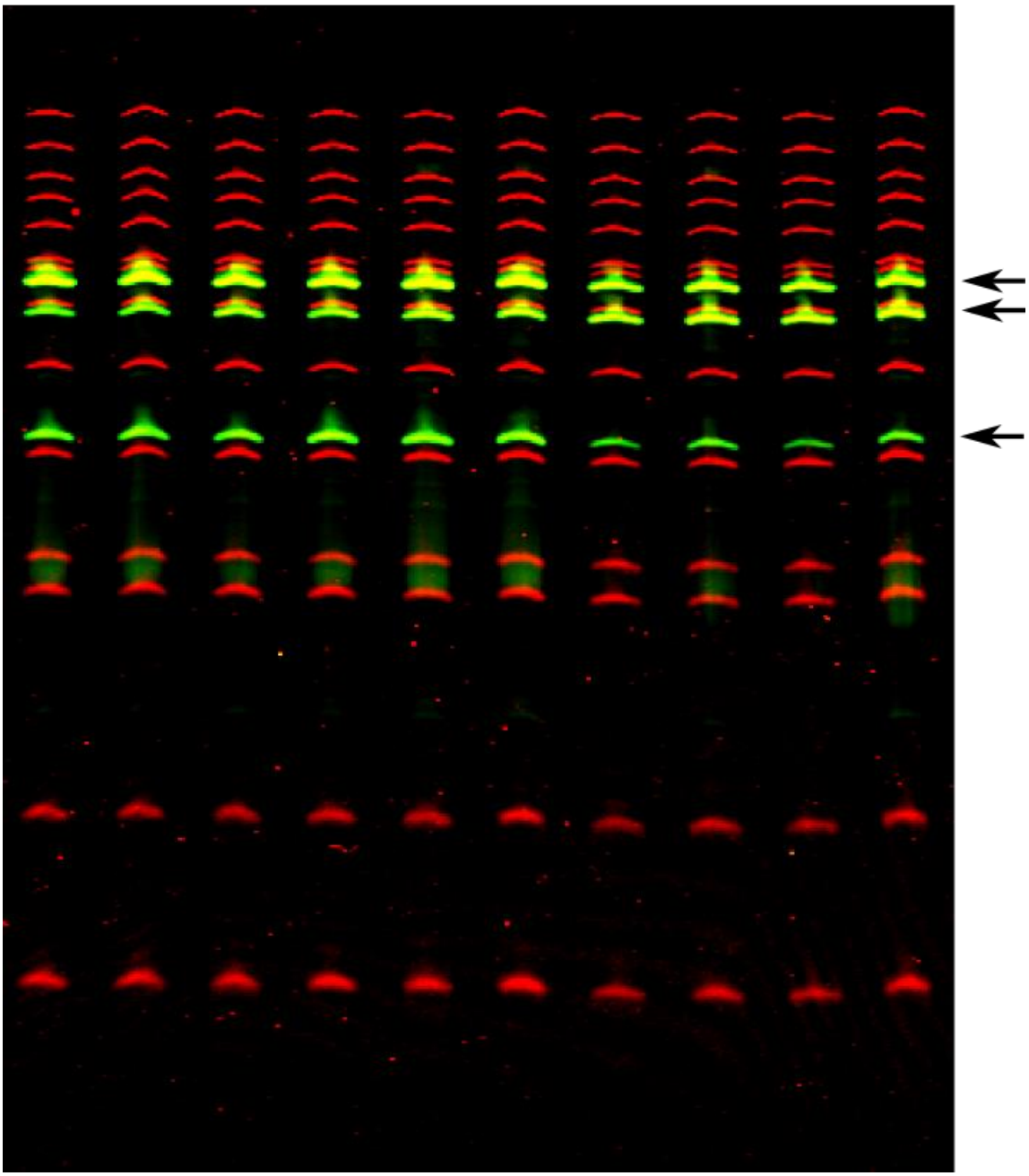

REPRINTED WITH PERMISSION FROM SPRINGER PUBLISHING.

Chapter 3: Book Chapter. Springer's Methods in Molecular Biology - RNA-Protein Complexes and Interactions: Methods and Protocols. In Press

Analysis of alternative splicing in the mouse retina using a fluorescent reporter.

Daniel Murphy, Saravanan Kolandaivelu, Visvanathan Ramamurthy, and Peter Stoilov

Author Contributions

DM: experimental design, data acquisition, data analysis and interpretation, drafting and revising the article.

SK: experimental design, data acquisition, data analysis and interpretation.

VR: conception, experimental design, data analysis and interpretation, revising the article.

PS: conception, experimental design, data acquisition, data analysis and interpretation, drafting and revising the article.

Springer's Methods in Molecular Biology - RNA-Protein Complexes and Interactions: Methods and Protocols.

Analysis of alternative splicing in the mouse retina using a fluorescent reporter.

Daniel Murphy, Saravanan Kolandaivelu, Visvanathan Ramamurthy, Peter Stoilov

Summary/Abstract

In vivo alternative splicing is controlled in a tissue and cell type specific manner. Often individual cellular components of complex tissues will express different splicing programs. Thus, when studying splicing in multicellular organisms it is critical to determine the exon inclusion levels in individual cells positioned in the context of their native tissue or organ. Here we describe how a fluorescent splicing reporter in combination with in vivo electroporation can be used to visualize alternative splicing in individual cells within mature tissues. In a test case we show how the splicing of a photoreceptor specific exon can be visualized within the mouse retina. The retina was chosen as an example of a complex tissue that is fragile and whose cells cannot be studied in culture. With minor modifications to the injection and electroporation procedure, the protocol we outline can be applied to other tissues and organs.

Key Words: *In vivo* reporter, alternative splicing, retina, photoreceptor

Introduction

Alternative splicing is a major mechanism for generating protein diversity in higher eukaryotes. Expression of tissue and cell type specific splicing isoforms is critical for the development and maintenance of differentiated cell types such as neurons, muscle, and epithelial cells. On aggregate each of these differentiated cell types expresses a distinct splicing program and set of splicing regulators. However, the gross picture painted by tissue wide analysis of splicing and expression masks the significant variability of specialized cellular

subtypes, particularly among neurons and epithelial cells. To understand the organization and functions of complex vertebrate tissues, gene expression and splicing need to be analyzed at the level of the individual cell within the context of the native tissue. Naturally, such studies face significant technical challenges in segregating the signals derived from individual cells. One approach to address these challenges is the use of fluorescent reporters which provide a convenient way to visualize gene expression and splicing at the individual cell level. The recent development of two-color fluorescent splicing reporters that produce either Green (GFP) or Red Fluorescent Protein (RFP) depending on the splicing of an alternative exon has provided an opportunity to study alternative splicing *in vivo*[1–6]. Transgenes expressing fluorescent splicing reporters have successfully been used to visualize FGFR2 splicing in mice and *let-2* splicing in C. elegans[3,6,7]. However, the relatively high cost and long time frames required for the establishment of mouse transgenes have limited the utility of the splicing reporters *in vivo*.

Here, we describe a protocol that uses electroporation to introduce splicing reporters into the retina of mice, followed by RT-PCR analysis and fluorescent microscopy imaging to investigate alternative splicing. The protocol is based on an *in vivo* subretinal injection and electroporation method [8]. The technique involves injection of the plasmid DNA into the space between the retinal pigmented epithelial (RPE) cell layer and retina followed by electroporation using tweezer-type electrodes. Electroporation facilitates the movement of plasmid DNA into the retinal precursor cells. This system is highly customizable, allowing for multiple DNA constructs driven by various promoters to be expressed in rod, bipolar, amacrine, and muller glial cells, with expression lasting upwards of 50 days[8]. It has also been adapted for gain of function and loss of function studies using plasmids and si-RNAs, and has been demonstrated in both neonatal and adult mice as well as other species[8,9]. The *in vivo* electroporation approach is remarkably tolerant to variations in the size of the DNA. We and others have reproducibly electroporated bacterial artificial chromosome (BAC) clones reaching 100Kbp in size[10,11].

In vivo electroporation of DNA constructs provides a rapid and cost-efficient alternative to the use of transgenic animals. The time frame of a typical experiment is dictated mainly by the developmental timeline of the mouse retina and typically lasts 20 to 30 days. A significant advantage over the use of transgenic animals is the ability to quickly analyze the splicing of a large number of minigenes. This approach has allowed us to carry out extensive mutagenesis experiments involving more than 20 different constructs that were tested in multiple replicates.

A key component of the protocol described here is a two-color fluorescent splicing reporter. The splicing reporter, which was described previously, expresses either GFP or RFP fluorescent protein depending on the splicing of an alternative exon[1]. The reporter is designed to accommodate virtually any alternative exon. The test exon is cloned in an intron that splits the AUG translation initiation codon of the GFP reading frame (Figure 1). When the exon is skipped from the mature RNA, the AUG codon of the GFP reading frame is joined together by splicing out the intervening sequences and GFP protein is expressed from the mature RNA. In this scenario the translation of the downstream RFP reading frame, which lacks an internal ribosome entry site, is suppressed. In the alternative scenario, the exon is spliced in, leading to disruption of the translation initiation codon of the GFP reading frame, and the downstream RFP reading frame is translated instead. This reporter design (pFlare A in Figure 1) accommodates exons that do not terminate on adenosine or carry a translation initiation codon with good match to the Kozak consensus. These types of exons are accommodated by a second backbone (pFlare G on Figure 1) in which the upstream exon no longer carries the adenosine of the GFP reading frame AUG codon. Under this design GFP will be expressed upon inclusion of the alternative exon. This can be achieved by either recreation of the AUG codon of the GFP reading frame by exons terminating on adenosine or by initiation of GFP translation from AUG codon encoded by the exon. In the latter case care must be taken to ensure that GFP is in frame with the AUG codon carried by the exon.

While the focus of this protocol is on studying splicing in the retina, the combination of *in vivo* electroporation and fluorescent reporters can be applied with some modifications to other tissues and organs. Reliable electroporation protocols have been established for introducing DNA in brain, lung, liver, muscle, heart, skin, and testis[12–19].

Materials

1. Laboratory animal and regulatory approval.
    1.1. Pregnant (untimed pregnancy) mice such as CD-1 IGS (Charles River). (see **note 1**)
    1.2. All procedures that are carried out on mice must be approved by the institutional regulatory bodies that oversee the use and human treatment of laboratory animals.
2. Tools and equipment.
    2.1. Surgery and dissection.
        2.1.1. Microscope for performing surgery and dissections, such as Zeiss Stemi DV4.
        2.1.2. Hamilton blunt end syringe, 33G or 32G. (7634-01).
        2.1.3. Water heated warming blanket such as HTP-1500, Adroit Medical.
        2.1.4. Square Wave Electroporation System, Nepagene CUY21, or BTX ECM 830.
        2.1.5. Tweezer-type electrodes- BTX model 520, 7mm diameter.
        2.1.6. Two pairs of tweezers, and scissors for dissection of retina prior to both RNA isolation and sectioning and imaging
        2.1.7. Chamber for euthanization by asphyxiation from CO_2.
        2.1.8. CO_2 tank and regulator.
    2.2. Microscopy
        2.2.1. Cryostat such as Leica cm 1850.
        2.2.2. Zeiss LSM 510 laser scanning confocal microscope or equivalent.
    2.3. RNA isolation, cDNA synthesis, PCR amplification, and gel electrophoresis

2.3.1. Handheld homogenizer such as (VWR 47747-370) with RNAse free pestles (VWR 47747-358).

2.3.2. Tabletop microcentrifuge such as Sorvall Legend Micro 17 (Thermo 75002430).

2.3.3. Nanodrop spectrophotometer (Thermo).

2.3.4. Thermocycler.

2.3.5. Vertical gel electrophoresis apparatus (Labrepco model v16 or equivalent).

2.3.6. High voltage power supply capable of producing 500V DC, such as Bio-Rad Power Pac 3000.

2.3.7. 18G disposable needle.

2.3.8. 50ml syringe.

2.3.9. Laser scanning capable of imaging two fluorescence channels, such as Typhoon 9410 Phosphorimager (GE).

3. Reagents and consumables.

3.1. Subretinal injection.

3.1.1. DNA at approximately 2-6µg/µl diluted in PBS with 0.1% fluorescein sodium.

3.1.2. Ice.

3.1.3. Sterile Single use needle 22G1 for dissection (Becton Dickinson 305159).

3.1.4. Phosphate Buffered Saline (PBS).

3.1.5. Absolute, Anhydrous ACS/USP grade Ethanol (Pharmaco-AAPER, 111ACS200).

3.1.6. Cotton swabs.

3.1.7. 1:40 dilution (0.05% final concentration) of Nolvasan (2% Chlorhexidine (1,1'-Hexamethylenebis [5-(p-chlorophenyl) biguanide]) diacetate, Zoetis) in water.

3.2. RNA Isolation, cDNA synthesis, PCR amplification, and gel electrophoresis

3.2.1. Sterile Polystyrene Petri Dish (VWR 470175-016).

3.2.2. Filter paper (Fisher 22-279539).

3.2.3. Ultrapure water.

3.2.4. Dry Ice.

3.2.5. TRIzol reagent (Sigma T9424-200ML).

3.2.6. Chloroform, ACS Spectrophotometric grade (Sigma 154733).

3.2.7. Isopropanol HPLC Grade (Sigma Aldrich 650447).

3.2.8. Absolute, Anhydrous ACS/USP grade Ethanol (Pharmaco-AAPER, 111ACS200).

3.2.9. 1.5ml microcentrifuge tubes. (World Wide Medical Products 41021009).

3.2.10. DNAse 1 RNAse Free enzyme and 10x DNAse 1 Buffer (Roche 04716728001).

3.2.11. 3 Molar Sodium acetate solution, pH 5.2.

3.2.12. PCR tube strips and caps (8 or 12-tube) (VWR 20170-004 or 53509-306).

3.2.13. 10mM dNTP mix (dATP, dCTP. dGTP and dTTP at 10mM concentration each). (Denville Scientific CB4420-4).

3.2.14. Reverse transcription primer mix: 10uM anchored oligo dT ($dT_{24}VN$) and 50uM random hexamers.

3.2.15. 10x Reverse Transcriptase Buffer: 500mM Tris-HCL (pH 8.3), 750mM KCL, 30mM $MgCl_2$.

3.2.16. RNAse H (-) Reverse Transcriptase.

3.2.17. Primers combined at 10uM final concentration each:

pFlare-BGL-F: aaacagatctaccattggtgc

EGFP-N carrying 5' end 6-FAM label: [6-FAM] cgtcgccgtccagctcgacca

3.2.18. 10x Taq buffer: 500mM KCL, 100mM Tris-HCl, (pH 9.0), 15mM $MgCl_2$, and 1% Triton X-100.

3.2.19. Taq polymerase at 15U/µl.

3.2.20. Sigmacote (Sigma Aldrich) or equivalent siliconizing reagent.

3.2.21. 10% Ammonium Persulfate (APS) solution in water.

3.2.22. Tetramethylenediamine (TEMED).

3.2.23. 1x Tris-Borate EDTA Buffer (TBE): 89mM Tris, 89mM Boric Acid, 2mM EDTA. This buffer can be made as a 5x stock solution and diluted before use.

3.2.24. Acrylamide gel solution: 4% Acrylamide/Bis-acrylamide (19:1 crosslink ratio), 1x TBE, 7.5M Urea. Filter through .45µM filter and store in a dark bottle at 4˚C.

3.2.25. Clear formamide loading buffer: Deionized formamide, 2mM EDTA.

3.2.26. Formamide loading buffer with tracking dyes: Deionized formamide, 2mM EDTA, 0.25% (w/v) bromophenol blue and 0.25% (w/v) xylene cyanol FF.

3.2.27. Fluorescently labeled size standards: Life technologies/ABI GeneScan 1000 Rox or GeneScan 1200 Liz. Alternatively custom size standards can be prepared by a simple PCR amplification with Rox-labelled primer [20].

3.3. Tissue sectioning and fluorescent microscopy.

3.3.1. Sterile Polystyrene Petri Dish (VWR 470175-016).

3.3.2. 24 well polystyrene tissue culture plate (VWR 662 0160).

3.3.3. Filter paper (Fisher 22-279539**).**

3.3.4. Phosphate-buffered Saline (PBS).

3.3.5. 4% paraformaldehyde (PFA) in PBS.

3.3.6. 20% sucrose (Jt Baker 4097) solution in PBS.

3.3.7. Hanks Balanced Salt Solution (HBSS) (Fisher, cat no SH30268.01).

3.3.8. Sterile Single use needle 22G1 for dissection (Becton Dickinson 305159).

3.3.9. Dry ice.

3.3.10. Optimal Cutting Temperature Compound (O.C.T.) Tissue Tek (Ref 4583).

3.3.11. Cryomolds Tissue Tek (ref 4565).

3.3.12. Fisher SuperFrost Plus slides (cat no 12-550-15).

3.3.13. ProLong-Gold Antifade reagent with DAPI (life technologies P36935).

3.3.14. Cover slips.

3.3.15. Clear nail polish.

Methods

Generation of reporter construct

The procedures for cloning the exon to be tested for inclusion can be found elsewhere[21]. The cassette exon cloned into the reporter construct should contain part of flanking native introns to ensure that all elements necessary for the regulation of its splicing are present. Typically, intronic regulator elements will be located within 100nt from the exon borders. The sequence conservation of the flanking introns should serve as a guide in the identification of such cis-acting sequences[22]. We recommend incorporating 200 to 300 nucleotides of each flanking intron. If the sequence conservation extends beyond this range, larger portions of the introns will need to be incorporated into the minigene to ensure that all regulatory sequences are present. It is important to confirm that the regulation of the alternative exon in the minigene construct mirrors the regulation of the exon in the native gene. This can be achieved by transfecting the minigene in cell lines that differentially splice the exon of the native gene and using RT-PCR to confirm that the splicing of the minigene is regulated similarly to the native transcript. It is possible that suitable cell lines may not exist for some cell type specific exons (the *Bbs8* exon 2A example used in this protocol is one such exon). Should this be the case, testing the minigenes will have to be carried out directly in animal tissue and suitable controls will need to be considered to ensure that negative results are not due to failure to incorporate the required regulatory sequences into the minigene. The nature of these controls is beyond the scope of this protocol as it strongly depends on the exon and tissue being studied. (see **note 2**)

1. Subretinal Injection and electroporation.

This technique requires a minor surgery to open the eye in a neonatal pup followed by an incision in the sclera. A blunt end syringe is then used to deliver the DNA through the incision created in the sclera. The use of a blunt end needle is necessary to prevent piercing through the back of the eye. The depth at which the DNA needs to be injected is determined by the slight increase in resistance which is felt when the blunt end needle reaches the end of scleral wall. Following injection in the subretinal space, electroporation is used to introduce the DNA into the retinal precursor cells. The steps in the procedure will require some practice, patience, and a steady hand in order to deliver the DNA at the correct site. We typically see the expression of the minigene constructs in 60 to 70% of the injections. The entire process (excluding time for anesthetization) should take less than 3-5 minutes per pup, cause little if any bleeding, and result in a 100% survival rate.

1.1. Prepare purified DNA according to plasmid purification kit. For large DNA constructs such as Bacterial Artificial Chromosomes (BACs), we recommend using CsCl gradient to purify the DNA.
1.2. Resuspend DNA at 2-6µg/µl in PBS.
1.3. Monitor untimed pregnant moms daily to check for delivery of pups.
1.4. To 15-20µl of DNA in PBS, add 1/10 volume of 1% fluorescein sodium.
1.5. Remove newborn pups from cage and anesthetize individually on ice for several minutes. To avoid frostbite from direct contact with ice, place each mouse in a latex sleeve made from the finger of an examination glove (See Figure 2 A). Mice are fully anesthetized when they no longer respond to a toe pinch.
1.6. Clean the eyelid with ethanol using a cotton swab.
1.7. Repeat the cleaning with a 1:40 solution of Nolvasan.
1.8. Under the microscope using a 32-guage needle, carefully make an incision along the future edge of the eyelid (Figure 2 B and C).

1.9. Expose the eye by spreading the eyelids.

1.10. Make a pinpoint incision through the sclera using the tip of the needle (Figure 2 C and D).

1.11. Insert a blunt end syringe containing 0.5µl of the DNA and dye solution into the incision, carefully maneuver the syringe around the lens toward the back of the eye until the retinal pigmented epithelium (RPE), is reached, you should feel some resistance (Figure 2 E).

1.12. Slowly inject the DNA into the subretinal space. The dye should be visible as it spreads across a small area of the retina (Figure 2 E).

1.13. Dip tweezer-type electrodes in PBS and apply them to the head of the pup with light pressure. The positive electrode is indicated by the screw, and should be oriented on the same side as the injection (Figure 2F).

1.14. Apply five pulses of 80 volts at 50 millisecond durations with 950 millisecond duration between pulses.

1.15. Place pups on a warming blanket (HTP-1500, Adroit Medical) for recovery before returning them to their mother.

2. Dissection of the retina for RNA Isolation.

At postnatal day 16 (P16), the photoreceptors should be fully developed (although the outer segments may not be fully elongated) and retinae can be harvested for RNA isolation. The following protocol outlines the dissection of the eye in order to isolate the retina. All procedures should be carried out in an RNAse-free environment. (see **note 3**)

2.1. Euthanize animals according to IACUC approved protocol.

2.2. To remove injected eye spread eyelids with thumb and forefinger. With the other hand, apply tweezers over and around the eyeball to pop it out of the eye socket. Grasp the optic nerve and enucleate the eye (Figure 3 A). (see **note 4**)

2.3. Place eye on a small square of filter paper dampened with HBSS, under microscope (Figure 3 A).

2.4. Using a needle, puncture the eye at the border of the cornea and sclera. This will release pressure and allow for further dissection (Figure 3 B).

2.5. Using the needle incision as a starting point, cut out the cornea with scissors (Figure 3 C).

2.6. Carefully pull the lens out with tweezers. Before and after images shown on Figures 3 D and E.

2.7. Place eye in 1 drop of RNAse-free water or HBSS on a plastic petri dish

2.8. Using two tweezers, separate the retina from the sclera as shown on Figure 3F-H:

2.8.1. With one tweezers, grip the sclera near the optic nerve. With the second, lightly clamp down on the back of the eye near optic nerve (Figure 3 G).

2.8.2. Gently push the second pair of tweezers away from the optic nerve into the drop of water or HBSS. The retina (clear) will separate from the sclera (Figure 3 H).

2.9. Place retina into a 1.5ml centrifuge tube containing 200µl TRIzol. Freeze on dry ice while collecting other samples.

2.10. To serve as a negative control, collect the retina of the other, uninjected eye as described above and add to separate TRIzol containing tube.

3. RNA isolation and DNAse treatment.

3.1. Homogenize each retina by pulsing 10-15 times for 1-2 seconds with handheld homogenizer.

3.2. Add additional 200µl of TRIzol to each tube containing homogenized retina and mix by vortexing.

3.3. Add 1/10 volume of Chloroform to each sample.

3.4. Vortex well.

3.5. Spin samples at 15000xG for 10minutes.

3.6. Transfer the aqueous (top) phase, which should be approximately 200-250µl to a new tube. (see **note 5**)

3.7. Add 1.5 volumes of isopropanol to each sample and mix by vortexing.

3.8. Incubate at room temperature for 15 minutes.

3.9. Spin each sample at 15000xG for 10-15 minutes to precipitate RNA.

3.10. Carefully remove the supernatant.

3.11. Add 0.5ml of 75% ethanol.

3.12. Centrifuge at 15000xG for 5 minutes.

3.13. Remove ethanol and briefly air-dry pellets.

3.14. Resuspend each pellet in 100µl of ultrapure water.

3.15. Make a 2x concentrated master mix containing 20µl of 10x DNAse1 Buffer, 79µl of water, and 1µl DNAse 1 per tube.

3.16. Add 100µl of the master mix to each sample.

3.17. Mix samples and incubate at 37˚C for 20 minutes.

3.18. Add 200µl of chloroform and vortex well.

3.19. Centrifuge at 15000xG for 10 minutes.

3.20. Transfer the aqueous (top) phase to a new tube. Take care not to carry over the interphase, containing the denatured proteins.

3.21. Add 1/10 volume, or 20µl of 3M sodium acetate ph5.2.

3.22. Add 3 volumes or 600µl ice-cold ethanol and mix well.

3.23. Incubate each sample at -20˚C for at least 30 minutes.

3.24. Resuspend RNA in 25µl of ultrapure water.

3.25. Determine the RNA concentration on a Nanodrop spectrophotometer (Thermo Fisher). The typical yield is approximately 1ug of RNA per retina.

4. cDNA synthesis

4.1. Prepare a 2x Reverse transcription master mix (2µl of 10xRT buffer; 1µl of 10mM dNTPs; 0.5µl Oligo dT/random hexamer primer mix; 6µl water, and 0.5µl reverse transcriptase per reaction)

4.2. Dispense 10µl of master mix into each tube of a PCR tube strip.

4.3. Add 10µl of RNA solution containing up to 1ug of RNA to each reaction and mix by pipetting. 100ng of RNA are typically sufficient to reliably quantify the splicing of the minigene.

4.4. Cap the strip and incubate in a thermal cycler under the following conditions: 25˚C for 5 minutes; 43˚C for 40 min; 75˚C for 15 min; hold at 10˚C until the strip is removed.

5. PCR

5.1. Prepare a master mix (2µl of 10x Taq PCR buffer; 0.4µl of 10mM dNTPs, 2µl of 10µM primer mix, 0.2 µl of Taq DNA polymerase per reaction)

5.2. Dispense 19.5 µl to each tube of a PCR tube strip.

5.3. Transfer 0.5µl of cDNA to each reaction.

5.4. Mix by pipette and cap the strip. Make sure there are no air bubbles at the bottom of each tube.

5.5. Amplify the templates using the following conditions. Initial denaturation step at 94˚C for 4 minutes, followed by 20-30 cycles of 94˚C for 30 seconds, 62˚C for 30 seconds, and 72˚C for 30-60 seconds, followed by a final extension at 72 for 5 minutes. Then hold the reactions at 10˚C until ready to remove.

6. Electrophoresis and imaging

The electrophoresis protocol described here uses denaturing urea/polyacrylamide gels to resolve the PCR products. The gels are then imaged on a fluorescent imager without being disassembled.

6.1. Clean slides of each glass plate with ethanol and dry with paper towels

6.2. If the plates have not been siliconized before, apply Sigmacote to the cleaned plates and spread it with a paper towel until dry. Clean the plates with ethanol again as in step 6.1.

6.3. Place spacers on the clean side of the larger of the two glass plates- place the two side spacers with the foam dam toward the top, and the bottom spacer across the bottom edge. Place the smaller of the two glass, clean side facing down, on top of the larger glass plate to create a plate-spacer-plate sandwich.

6.4. Clip the sandwich together with binder clips and set aside.

6.5. Repeat for as many gels as needed

6.6. In a clean flask mix acrylamide solution (25ml per gel) with 1/100 volume of 10% APS (250µl per gel) and 1/1,000 volume TEMED (25µl per gel) and pour the gels.

6.7. Holding the plate sandwich at approximately 15-20 degrees from horizontal, pour the gel solution in a steady stream along one of the side spacers allowing it to flow smoothly between the two glass plates while ensuring that no air bubbles are formed. Once filled to the top, place the gel horizontally to insert the comb. Leave the gel in this position until the gel polymerizes (approximately 20-30 minutes).

6.8. After the gel has solidified, remove the clips and the bottom spacer, as well as the well comb.

6.9. Place the sandwich onto the running apparatus with the larger glass plate facing out. Use two clips on each side of the gel to clip the sandwich to the gel.

6.10. Fill the upper and lower reservoirs with 1x TBE buffer ensuring that the gel is covered. Flush with TBE any air that was trapped at the bottom of the gel.

6.11. Immediately rinse the wells using an 18G needle on a 50ml syringe filled with 1x TBE.

6.12. Apply a piece of clear adhesive tape such as Scotch tape, to the outside glass plate directly over the wells. Use a sharpie pen to label on the tape each well with a number that corresponds to the sample that will be loaded in the well. It is critical to label the

wells as the loading buffer contains no running dye and it is impossible to determine which lanes have been loaded.

6.13. Attach the cover of the gel apparatus and pre-run the gel for 30-50 minutes at 400 V. While the gel is running, prepare the PCR amplicons for loading as described in steps 14-16 below.

6.14. Prepare a loading buffer mix containing 10µl of clear formamide loading buffer and 0.3µl fluorescent size standard for each sample loaded onto the gel.

6.15. Dispense 10µl of loading buffer mix to each tube on a PCR tube strip, according to the number of samples being analyzed.

6.16. Transfer 1µl of the PCR amplicon to each of the tubes containing the loading buffer mix.

6.17. Seal the tubes and incubate in a thermal cycler at 95˚C for 5 minutes to denature the samples. Place the tubes on ice.

6.18. Turn off the gel power supply. Remove the urea that has accumulated in the wells by rinsing them again as described in step 11. Failing to remove the urea will result in distorted bands.

6.19. Load 10µl of the denatured samples in each well.

6.20. Run the gel at 400V for 55 min then turn off the power supply.

6.21. Remove the gel sandwich from the apparatus.

6.22. Remove the side spacers, but do not disassemble the gel sandwich.

6.23. Clean the plates with deionized water to remove any acrylamide or urea attached to the outside of the plates.

6.24. Dry the plates with a paper towel.

6.25. Clean the surface of the phosphorimager with a moist paper towel and dry it.

6.26. Place the gel sandwiches on the phosphorimager glass plate.

6.27. Select the scan area in the typhoon software and close the lid.

6.28. Select the appropriate combination of excitation lasers and bandpass emission filters depending on the labels present in the samples and the size standards. For FAM-labeled primers, we recommend blue laser (480nm) excitation and 520nm bandpass emission filter.

6.29. Set the focal plane to +3 mm to adjust the focal point above the surface of the phosphorimager, to account for the width of the glass plate and gel.

6.30. Choose the appropriate orientation for your output image.

6.31. Scan the gel. While scanning make sure that there are no saturated pixels, indicated by red dots on the preview window. If there are saturated pixels, rescan the gel after lowering the photomultiplier (PMT) voltage for the appropriate channel. (See Figure 4 for example results).

7. Dissection of the retina for tissue sectioning

To ensure that photoreceptor maturation is complete, we allow 20 days post-injection before the injected eyes are taken for tissue sectioning. The procedure outlined here is very similar to the retinal dissection for RNA isolation described above and shown in Figure 3 A-E. Here, however, maintaining retinal morphology throughout the process is vital for obtaining unblemished tissue sections. Excessive pressure or shearing forces on the eye can cause the retina to detach or tear, making interpretation of results difficult. While some retinal detachment and malformation can be expected from the injection process, most of the tissue expressing the reporter should still display normal morphology.

7.1. In a petri dish, soak a piece of filter paper in HBSS.

7.2. Carefully enucleate the injected eye, and place it on the filter paper. This may require removal of fascia surrounding eye. Retinal detachment may occur if excess pressure is exerted on the eye.

7.3. Puncture with a 33 gauge needle at the border of the cornea and sclera. Figure 3 B.

7.4. Place the eye in a well of a 24 well plate containing 500µl of 4% PFA in PBS. Incubate 5-10 minutes at room temperature (RT).

7.5. Place the eye back under the microscope and remove the cornea and lens to prepare eye cup (Figure 3 C). Alternatively, the lens can be removed at the end of step 7.9.

7.6. Place the eye cup into the well containing 4% PFA. Incubate for 30-60 minutes at RT for fixation.

7.7. Wash the eye cup three times for 5 minutes each with PBS at RT.

7.8. Remove PBS and immerse the eye cup in 20% sucrose in PBS solution and incubate with shaking overnight at 4˚C.

7.9. Replace the 20% Sucrose solution with a 1:1 mixture of O.C.T. compound and 20% sucrose in PBS. Incubate with shaking for 1 hour.

7.10. Prepare an ethanol/dry ice bath in a container with wide opening.

7.11. Fill a labeled cryomold container with O.C.T compound. Rather than writing on the plastic itself, label a piece of tape and attach it to the lip of the cryomold to prevent the ethanol from washing off marker.

7.12. Remove the eye and blot off excess O.C.T./Sucrose in PBS. Place the eye in the cryomold containing O.C.T.

7.13. Orient the eye such that the opening (where cornea and lens were removed) is facing to the right. (see **note 6**)

7.14. Snap freeze the eye in O.C.T by submerging the well of the cryomold in ethanol/dry ice bath.

7.15. Store the eye at -80°C. Eyes can be stored at -80°C for more than a year.

8. Sectioning and staining

Once the dissected eye is properly fixed and frozen in a block of O.C.T compound it can be cut into 16µm thick sections using a cryostat. Cryostat operation will require training which is beyond the scope of this protocol. Properly oriented, the sectioned retina should

resemble a “C” with the opening formed from the removal of the cornea and lens. As many “C” sections as is practical for mounting can be arranged on each slide. For mounting, we use a reagent containing DAPI to stain the nuclei. The RFP and GFP expression from the minigene are visible without any further staining (Figure 4). If necessary, immunofluorescence staining following standard protocols can be used to visualize cell type specific markers or other proteins of interest. We recommend using secondary antibodies labeled with Cy5 or equivalent infrared fluorescent dye, to prevent overlap with the fluorescence of the GFP and RFP proteins.

8.1. Using a cryostat, cut sections at 16um.

8.2. Arrange 5-10 tissue sections on the stage of the cryostat.

8.3. Quickly but carefully apply the slide (treated side facing down) to the sections. The tissue sections will adhere to the slide. The slide should be at room temperature. This process should be done quickly to ensure that the slide will not cool, which can inhibit proper attachment of sections. Do not press the slide firmly onto the stage.

8.4. Air-dry sections on each slide for 30 minutes and mount or store at -20˚C. Slides can be stored for several months.

8.5. To room temperature slides add a drop of ProLong Gold with DAPI. To avoid bubbles, use a cut pipette tip to apply the Pro-Gold to the retinal sections. Very little is needed as the solution will spread once cover slip is applied.

8.6. Carefully apply the cover slip and ensure each retina is coated with Pro-Gold.

8.7. Air-dry for 30 minutes.

8.8. Seal the cover and slide edge with clear nail polish and store at 4˚C.

8.9. Image the slides on a confocal microscope.

Notes

1. Many mouse strains carry mutations causing retinal degeneration, such as rd1 and rd8. In some cases the same mouse strain may or may not carry retinal degeneration mutations depending on the commercial source. It is critical to ensure that the experimental animals do not carry rd alleles.

2. The nature of these controls is beyond the scope of this protocol as it strongly depends on the exon and tissue being studied.

3. Preventing RNase contamination:

- Maintain clean bench surfaces.
- If necessary RNase contamination on equipment and bench surfaces can be inactivated by treating with RNaseZap reagent (Life Technologies).
- Always wear gloves.
- Use ultrapure or DEPC treated water to prepare reagents.
- Where applicable autoclave or filter sterilize the reagents.
- Use RNase- and DNase-free plasticware. If possible use aerosol resistant tips.

4. Keeping the optic nerve intact provides a convenient method for handling the eye throughout the procedure with minimal risk for causing damage.
5. Adding 1 µl GlycoBlue™ Coprecipitant to the supernatant (optional) helps to visualize the RNA pellet after the precipitation steps.
6. Ensure that there are no air bubbles inside or surrounding the eye cup. Trapped air can make it impossible to obtain intact sections.

Acknowledgements and Funding.

We thank Zachary Wright and Abigail Hayes for advice and assistance in taking pictures. This work was supported by grants from the National Institutes of Health (EY017035), West Virginia Lions, Lions Club International Fund and an internal grant from West Virginia University. Imaging experiments were performed in the West Virginia University Microscope Imaging Facility, which has been supported by the Mary Babb Randolph Cancer Center and NIH grants P20 RR016440, P30 GM103488 and P20 GM103434.

References

1. Stoilov, P., Lin, C.-H., Damoiseaux, R., Nikolic, J. & Black, D. L. A high-throughput screening strategy identifies cardiotonic steroids as alternative splicing modulators. *Proc. Natl. Acad. Sci.* **105,** 11218–11223 (2008).
2. Orengo, J. P., Bundman, D. & Cooper, T. A. A bichromatic fluorescent reporter for cell-based screens of alternative splicing. *Nucleic Acids Res.* **34,** e148 (2006).
3. Kuroyanagi, H., Ohno, G., Sakane, H., Maruoka, H. & Hagiwara, M. Visualization and genetic analysis of alternative splicing regulation in vivo using fluorescence reporters in transgenic Caenorhabditis elegans. *Nat. Protoc.* **5,** 1495–1517 (2010).
4. Somarelli, J. A. *et al.* Fluorescence-based alternative splicing reporters for the study of epithelial plasticity in vivo. *RNA N. Y. N* **19,** 116–127 (2013).
5. Newman, E. A. *et al.* Identification of RNA-binding proteins that regulate FGFR2 splicing through the use of sensitive and specific dual color fluorescence minigene assays. *RNA* **12,** 1129–1141 (2006).
6. Takeuchi, A., Hosokawa, M., Nojima, T. & Hagiwara, M. Splicing reporter mice revealed the evolutionally conserved switching mechanism of tissue-specific alternative exon selection. *PloS One* **5,** e10946 (2010).
7. Ohno, G., Hagiwara, M. & Kuroyanagi, H. STAR family RNA-binding protein ASD-2 regulates developmental switching of mutually exclusive alternative splicing in vivo. *Genes Dev.* **22,** 360–374 (2008).
8. Matsuda, T. & Cepko, C. L. Electroporation and RNA interference in the rodent retina in vivo and in vitro. *Proc. Natl. Acad. Sci.* **101,** 16–22 (2004).
9. Nickerson, J. M. *et al.* Subretinal delivery and electroporation in pigmented and nonpigmented adult mouse eyes. *Methods Mol. Biol. Clifton NJ* **884,** 53–69 (2012).

10. Magin-Lachmann, C. *et al.* In vitro and in vivo delivery of intact BAC DNA – comparison of different methods. *J. Gene Med.* **6,** 195–209 (2004).
11. Barnabé-Heider, F. *et al.* Genetic manipulation of adult mouse neurogenic niches by in vivo electroporation. *Nat. Methods* **5,** 189–196 (2008).
12. Young, J. L. & Dean, D. A. in *Advances in Genetics* (ed. Leaf Huang, D. L. and E. W.) **89,** 49–88 (Academic Press, 2015).
13. Heller, R., Cruz, Y., Heller, L. C., Gilbert, R. A. & Jaroszeski, M. J. Electrically Mediated Delivery of Plasmid DNA to the Skin, Using a Multielectrode Array. *Hum. Gene Ther.* **21,** 357–362 (2010).
14. Young, J. L., Barravecchia, M. S. & Dean, D. A. Electroporation-mediated gene delivery to the lungs. *Methods Mol. Biol. Clifton NJ* **1121,** 189–204 (2014).
15. Aihara, H. & Miyazaki, J. Gene transfer into muscle by electroporation in vivo. *Nat. Biotechnol.* **16,** 867–870 (1998).
16. Tevaearai, H. T., Gazdhar, A., Giraud, M.-N. & Flück, M. In vivo electroporation-mediated gene delivery to the beating heart. *Methods Mol. Biol. Clifton NJ* **1121,** 223–229 (2014).
17. De Vry, J. *et al.* In vivo electroporation of the central nervous system: A non-viral approach for targeted gene delivery. *Prog. Neurobiol.* **92,** 227–244 (2010).
18. Heller, R. *et al.* In vivo gene electroinjection and expression in rat liver. *FEBS Lett.* **389,** 225–228 (1996).
19. Michaelis, M., Sobczak, A. & Weitzel, J. M. In vivo microinjection and electroporation of mouse testis. *J. Vis. Exp. JoVE* (2014). doi:10.3791/51802
20. DeWoody, J. A. *et al.* Universal method for producing ROX-labeled size standards suitable for automated genotyping. *BioTechniques* **37,** 348, 350, 352 (2004).
21. Green, M. R. & Sambrook, J. *Molecular Cloning: A Laboratory Manual (Fourth Edition): Three-volume set*. (Cold Spring Harbor Laboratory Press, 2012).

22. Cooper, T. A. Use of minigene systems to dissect alternative splicing elements. *Methods San Diego Calif* **37,** 331–340 (2005).

Figure legends

Figure 1. Two-color fluorescent splicing reporter. Diagram of pFlare splicing reporters. The alternative exon being tested is shown in blue, constitutive 5' and 3' exons of the backbone are shown in cyan and green/red, respectively. The upper panel shows the pFlare A backbone, which accommodates exons ending in C, T or G. The lower panel depicts the pFlare G backbone for use with exons ending in adenosine. In each panel, transcripts resulting from alternative splicing and the subsequent fluorescent protein expression are shown below. For pFlare A, exon inclusion abolishes the AUG start codon for GFP, resulting in RFP expression, whereas exon skipping reforms the AUG, allowing for GFP expression. Conversely, in pFlare G, exon inclusion establishes the AUG start codon for GFP translation, while exon skipping prevents GFP expression and results in expression of a downstream RFP.

Figure 2. Subretinal injection and electroporation at postnatal day 0. A. Image of neonatal mouse pup in examination glove sleeve. **B.** Image of neonatal mouse pup, using thumb and forefinger to gently spread the skin around the eye. The outline of the eye and the future edge of the eyelid are shown by dotted lines. The approximate location of the scleral incision is denoted by a round dot. **C.** Cartoon of an aerial view of neonatal mouse eye showing position of future edge of the eyelid and needle used for incision. Skin is shown in beige, future edge of the eyelid, lens, sclera (black), RPE (grey), subretinal space, and retinal precursor cells (orange) are denoted by arrows. **D.** Cartoon showing the location of pinpoint incision through the sclera. **E.** Cartoon showing the DNA injection using blunt end needle. The injected DNA is shown in green. **F.** Cartoon showing direction of current in electroporation. Cells that have taken up injected DNA are shown in green.

Figure 3. Retinal Dissection. A. Image of adult pigmented mouse eye. The border of the cornea and sclera is indicated by a dotted line. Black arrow indicates optic nerve **B.** Image of needle puncture at border of cornea and sclera. **C.** Image of removing the cornea. **D.** Image of eye once cornea (black arrow) is removed. **E.** Image of eye once lens (black arrow) is removed. **F.** Expansive view of using tweezers to separate the retina from the sclera. **G.** magnified view of the same image as in panel F. **H.** Image of retina in a drop of HBSS.

Figure 4. RT-PCR and Fluorescence microscopy. The left panel in each set shows RT-PCR results for injected eyes after gel electrophoresis and imaging. "+" denotes exon inclusion and "-" denotes exon skipping. The green and red bands are PCR amplicons and ROX size standard, respectively. The right panel in each set shows fluorescence microscopy images of sections taken from injected eyes. The layers of the retina are indicated with brackets on the side of the image. **A.** Example of photoreceptor specific *Bbs8* Exon 2a wild type (WT) minigene. RT-PCR indicates a very high level of exon inclusion. Fluorescence microscopy shows high RFP fluorescence in Outer Nuclear Layer (ONL) containing the photoreceptor cell nuclei. Few neuronal cells expressing the minigene in the Inner Nuclear Layer (INL) produce GFP which indicates exon skipping. **B.** Example of *Bbs8* Exon 2a minigene once the critical intronic splicing enhancers have been deleted. RT-PCR indicates majority of transcripts skip exon 2a. Fluorescence microscopy shows high levels of GFP in all cell layers, and low levels of RFP in ONL. **C.** Control minigene containing the Dup34 synthetic exon. RT-PCR and fluorescence microscopy show the exon being skipped in all cell layers. **D.** Control minigene containing the Dup51 synthetic exon. RT-PCR and fluorescence microscopy show high levels of exon inclusion regardless of cell type.

Figure 1

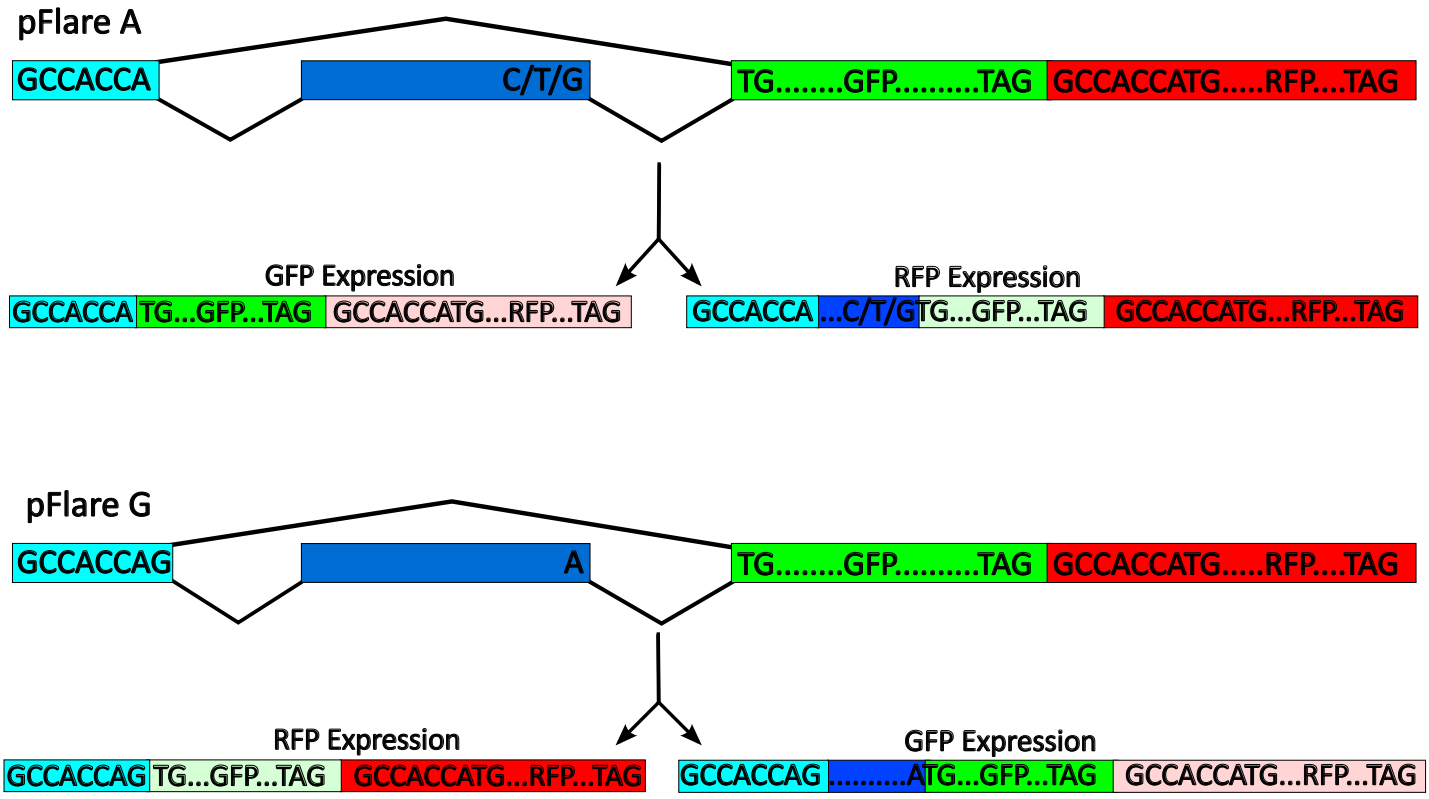
pFlare A
GCCACCA
C/T/G
TG.....GFP.....TAG
GCCACCATG.....RFP....TAG
GFP Expression
GCCACCA
TG...GFP...TAG
GCCACCATG...RFP...TAG
RFP Expression
GCCACCA
...C/T/G
TG...GFP...TAG
GCCACCATG...RFP...TAG
pFlare G
GCCACCAG
A
TG.....GFP.....TAG
GCCACCATG.....RFP....TAG
RFP Expression
GCCACCAG
TG...GFP...TAG
GCCACCATG...RFP...TAG
GFP Expression
GCCACCAG
.....A
TG...GFP...TAG
GCCACCATG...RFP...TAG

Figure 2

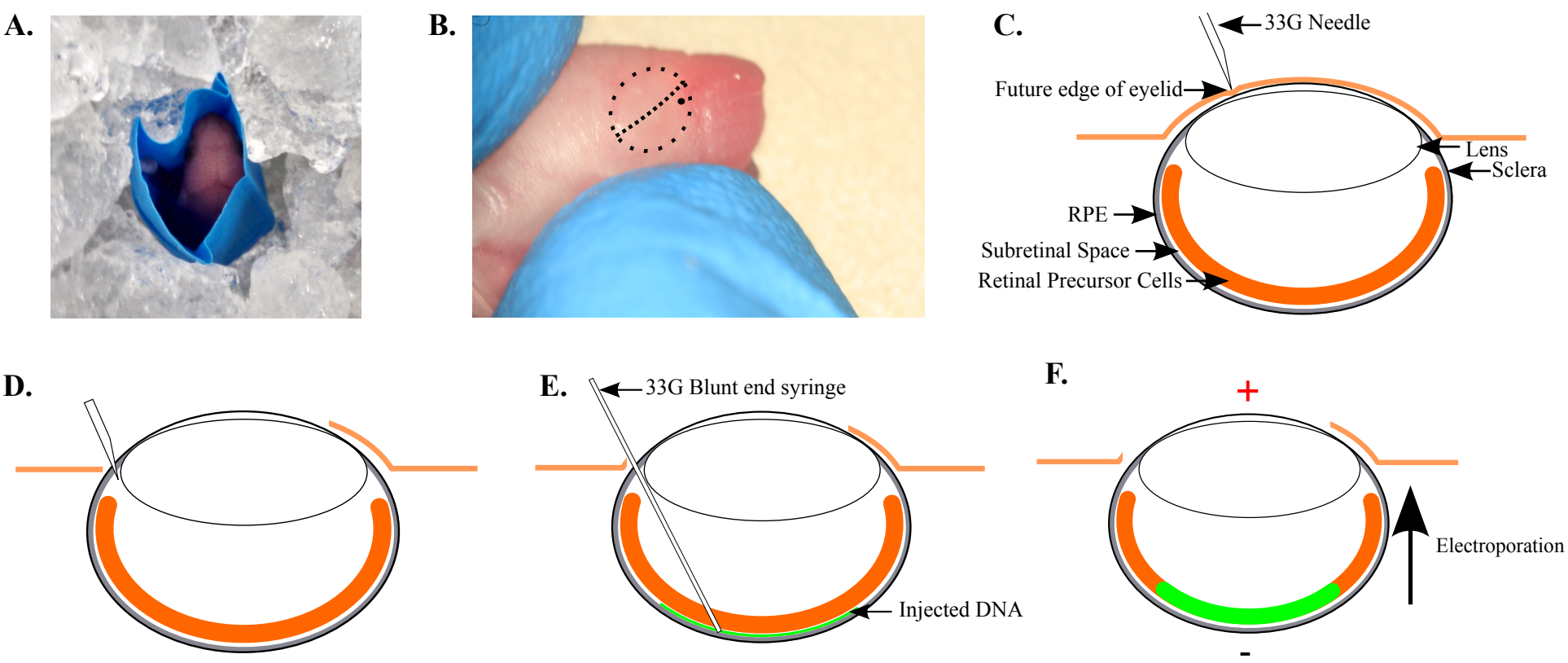
A.
B.
C.
33G Needle
Future edge of eyelid
Lens
Sclera
RPE
Subretinal Space
Retinal Precursor Cells
D.
E.
33G Blunt end syringe
Injected DNA
F.
+
Electroporation
-

Figure 3

A.

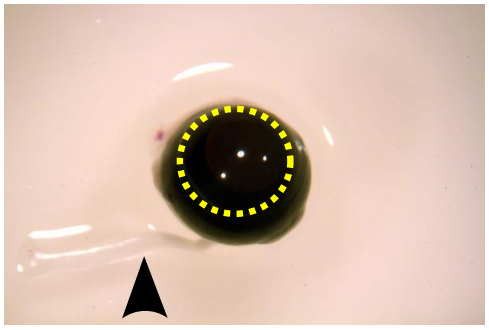

B.

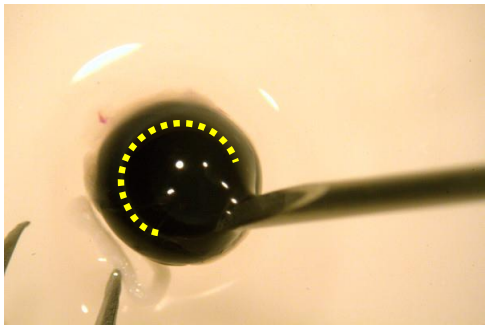

C.

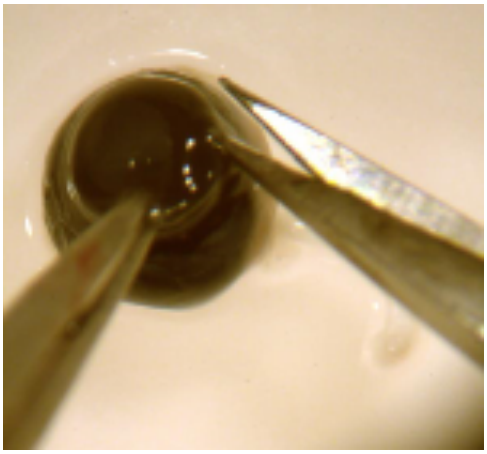

D.

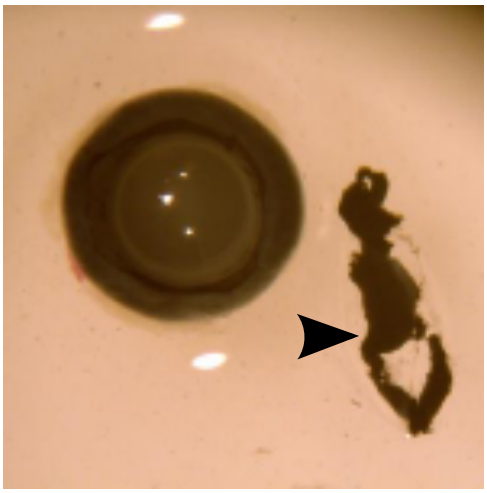

E.

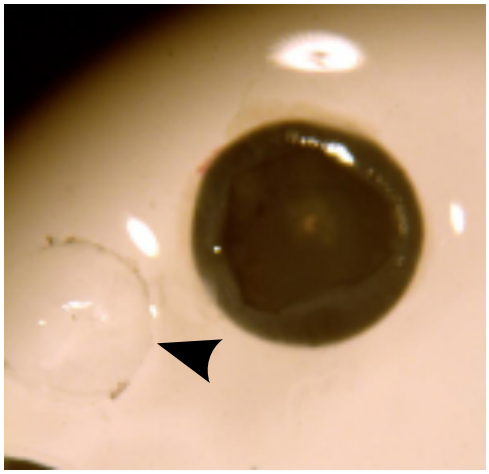

F.

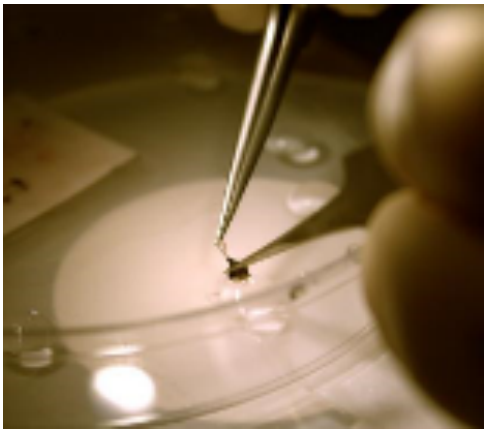

G.

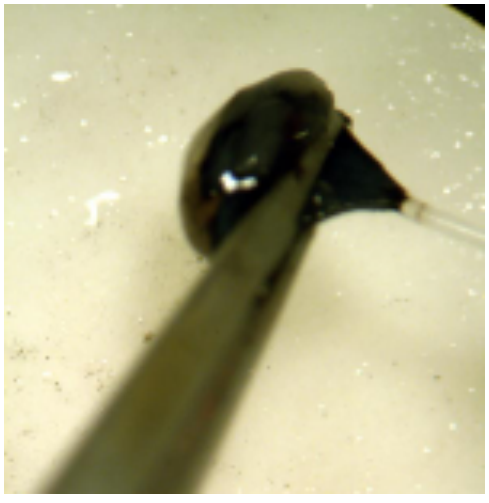

H.

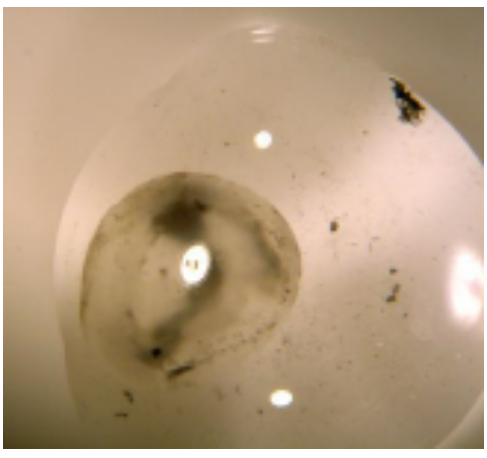

Figure 4

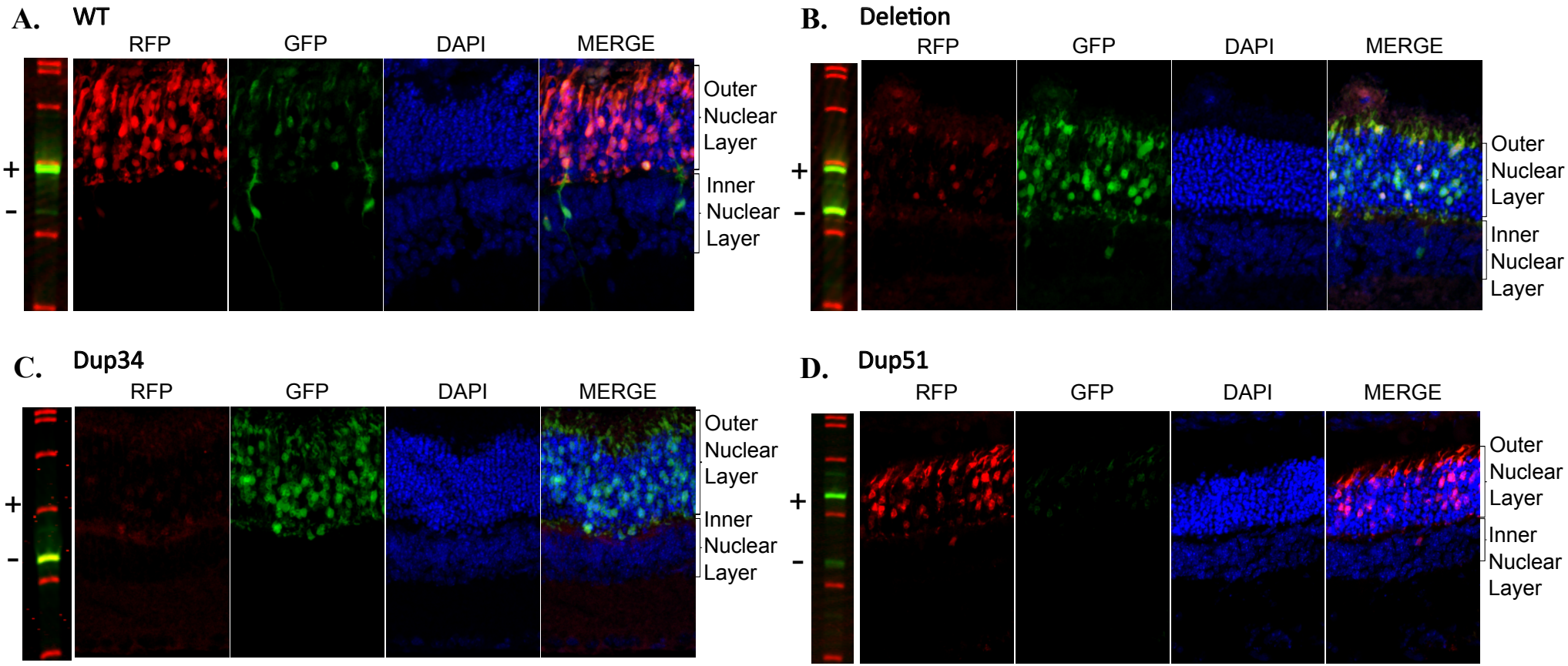
A.
WT
RFP
GFP
DAPI
MERGE
+
-
Outer Nuclear Layer
Inner Nuclear Layer
B.
Deletion
RFP
GFP
DAPI
MERGE
+
-
Outer Nuclear Layer
Inner Nuclear Layer
C.
Dup34
RFP
GFP
DAPI
MERGE
+
-
Outer Nuclear Layer
Inner Nuclear Layer
D.
Dup51
RFP
GFP
DAPI
MERGE
+
-
Outer Nuclear Layer
Inner Nuclear Layer

Chapter 4. Paper Published in the journal Molecular and Cellular Biology, 2015.

Alternative splicing shapes the phenotype of a mutation in *BBS8* to cause nonsyndromic Retinitis Pigmentosa

Daniel Murphy [a], Ratnesh Singh [b], Saravanan Kolandaivelu [b], Visvanathan Ramamurthy [a,b,c,#] and Peter Stoilov [a,#]

Departments of [a]Biochemistry, [b]Ophthalmology and [c]Center for Neuroscience, Robert C. Byrd Health Sciences Center, West Virginia University, Morgantown, West Virginia, 26505, USA

#Address for correspondence: Peter Stoilov, pstoilov@hsc.wvu.edu or Visvanathan Ramamurthy, ramamurthyv@wvuhealthcare.com

Department of Biochemistry, West Virginia University School of Medicine, 1 Medical Center Dr, Morgantown WV 26505. Phone: 304 293-6334 or 304-598-6940; Fax: +1 304 293-6846

Author Contributions

DM: experimental design, data acquisition, data analysis and interpretation, drafting and revising the article

RS: experimental design, data acquisition, data analysis and interpretation, drafting and revising the article

SK: experimental design, revising the article

VR: conception, experimental design, data analysis and interpretation, drafting and revising the article

PS: conception, experimental design, data acquisition, data analysis and interpretation, drafting and revising the article

ABSTRACT

Bardet-Biedl syndrome is a genetic disorder affecting multiple systems and organs in the body. Several mutations in genes associated with Bardet-Biedl syndrome (BBS) affect only photoreceptor cells and cause nonsyndromic Retinitis Pigmentosa (RP), raising the question why certain mutations manifest as a systemic disorder, while other changes in the same gene affect only a specific cell type. Here, we show that cell type specific alternative splicing is responsible for confining the phenotype of the IVS1-2A>G mutation in the *BBS8* gene to photoreceptor cells. The IVS1-2A>G mutation leads to mis-splicing of *BBS8* exon 2A producing a frameshift in the *BBS8* reading frame and thus eliminating the protein specifically in photoreceptor cells. Cell types other than photoreceptors skip exon 2A from the mature *BBS8* transcript, which renders them immune to the mutation. We also show that the splicing of *Bbs8* exon 2A in photoreceptors is directed exclusively by redundant splicing enhancers located in the adjacent introns. These intronic sequences are sufficient for photoreceptor cell-specific splicing of heterologous exons, including an exon with randomized sequence.

INTRODUCTION

The BBSome is a multi-protein complex that is thought be required for the transport of proteins in and out of the cilia. The BBSome interacts with IFT-A and IFT-B complexes and promotes the assembly of the intraflagellar transport (IFT) machinery (1–7). Several proteins such as the G-protein coupled receptors Smo, Sstr3, Mchr1 and Vipr2, depend on the BBSome for their ciliary transport, suggesting a possible role for the BBSome as an adapter that connects the IFT complex to its cargo in primary cilia (2, 8, 9). Mutations in genes that encode BBSome components and proteins associated with the BBSome are linked to the systemic Bardet-Biedl syndrome (BBS). BBS is an autosomal recessive ciliopathy caused by defects in the BBSome that disrupt the normal ciliary function throughout the body. The BBS symptoms include Retinitis Pigmentosa (RP), skeletal malformations, mental retardation, obesity, hearing impairment, shortened limbs, polydactyly and kidney cysts (10, 11). In photoreceptor cells, BBSome deficiency leads to defects in rod outer segment formation and localization of rod opsin, and ultimately photoreceptor cell death (10–13). The severity of the BBS symptoms can vary considerably due to the nature of the mutation and the genetic background. Interestingly, phenotypes of different mutations in the same gene can range from a classical BBS that affects multiple systems to nonsyndromic RP, where the phenotype is limited to loss of photoreceptor function. For example, *ARL6* (*BBS3*) A89V, *BBS1* M390R and *BBS8* IVS1-2A>G mutations cause nonsyndromic RP, while several other mutations in the same genes manifest as classical BBS presenting additional symptoms such as obesity, hearing impairment, polydactyly and mental retardation in addition to the loss of vision (7, 14–19). The existence of BBSome mutations that cause nonsyndromic RP is interpreted to indicate a specific function for this protein complex in vision. This hypothesis is further supported by the requirement for the Arl6 long (Arl6L) splice isoform that is specific to the retina for photoreceptor survival (20, 21).

BBS8 is a tetratricopeptide repeat (TPR) protein that is part of the core BBSome particle. BBS8 was recently shown play a role in establishing planar cell polarity and cilia orientation in epithelial cells (22). To date, six mutations in the *BBS8* gene have been linked to classical BBS (18, 23, 24). An exception from this pattern is the *BBS8* IVS1-2A>G mutation, which disrupts the 3' splice site of *BBS8* exon 2A and causes nonsyndromic RP. It was postulated that the IVS1-2A>G mutation induces skipping of the exon to produce a shorter splice variant (BBS8S) (19). The long form of *BBS8* containing the 30nt exon 2A (BBS8L) is detected exclusively in the photoreceptor outer nuclear layer (ONL), but not in other parts of the retina which express the short BBS8S isoform (19). Analogous to Arl6, where the splicing isoform Arl6L is needed for photoreceptor survival, it was proposed that the RP phenotype is due to the inability of BBS8S protein to substitute for a crucial function performed by the longer BBS8L isoform in photoreceptor cells (19–21).

Here, we show that *BBS8* exon 2A is highly photoreceptor specific. We dissect the sequences that direct Bbs8 exon 2A splicing and show that splicing enhancers within the flanking introns are sufficient to drive photoreceptor specific inclusion of exon 2A and unrelated exons. The mechanisms controlling the cell type specific splicing of *BBS8* exon 2A modify the phenotype of the IVS1-2A>G mutation to eliminate the BBS8 protein specifically in photoreceptors and cause nonsyndromic RP.

MATERIALS AND METHODS

Mice

The procedures used in this work were approved by Institutional Animal Care and Use Committee at West Virginia University. The *in vivo* subretinal injection and electroporation experiments were carried out in CD-1 mice (Charles River). The *Aipl1* and *Nrl* knockouts were described previously (25, 26). *Nrl* knockouts were a generous donation from Dr. Anand

Swaroop (NEI). The two knockout alleles were maintained in C57BL/6J genetic background. (Jackson Laboratory, Bar Harbor, ME).

RNA isolation and RT-PCR

Mouse eyes were enucleated at P16 and dissected under microscope (Zeiss Stemi DV4) to isolate the retina. Retinal RNA was isolated with TRI reagent (Sigma) according to manufacturer's guidelines. Reverse-transcription PCR reactions containing 0.1-0.5 μg RNA were primed with Oligo-dT and random hexamers to generate cDNA. The alternatively spliced regions were amplified using fluorescently labeled primers (listed in Supplementary Table 2) positioned in the flanking constitutive exons (27). The amplified products were separated by gel electrophoresis under denaturing conditions (Urea/polyacrylamide gels) and imaged on typhoon imager 9410 (GE). The band intensities on the gels were quantified using the Image Quant software (GE). For sequencing, the PCR products were isolated from agarose gels, purified using QIAquick Gel Extraction Kit (Qiagen) and either sequenced directly or cloned into pGEM T-Easy vector (Promega) prior to sequencing.

Real Time-PCR.

Rho, *Opn1sw*, *Gnat1*, *Gnat2*, *Pde6a* and *Pde6c* expression was quantified by SYBR-green qPCR. The expression of each gene was normalized to the average expression of three reference genes: β- Glucuronidase (*GusB*), β-Actin (*ActB*), and Glyceraldehyde-3-Phoshpate Dehydrogenase (*Gapdh*). See Supplementary Table 2 for primer sequences.

Antibodies

The *Bbs8* exon 2A antiserum was produced by Pacific Immunology. The serum was raised in rabbits against a peptide antigen (C-SPYDQEPAPDLPVSQA) that corresponds to the mouse exon 2A and includes six amino acid residues from the flanking exons to improve its

immunogenicity. The antibody was affinity purified using the antigen peptide coupled to sulfo-link resin (Pierce). We also used the following commercial antibodies: pan-Bbs8 rabbit polyclonal antibody E-2 (Santa-Cruz Biotech); GAPDH mouse monoclonal antibody 10RG109a (Fitzgerald). The antibodies to Pdc, Chx and Pax6 were kind gifts by Drs Maxim Sokolov and Peter Mathers (WVU).

Western blotting

Flash frozen retinal samples (*Aipl1*$^{+/+}$; *Aipl1*$^{-/-}$) and lysates of N2A cells transiently transfected with *BBS8* expressing construct were homogenized by sonication (Microson Ultrasonic cell disruptor) in 1xPhosphate Buffered Saline (PBS) containing protease inhibitors (Roche complete). The protein concentration was measured by using NanoDrop spectrophotometer (ND-1000, Thermo Scientific). Equal concentrations (150 µg) of protein samples were resolved in 10% SDS-PAGE gel electrophoresis and then transferred to Immobilon-FL membrane (Millipore). Membranes were blocked with blocking buffer (Rockland) for 30 min at room temperature. After blocking, membranes were incubated with primary anti-Bbs8 antibodies at 1:1000 dilution for 4 hrs at room temperature. The secondary antibodies, odyssey goat anti-rabbit Alexa 680 and odyssey goat anti-mouse Alexa 680 (LI-COR Biosciences) were used at 1:50,000 dilution for 30 min at room temperature. Membranes were scanned using an Odyssey Infrared Imaging System (LI-COR Biosciences).

Retinal tissue sections and fluorescence imaging

Mouse eyes were enucleated at P20 and incubated in 4% paraformaldehyde for 10 minutes. After removal of the cornea, the dissected eye was incubated in 4% paraformaldehyde for an additional 1 hr with shaking. After three 5 min washes in PBS, the eye were cryoprotected by shaking at 4°C overnight in PBS containing 20% sucrose. Eyes were then incubated for 1 hr with shaking in a 1:1 mixture of optimal cutting temperature (OCT) (Tissue Tek) compound and

20%sucrose in PBS, during which time the lens was removed. Eye cups were then flash frozen in OCT compound and stored at -80°C. Retinal sections (16 µm) were cut (Lecia cm 1850) and mounted on Superfrost Plus (Fisher) slides and stored at -20°C. Slides were washed in PBS to remove excess OCT and mounted with Prolong-Gold reagent containing 4′,6-Diamidino-2-phenylindole (DAPI) (Life technologies). The slides were imaged on Zeiss LSM 510 laser scanning confocal microscope.

Generation of minigenes

The *Bbs8* exon 2a minigene was created by inserting a 700bp fragment containing Bbs8 exon 2a and surrounding intron sequences into the EcoR1 and BamH1 sites of pFLare9a. The Bbs8 site directed mutagenesis was performed using PCR overlap extension. The sequences of the primers used for cloning are in Supplementary Table 2. The construction of Dup 51 and Dup 34 exon minigenes were described in our earlier publication (28).

Modification of BAC clones

The RP11-99F24 BAC clone carrying the full length human *BBS8* gene was purchased from BACPAC Resources Center at Children's Hospital Oakland Research Institute (Oakland, California) and verified by end sequencing and restriction fragment analysis. The IVS1-2A>G mutation and the tandem Flag/HA tag at the C-terminus of the *BBS8* ORF were introduced into the RP11-99F24 BAC clone using recombineering following previously described procedures (29). Restriction digests and sequencing of the targeted sites was used to ensure that the expected recombination events have occurred without unintended changes in the surrounding sequences.

Subretinal injection and electroporation

Minigene plasmid DNA was isolated at 4-7μg/μl using the Qiagen Plasmid Plus Midi kit. DNA containing 0.1% fluorescein sodium (NDC) was injected into the subretinal space of newborn CD-1 pups as described (30). Briefly, after anesthesia, an incision was made at the future eyelid with a 33 gauge needle under a dissecting microscope. The needle was used to make a pinhole puncture in the sclera away from the lens. 0.5 μl of DNA was injected through the puncture into the subretinal space using a blunt-end syringe. Five pulses of 80v at 50-ms duration with 950-ms intervals were then applied with tweezer type electrodes BTX model 520, 7 mm diameter. All experimental results and conclusions are based on at least three independent experiments (see Supplementary Table 1 for the number of replicates used in each experiment).

RESULTS

The long form of BBS8 (BBS8L) is predominantly expressed in photoreceptor cells.

A previous study analyzing *Bbs8* message from various retinal layers obtained by laser captured microdissection showed that exon 2A is included in the photoreceptor layer. It was unclear if exon 2A inclusion in the mature *Bbs8* transcripts is a general feature of photoreceptor cells or if it is restricted to rods, which comprise 97% of the mouse retina. We first established the tissue specificity of exon 2A inclusion using RT-PCR to analyze the splicing of *Bbs8* in various mouse tissues. Other than the retina, we did not observe significant exon 2A inclusion in any of the tissues that we examined (Figures 1A and 1B). Low levels of exon 2A inclusion can be detected in cortex and cerebellum after overexposing the gel with the RT-PCR products (Figure 1A, lower panel).

To confirm that exon 2A containing transcripts in the retina are specific to photoreceptor cells, we analyzed *Bbs8* splicing in the retina of Aryl hydrocarbon receptor Interacting Protein Like -1 (*Aipl1*) knockout mice at P60 and compared it to age matched littermates. *Aipl1* is required for photoreceptor cell survival. Consequently, the retina of *Aipl1* knockout mice lacks photoreceptor cells by P30, but retain their inner neurons and retinal pigmented epithelium (25). RT-qPCR analysis of the expression of cone and rod photoreceptor markers (*Opn1sw*, *Gnat2*, *Pde6c*, *Rho*, *Gnat1* and *Pde6a*) in the *Aipl1* knockout retina confirmed that there are little if any photoreceptor cells left (Supplementary Figure 1). We reasoned that if *Bbs8* exon 2A is expressed exclusively in photoreceptor cells, we should see a dramatic reduction in its inclusion in *Aipl1* knockout animals compared to wild type littermates. In agreement with the previous study characterizing *Bbs8* exon 2A splicing, we find that the expression of the *Bbs8L* isoform is severely reduced in the retina of the adult *Aipl1* knockout animals (Figure 1B) (19). This result demonstrates that exon 2A is included in the mature *Bbs8* RNA in photoreceptor cells. To

determine if *Bbs8* exon inclusion is specific to a particular photoreceptor cell type in the retina, we compared the splicing of the *Bbs8* transcripts in retina from wild type to retina from mice lacking the *Nrl* transcription factor. The retina from the *Nrl* knockout animal is enriched in cones and lack rods (26). RT-qPCR analysis of the expression of photoreceptor specific genes confirmed elevated expression of cone markers (*Opn1sw*, *Gnat2* and *Pde6c*) and loss of rod markers (*Rho*, *Gnat1* and *Pde6a*) in the retina of *Nrl* knockout mice (Supplementary Figure 1). The level of exon 2A inclusion in the retina of the *Nrl* knockout was indistinguishable from that in wild type mouse retina (Figure 1B), indicating that rods and cones include *Bbs8* exon 2A.

We next examined the splicing of *Bbs8* exon 2A in the course of retinal development. Inclusion of exon 2A was not detectable in the retina at embryonic day 17.5. Exon 2A was detected first at P0 and its inclusion increases rapidly thereafter (Figure 1C). This change in exon 2A inclusion levels closely correlates with photoreceptor outer segment morphogenesis as well as expression of rod opsin, which is not detectable at E17.5 and rapidly rises after birth (Figure 1C) (31). Thus, the developmental regulation of exon 2A splicing and its splicing pattern in the retina of adult *Aipl1* and *Nrl* knockout mice strongly support photoreceptor cell specific splicing of this alternative exon.

To assess the Bbs8L protein expression in the retina, we raised a rabbit polyclonal antibody against the peptide sequence encoded by exon 2A. Unfortunately, this Bbs8L antibody was not suitable for immunolocalization in retinal sections. However, we were able to use the anti-exon 2A antibody to compare the Bbs8L expression by western blotting in the retina from wild type and *Aipl1* knockout animals. Wild type retina expressed high levels of Bbs8L protein that matched in mobility to the recombinant Bbs8L protein overexpressed in N2A cells, a mouse neuronal cell line (Figure 1D). Consistent with the photoreceptor cell specific splicing of exon 2A, the Bbs8L protein was undetectable in the retina lacking Aipl1 and in untransfected N2A cells. To determine the overall expression pattern of the Bbs8S and Bbs8L proteins in the retina,

we probed the protein extracts with a commercially available pan-Bbs8 antibody that recognizes both isoforms. Similar to the results obtained with the Bbs8L specific antibody, the pan-Bbs8 antibody detected high levels of Bbs8 protein in the wild type retina, which was absent in the retina from the *Aipl1* knockouts. We also noticed that the retina lacking Aipl1 and the untransfected N2A cells express the shorter BBS8S protein albeit at low levels. Overall, our results show that the Bbs8L protein is expressed at high levels in photoreceptor cells.

The splice site mutation upstream of exon 2A results in cryptic splicing

The A to G substitution (IVS1-2A>G) in the 3' splice site of *BBS8* exon 2A was postulated to cause nonsyndromic Retinitis Pigmentosa (RP) by preventing the inclusion of exon 2A in the mature transcripts (19). To test this hypothesis, we established a robust system to investigate the mechanism that controls the inclusion of exon 2A in *Bbs8*. This assay would also aid in visualizing the *Bbs8* exon 2A splicing event in a particular cell type in the retina. We cloned a 700bp fragment containing the mouse exon 2A and portions of its flanking introns into a splicing reporter minigene under the control of ubiquitously active cytomegalovirus promoter (CMV) (Figure 2A). In addition to the wild type construct, we also created an exon 2A minigene carrying the IVS1-2A>G mutation. The splicing reporter is designed to produce red fluorescent protein (RFP) when exon 2A is included and green fluorescent protein (GFP) when the exon is skipped (28). This reporter construct allows us to use fluorescent microscopy to assess the inclusion of exon 2A by comparing the RFP to GFP expression in individual cells. The splicing of exon 2A in the context of the minigene can also be quantified by RT-PCR using primers specific to the backbone.

We first analyzed the splicing of the wild type and mutant exon 2A minigenes after transfecting them into human embryonic kidney (HEK293) tissue culture cells. Both minigenes produced mRNA that did not include exon 2A (Figure 2B, product A). Next, we used subretinal injection

and electroporation to introduce the *Bbs8* exon 2A minigenes into developing photoreceptor cells at postnatal day 0 (P0) and analyzed their splicing by RT-PCR at P16 (30). We harvested retina at this time point as our results indicated that the inclusion of exon 2A is near its maximum at P16 (Figure 1C). In addition, splicing of minigenes was visualized by fluorescence microscopy at P20 in retinas dissected from littermates of animals used for the RT-PCR experiments. Exon 2A was included in 98% of the minigene transcripts as determined by RT-PCR (Figure 2B, product B). Surprisingly, introducing the 3' splice site mutation into the minigene caused mis-splicing rather than exon skipping. Sequencing the PCR product showed that the shorter transcript is derived from the inclusion of a truncated exon 2A (represented as 2A*) due to the use of a cryptic 3' splice site 7 nucleotides downstream of the normal acceptor site (Figure 2B, product D). The minigene also produced two minor splice products, one migrating significantly higher than the wild type exon 2A and one migrating at the same position as the wild type exon. We determined by sequencing that the higher molecular weight splice product is generated by the use of a cryptic 3' splice site upstream of exon 2A (Product C). Splicing to both the intronic (Product C) and the exonic (Product D) cryptic splice site is predicted to cause frame shift and premature termination of the Bbs8 reading frame in the downstream exon 2.

Fluorescent microscopy imaging of the electroporated retinas shows that the electroporated minigenes are expressed mostly in photoreceptor cells, as very few inner neurons express the reporter fluorescent proteins (Figure 3 and Supplementary Figures 2, 3 and 4). Thus, the RT-PCR signal is largely derived from the photoreceptor cells. In agreement with photoreceptor cell specific inclusion of exon 2A, we see high levels of RFP expression in the photoreceptor outer nuclear layer (ONL) (Figure 3A). Similar high RFP expression, that is indicative of exon inclusion was observed with the minigene carrying the IVS1-2A>G mutation (Figure 3B). To determine the exon 2A inclusion levels in inner neurons, we analyzed by fluorescent microscopy

sections from animals electroporated with the exon 2A minigenes (Figure 3A, 3B and Supplementary Figures 2 and 3). Invariably, the inner neurons displayed high GFP to RFP ratio, which is indicative of skipping of exon 2A from the mature transcript (Figure 3A, indicated with yellow arrows). Taken together, the fluorescence imaging of the mutant minigene in the retina and the RT-PCR analysis show that the cryptic splice sites are used exclusively by the photoreceptor cells (Figure 3B and Supplementary Figure 3). In contrast, inner neurons skip both the wild type and mutant exon 2A altogether (Figure 3A, 3B and Supplementary Figures 2 and 3).

To ensure that the observed splicing pattern is not influenced by the vector backbone, we electroporated two minigenes that carried synthetic alternative exons, Dup34 and Dup51, derived from the human β-globin gene (28). Dup34 is universally skipped, while Dup51 has approximately 50% inclusion level in cultured cells (28, 32). We observed by RT-PCR and fluorescence microscopy that the Dup34 exon was completely skipped (high GFP) (Figure 3C and Supplementary Figure 4) and the Dup51 exon was included at a high rate (high RFP) (Figure 3D and Supplementary Figure 4). Neither of the two exons displayed a photoreceptor specific splicing pattern.

We next examined the inclusion of exon 2A in the context of full-length introns and exons in human *BBS8* gene. To do so, we used recombineering to modify a BAC clone containing the full length human *BBS8* gene and created an A to G substitution in the 3' splice site of exon 2A (Figure 4A). The wild type and mutant BAC were then introduced into the developing photoreceptor cells of neonatal mice by subretinal injection and electroporation (30). The splicing of exon 2A in the retina was analyzed at P16 by RT-PCR using primers specific to the human sequence. We observed high levels of exon 2A inclusion in retina expressing the wild type *BBS8* gene (Figure 4B). Similar to our minigene experiments, the IVS1-2A>G mutation did not cause skipping of exon 2A from the *BBS8* transcripts (Figure 4B). Instead, the exon 2A

isoform was replaced by an mRNA variant that included a slightly shorter exon. The shorter transcript contained a truncated exon 2A* with the use of the cryptic 3' splice site 7 nucleotides downstream of the normal acceptor site, which we observed in our minigene experiments (Figure 4C and Supplementary Figure 5).

Our results show that the molecular mechanism by which mutation of *Bbs8* exon 2A causes the loss of photoreceptor cells is mis-splicing leading to the inclusion of a truncated exon 2A, rather than skipping of exon 2A.

The sequence of exon 2A does not direct its inclusion in photoreceptor cells.

Our studies establish that *Bbs8* exon 2A is specifically included in photoreceptor cells. To determine how such specificity is achieved, we mapped the sequence elements that direct the splicing of exon2A in photoreceptor cells. The sequence elements located within the exons (exonic splicing enhancers or ESEs) are typically required for exon recognition and inclusion in the mature transcript (33–35). To determine if ESE sequences are involved in the photoreceptor specific splicing of *Bbs8* exon 2A we created four minigenes (LS1-4) in which overlapping 8 nucleotide segments of the exon were replaced with a PvuI linker sequence (Figure 5A). To our surprise, all linker scanning mutants retained a high level of exon 2A inclusion in the retina (Figure 5B). The LS1 mutant was the only one that showed minor but significant decrease of approximately 14% in its inclusion level compared to the wild type exon (Figure 3 top left panel and Figure 5B). We reasoned that rather than carrying ESEs recognized by photoreceptor specific splicing factors, *Bbs8* exon 2A might contain exonic splicing silencers (ESS) that repress its inclusion in other cell types. Alternatively, the linker sequence itself may contain an ESE. To test this hypothesis, we introduced the linker scanning mutants into N2A cells. In comparison to HEK293 cells where exon 2A was not included, we observed minor levels (10%) of wild-type (WT) exon 2A inclusion in N2A cells. However, this was significantly lower than the

98% inclusion levels in photoreceptor cells. We expected that mutants which disrupt ESS elements in exon 2A or add an ESE will increase its inclusion in the N2A cell line. We did not observe significant increase in the exon 2A inclusion levels in any of the linker scanning mutations (Figure 5C). As in our *in vivo* electroporation experiments, the LS1 mutant showed minor but significant decrease in the exon 2A inclusion level (Figure 5C).

To rule out the possibility that exon 2A may contain redundant ESEs we scrambled the exon 2A sequence (Core-SCR), while preserving the first and the last three nucleotides, and the overall nucleotide composition (Figure 5A). The first nucleotide and the last three nucleotides of the exon are part of the consensus splice site sequences and are directly contacted by the core spliceosome (36–38). By preserving these nucleotides in the Core-Scr minigene, we avoided disrupting interactions that are essential for splicing. MaxEnt splice site scores for the 3' splice sites of *Bbs8* exon 2A and Core-SCR are 8.82 and 8.61, respectively (39). The 5' splice sites of both exons have a MaxEnt score of 8.59. We also created a minigene construct in which *Bbs8* exon 2A was substituted with the Dup34 exon, while preserving the *Bbs8* intronic sequence (Bbs8-Dup34). The MaxEnt score of the 3' splice site of the Bbs8-Dup34 fusion is lower, 7.47, but still represents a good match to the 3' splice site consensus sequence. The 5' splice site score of the Bbs8-Dup34 fusion is 8.59, identical to that of Bbs8 exon 2A and the Core-SCR. After subretinal injection and electroporation, both the Core-SCR and Bbs8-Dup34 minigenes displayed high levels of inclusion of the alternative exon: 88% and 77%, respectively (Figure 5D, and Supplementary Figures 6 and 7). Importantly, both exons are specifically included in photoreceptor cells and not in inner neurons (Figure 5D and 5E). This result is in contrast to our previous observation where the Dup34 exon is completely skipped in photoreceptor cells when it is flanked by its original β-globin introns (Figure 3, bottom left).

Mutating the first and last three nucleotides of Bbs8 exon 2A (Edge-SCR) to reduce the strength of the 3' and 5' splice sites to 6.17 and -8.27, respectively, completely abolished the inclusion of

the exon (Figure 5D and Supplementary Figure 8). Lack of exon 2A inclusion in this mutant is likely due to the disruption of the 5' splice site as indicated by its negative MaxEnt score.

The results from our mutagenesis study demonstrate that exon2A does not contain splicing regulatory elements that are necessary for its inclusion in the photoreceptor cells and that the cis-elements that control *Bbs8* exon 2A splicing are likely intronic.

Redundant intronic splicing enhancers (ISEs) regulate the splicing of *Bbs8* exon 2A.

To map these regulatory elements in the introns flanking Bbs8 exon 2A, we created six deletion mutants, each one removing 100 nucleotides from the upstream and downstream introns cloned in the exon 2A minigene (Figure 6A). In all deletions we preserved the sequences of the 3' and 5' splice sites, and the putative branch point, which are recognized by the core spliceosome. We observed that deletion of the segments adjacent to the exon, labeled D3 and D4, resulted in significant reduction of exon 2A inclusion in the retina (Figure 6B and Figure 3 top left panel). Additionally, the deletion of segment D3 caused retention of the upstream intron in part of the mature transcripts. The remaining four deletions had minimal or no effect on the exon 2A inclusion levels or the splicing efficiency of the introns. Combined deletion of segments D3 and D4 dramatically reduced the exon 2A inclusion level in photoreceptor cells from 98% (Figure 2) to 23% (Figure 6C and Supplementary Figure 9). In agreement with decrease in inclusion levels of exon 2A in D3/D4 deletion, we saw increased expression of GFP in photoreceptor cells (Figure 6C). This is in contrast to our earlier result with intact exon 2A introns showing robust expression of RFP (Figure 3D). Altogether, these findings indicate that ISE elements located in both D3 and D4 segments in concert promote the splicing of exon 2A in photoreceptor cells.

To obtain a higher resolution map of the ISEs controlling exon 2A splicing, we generated six additional mutants that had overlapping 40 nucleotide deletions in segments D3 and D4 (Figure 6D). We did not observe any significant changes in levels of exon 2A inclusion in any of the

shorter deletion mutants (Figure 6E). We conclude that segments D3 and D4 contain multiple redundant ISEs, so that the deletion of any single ISE is insufficient to significantly impact the splicing of exon 2A.

Discussion

The lack of cellular models and the technical difficulty of analyzing the gene expression profiles of individual cell subtypes in the retina have presented significant obstacles to studying the regulation of gene expression and alternative splicing in photoreceptor cells. Here we demonstrate that these obstacles can be overcome by using genetically engineered mouse models to identify photoreceptor specific transcripts and subretinal injection and electroporation to dissect the regulation of their expression. In particular, the use of the fluorescent splicing reporter allowed us to visualize the splicing regulation of *Bbs8* exon 2A in individual retinal cells. As the fluorescent reporter minigene is designed to accommodate most alternative exons, our approach is generally applicable to studying splicing *in vivo*.

To our surprise the IVS1-2A>G mutation in the splice acceptor site of *Bbs8* exon 2A does not cause skipping of the exon, which in turn will result in the expression of the BBS8S protein in place of the photoreceptor specific BBS8L. Instead, the mutation forced the use of a cryptic splice site located 7nt downstream of the mutated site. The splicing of the mutant exon 2A is consistent with our finding that any exon placed in the context of the introns flanking *Bbs8* exon 2A will be spliced efficiently in photoreceptor cells as long as it carries functional splice sites. Based on the splicing pattern of the mutant exon 2A, we propose that the disease mechanism involves mis-splicing, which in turn results in premature termination of the *BBS8* reading frame and elimination of the BBS8 protein in photoreceptors (Figure 7). In this scenario, we expect no BBS8 protein (BBS8L or BBS8S) expression in photoreceptor cells. This is akin to generating photoreceptor specific BBS8 knockout. Our attempts to detect BBS8 protein expression in the retina from either the wild type or mutant BAC constructs were not fruitful. This is likely due to the low efficiency of the BAC electroporation. A robust test to examine the effect of the IVS1-2A>G mutation on BBS8 protein synthesis will require animal models in which the mutation is

introduced in the endogenous *Bbs8* locus or transgenes carrying the BAC constructs described here and bred into a *Bbs8* null animals.

How is the phenotype of the IVS1-2A>G mutation confined to photoreceptors? All cell types other than photoreceptor cells that we have tested skip exon 2A and consequently do not utilize the cryptic splice sites. These cells express the short BBS8 isoform (BBS8S) and are immune to the mutation (Figure 7). Thus, the phenotype of the IVS1-2A>G mutation is determined by the photoreceptor specific alternative splicing program. To our knowledge, such interaction between tissue specific alternative splicing and genetic mutations has been described only in Stickler syndrome. Stickler syndrome is caused by mutations in at least 4 collagen genes and presents as a systemic disorder characterized by facial and eye abnormalities, hearing loss and joint problems (40, 41). However, mutations in exon 2 of the COL2A1 gene, but not in other exons of the same gene, produce predominantly eye phenotype due to the tissue specific splicing of this exon (42–45). We are tempted to speculate that the BBS8 IVS1-2A>G and the COL2A1 exon 2 mutations may not be isolated cases. Neurons, epithelial cells and muscle cells express highly cell type specific splicing regulators and consequently present characteristic splicing programs. Furthermore, splicing regulatory sequences are rich and often underappreciated target for disease causing genetic mutations (46). Approximately 10% of disease causing mutations disrupt the canonical splice site and additional 25% are estimated to affect splicing regulatory sequences within the exons (47, 48). Thus, we expect the phenotype of many disease causing mutations to be modulated by the alternative splicing machinery.

Bbs8 exon 2A is highly photoreceptor specific with nearly 100% inclusion levels in photoreceptor cells, while it is not included or included at very low levels outside of the retina. After exhaustive mutagenesis, we find that efficient splicing of *Bbs8* exon 2A in photoreceptor cells does not depend on ESEs. Strikingly, even the randomized sequence of the Core-SCR exon and the unrelated Dup34 exon were spliced efficiently in photoreceptor cells as long as

they were in the context of the introns flanking *Bbs8* exon 2A. Two 100 nucleotide segments, D3 located upstream and D4 located downstream of exon 2A, work in concert to promote inclusion of exon 2A in photoreceptors. The D3 and D4 segments are likely composed of multiple redundant intronic splicing enhancers, as a series of shorter deletions did not significantly reduce the efficiency of exon 2A splicing. Intronic splicing regulatory elements have a well-established role in regulating alternative splicing and promoting alternative exon splicing in specific tissues and cell types. In particular, neuronal and muscle specific microexons are characterized by high degree of conservation of the adjacent intronic sequences, compared to longer exons with similar tissue specific regulation (49, 50). The intron sequence conservation in these exons is dictated by the presence of regulatory sequences that are recognized by Rbfox1/2/3, PTBP1/2 and SRRM3 splicing regulators (49, 50).

At present, we do not know the identity of the trans-acting factors that bind to the intronic splicing enhancers flanking *Bbs8* exon 2A to promote its inclusion in photoreceptor cells. We are also unaware of any RNA binding proteins that are specifically expressed in photoreceptors. Several genome wide studies provide evidence that the retina expresses a highly diverse set of alternative transcripts that are developmentally regulated (51–54). It is unclear to what degree the retina specific transcript variants identified in these studies are derived from photoreceptor cells. We believe that by expanding to a genomic scale, our approach of comparing the expression levels in the retina of Aipl1 knockout to wild type animals will make it possible to identify the splicing regulators and alternative transcripts specific to the photoreceptor cells. In the absence of photoreceptor specific proteins that directly bind to the *Bbs8* pre-mRNA, the splicing of the exon 2A may be controlled by a combination of otherwise ubiquitously expressed splicing factors that is unique to this cell type. Such mode of regulation will be consistent with the combinatorial nature of the mechanisms controlling alternative splicing (55–57).

ACKNOWLEDGEMENTS

We thank Dr. Anand Swaroop for generously providing the Nrl knockout animal used in this study. We thank Dr. Peter Mathers and Helen Rodgers for providing RNA samples from embryonic and early postnatal mouse retinas and the anti-Chx and anti-Pax6 antibodies. We thank Dr. Maxim Sokolov and Marycharmain Belcastro for the *Gnat1* qPCR primers and the anti-Pdc antibody. We appreciate the constructive criticisms received from Drs. Lisa Salati, Maxim Sokolov, Peter Mathers and Mike Schaller (West Virginia University), and Dr. Shalini Sharma (University of Arizona). Imaging experiments were performed in the West Virginia University Microscope Imaging Facility, which has been supported by the Mary Babb Randolph Cancer Center and NIH grants P20 RR016440, P30 GM103488 and P20 GM103434.

FUNDING

This work was supported by grants from the National Institutes of Health (EY017035), West Virginia Lions, Lions Club International Fund and an internal grant from West Virginia University.

CONFLICT OF INTEREST STATEMENT

None

REFERENCES

1. Wei Q, Zhang Y, Li Y, Zhang Q, Ling K, Hu J. 2012. The BBSome controls IFT assembly and turnaround in cilia. Nat. Cell Biol. 14:950–957.

2. Seo S, Zhang Q, Bugge K, Breslow DK, Searby CC, Nachury MV, Sheffield VC. 2011. A Novel Protein LZTFL1 Regulates Ciliary Trafficking of the BBSome and Smoothened. PLoS Genet 7:e1002358.

3. Domire JS, Green JA, Lee KG, Johnson AD, Askwith CC, Mykytyn K. 2011. Dopamine receptor 1 localizes to neuronal cilia in a dynamic process that requires the Bardet-Biedl syndrome proteins. Cell. Mol. Life Sci. 68:2951–2960.

4. Lechtreck K-F, Johnson EC, Sakai T, Cochran D, Ballif BA, Rush J, Pazour GJ, Ikebe M, Witman GB. 2009. The Chlamydomonas reinhardtii BBSome is an IFT cargo required for export of specific signaling proteins from flagella. J. Cell Biol. 187:1117–1132.

5. Berbari NF, Lewis JS, Bishop GA, Askwith CC, Mykytyn K. 2008. Bardet–Biedl syndrome proteins are required for the localization of G protein-coupled receptors to primary cilia. Proc. Natl. Acad. Sci. 105:4242–4246.

6. Su X, Driscoll K, Yao G, Raed A, Wu M, Beales PL, Zhou J. 2014. Bardet–Biedl syndrome proteins 1 and 3 regulate the ciliary trafficking of polycystic kidney disease 1 protein. Hum. Mol. Genet. 23:5441–5451.

7. Ansley SJ, Badano JL, Blacque OE, Hill J, Hoskins BE, Leitch CC, Chul Kim J, Ross AJ, Eichers ER, Teslovich TM, Mah AK, Johnsen RC, Cavender JC, Alan Lewis R, Leroux MR, Beales PL, Katsanis N. 2003. Basal body dysfunction is a likely cause of pleiotropic Bardet–Biedl syndrome. Nature 425:628–633.

8. Sung C-H, Leroux MR. 2013. The roles of evolutionarily conserved functional modules in cilia-related trafficking. Nat. Cell Biol. 15:1387–1397.

9. Barbelanne M, Hossain D, Chan DP, Peränen J, Tsang WY. 2014. Nephrocystin proteins NPHP5 and Cep290 regulate BBSome integrity, ciliary trafficking and cargo delivery. Hum. Mol. Genet.

10. Zaghloul NA, Katsanis N. 2009. Mechanistic insights into Bardet-Biedl syndrome, a model ciliopathy. J. Clin. Invest. 119:428–437.

11. M'hamdi O, Ouertani I, Chaabouni-Bouhamed H. 2014. Update on the Genetics of Bardet-Biedl Syndrome. Mol. Syndromol. 5:51–56.

12. Nishimura DY, Fath M, Mullins RF, Searby C, Andrews M, Davis R, Andorf JL, Mykytyn K, Swiderski RE, Yang B, Carmi R, Stone EM, Sheffield VC. 2004. Bbs2-null mice have neurosensory deficits, a defect in social dominance, and retinopathy associated with mislocalization of rhodopsin. Proc. Natl. Acad. Sci. U. S. A. 101:16588–16593.

13. Abd-El-Barr MM, Sykoudis K, Andrabi S, Eichers ER, Pennesi ME, Tan PL, Wilson JH, Katsanis N, Lupski JR, Wu SM. 2007. Impaired photoreceptor protein transport and synaptic transmission in a mouse model of Bardet–Biedl syndrome. Vision Res. 47:3394–3407.

14. Aldahmesh MA, Abu Safieh L, Alkuraya H, Al-Rajhi A, Shamseldin H, Hashem M, Alzahrani F, Khan AO, Alqahtani F, Rahbeeni Z, Alowain M, Khalak H, Al-Hazzaa S, Meyer BF, Alkuraya FS. 2009. Molecular characterization of retinitis pigmentosa in Saudi Arabia. Mol. Vis. 15:2464–2469.

15. Estrada-Cuzcano A, Koenekoop RK, Senechal A, et al. 2012. BBs1 mutations in a wide spectrum of phenotypes ranging from nonsyndromic retinitis pigmentosa to bardet-biedl syndrome. Arch. Ophthalmol. 130:1425–1432.

16. Safieh LA, Aldahmesh MA, Shamseldin H, Hashem M, Shaheen R, Alkuraya H, Hazzaa SAFA, Al-Rajhi A, Alkuraya FS. 2010. Clinical and molecular characterisation of Bardet–Biedl syndrome in consanguineous populations: the power of homozygosity mapping. J. Med. Genet. 47:236–241.

17. Fan Y, Esmail MA, Ansley SJ, Blacque OE, Boroevich K, Ross AJ, Moore SJ, Badano JL, May-Simera H, Compton DS, Green JS, Lewis RA, van Haelst MM, Parfrey PS, Baillie DL, Beales PL, Katsanis N, Davidson WS, Leroux MR. 2004. Mutations in a member of the Ras superfamily of small GTP-binding proteins causes Bardet-Biedl syndrome. Nat. Genet. 36:989–993.

18. Ansley SJ, Badano JL, Blacque OE, Hill J, Hoskins BE, Leitch CC, Chul Kim J, Ross AJ, Eichers ER, Teslovich TM, Mah AK, Johnsen RC, Cavender JC, Alan Lewis R, Leroux MR, Beales PL, Katsanis N. 2003. Basal body dysfunction is a likely cause of pleiotropic Bardet–Biedl syndrome. Nature 425:628–633.

19. Stoetzel C, Laurier V, Faivre L, Mégarbané A, Perrin-Schmitt F, Verloes A, Bonneau D, Mandel J-L, Cossee M, Dollfus H. 2005. BBS8 is rarely mutated in a cohort of 128 Bardet-Biedl syndrome families. J. Hum. Genet. 51:81–84.

20. Riazuddin SA, Iqbal M, Wang Y, Masuda T, Chen Y, Bowne S, Sullivan LS, Waseem NH, Bhattacharya S, Daiger SP, Zhang K, Khan SN, Riazuddin S, Hejtmancik JF, Sieving PA, Zack DJ, Katsanis N. 2010. A Splice-Site Mutation in a Retina-Specific Exon of BBS8 Causes Nonsyndromic Retinitis Pigmentosa. Am. J. Hum. Genet. 86:805–812.

21. Pretorius PR, Baye LM, Nishimura DY, Searby CC, Bugge K, Yang B, Mullins RF, Stone EM, Sheffield VC, Slusarski DC. 2010. Identification and Functional Analysis of the Vision-Specific BBS3 (ARL6) Long Isoform. PLoS Genet 6:e1000884.

22. Pretorius PR, Aldahmesh MA, Alkuraya FS, Sheffield VC, Slusarski DC. 2011. Functional analysis of BBS3 A89V that results in non-syndromic retinal degeneration. Hum. Mol. Genet. 20:1625–1632.

23. May-Simera HL, Petralia RS, Montcouquiol M, Wang Y-X, Szarama KB, Liu Y, Lin W, Deans MR, Pazour GJ, Kelley MW. 2015. Ciliary proteins Bbs8 and Ift20 promote planar cell polarity in the cochlea. Dev. Camb. Engl. 142:555–566.

24. Bin J, Madhavan J, Ferrini W, Mok CA, Billingsley G, Héon E. 2009. BBS7 and TTC8 (BBS8) mutations play a minor role in the mutational load of Bardet-Biedl syndrome in a multiethnic population. Hum. Mutat. 30:E737–E746.

25. Hichri H, Stoetzel C, Laurier V, Caron S, Sigaudy S, Sarda P, Hamel C, Martin-Coignard D, Gilles M, Leheup B, Holder M, Kaplan J, Bitoun P, Lacombe D, Verloes A, Bonneau D, Perrin-Schmitt F, Brandt C, Besancon A-F, Mandel J-L, Cossée M, Dollfus H. 2005. Testing for triallelism: analysis of six BBS genes in a Bardet–Biedl syndrome family cohort. Eur. J. Hum. Genet. 13:607–616.

26. Ramamurthy V, Niemi GA, Reh TA, Hurley JB. 2004. Leber congenital amaurosis linked to AIPL1: a mouse model reveals destabilization of cGMP phosphodiesterase. Proc. Natl. Acad. Sci. U. S. A. 101:13897–13902.

27. Mears AJ, Kondo M, Swain PK, Takada Y, Bush RA, Saunders TL, Sieving PA, Swaroop A. 2001. Nrl is required for rod photoreceptor development. Nat. Genet. 29:447–452.

28. Percifield R, Murphy D, Stoilov P. 2014. Medium throughput analysis of alternative splicing by fluorescently labeled RT-PCR. Methods Mol. Biol. Clifton NJ 1126:299–313.

29. Stoilov P, Lin C-H, Damoiseaux R, Nikolic J, Black DL. 2008. A high-throughput screening strategy identifies cardiotonic steroids as alternative splicing modulators. Proc. Natl. Acad. Sci. 105:11218–11223.

30. Copeland NG, Jenkins NA, Court DL. 2001. Recombineering: a powerful new tool for mouse functional genomics. Nat Rev Genet 2:769–779.

31. Matsuda T, Cepko CL. 2004. Electroporation and RNA interference in the rodent retina in vivo and in vitro. Proc. Natl. Acad. Sci. U. S. A. 101:16–22.

32. Swaroop A, Kim D, Forrest D. 2010. Transcriptional regulation of photoreceptor development and homeostasis in the mammalian retina. Nat. Rev. Neurosci. 11:563–576.

33. Modafferi EF, Black DL. 1997. A complex intronic splicing enhancer from the c-src pre-mRNA activates inclusion of a heterologous exon. Mol. Cell. Biol. 17:6537–45.

34. Blencowe BJ. 2000. Exonic splicing enhancers: mechanism of action, diversity and role in human genetic diseases. Trends Biochem. Sci. 25:106–110.

35. Matlin AJ, Clark F, Smith CWJ. 2005. Understanding alternative splicing: towards a cellular code. Nat. Rev. Mol. Cell Biol. 6:386–398.

36. Black DL. 2003. Mechanisms of alternative pre-messenger RNA splicing. Annu. Rev. Biochem. 72:291–336.

37. Wu S, Romfo CM, Nilsen TW, Green MR. 1999. Functional recognition of the 3′ splice site AG by the splicing factor U2AF35. Nature 402:832–835.

38. Seraphin B, Kretzner L, Rosbash M. 1988. A U1 snRNA:pre-mRNA base pairing interaction is required early in yeast spliceosome assembly but does not uniquely define the 5' cleavage site. EMBO J. 7:2533–2538.

39. Malca H, Shomron N, Ast G. 2003. The U1 snRNP Base Pairs with the 5? Splice Site within a Penta-snRNP Complex. Mol. Cell. Biol. 23:3442–3455.

40. Yeo G, Burge CB. 2004. Maximum entropy modeling of short sequence motifs with applications to RNA splicing signals. J. Comput. Biol. J. Comput. Mol. Cell Biol. 11:377–394.

41. Stickler GB, Belau PG, Farrell FJ, Jones JD, Pugh DG, Steinberg AG, Ward LE. 1965. Hereditary progressive arthro-ophthalmopathy. Mayo Clin. Proc. 40:433–455.

42. Stickler GB, Hughes W, Houchin P. 2001. Clinical features of hereditary progressive arthro-ophthalmopathy (Stickler syndrome): a survey. Genet. Med. Off. J. Am. Coll. Med. Genet. 3:192–196.

43. Bishop PN, Reardon AJ, Mcleod D, Ayad S. 1994. Identification of Alternatively Spliced Variants of Type II Procollagen in Vitreous. Biochem. Biophys. Res. Commun. 203:289–295.

44. Lui VCH, Ng LJ, Nicholls J, Tam PPL, Cheah KSE. 1995. Tissue-Specific and differential expression of alternatively spliced α1(II) collagen mRNAs in early human embryos. Dev. Dyn. 203:198–211.

45. Sandell LJ, Nalin AM, Reife RA. 1994. Alternative splice form of type II procollagen mRNA (IIA) is predominant in skeletal precursors and non-cartilaginous tissues during early mouse development. Dev. Dyn. 199:129–140.

46. Donoso LA, Edwards AO, Frost AT, Ritter III R, Ahmad N, Vrabec T, Rogers J, Meyer D, Parma S. 2003. Clinical Variability of Stickler Syndrome: Role of Exon 2 of the Collagen COL2A1 Gene. Surv. Ophthalmol. 48:191–203.

47. López-Bigas N, Audit B, Ouzounis C, Parra G, Guigó R. 2005. Are splicing mutations the most frequent cause of hereditary disease? FEBS Lett. 579:1900–1903.

48. Sterne-Weiler T, Howard J, Mort M, Cooper DN, Sanford JR. 2011. Loss of exon identity is a common mechanism of human inherited disease. Genome Res. 21:1563–1571.

49. Krawczak M, Thomas NST, Hundrieser B, Mort M, Wittig M, Hampe J, Cooper DN. 2007. Single base-pair substitutions in exon–intron junctions of human genes: nature, distribution, and consequences for mRNA splicing. Hum. Mutat. 28:150–158.

50. Irimia M, Weatheritt RJ, Ellis JD, Parikshak NN, Gonatopoulos-Pournatzis T, Babor M, Quesnel-Vallières M, Tapial J, Raj B, O'Hanlon D, Barrios-Rodiles M, Sternberg MJE, Cordes SP, Roth FP, Wrana JL, Geschwind DH, Blencowe BJ. 2014. A Highly Conserved Program of Neuronal Microexons Is Misregulated in Autistic Brains. Cell 159:1511–1523.

51. Li YI, Sanchez-Pulido L, Haerty W, Ponting CP. 2014. RBFOX and PTBP1 proteins regulate the alternative splicing of micro-exons in human brain transcripts. Genome Res. gr.181990.114.

52. Farkas MH, Grant GR, White JA, Sousa ME, Consugar MB, Pierce EA. 2013. Transcriptome analyses of the human retina identify unprecedented transcript diversity and 3.5 Mb of novel transcribed sequence via significant alternative splicing and novel genes. BMC Genomics 14:486.

53. Hackam AS, Qian J, Liu D, Gunatilaka T, Farkas RH, Chowers I, Kageyama M, Parmigiani G, Zack DJ. 2004. Comparative gene expression analysis of murine retina and brain. Mol. Vis. 10:637–649.

54. Wan J, Masuda T, Hackler L, Torres KM, Merbs SL, Zack DJ, Qian J. 2011. Dynamic usage of alternative splicing exons during mouse retina development. Nucleic Acids Res. 39:7920–7930.

55. Gamsiz ED, Ouyang Q, Schmidt M, Nagpal S, Morrow EM. 2012. Genome-wide transcriptome analysis in murine neural retina using high-throughput RNA sequencing. Genomics 99:44–51.

56. Hertel KJ. 2008. Combinatorial Control of Exon Recognition. J. Biol. Chem. 283:1211–1215.

57. Modafferi EF, Black DL. 1999. Combinatorial control of a neuron-specific exon. RNA 5:687–706.

58. Singh NN, Androphy EJ, Singh RN. 2004. In vivo selection reveals combinatorial controls that define a critical exon in the spinal muscular atrophy genes. RNA 10:1291–1305.

Figure Legends

Figure 1. *Bbs8* transcripts containing exon 2A are specifically expressed in photoreceptor cells. (A) *Bbs8* exon 2A splicing was analyzed by RT-PCR in a panel of mouse tissues. Exon 2A is skipped or included at very low levels in all of the tissues we examined ("+" and "-" indicate exon inclusion and skipping, respectively). Some exon 2A inclusion is detected after overexposing the gel (panel below) in neural tissues from wild type animals. **(B)** RT-PCR analysis of *Bbs8* exon 2A splicing in the retina of wild type, *Aipl1* knockout and *Nrl* knockout animals. Exon 2A is included at high levels in the retina of wild type and *Nrl* knockout mice and is largely skipped in the retina of the *Aipl1* knockout mice. **(C)** Exon 2A inclusion in the mature *Bbs8* transcript is first detected at postnatal day 0 (left), and increases rapidly thereafter. The increase in exon 2A inclusion correlates with the increase in rod opsin expression as detected by qRT-PCR (right). **(D)** Protein extracts from wild type mouse retina, Aipl1 knockout retina, N2A cells transfected with BBS8L expression, and mock transfected N2A cells were probed with rabbit polyclonal antibody raised against a peptide antigen containing the exon 2A sequence (Top) and a pan-BBS8 antibody (Bottom). The BBS8L protein, recognized specifically by the anti-exon 2A antibody, is not detected in the mock transfected N2A cells and is lost in the Aipl1 knockout retina. Similarly, low levels of the BBS8S protein are detected by the pan-BBS8 antibody in Aipl1 knockout retina and mock transfected N2A cells.

Figure 2. The *Bbs8* exon2A minigene recapitulates the splicing of the full length gene. (A) Schematic of the splicing minigene carrying the mouse *Bbs8* exon 2A. The exon and portions of the flanking introns are cloned in the fluorescent reporter minigene (28). The ATG translation start codon of the GFP reading frame is split between the first and last exon of the minigene and is reconstituted when the alternative exon is spliced out. This leads to GFP expression, while

the translation of the downstream RFP reading frame is suppressed. Inclusion of the alternative exon will disrupt the ATG codon of the GFP reading frame, which blocks the GFP protein expression and simultaneously allows the downstream RFP reading frame to be translated. **(B)** RT-PCR analysis of the splicing of the wild type (WT) and mutant (MT) exon 2A minigenes in HEK293 cells and mouse retina. HEK293 cells skip both the wild type and mutant exon 2A from the mature transcripts (skipped isoform labeled A). In retina, the wild type exon 2A is included in the majority of transcripts. The major splice product of the mutant minigene, labeled D, is inclusion of truncated exon that utilizes the same cryptic splice site as the exon in the context of the full length human *BBS8* gene. A second high molecular weight splice product, labeled *C*, is derived from the use of a cryptic splice site upstream of exon 2A. **(C)** Sequence of the mouse *Bbs8* exon 2A and portions of the adjacent introns. The mutation in the 3'splice site is underlined. The exon included in the minigene mRNA is outlined with white (splice product *B*), dark gray (splice product *D*) and light gray (splice product *C*) boxes. Black arrow indicates the position of the wild type 3' splice site. White arrows indicate the positions of the cryptic 3' and 5' splice sites that are activated in the mutant minigene.

Figure 3. Photoreceptor specific splicing of exon 2A in the context of the *Bbs8* minigene. Retinal sections from animals after electroporation with indicated minigenes were imaged for GFP (Green) and RFP (Red). The nuclei are stained by DAPI (Blue). ONL, INL and GCL indicate outer nuclear, inner nuclear and ganglion cell layer, respectively. The RT-PCR analysis of minigene splicing in the retina is shown on the left. The percent exon inclusion ± standard error is shown under each gel image. **(A)** The wild type exon 2A is included in photoreceptors as indicated by the high RFP expression observed on immunofluorescence and by RT-PCR analysis of total retinal RNA ("+" and "-" indicate exon inclusion and skipping, respectively). In contrast, higher GFP expression in the inner neurons demonstrates skipping of exon 2A in these cells (indicated by yellow arrows). **(B)** Similar to the wild type exon 2A, the exon included

products from the mutant exon 2A are specifically detected in photoreceptors and not inner neurons . The Dup34 and Dup51 exons show uniform fluorescent protein expression throughout the retina (Bottom two panels; inner neurons are indicated by yellow arrows). Both Dup34 **(C)** and Dup51 **(D)** produce unspliced RNA (indicated by "~" next to the RT-PCR gel). This unspliced RNA does not express RFP or GFP, because a small ORF in the downstream intron inhibits the translation of the downstream RFP reading frame (28).

Figure 4. Inclusion of a truncated exon 2A in *BBS8* patient mutation linked to RP. (A) Schematic of the wild-type BAC clones containing the full length human *BBS8* gene. The mutant BAC clone harbors an IVS1-2A>G mutation in the 3' splice of exon 2A. **(B)** RT-PCR analysis of the splicing of the BAC transcripts in mouse retina at P16 after electroporation at P0 using primers specific to the human *BBS8* sequence. The wild type BAC produces the exon 2A included isoform of the mature *BBS8* mRNA. The mutation causes the inclusion of a shorter exon 2A* in the mature mRNAs. Also indicated on the right is the minor isoform that excludes exon 2A in retina electroporated with both wild type and mutant *BBS8* BAC. **(C)** Genomic sequence of exon 2A and the adjacent introns showing the mutated splice site (underlines), the 3'-splice sites being used for the wild type (black arrow) and the mutant (open arrow) exons. The sequence of the exon being spliced is outlined with a white (wild type) or gray (mutant) box.

Figure 5. The sequence of *Bbs8* exon 2A does not control its splicing. (A) Sequences of the wild type *Bbs8* exon 2A along with the sequences of the exon in mutant *Bbs8* minigenes. Four linker scanning mutants were created by substituting overlapping 8 nucleotide (nt) segments of the exon with a PvuI linker (the linker sequences is shown in bold). Two minigenes scramble the sequence of nucleotides 2 to 27 (Core-Scr) or mutate nucleotides 1, 28, 29 and 20 (Edge-Scr) of the *Bbs8* exon 2A. The mutated nucleotides are shown in bold. In *Bbs8*-Dup34 exon 2A is replaced by the Dup34 exon, while preserving the *Bbs8* introns. **(B)** RT-PCR analysis of the splicing of the linker scanning minigenes in the retina at postnatal day 16, and in

N2A cells 48 hours post transfection. All linker scanning mutants are included at high rate in the retina and skipped in N2A cells ("+" and "-" indicate exon inclusion and skipping, respectively). **(C)** RT-PCR and fluorescence microscopy analysis of the splicing of the Core-SCR, *Bbs8*-Dup34 and Edge-SCR minigenes in mouse retina. Each panel represents fluorescence microscopy images of the retinal sections accompanied by RT-PCR analysis of the minigene splicing. The percent exon inclusion ± standard error is shown under each gel image. The Core-SCR and *Bbs8*-Dup34 exons are included at high rate in the photoreceptors and skipped from the minigene transcripts in the inner neurons (indicated by yellow markers). The Edge-SCR exon is skipped uniformly throughout the retina.

Figure 6. Intronic splicing enhancers promote exon 2A splicing in photoreceptor cells. **(A)** Schematic showing the positions six 100nt intronic deletions relative to *Bbs8* exon 2A. **(B)** RT-PCR analysis of the splicing of the intron deletion minigenes in mouse retina. The percent exon inclusion ± standard error is shown under each gel image. Most deletions with exception of D3 and D4 do not affect significantly the splicing of *Bbs8* exon 2A. D3 and D4 cause reduction of *Bbs8* exon inclusion ("+" and "-" indicate exon inclusion and skipping, respectively). In addition, the D3 mutant expresses significant amounts of mRNA which retains the upstream intron (indicated by "~"). The numbers under the gel images represent the percent of the transcripts including the exon and the standard error. **(C)** The simultaneous deletion of segments 3 and 4 reduces exon 2A inclusion levels in the retina to 23% (RT-PCR analysis gel shown on the left), which is accompanied by increase of GFP and reduction of RFP expression in the photoreceptor cells (right). The yellow marker points to an inner neuron. **(D)** Schematic showing the relative positions of six 40nt deletions within the sequence of segments D3 and D4. **(E)** The 40nt deletions shown on panel D do not alter *Bbs8* exon inclusion in the retina as detected by RT-PCR. The percent exon inclusion ± standard error is shown under each gel image.

Figure 7. Model explaining the confinement of the phenotype of the *BBS8* IVS1-2A>G mutation to photoreceptor cells. *BBS8* exon 2A is included specifically in the photoreceptor cells to produce BBS8L protein. All other cell types skip exon 2A and produce the shorter BBS8S protein. Disruption of the exon 2A splice site by the IVS1-2A>G mutation causes the use of a cryptic splice site, resulting in frameshift. As a result of the frameshift, the *BBS8* reading frame will end with a premature termination codon (PTC) in exon 2. As BBS8L is the exclusive isoform in photoreceptors, the mutation ultimately results in elimination of the BBS8 protein from this cell type. All other cell types are immune to the mutation as they skip exon 2A and do not utilize the cryptic splice site.

Figure 1

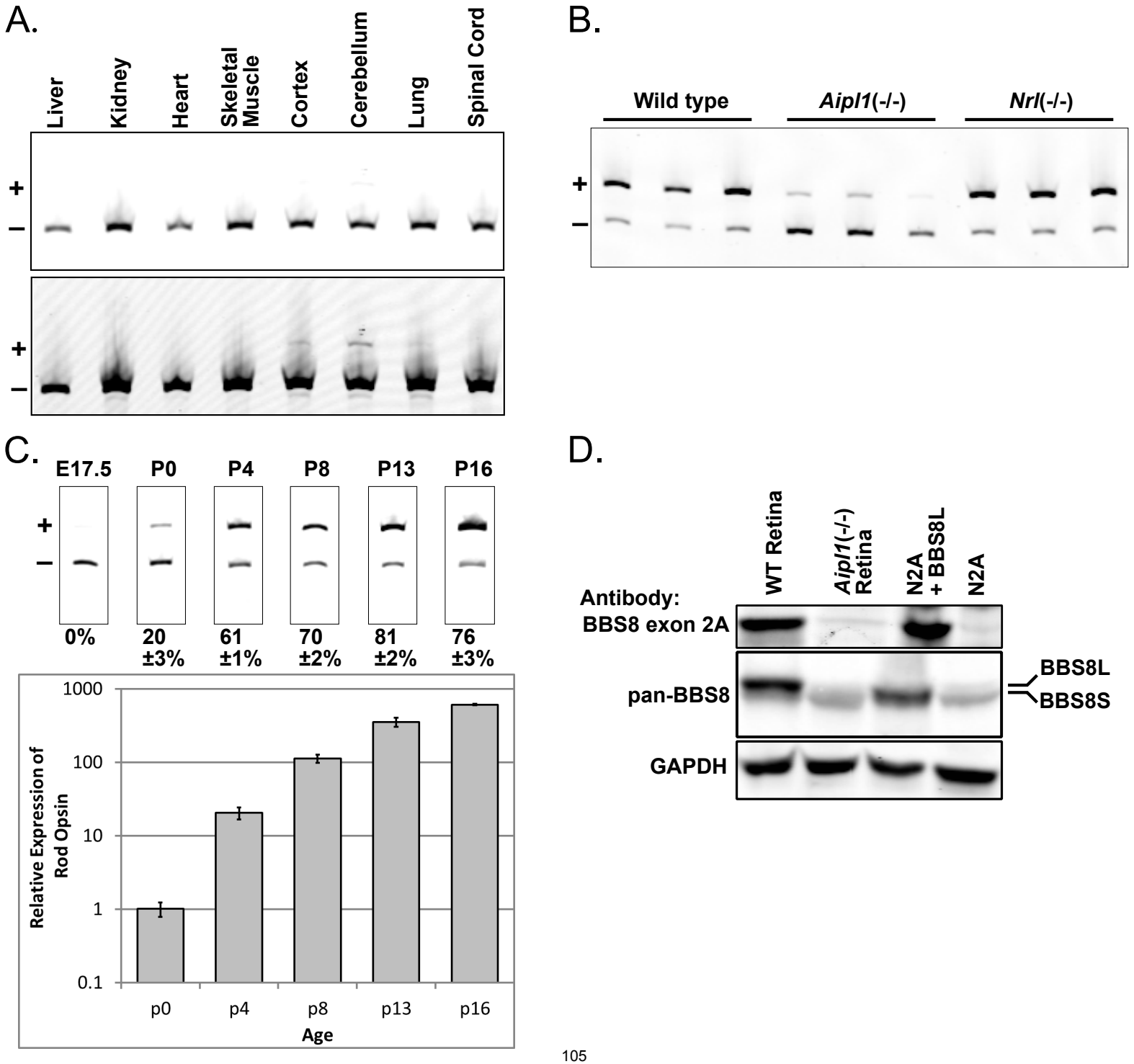
A.
Liver
Kidney
Heart
Skeletal Muscle
Cortex
Cerebellum
Lung
Spinal Cord
+
–
+
–
B.
Wild type
Aipl1(-/-)
Nrl(-/-)
+
–
C.
E17.5
P0
P4
P8
P13
P16
+
–
0%
20 ±3%
61 ±1%
70 ±2%
81 ±2%
76 ±3%
Relative Expression of Rod Opsin
1000
100
10
1
0.1
p0
p4
p8
p13
p16
Age
D.
WT Retina
Aipl1(-/-) Retina
N2A + BBS8L
N2A
Antibody:
BBS8 exon 2A
pan-BBS8
BBS8L
BBS8S
GAPDH

Figure 2

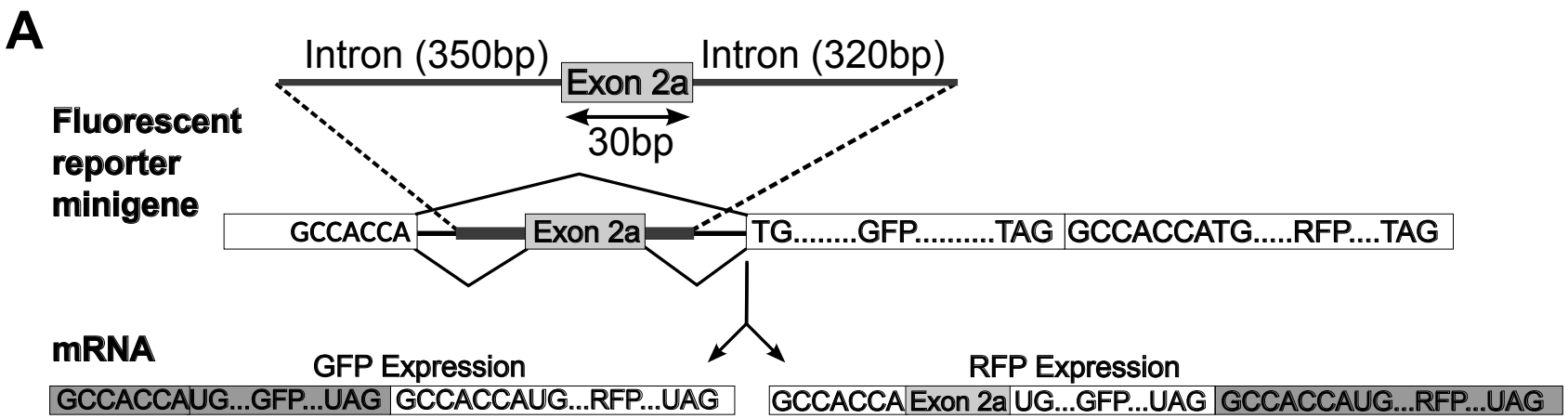

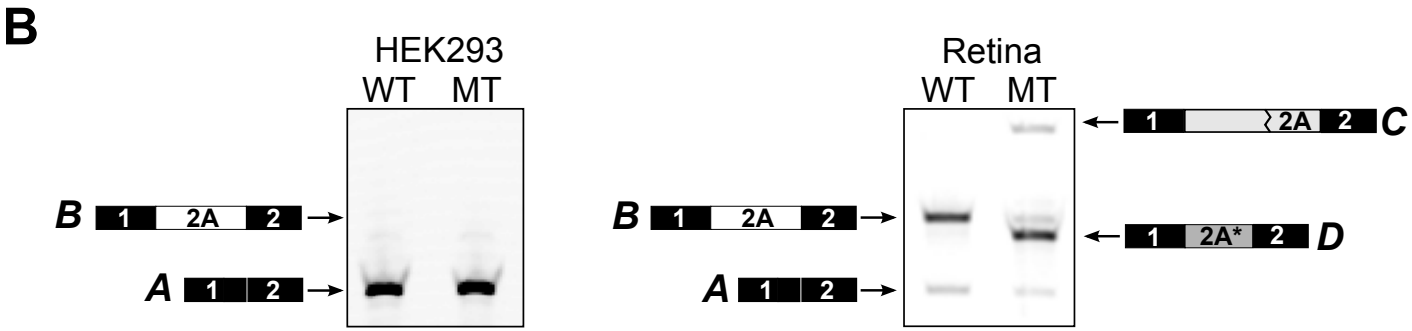

C

WT

Splice product B

TCTTCAGAAATTGCATGCCTTAAAAATGTTTACAACCTTCTTAACGCTTTCCAGGAACCAGCTCCTGATTTGCCAGTGTCTCAGGTAAAAAGTTAGC

MT

Splice product D

TCTTCAGAAATTGCATGCCTTAAAAATGTTTACAACCTTCTTAACGCTTTCCGGGAACCAGCTCCTGATTTGCCAGTGTCTCAGGTAAAAAGTTAGC

Splice product C

TCTTCAGAAATTGCATGCCTTAAAAATGTTTACAACCTTCTTAACGCTTTCCGGGAACCAGCTCCTGATTTGCCAGTGTCTCAGGTAAAAAGTTAGC

Figure 3.

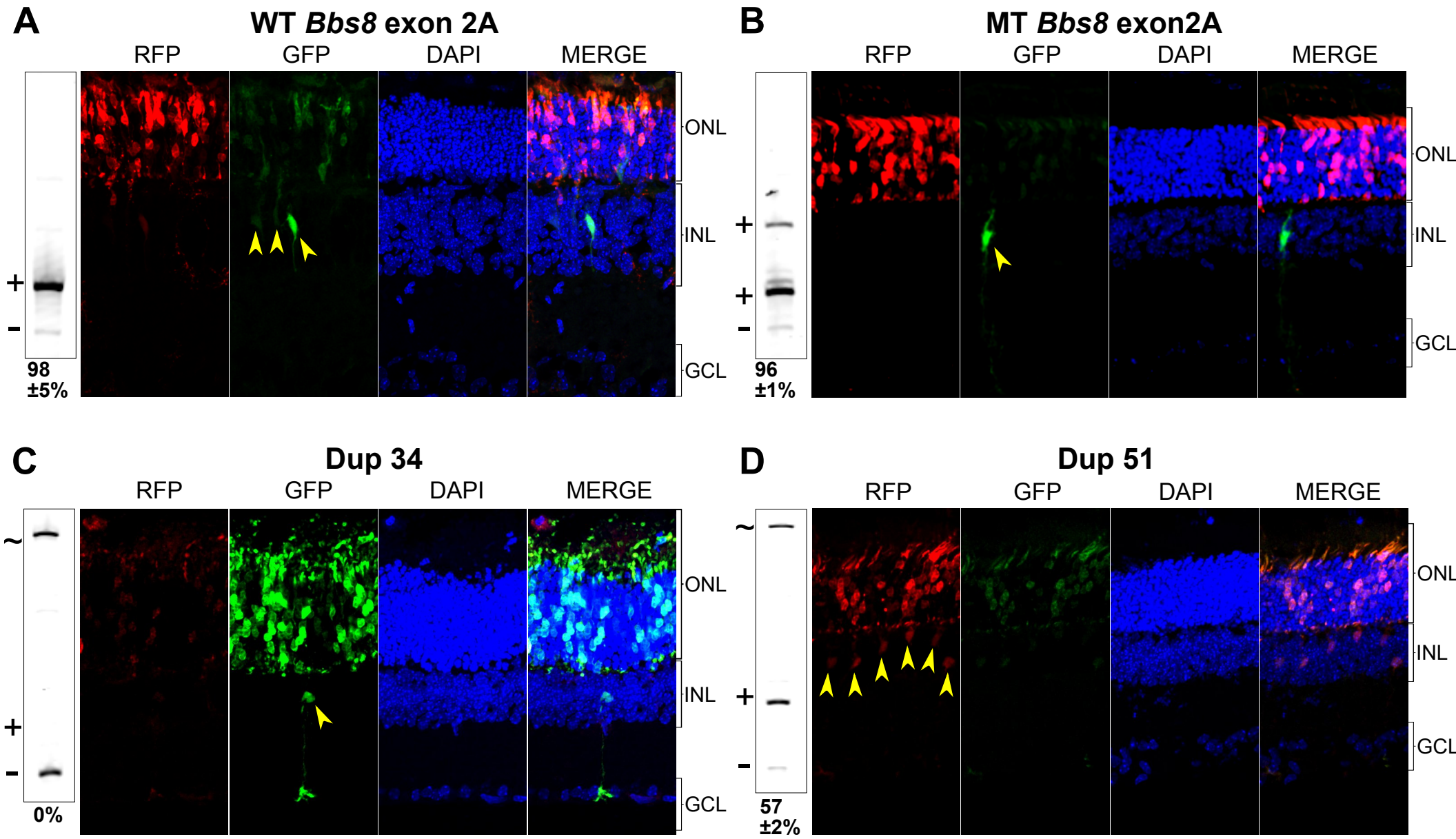
A
WT Bbs8 exon 2A
RFP
GFP
DAPI
MERGE
ONL
INL
GCL
+
-
98
±5%
B
MT Bbs8 exon2A
RFP
GFP
DAPI
MERGE
ONL
INL
GCL
+
+
-
96
±1%
C
Dup 34
RFP
GFP
DAPI
MERGE
ONL
INL
GCL
~
+
-
0%
D
Dup 51
RFP
GFP
DAPI
MERGE
ONL
INL
GCL
~
+
-
57
±2%

Figure 4

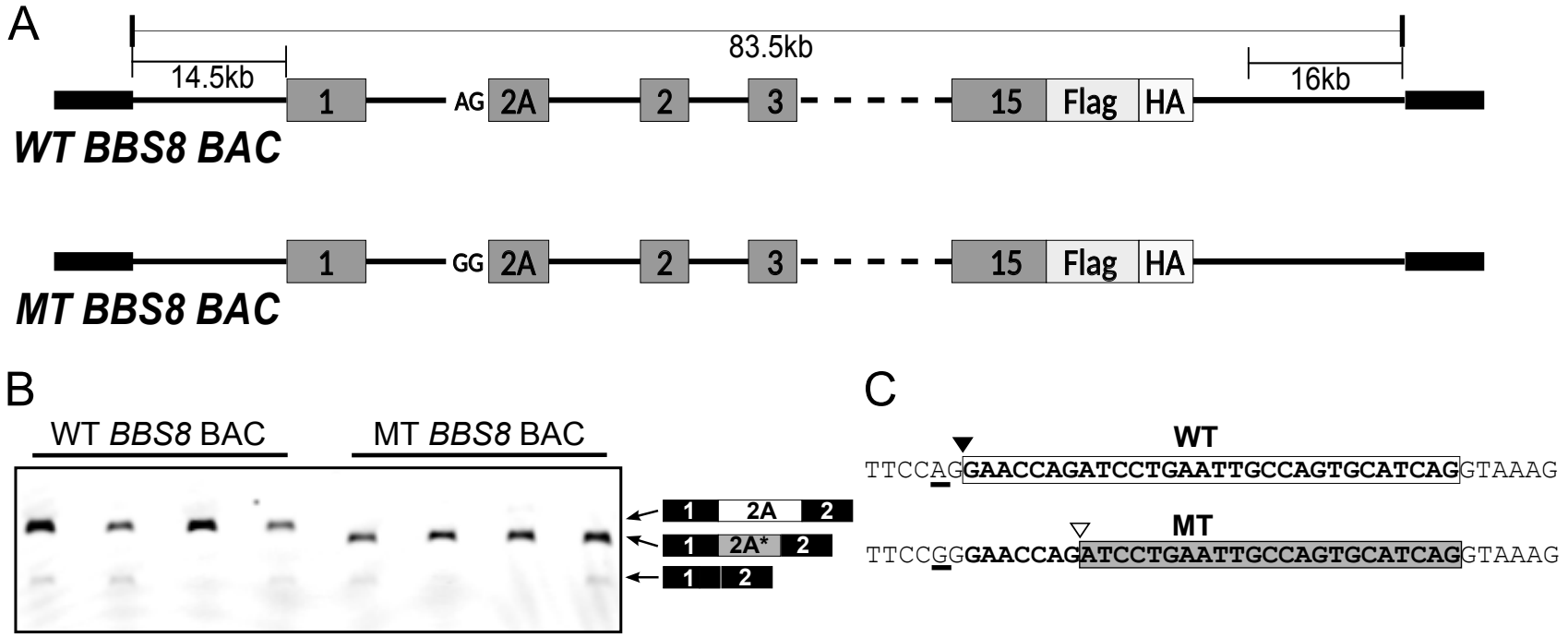
A
83.5kb
14.5kb
16kb
1
AG
2A
2
3
15
Flag
HA
WT BBS8 BAC
1
GG
2A
2
3
15
Flag
HA
MT BBS8 BAC
B
WT BBS8 BAC
MT BBS8 BAC
1
2A
2
1
2A*
2
1
2
C
WT
TTCCAGGAACCAGATCCTGAATTGCCAGTGCATCAGGTAAAG
MT
TTCCGGGAACCAGATCCTGAATTGCCAGTGCATCAGGTAAAG

Figure 5

A.

Bbs8 Exon2A GAACCAGCTCCTGATTTGCCAGTGTCTCAG
LS1 G**ACGATCG**TCCTGATTTGCCAGTGTCTCAG
LS2 GAACCAG**ACGATCG**TTTGCCAGTGTCTCAG
LS3 GAACCAGCTCCTG**ACGATCG**TGTGTCTCAG
LS4 GAACCAGCTCCTGATTTGC**ACGATCG**TCAG
Core-SCR G**ATTACTAGTTCCGGCGTTACACTCGC**CAG
Edge-SCR **T**AACCAGCTCCTGATTTGCCAGTGTCT**GTC**
Bbs8-Dup34 GCTGCTGGTGGTGCCATGGCAGGCCCTGGGCAG

B.

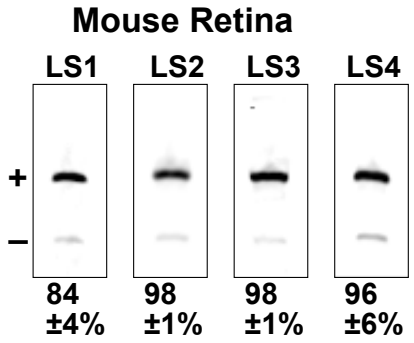

C.

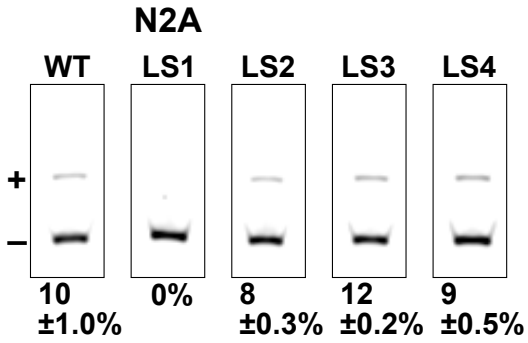

D.

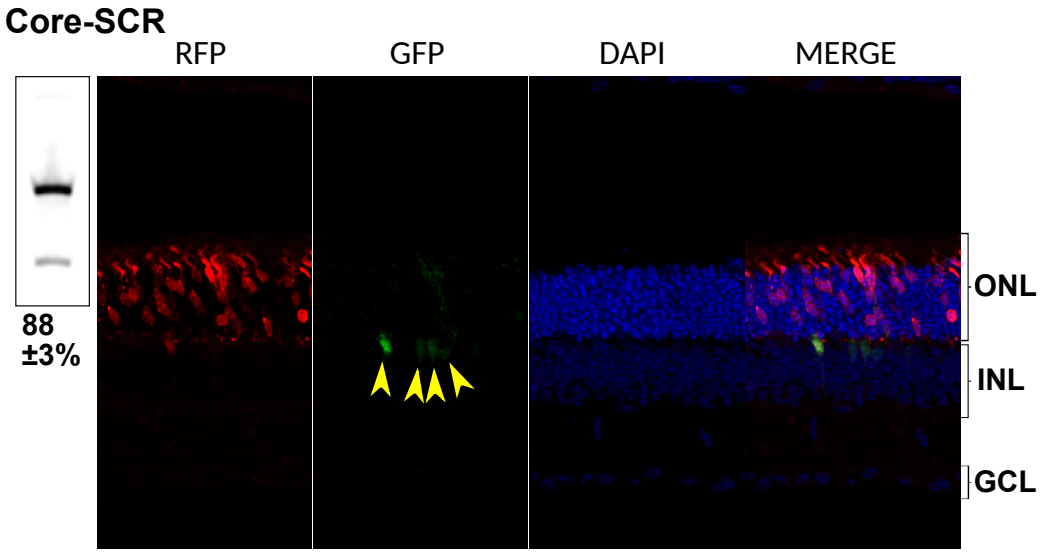

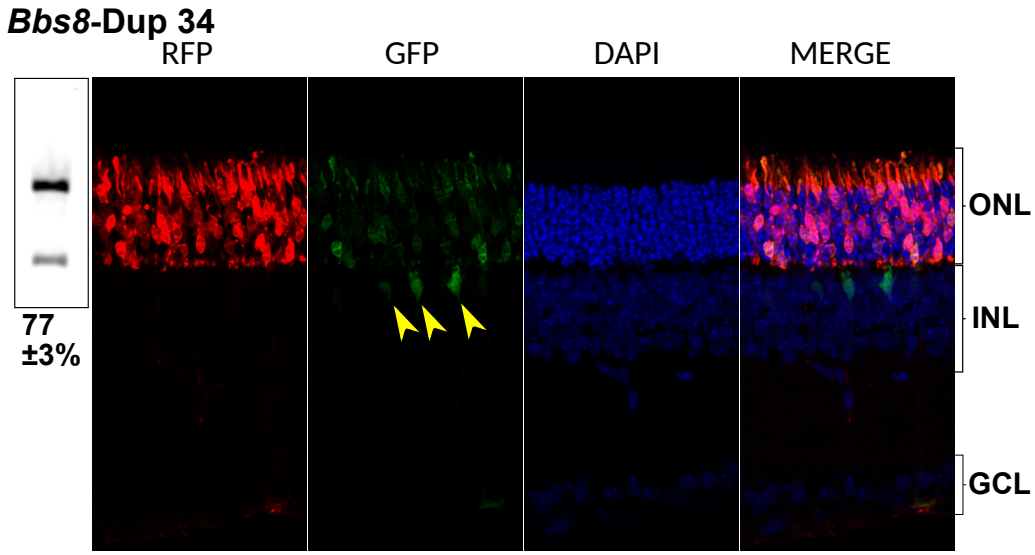

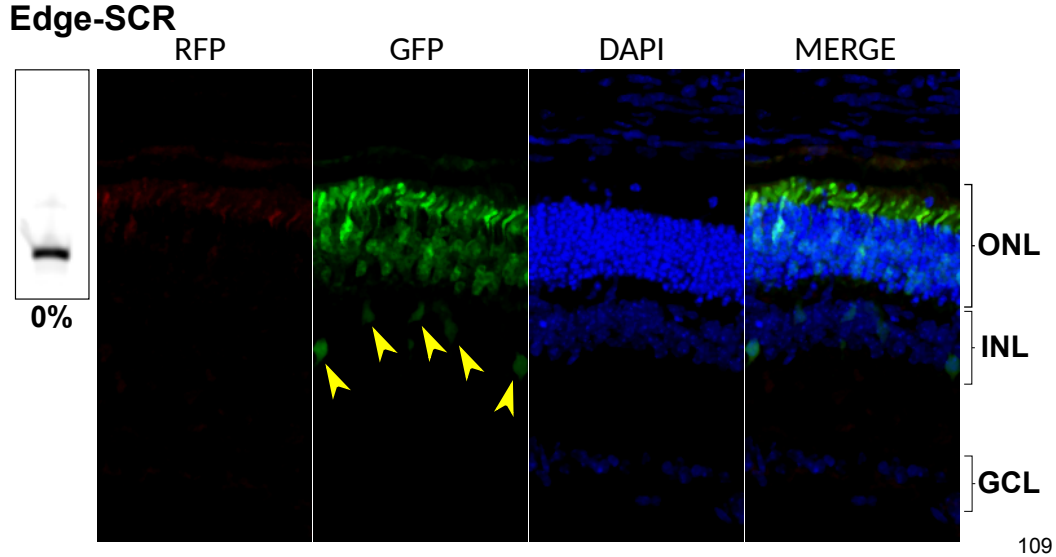

Figure 6

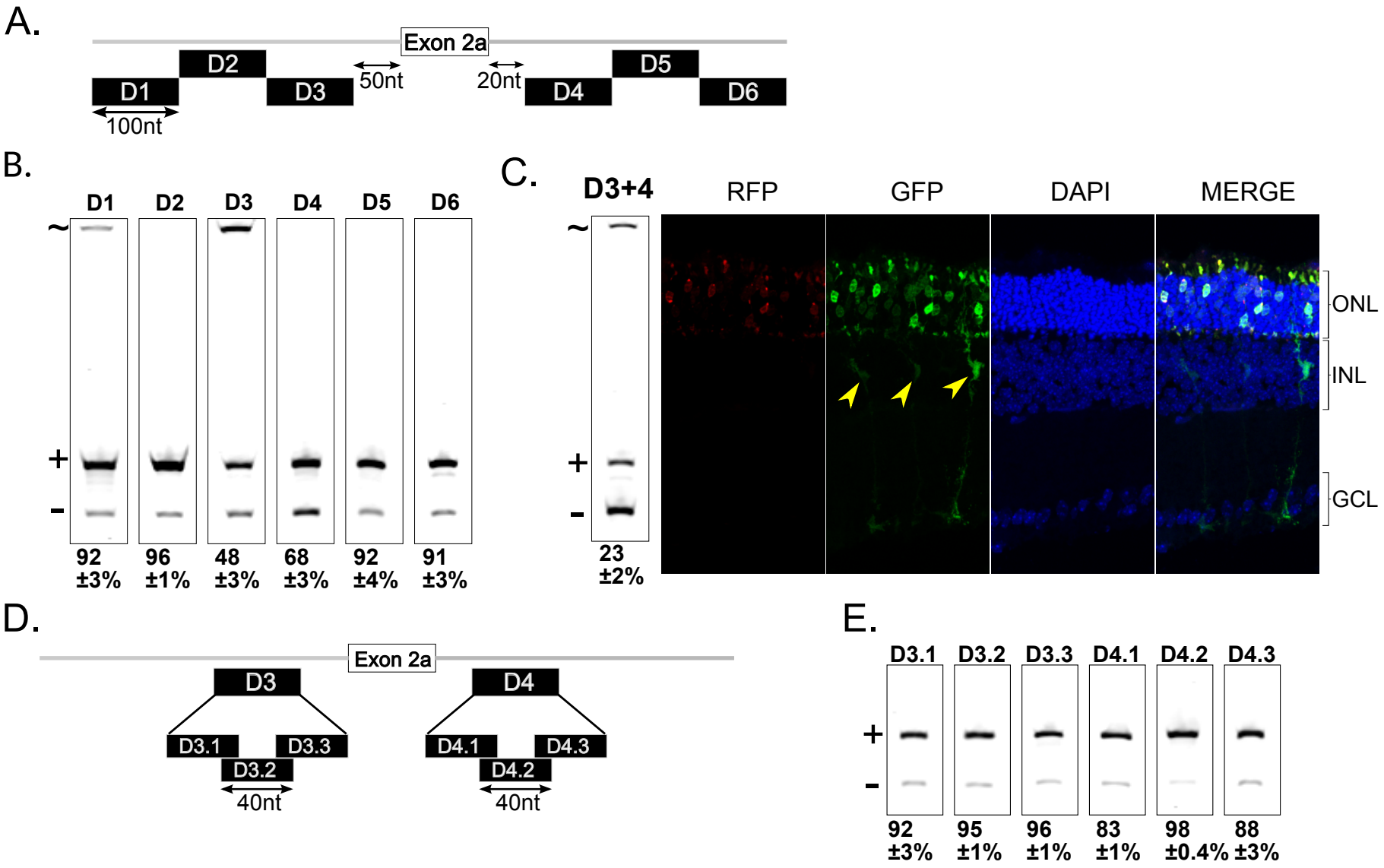
A.
Exon 2a
D1
D2
D3
D4
D5
D6
50nt
20nt
100nt
B.
D1
D2
D3
D4
D5
D6
~
+
-
92 ±3%
96 ±1%
48 ±3%
68 ±3%
92 ±4%
91 ±3%
C.
D3+4
RFP
GFP
DAPI
MERGE
~
+
-
23 ±2%
ONL
INL
GCL
D.
Exon 2a
D3
D4
D3.1
D3.3
D3.2
D4.1
D4.3
D4.2
40nt
40nt
E.
D3.1
D3.2
D3.3
D4.1
D4.2
D4.3
+
-
92 ±3%
95 ±1%
96 ±1%
83 ±1%
98 ±0.4%
88 ±3%

Figure 7

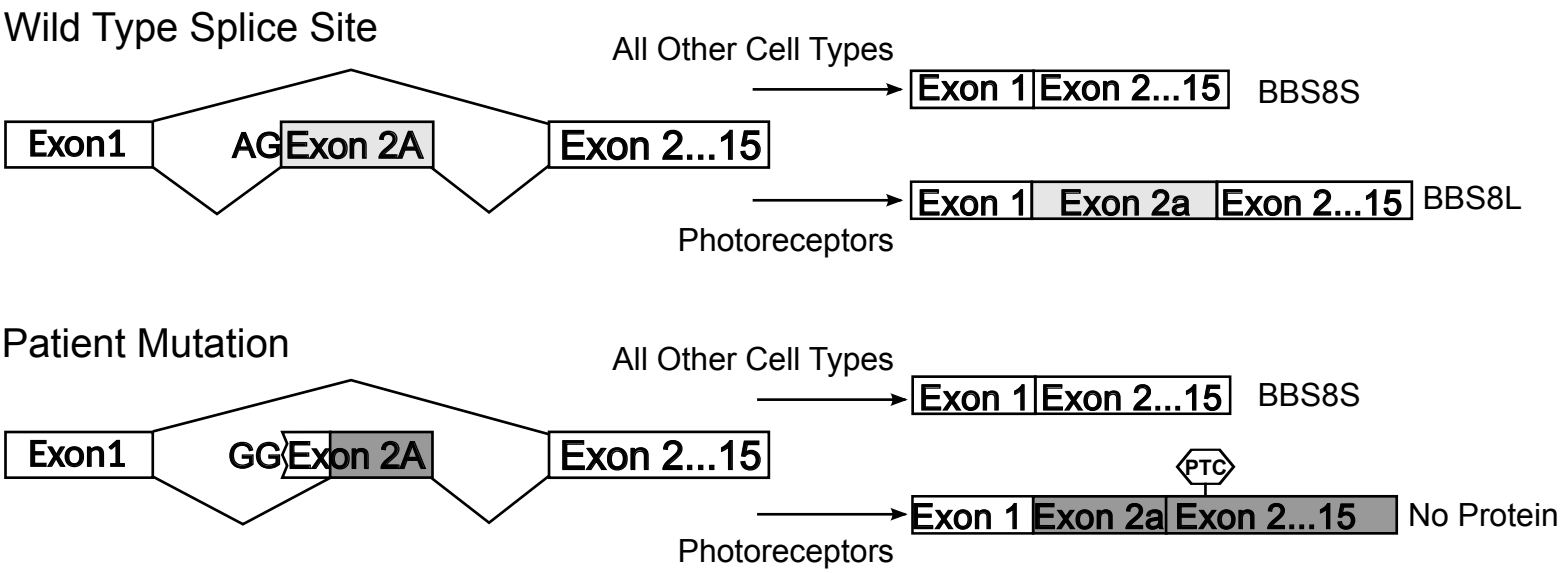
Wild Type Splice Site
All Other Cell Types
Exon1
AG
Exon 2A
Exon 2...15
Exon 1
Exon 2...15
BBS8S
Exon 1
Exon 2a
Exon 2...15
BBS8L
Photoreceptors

Patient Mutation
All Other Cell Types
Exon1
GG
Exon 2A
Exon 2...15
Exon 1
Exon 2...15
BBS8S
PTC
Exon 1
Exon 2a
Exon 2...15
No Protein
Photoreceptors

SUPPLEMENTARY MATERIAL

Tables

Supplementary table 1. Number of replicates used in the RT-PCR experiments.

Minigene electroporated into mouse retina	Figure #	Replicates (animals)
WT Bbs8	3	4
A>G Mutant Bbs8	3	6
D1	6	9
D2	6	5
D3	6	5
D4	6	7
D5	6	5
D6	6	8
D3.1	6	7
D3.2	6	6
D3.3	6	8
D4.1	6	8
D4.2	6	6
D4.3	6	9
LS1	5	5
LS2	5	10
LS3	5	6
LS4	5	8
EdgeScR	5	7
CoreScr	5	5
D3+4	6	8
pFlare Dup 51	3	10
pFlare Dup 34	3	3
Bbs8 Dup 34	4	4
Minigenes transfected into N2a cells	**Figure #**	**Replicates (independent transfections)**
Bbs8 WT	5	3
LS1	5	3
LS2	5	3
LS3	5	3
LS4	5	3

Supplementary Table 2. Primer Sequences

pFlare Minigene Primers			
Gene name	**Primer name**	**Sequence**	**Label**
pFlare-minigenes	EGFP-N-R-FAM	cgtcgccgtccagctcgacca	FAM
pFlare-minigenes	Dup-e1-bgl-F	aaacagatctaccattggtgc	none

Real-Time PCR Primers			
Species	**Gene name**	**Primer name**	**Primer sequence**
mouse	Rho	mRhodopsin-Left	AGGGCTTCTTTGCCACACTT
mouse	Rho	mRhodopsin-Right	CACACCCATGATAGCGTGAT
mouse	Pde6a	mPDE6a-Left	CCGACTCCGAGATTGTCTTC
mouse	Pde6a	mPDE6a-Right	CCACGAAGTCACAGAAATGC
mouse	Gnat1	Gnat1-F	TGCCATCATCTACGGCAACACTCT
mouse	Gnat1	Gnat1-R	CTTGGGCATTGTGCCTTCCTCAAT
mouse	Gnat2	FP900	AACTACCTCCCTAACGAGCAG
mouse	Gnat2	RP901	GGCCGCACAGAAAATGATGC
mouse	Pde6c	FP902	CAGTTTGAAACGGTGATCCA
mouse	Pde6c	RP903	CGGGTCGGAGGTTACGTATT
mouse	Gapdh	mGAPDH-Left	GGTCCTCAGTGTAGCCCAAG
mouse	Gapdh	mGAPDH-Right	AATGTGTCCGTCGTGGATCT
mouse	Actb	mActB-Left	ACGATGGAGGGGAATACAGC
mouse	Actb	mActB-Right	CTTTGCAGCTCCTTCGTTG
mouse	GusB	mGusB-Left	CAGCCAATAAAGTCCCGAAG
mouse	GusB	mGusB-Right	GGTTTCGAGCAGCAATGGTA

Cloning Primers			
Primer Name	**Minigene Name**	**Primer Sequence**	
mBbs8-F-Eco	WT (mouse)	actgaaTTCgcagtaaaggcttgctgagg	
mBbs8-R-Bam	WT (mouse)	actggatccgcccagctccctctaaagtc	
mBbs8-GG-F	A>G mutant	aacgctTTCcggGAACCAGCTCCTG	

	(mouse)	
mBbs8-GG-R	A>G mutant (mouse)	CAGGAGCTGGTTCccggaaagcgtt
D1-100-F-Eco	D1	actgaaTTCTGCAAACTCTAGGTTGAGTGA
D2-100-200-F	D2	ccacgctagctgacttAGGCAAAATAAGCCACACCC
D2-100-200-R	D2	tggcttattttgcctAAGTCAGCTAGCGTGGCTGTT
D3-200-300-F	D3	ctcccgccatgtgcacCAGAAATTGCATGCCTTAAAA
D3-200-300-R	D3	aggcatgcaatTTCtgGTGCACATGGCGGGAGGAGAA
D4-400-500-F	D4	aagttagctgcaaactTACCAGCTGTTCTGTTTTTTT
D4-400-500-R	D4	aacagaacagctggtaAGTTTGCAGCTAACTTTTTAC
D5-500-600-F	D5	aaacttagctgcatctACTGAGGCTTGGGGCTTCAGT
D5-500-600-R	D5	agccccaagcctcagtAGATGCAGCTAAGTTTCTAAT
D6-600-700-R-Bam	D6	actggatccACTGAAGCCCCAAGCCTCAGT
Bbs8_LS1_2-9-F	LS1	CTTAACGCTTTCCAGGacgatcgtCCTGATTTGCCAGTGTCTCAG
Bbs8_LS1_2-9-R	LS1	ACACTGGCAAATCAGGacgatcgtCCTGGAAAGCGTTAAGAAGGT
Bbs8_LS1_7-15-F	LS2	GCTTTCCAGGAACCAGacgatcgtTTGCCAGTGTCTCAGGTAAAA
Bbs8_LS1_7-15-R	LS2	CCTGAGACACTGGCAAacgatcgtCTGGTTCCTGGAAAGCGTTAA
Bbs8_LS1_13-21-F	LS3	CAGGAACCAGCTCCTGacgatcgtGTGTCTCAGGTAAAAAGTTAG
Bbs8_LS1_13-21-R	LS3	TTTTTACCTGAGACACacgatcgtCAGGAGCTGGTTCCTGGAAAG
Bbs8_LS1_19-27-F	LS4	CCAGCTCCTGATTTGCacgatcgtCAGGTAAAAAGTTAGCTGCAA
Bbs8_LS1_19-27-R	LS4	GCTAACTTTTTACCTGacgatcgtGCAAATCAGGAGCTGGTTCCT
D3.1-200-240-F	D3.1	ctcccgccatgtgcacGCACACATACATTTAATATTT

D3.1-200-240-R	D3.1	ttaaatgtatgtgtgcGTGCACATGGCGGGAGGAGAA
D3.2-230-270-F	D3.2	acacccatgcatatgcTTGATTAATACTCATTAAGAC
D3.2-230-270-R	D3.2	aatgagtattaatcaaGCATATGCATGGGTGTGGCTT
D3.3-260-300-F	D3.3	catacatttaatatTTCAGAAATTGCATGCCTTAAAA
D3.3-260-300-R	D3.3	aggcatgcaatTTCtgAAATATTAAATGTATGTGTGC
D4.1-400-440-F	D4.1	aagttagctgcaaacTTCCTGAAGATTGGAAAATGTG
D4.1-400-440-R	D4.1	tTTCcaatcTTCaggaAGTTTGCAGCTAACTTTTTAC
D4.2-430-470-F	D4.2	agcttagttgctgtcgCGCTCATAGTATTAGAAACTT
D4.2-430-470-R	D4.2	tctaatactatgagcgCGACAGCAACTAAGCTACTCT
D4.3-460-500-F	D4.3	aagattggaaaatgtgTACCAGCTGTTCTGTTTTTTT
D4.3-460-500-R	D4.3	aacagaacagctggtaCACATTTTCCAATCTTCAGGA
D5.1-500-540-F	D5.1	aaacttagctgcatctTTCATATTCCTAAACCTTTTA
D5.1-500-540-R	D5.1	ggtttaggaatatgaaAGATGCAGCTAAGTTTCTAAT
D5.2-530-570-F	D5.2	ttttttttattgtgtCTAGCCTTGTAGAACTAGTGT
D5.2-530-570-R	D5.2	agTTCtacaaggctagACACAATAAAAAAAAAACAGA
D5.3-560-600-F	D5.3	aTTCctaaacctttaACTGAGGCTTGGGGCTTCAGT

D5.3-560-600-R	D5.3	agccccaagcctcagtTAAAAGGTTTAGGAATATGAA
D6.1-600-640-F	D6.1	tagtgtgaactgcttaTAGGATGGGGAGAAGAAGGAA
D6.1-600-640-R	D6.1	tcTTCtccccatcctaTAAGCAGTTCACACTAGTTCT
D6.2-630-670-F	D6.2	TTCagtaacgattgccATAGTAGTATCAGACTTTAGA
D6.2-630-670-R	D6.2	agtctgatactactatGGCAATCGTTACTGAAGCCCC
D6.3-660-700-F	D6.3	tggggagaagaaggaaGCGGATCCATAGTCGACCACC
D6.3 Reverse-Bam	D6.3	GATCCATAGTCGACCACCATGGTGGCTTA
BBS8-F-Mlu1	WT (human)	actACGCGTcttatttttgaataaaagga
BBS8-R-Bam	WT (human)	actggatcccgctccctTTCtaagccctt
BBS8-A>G-F	A>G mutant (human)	TTCttaatgctTTCcGgGAACCAGATCCTGAATTGCC
BBS8-A>G-R	A>G mutant (human)	ATTCAGGATCTGGTTCcCggaaagcattaagaaggca
Bbs8-ExonDup51-F	DUP51 fusion	GCTGCTGGGCAAGGTGAACGTGGATGAAGTTGGTGGTGAGGCCCTGGGCAGgtaaaaagttagctgcaaact
Bbs8-ExonDup51-R	DUP51 fusion	CTGCCCAGGGCCTCACCACCAACTTCATCCACGTTCACCTTGCCCAGCAGCctggaaagcgttaagaaggtt
Bbs8-ExonDup34-F	DUP34 fusion	GCTGCTGGTGGTGCcATGgcAGGCCCTGGGCAGgtaaaaagttagctgcaaact
Bbs8-ExonDup34-R	DUP34 fusion	CTGCCCAGGGCCTgcCATgGCACCACCAGCAGCctggaaagcgttaagaaggtt
NewScr-Exon-F	Core-SCR	GattactagTTCcggcgttacactcgcCAGgtaaaaagttagctgcaaact

NewScr-Exon-R	Core-SCR	CTGgcgagtgtaacgccggaactagtaatCctggaaagcgttaagaaggtt
EdgeScr-Exon-F	Edge-SCR	TAACCAGCTCCTGATTTGCCAGTGTCTGTCgtaaaaagttagctgcaaact
EdgeScr-Exon-R	Edge-SCR	GACAGACACTGGCAAATCAGGAGCTGGTTActggaaagcgttaagaaggtt

Fluorescent PCR for alternative splicing detection										
Species	**Primer Set**	**Alt exon position**	**Alt exon types**	**Alt exon sizes**	**Primer name**	**Primer sequence**	**direction**	**Label**	**Skipped PCR size**	**Included PCR size**
mouse	mBbs8	chr12:98,937,120-98,937,149	CA	30	mBbs8-F	GGGCCTGGAGCTATTTTAGA	F	FAM	236	266
mouse	mBbs8	chr12:98,937,120-98,937,149	CA	30	mBbs8-R	GCCAGGGAGCBbsAAAGATG	R	none	236	266
human	hBBS8	chr14:89,300,037-89,300,066	CA	30	BBS8-F	TGGCCTGGAGCTATTTTAGG	F	FAM	236	266
human	hBBS8	chr14:89,300,037-89,300,066	CA	30	BBS8-R	TCCAGGGAGTBbsAAAGACG	R	none	236	266

Supplementary Figure Legends

Supplementary Figure 1. Rod and cone marker gene expression in wild type, *Aipl1* (-/-) and *Nrl* (-/-) mice. RT-qPCR quantification of the cone (*Opn1sw*, *Gnat2* and *Pde6c*) and rod (*Rho*, *Gnat1*, *Pde6a*) markers. The values are normalized to the expression levels in the *Aipl1* (-/-) retina. Each bar is an average of three animals. The cone marker expression is significantly upregulated in the *Nrl* (-/-) retina as it is enriched in cone photoreceptor cells, compared to the wild type (3% cones) retina. The rod markers have highest expression in the wild type retina (97% rods) and are lost in the *Nrl* (-/-) retina. In contrast, expression of both rod and cone markers are absent in the *Aipl1*(-/-) retinas supporting the loss of photoreceptor cells.

Supplementary Figure 2. *Bbs8* exon 2A splicing of reporter minigene in mouse retina. These additional images were collected from retinal sections from four different mice. Panel A shows unstained retinal sections. Panels B, C and D show sections stained with the photoreceptor marker Pdc, the bipolar neuron marker Chx, and the amacrine and ganglion neuron marker Pax 6, respectively. The Pdc, Chx and Pax6 markers outline the positions of the photoreceptor and neuronal layers in the retina. Inner neurons expressing the minigene are indicated by yellow markers. All inner neurons express high GFP to RFP ratio, which is indicative of exon skipping. In contrast, photoreceptor cells express high levels of RFP (low GFP to RFP ratio), indicative of exon inclusion.

Supplementary Figure 3. *Bbs8* mutant (IVS1-2A>G) exon 2A splicing of reporter minigene in mouse retina. These additional images were collected from retinal sections from four different animals. Panel A shows unstained retinal sections. Panels B, C and D show sections stained with the photoreceptor marker Pdc, the bipolar neuron marker Chx, and the amacrine and ganglion neuron marker Pax 6, respectively. The Pdc, Chx and Pax6 markers outline the positions of the photoreceptor and neuronal layers in the retina. Inner neurons expressing the minigene are indicated by yellow markers. The blue marker points to a Mueller glia cell. A total of 7 inner neurons and one Mueller glia cell can be observed, all of which express high GFP to RFP ratio, which is indicative of exon skipping. In contrast all photoreceptors express high levels of RFP (low GFP to RFP ratio), indicative of exon inclusion.

Supplementary Figure 4. Mouse retina electroporated with the splicing reporter minigene carrying the Dup34 and Dup51 exons. These additional images were collected from retinal sections from two mice. Inner neurons expressing the minigene are indicated by yellow markers. The Dup34 exon is skipped resulting GFP expression, while Dup51 is mostly included producing high levels of RFP. Both Dup34 and Dup51 exons are included at the same rate in photoreceptors and inner neurons.

Supplementary Figure 5. Sequencing traces of the RT-PCR products produced by amplification of the wild type and mutant *Bbs8* transcripts. The exon boundaries are marked by black arrows. The position of the 7 nucleotide deletion in the transcript from the mutant gene relative to the wild type transcript is shown by dotted line.

Supplementary Figure 6. Mouse retina electroporated with the splicing reporter minigene carrying the Core-SCR exon. The images were collected from retinal sections from three mice. Inner neurons expressing the minigene are indicated by yellow markers. Blue markers point to the Mueller glia cells. A total of 12 inner neurons and two Mueller glia cells can be observed, all of which express high GFP to RFP ratio, which is indicative of exon skipping. In contrast,

photoreceptor cells express high levels of RFP (low GFP to RFP ratio), indicative of exon inclusion.

Supplementary Figure 7. Mouse retina electroporated with the splicing reporter minigene carrying the Bbs8-Dup34 fusion. These additional images were collected from retinal sections from three different mice. Inner neurons expressing the minigene are indicated by yellow markers. A total of 19 inner neurons can be observed, all of which express high GFP to RFP ratio, which is indicative of exon skipping. On the other hand, photoreceptor cells express high levels of RFP (low GFP to RFP ratio), indicative of exon inclusion.

Supplementary Figure 8. Mouse retina electroporated with the splicing reporter minigene carrying the Edge-SCR exon. The images were collected from retinal sections from two mice. Inner neurons expressing the minigene are indicated by yellow markers. A total of 15 inner neurons can be observed. Both photoreceptor and inner neurons express high GFP to RFP ratio, which is indicative of exon skipping.

Supplementary Figure 9. Mouse retina electroporated with the splicing reporter minigene carrying the double D3+D4 deletion. The images were collected from retinal sections from two mice. Inner neurons expressing the minigene are indicated by yellow markers. A total of 9 inner neurons can be observed. Photoreceptor neurons express high levels of GFP and low to moderate levels of RFP, pointing to low rate of exon 2a inclusion. Inner neurons express high GFP to RFP ratio, which is indicative of exon skipping.

Supplementary Figure 1

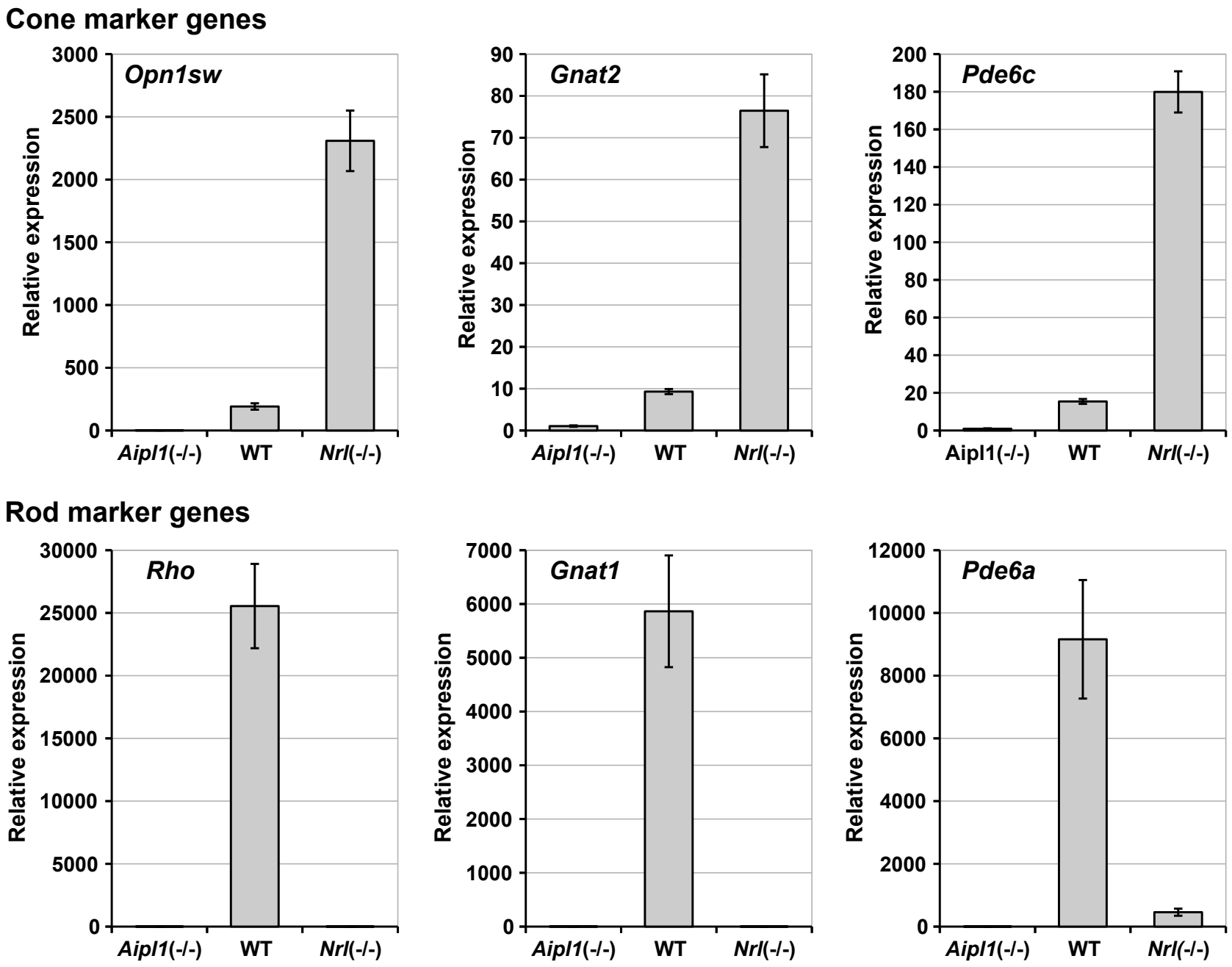

Supplementary Figure 2

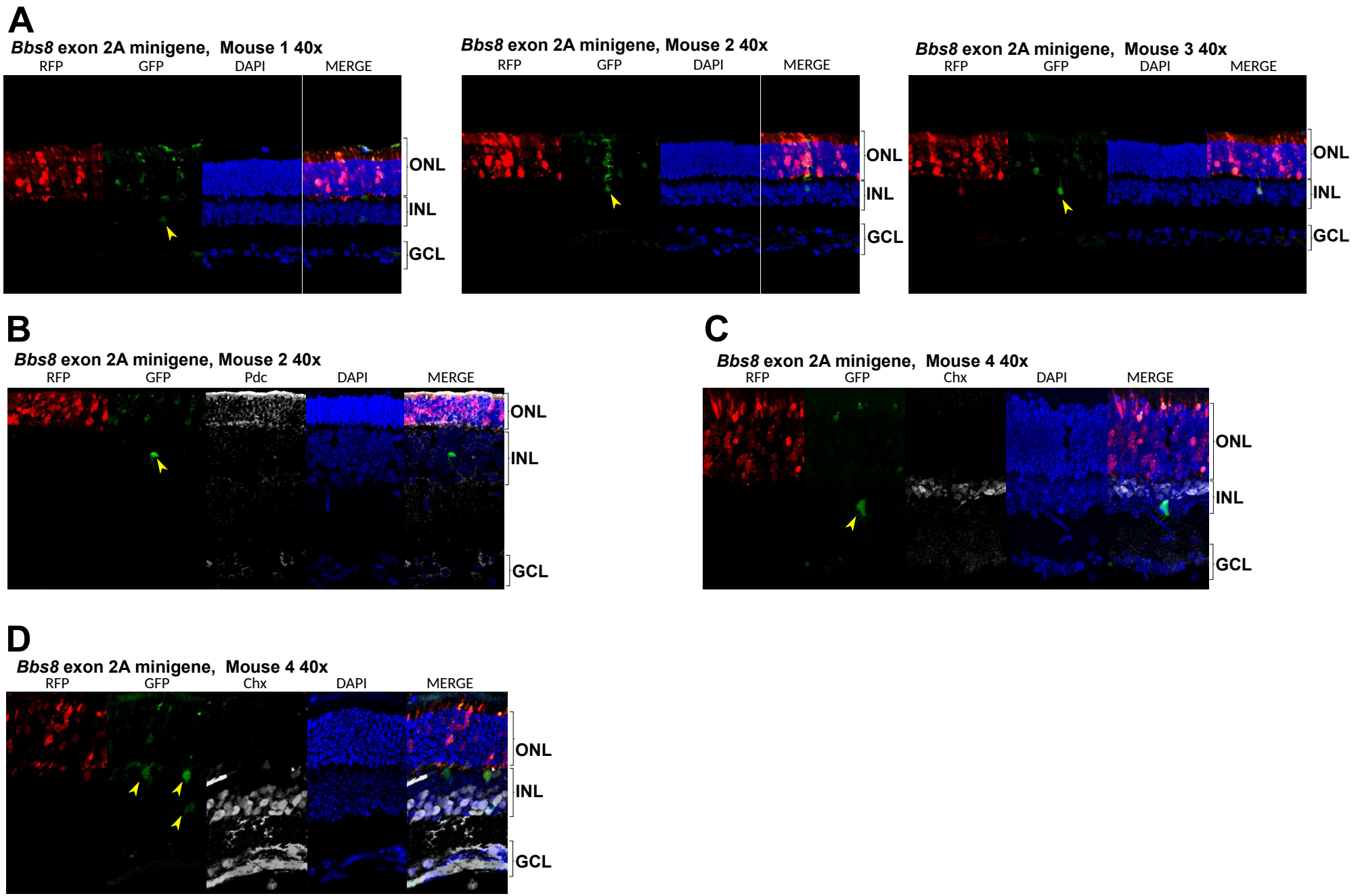

Supplementary Figure 3

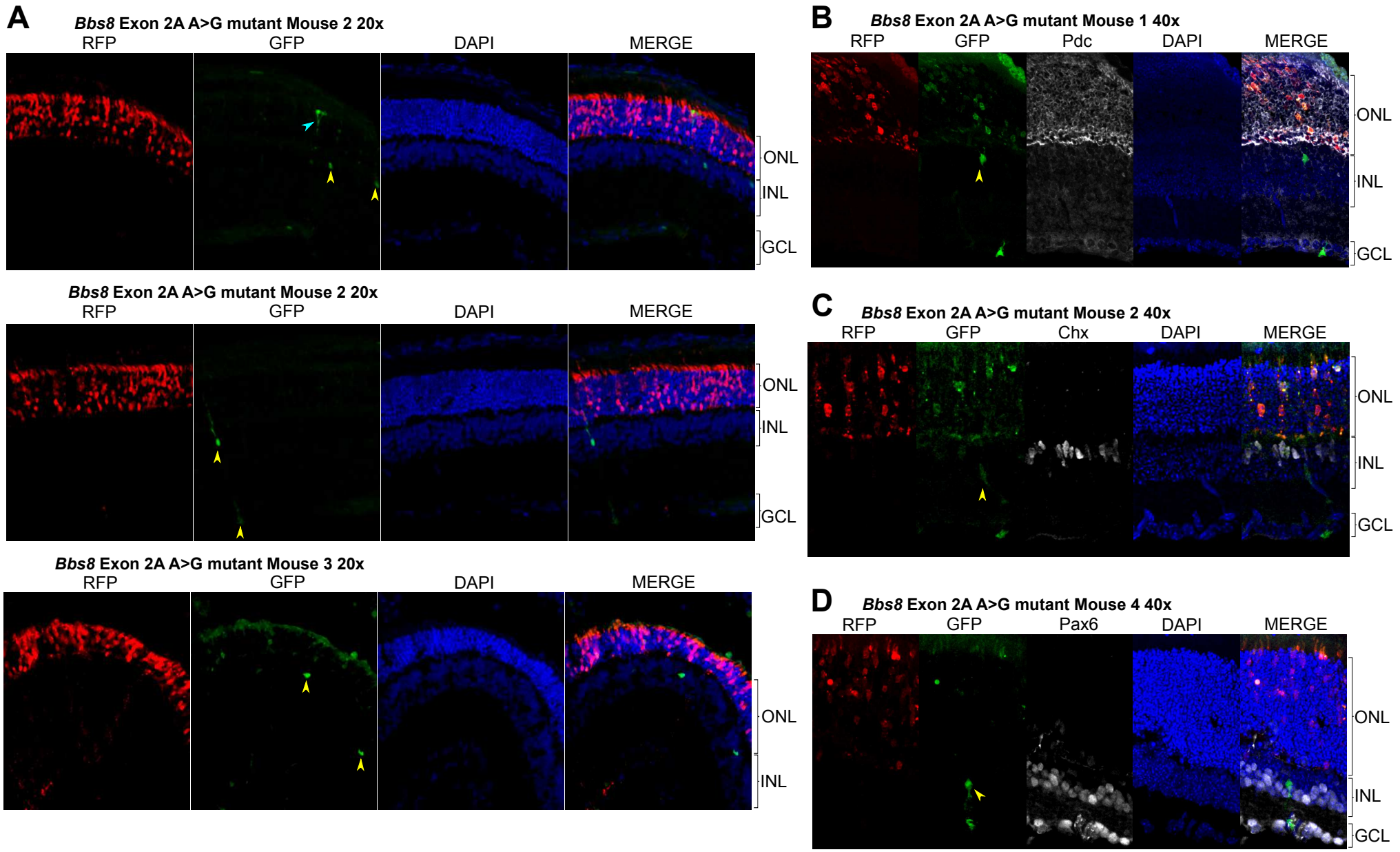

Supplementary Figure 4

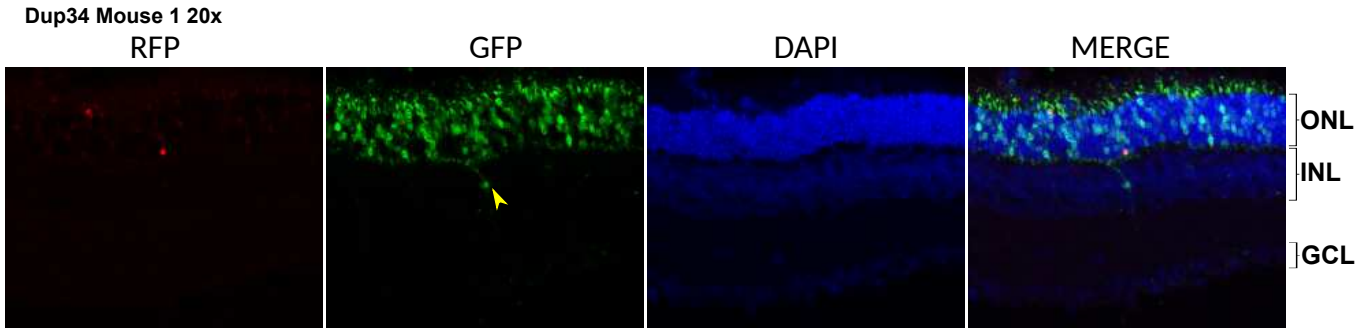

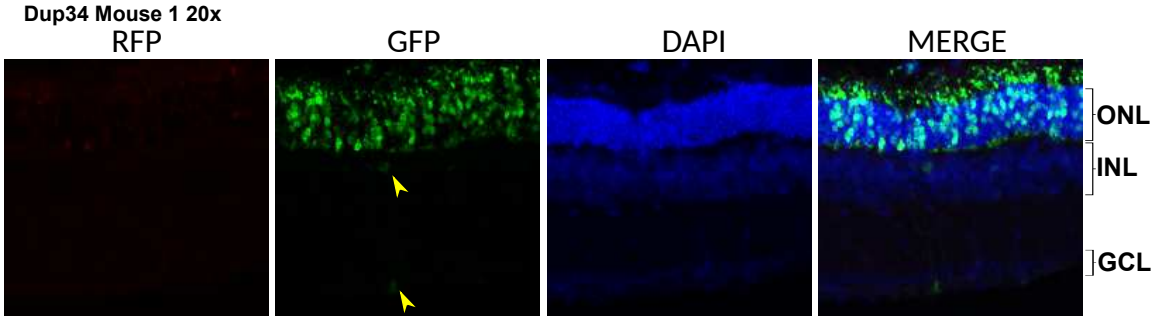

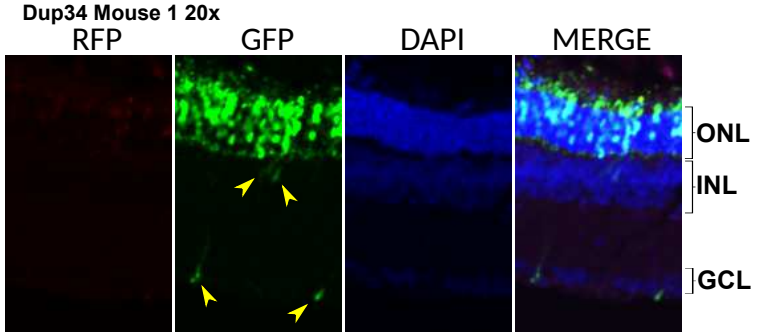

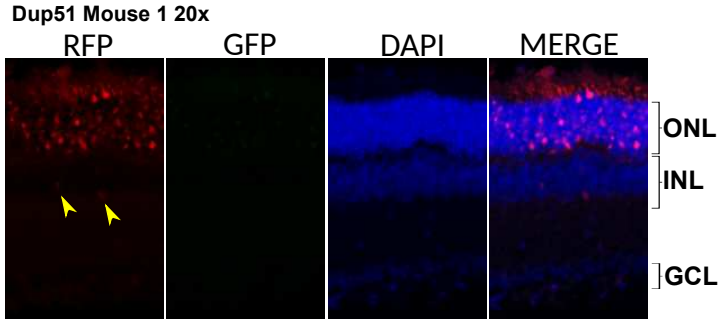

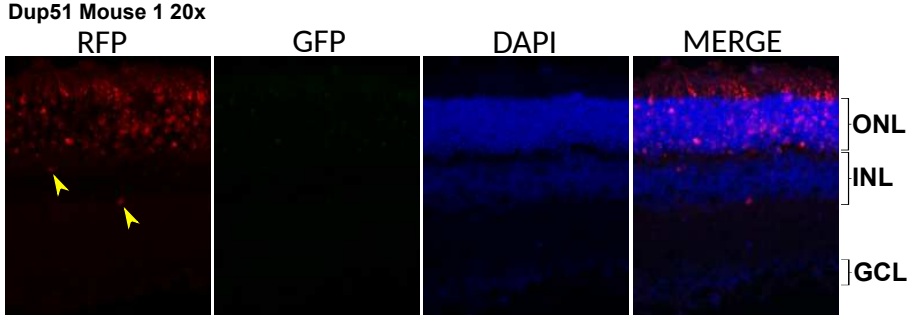

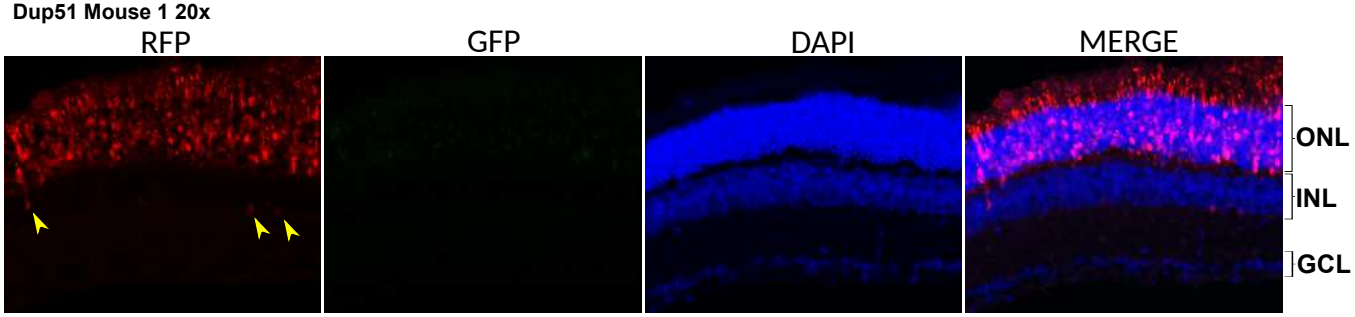

Supplementary Figure 5

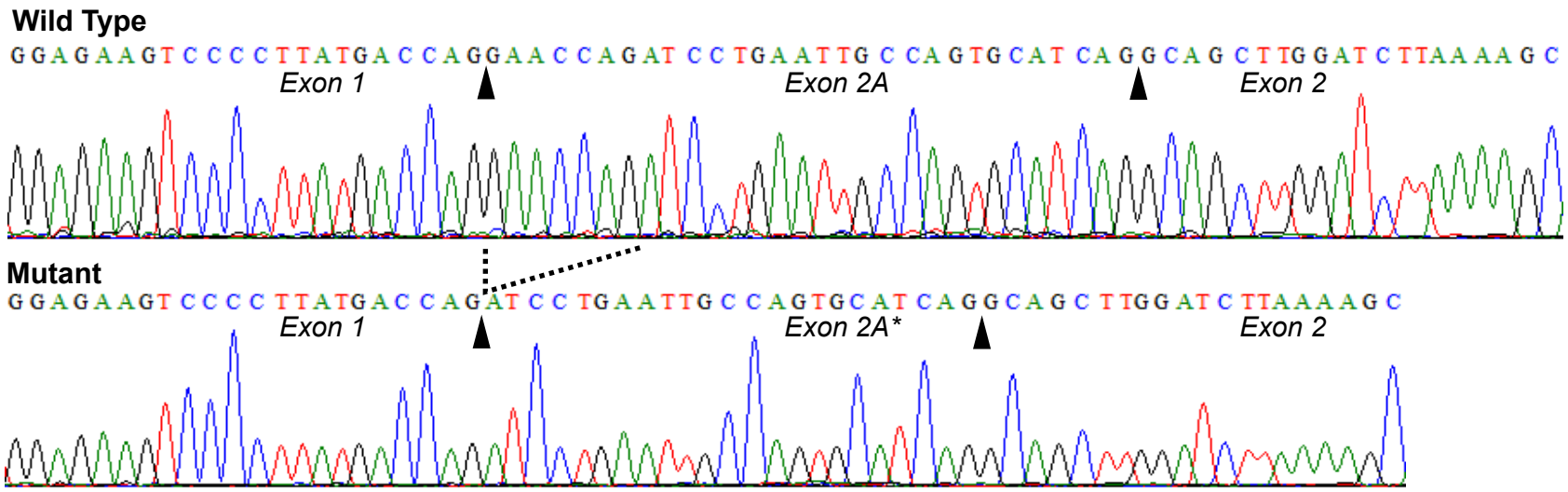

Supplementary Figure 6

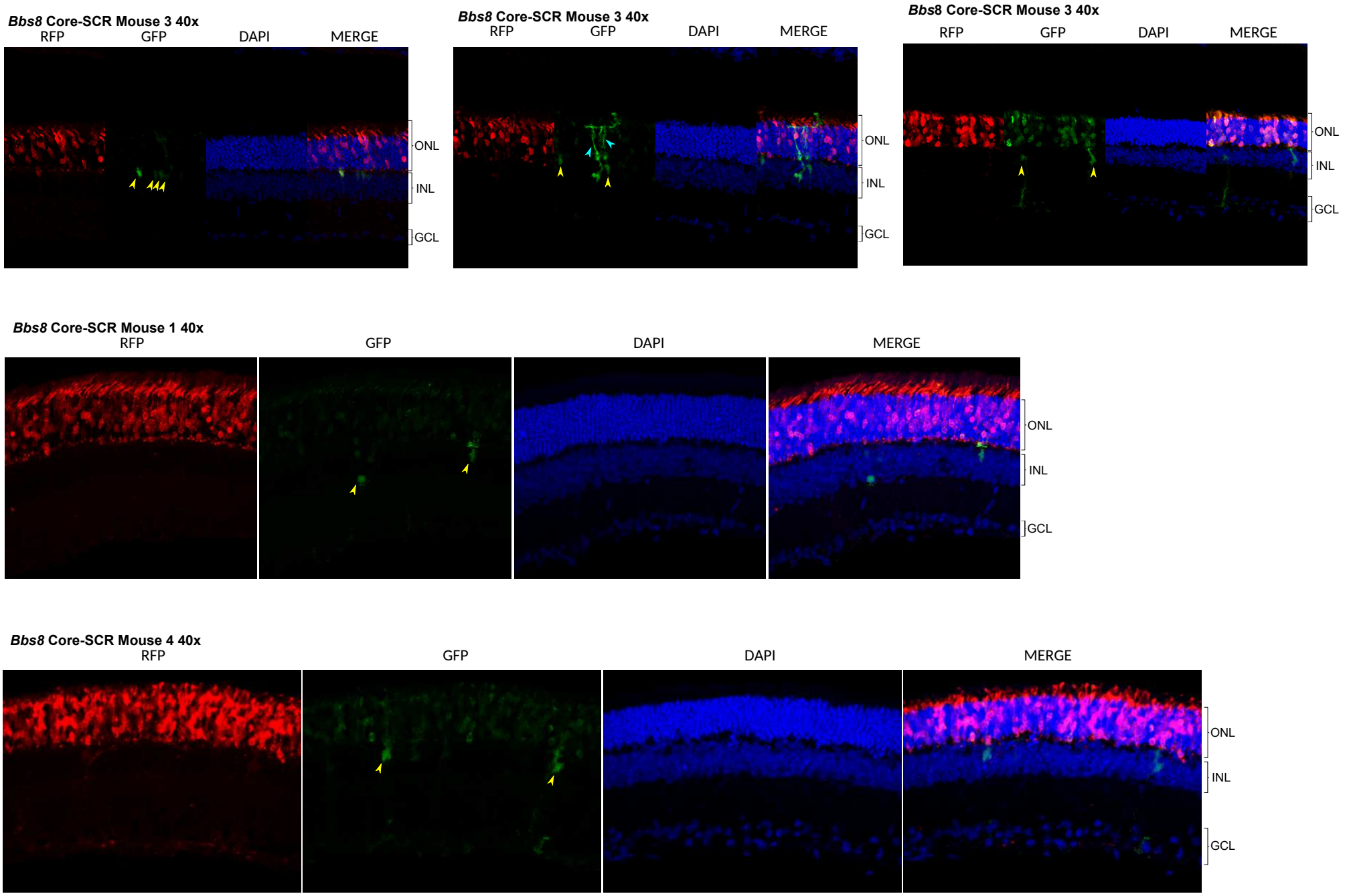

Supplementary Figure 7

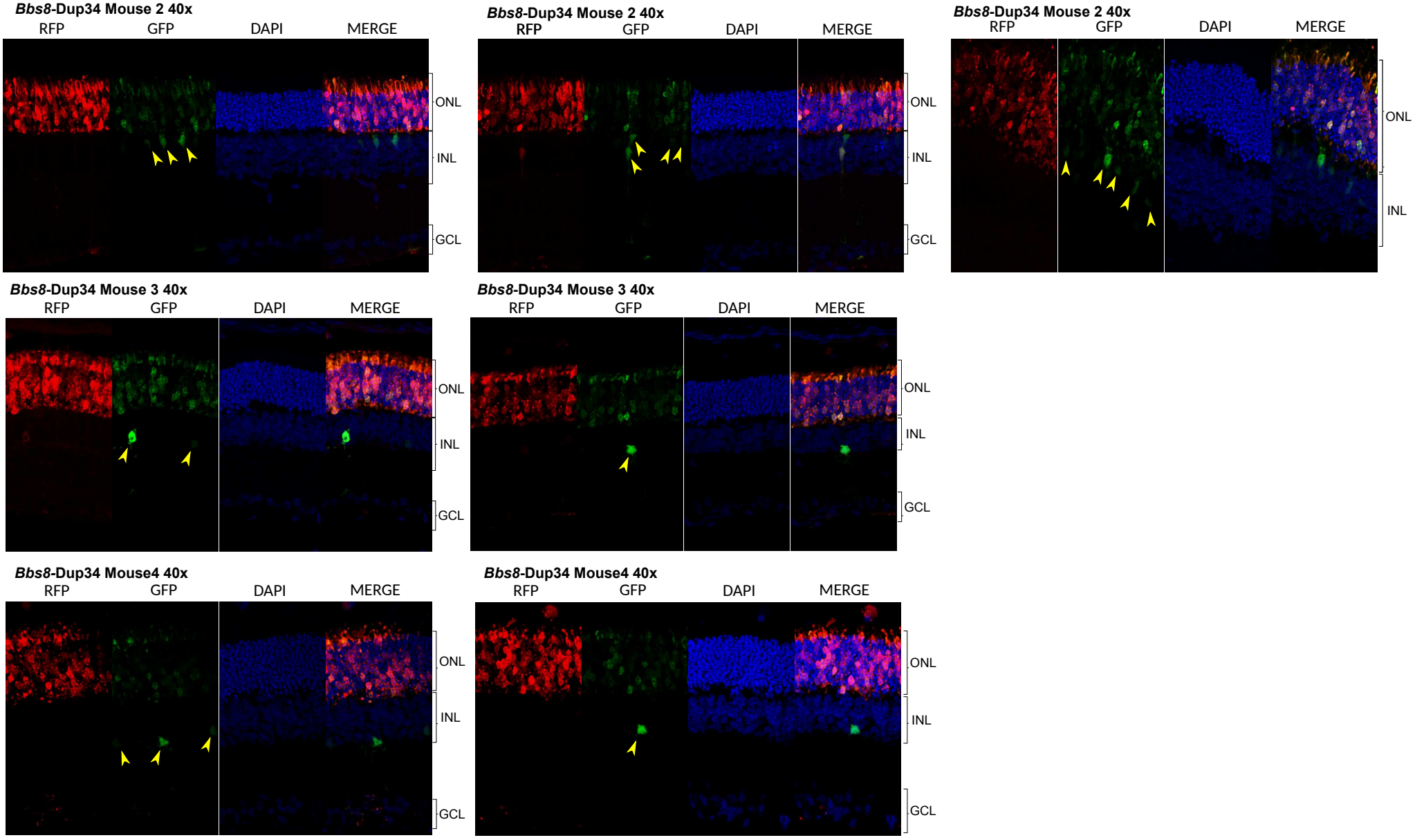

Supplementary Figure 8

Bbs8 **Edge-SCR Mouse 1 40x**

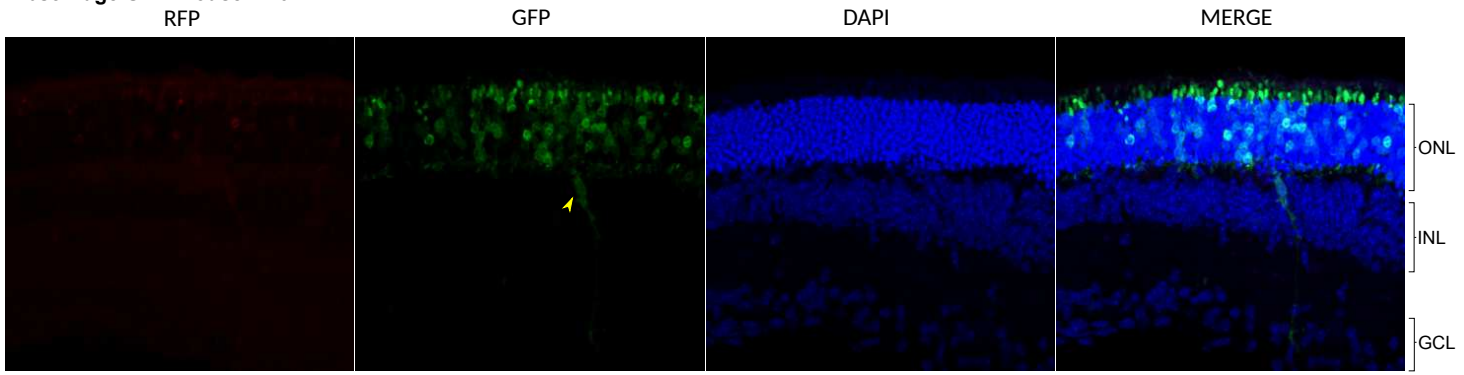

Bbs8 **Edge-SCR Mouse 2 40x**

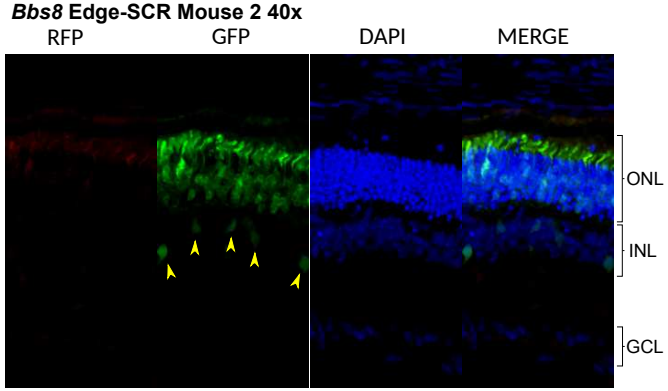

Bbs8 **Edge-SCR Mouse2 40x**

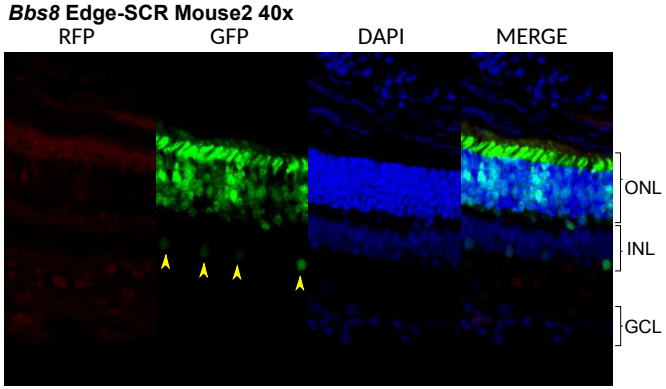

Bbs8 **Edge-SCR Mouse2 40x**

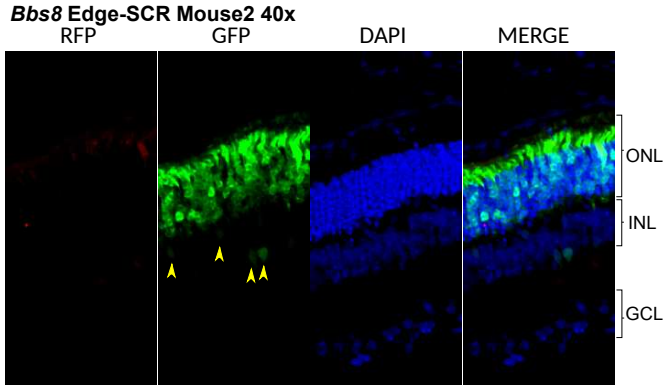

Supplementary Figure 9

Bbs8 **D3+4 mouse 2 40x**

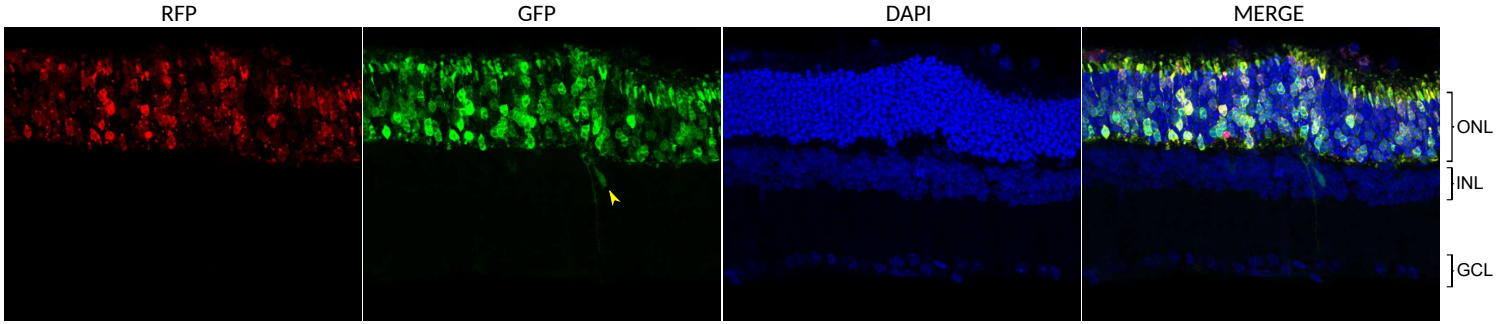

Bbs8 **D3+4 mouse 2 40x**

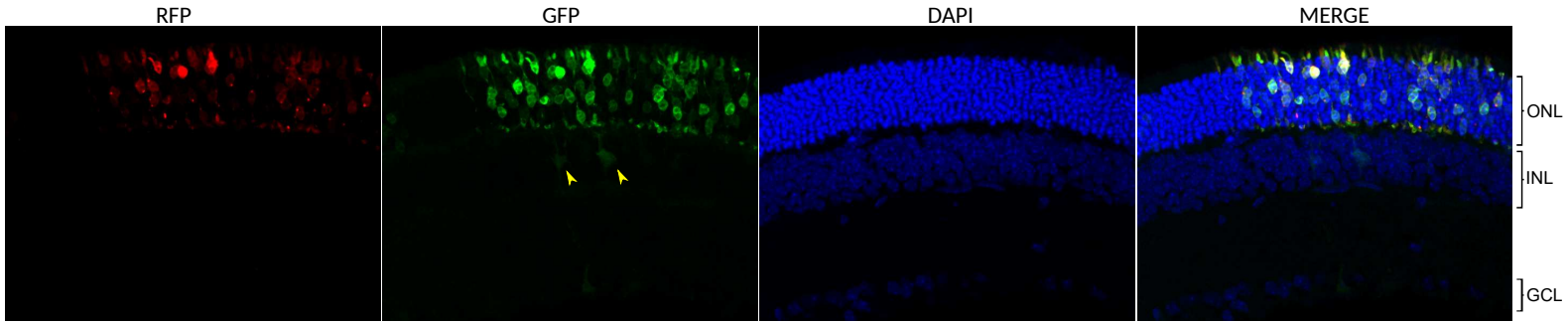

Bbs8 **D3+4 mouse 4 40x**

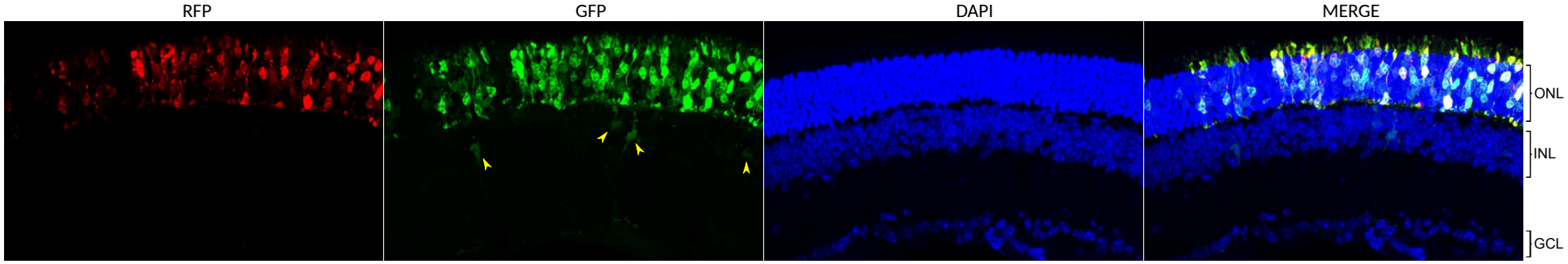

Chapter 5. Manuscript in preparation.

The Musashi proteins control the splicing of photoreceptor specific exons in the vertebrate retina

Daniel Murphy[a], Benjamin Cieply[b], Russ Carstens[b], Visvanathan Ramamurthy[a,c,d], Peter Stoilov[a,#]

Departments of [a]Biochemistry, [c]Ophthalmology and [d]Center for Neuroscience, Robert C. Byrd Health Sciences Center, West Virginia University, Morgantown, West Virginia, 26505, USA

[b]Department of Medicine, University of Pennsylvania, Perelman School of Medicine, Philadelphia, PA, USA

[#]Address for correspondence:

Peter Stoilov, pstoilov@hsc.wvu.edu

Department of Biochemistry, West Virginia University School of Medicine

1 Medical Center Dr, Morgantown WV 26505

Phone: +1 304 293-6334

Fax: +1 304 293-6846

Author Contributions

DM: experimental design, data acquisition, data analysis and interpretation, drafting and revising the article

BC: experimental design, data acquisition, data analysis and interpretation, drafting and revising the article

RC: experimental design, revising the article

VR: conception, experimental design, data analysis and interpretation, drafting and revising the article

PS: conception, experimental design, data acquisition, data analysis and interpretation, drafting and revising the article

Abstract

Alternative pre-mRNA splicing expands the coding capacity of eukaryotic genomes, potentially enabling a limited number of genes to govern the development of complex structures such as the vertebrate nervous system. Here, we show that photoreceptors, a type of sensory neuron, express a specific splicing program that affects a broad set of genes. The photoreceptor splicing program is initiated early in retinal development, prior to the morphogenesis of their light sensing outer segments. A striking feature of alternative splicing in photoreceptors are exons with a "switch-like" pattern of high inclusion levels in photoreceptors and near complete exclusion outside of the retina. Presence of "switch-like" exons in genes that are involved in biogenesis and maintenance of primary cilia suggests a role for alternative splicing in the development of the photoreceptor outer segment. Photoreceptors lack prototypical neuronal splicing factors and photoreceptor specific exons are spliced by a combinatorial mechanism that involves the Musashi proteins.

Introduction

Vertebrate nervous systems contain numerous types of neuronal cells distinguished by their morphology, connectivity, electrophysiological properties, and neurotransmitter signatures. Differences in marker gene expression among the neuronal subtypes suggest that their identity is established and maintained by specific gene expression programs. Consistent with this, single cell transcriptome profiling studies reveal dozens of distinct gene expression profiles in the central nervous system (CNS) and the retina (Rotem et al. 2015; Johnson et al. 2015; Shin et al. 2015; Zeisel et al. 2015). A limitation of the single cell approaches is the relatively low coverage of the transcriptome that is biased towards the 3'-end of the transcripts (Wu et al. 2014). The depth and distribution of the reads produced by the current single cell transcriptome profiling approaches do not allow the reliable assessment of the levels of transcript isoforms produced by alternative splicing. Thus, the posttranscriptional layer in the regulation of gene expression in neurons, which is required for the normal development and function of the CNS, remains hidden (Lauren T Gehman et al. 2011; L. T. Gehman et al. 2012; Q. Li et al. 2014, 2; Irimia et al. 2014; Jensen et al. 2000, -1; Kim et al. 2013, 3).

The vertebrate retina offers a relatively simple model for carrying out gene expression profiling of specific neuronal subtypes (Siegert et al. 2012; Rotem et al. 2015; Macosko et al. 2015). The retina is an extension of the CNS that is formed by approximately 60 different types of neurons belonging to six major classes (photoreceptor, horizontal, bipolar, amacrine and ganglion cells). While less complex than the CNS, the retina is a fully developed neural network that encodes the visual input in modalities that reflect color, edges, and direction of movement (Masland 2012).

Retinal photoreceptor cells in particular provide an intriguing model to study how gene expression programs shape the cell structure and properties. Photoreceptors have a distinct morphology with a characteristic light sensing organelle termed the outer segment. The

photoreceptor outer segment is a sensory cilium with an elaborate structure of membrane stacks which hold the phototransduction machinery. Surprisingly, the genes involved in the biogenesis and maintenance of the photoreceptor cilium are ubiquitously expressed in all ciliated cells. Recently, isoforms for two of these proteins, Arl6 (BBS3) and Ttc8 (BBS8), were shown to be preferentially expressed in photoreceptors (Pretorius et al. 2011; Pretorius et al. 2010; Riazuddin et al. 2010; Murphy et al. 2015). The photoreceptor variant of Arl6, a Ras related GTP-binding protein, is required for the survival of zebrafish photoreceptor cells and the morphogenesis of the photoreceptor layer in the mouse retina (Pretorius et al. 2010; Pretorius et al. 2011). These findings raise the possibility that photoreceptor cells are at least in part shaped by post-transcriptional processes such as alternative pre-mRNA splicing.

Alternative pre-mRNA splicing is a major mechanism for generating protein diversity in vertebrates. In particular, neurons use alternative splicing for generating protein diversity to a significantly higher degree than any other cell type (Zheng and Black 2013; Raj and Blencowe 2015). Additionally, neurons broadly utilize alternative microexons. Microexons are short exons that are defined by different groups as being no longer than 27nt or 51nt (Irimia et al. 2014; Y. I. Li et al. 2014). Examination of the conservation of microexons and the surrounding sequence indicates that their splicing is controlled to a large degree by sequence elements in the adjacent introns (Irimia et al. 2014; Y. I. Li et al. 2014). The neuronal splicing program and the inclusion of neuronal microexons are governed by splicing factors belonging to several families of RNA binding proteins such as PTBP, ELAVL, NOVA, KHDRBS, SRRM and RBFOX (Q. Li, Lee, and Black 2007; Raj and Blencowe 2015; Iijima et al. 2014; Iijima et al. 2011; Ehrmann et al. 2013). With the exception of Ptbp1, these proteins have high expression levels in neurons and are not expressed or have limited expression outside of the nervous system. Ptbp1, which represses splicing of neuronal exons outside of the nervous system, is replaced by the Ptbp2 in the early stages of neuronal differentiation.

Here we use animal models to characterize in depth the alternative splicing profiles of photoreceptor cells, a sensory neuron type. We find that photoreceptors express a characteristic splicing program. This program includes a set of photoreceptor specific isoforms that are absent from retinal and CNS neurons, or any other tissue we examined. Surprisingly, key neuronal splicing regulators are either not expressed or downregulated in photoreceptor cells. We show that the Musashi proteins, MSI1 and MSI2, promote the splicing of photoreceptor specific exons as part of a combinatorial mechanism that controls splicing in photoreceptor cells.

Results

Mouse models for retinal degeneration can be used to isolate the photoreceptor transcriptome

To identify the features of the retina transcriptome that are specific to photoreceptor cells we used RNA-Seq to analyze the transcriptomes of retina samples from wild type and Aipl1 knockout mice. AIPL1 is a molecular chaperone that is mutated in patients with Leber Congenital Amaurosis, a retinopathy caused by rapid loss of photoreceptors (Daiger, Sullivan, and Bowne 2013; Ramamurthy et al. 2004, 1; Kolandaivelu, Singh, and Ramamurthy 2014, 1). The Aipl1 mouse knockout phenocopies the human disease and by postnatal day 30, the retina lacking AIPL1 is devoid of photoreceptors (Figure 1A) (Ramamurthy et al. 2004, 1). The remaining cells in the retina, apart from the missing photoreceptors, have grossly normal anatomy (Figure 1A) (Ramamurthy et al. 2004). In a comparison between the transcriptomes of Aipl1 knockout and wild type retina, transcripts with higher expression levels in photoreceptors will appear downregulated in the Aipl1(-/-) sample due to the altered cell composition (Figure 1B). Conversely, transcripts expressed at higher levels in the inner neurons will show elevated expression levels in the Aipl1 knockout retina.

We first validated our approach by performing gene level expression analysis and tracking the expression levels of transcripts known to be specific to photoreceptors. We identified 5377 genes with more than 2 fold difference in their expression level between Aipl1 knockout and wild type retina (false discovery rate corrected p-value <0.01; see Supplementary Table 1). In the Aipl1 knockout, we observed loss of all genes known to encode photoreceptor specific transcription factors, (e.g. NR2E3, NRL), proteins involved in phototransduction, (e.g RHO, CNGA1, PDE6B), and photoreceptor morphogenesis (e.g PRPH2, RM1, FSCN2) (Supplementary Table 1). The genes with higher expression in the wild type retina compared to the Aipl1 knockout, showed enrichment of Gene Ontology (GO) categories directly related to photoreceptor development, structure and function (Table 1 and Supplementary Table 2). This enrichment is consistent with the loss of photoreceptor cells in the Aipl1 knockout. In contrast, the genes with lower expression levels in the wild type retina were part of broad GO categories related to organ development, neuronal cell structure and function (Table 1 and Supplementary Table 3). The GO categories enriched in downregulated transcripts reflect the preservation of the inner neuronal layers in the retina of the Aipl1 knockout mice. Thus, the gene level expression data demonstrates that comparing the retinal transcriptome of Aipl1 knockout with that of the wild type retina correctly identifies the transcripts characteristic to photoreceptors.

Photoreceptors express a characteristic splicing program

We used the RNA-Seq data to determine the inclusion levels of alternative exons in the mouse retina (Supplementary Table 4). Hierarchical clustering shows that the retina samples form a separate cluster with a splicing profile related to that of other neuronal tissues (Supplementary figure 1). Similar to central nervous system samples, the retina utilizes a significant number of microexons (Supplementary Figure 1).

We next analyzed the differences in exon inclusion levels in the wild type retina compared to the retina of the Aipl1 knockout. For this purpose we used the rMATS software,

which we modified by adding an algorithm to discover novel exons (S. Shen et al. 2012). Interestingly, approximately 40% of the differentially spliced exons between wild type and Aipl1 knockout retina were not annotated in the GRCm38 mouse genome assembly. The large number of novel exons prompted us to use Cufflinks to carry out guided transcriptome assembly based on the ENSEMBL GRCm38 transcript annotation and our RNA-Seq data. We then repeated the analysis of the differential splicing using the updated annotation and identified 540 differentially spliced exons (delta-Psi >= 0.1, FDR corrected p-value<0.01) in 372 genes (Supplementary Table 4). Of these 318 exons showed higher inclusion levels in wild type retina and 222 had lower inclusion levels. The alternative exons in the Bsg and Ttc8 (Bbs8) genes that are known to be used exclusively in photoreceptors were among the exons with higher inclusion levels in wild type retina, verifying that our approach correctly identifies photoreceptor specific exons (Ochrietor et al. 2003; Riazuddin et al. 2010; Murphy et al. 2015). We validated using RT-PCR 18 alternative exons that showed differences in inclusion level between 10% and 90% in our RNA-Seq data. All changes in exon inclusion level that were predicted by RNA-Seq were confirmed by the RT-PCR experiment (Figure 1C and Supplementary Figure 2). Exons in multiple genes such as Cep290, Cc2d2a, Cacna2d4, Prom1 and Kif1b showed large differences in inclusion levels between the wild type and Aipl1 knockout retina consistent with a “switch-like” splicing pattern. Similar to the Bsg and Ttc8 exons, these “switch-like” exons appear to be included at high levels in photoreceptors and skipped in all other tissues we examined (Figure 1B and Figure 2).

Unsupervised hierarchical clustering of the mouse tissue panel based on the inclusion levels of the exons differentially spliced in photoreceptors places the retina along with the other neuronal tissues (Figure 2). Interestingly, in this clustering the profile of the Aipl1 knockout retina is more closely related to that of the CNS samples than the wild type retina. The

expression of a distinct splicing profile by the photoreceptor cells is likely responsible for the separation of the Aipl1 knockouts from the cluster containing the wild type retinal samples.

As cone photoreceptors comprise only 3% of the retina, it was unclear if the splicing profile we discovered is shared between photoreceptors of different types or if it is specific to rod photoreceptors. To determine if rods and cones share the same splicing program we analyzed the splicing in the retina of Nrl knockout mice by RT-PCR. Nrl is a transcription factor required for rod photoreceptor development and its disruption leads to the conversion of all rod photoreceptors into cone like cells (Mears et al. 2001). All tested exons, with exception of an exon in the Glb1l2 gene, showed identical inclusion levels in the wild type and Nrl knockout retina (Figure 1B and Supplementary Figure 2). Thus, rods and cones share largely the same splicing program.

We next carried out gene ontology enrichment analysis to determine if alternative splicing in photoreceptors modifies particular processes or cellular components (Table 2 and Supplementary Table 5). Several of the enriched categories point to a significant impact of alternative splicing on the cytoskeleton of photoreceptor cells. Apart from the cytoskeleton we see enrichment of genes in broadly defined categories that are partially related to cell differentiation and neurogenesis. Such enrichment is evidence that alternative splicing modifies multiple systems and processes in the photoreceptor cells.

The photoreceptor splicing program is executed prior to photoreceptor differentiation

To gain insight into the developmental mechanisms that control splicing in photoreceptors, we analyzed exon inclusion levels in a panel of published retinal RNASeq datasets from wild type mice and genetic models that disrupt normal photoreceptor development and function. In addition to the Aipl1 and Nrl knockouts described above, these

models include a Crx knockout (Furukawa et al. 1999), a Crx-dominant negative (Crx-DN) mutant (Roger et al. 2014), and the RD10 mutant (Gargini et al. 2007). Deletion of Crx or expression of the CRX-DN protein block the transcription of the genes involved in phototransduction and the development of the outer segment by the post-mitotic photoreceptor progenitors (Furukawa et al. 1999; Morrow et al. 2005; Roger et al. 2014). The RD10 mutant, similar to the Aipl1 knockout, loses its photoreceptors in adulthood (Gargini et al. 2007). The wild type samples included retina from postnatal day 2, which contain early post-mitotic rod photoreceptor progenitors, and fully developed retina from juvenile and adult animals (postnatal days 21 and 50).

Unsupervised hierarchical clustering of the exons differentially spliced in photoreceptors revealed two major clusters (Figure 3A). One cluster is formed by samples derived from the Aipl1 knockout and the RD10 mutant retinas, both devoid of photoreceptor cells, and also includes the postnatal day 2 retina samples. The similarity between the Aipl1 and RD10 samples indicates that these splicing profiles are characteristic to retina devoid of photoreceptors and not a particular mouse model, further validating our approach.

A second cluster is formed by the adult wild type retina, the Nrl and Crx knockouts, and the Crx-DN mutant. The samples in this cluster preserved the photoreceptor splicing profile, a finding that we confirmed for the Nrl knockout by RT-PCR (Figure 1C and Supplementary Figure 2). Crx is a transcriptional factor required for photoreceptor differentiation (Swaroop, Kim, and Forrest 2010; Roger et al. 2014). The CRX-DN mutant protein heterodimerizes with OTX2, an upstream transcriptional regulator of Crx, and blocks its activity (Roger et al. 2014). Thus the presence of the photoreceptor specific splicing profile in the Crx knockout and Crx-DN mutant shows that the alternative splicing in photoreceptors is controlled independently of the known transcriptional regulators of photoreceptor morphogenesis.

At postnatal day 2 the rod photoreceptors are at the stage of immature progenitors. Interestingly, the splicing profile of the postnatal day 2 retina does not cluster with the samples containing immature photoreceptors that are derived from Crx knockout and Crx-DN retinas at postnatal day 21. The segregation of the postnatal day 2 retina from the juvenile Crx knockout and Crx-DN retina suggests that the photoreceptor splicing program is established in the post-mitotic photoreceptor progenitors prior to their final differentiation. To characterize the temporal control of alternative splicing during photoreceptor differentiation we analyzed by RT-PCR the inclusion levels of four photoreceptor specific exons in the Ttc8, Prom1, Cep290 and Cc2d2a genes between postnatal days 0 and 16 (Figure 3B). All four exons showed low levels of exon inclusion between postnatal day 0, which marks the peak of rod progenitor cell birth, and postnatal day 2. The inclusion levels of the four exons steadily increase thereafter, reaching approximately half of the maximum inclusion levels at postnatal day 8, when the photoreceptor outer segments begin to develop. Maximum inclusion levels are reached at postnatal day 14-16, shortly after the eyes open. Thus, the shift towards photoreceptor specific isoform expression is initiated in advance of the final stages of photoreceptor cell differentiation and the development of the critical for vision photoreceptor outer segments.

Motifs for several RNA binding proteins are enriched in proximity to exons differentially spliced in photoreceptors

After determining that photoreceptors express a characteristic splicing program we explored how this splicing program is controlled. To determine if a specific subset of splicing regulators bind in proximity to the exons differentially spliced in photoreceptors we performed motif enrichment analysis. For this purpose we used the position weight matrices (PWM) from the Cis-BP-RNA database that describe the sites recognized by RNA binding proteins (Ray et al. 2013). As these matrices are derived from the alignment of 7-mers, they fail to represent the true binding site for certain RNA binding proteins that recognize significantly shorter, 3 to 4

nucleotides long, sequences. To correct this deficiency we substituted the matrices for PTBP, NOVA, MBNL and MSI proteins with matrices corresponding to the sequences recognized by their RNA binding domains, i.e. YCU/UCY for PTBP, YCAY for NOVA, YGCY for MBNL, and UAG for MSI1.

Intronic sequences surrounding the differentially spliced exons showed enrichment of binding sites for several RNA binding proteins when exons differentially spliced in photoreceptors were compared to exons whose inclusion levels were the same in wild type and Aipl1 knockout retina (Table 3 and Supplementary Table 6). We observed enrichment of RBFOX and EIF2S1 binding sites, and marginal, but statistically significant enrichment of Nova binding sites downstream of exons with lower inclusion levels in photoreceptors. EIF2S1 is a cytoplasmic protein involved in translation initiation. The enrichment we observed for the EIF2S1 binding sites is likely due to the high degree of similarity between the sequence it recognizes (WGCAUG) and the binding site of the RBFOX splicing factors (UGCAUG). Weak, but statistically significant enrichment of PTBP binding sites was observed upstream of all differentially spliced exons, regardless if they were included at higher rate or skipped at higher rate in photoreceptors compared to inner neurons. Msi binding sites were enriched downstream of exons with higher inclusion levels in photoreceptors, compared to inner neurons. Elavl binding sites were partially depleted in exons with higher inclusion levels in photoreceptors and enriched in exons with lower inclusion levels in photoreceptors. Exons that had lower inclusion levels in photoreceptors showed enrichment of binding sites recognized by the KHDRBS, A1CF, LIN28, MEX3 and RBM41 proteins, all of which bind to for A/U rich sequences. Binding sites for two SR proteins, SRSF2 and SRSF9 that recognize G/A rich sequences, were depleted in these exons.

The cis-acting elements that efficiently recruit the PTBP, NOVA, MBNL and MSI proteins typically contain clusters of the short sequences recognized by their RNA binding domains (Han

et al. 2014; Licatalosi et al. 2008; Zearfoss et al. 2014; Goers et al. 2010; E. T. Wang et al. 2012). Thus, we tested if the number of PTBP, NOVA, MBNL and MSI motifs that are located in clusters is higher in proximity to the exons that are differentially spliced in photoreceptors. We examined clusters containing two to five motifs while varying the spacing between the motifs from 0 to 30 nucleotides. PTBP binding sites in clusters containing at least 5 motifs spaced by less than 2 nucleotides were significantly enriched upstream of all differentially spliced exons (Figure 4A and, Supplementary Figures 3 and 4). Such clustering of PTBP motifs is consistent with the well characterized mode of binding of the PTBP proteins to RNA. MSI binding sites in clusters containing at least three UAG motifs spaced by 10 to 15 nucleotides were enriched up to 8 fold downstream of the exons with elevated inclusion levels in photoreceptors (Figure 4A). Similar enrichment of pairs of Msi binding sites, albeit with larger spacing, was previously reported in the 3' UTRs of transcripts whose stability and translational efficiency is controlled by MSI (Zearfoss et al. 2014). NOVA binding sites were also enriched in clusters downstream of exons with lower inclusion levels in photoreceptors compared to inner neurons. We did not observe enrichment in the number of MBNL binding site located in clusters.

The motif enrichment analysis suggests a potential role in photoreceptors for several neuronal splicing regulators: RBFOX, NOVA, PTBP, KHDRBS and ELAVL.

Neuronal splicing factors are downregulated in photoreceptors

In an attempt to identify splicing factors specific to photoreceptors we examined the expression of 1039 known and potential splicing regulators in the panel of mouse retinal samples used in our splicing analysis (Supplementary table 7). None of these genes had expression restricted to photoreceptor cells that would suggest a role in the regulation of the photoreceptor specific exons. We observed that several key regulators of alternative splicing in neurons, Rbfox, Nova and Elavl family members, Ptbp1, Khdrbs2, and Srrm4 are

downregulated in the wild type retina compared to the Aipl1 knockout (Table 4 and Supplementary Table 1).

We used immunofluorescence staining to determine the expression pattern of RBFOX, NOVA, PTBP, KHDRBS, and ELAVL proteins in the mouse retina (Figure 4B). We were unable to test the expression of the SRRM4 protein in the retina due to the lack of selective antibodies suitable for immunofluorescence. In agreement with the RNA-Seq data showing lower expression levels in the wild type retina compared to the Aipl1 knockout, RBFOX and NOVA1 proteins were expressed in the inner neuronal layers but were completely absent from the photoreceptors. RBFOX and NOVA proteins act as splicing activators when bound downstream of alternative exons (Weyn-Vanhentenryck et al. 2014; Licatalosi et al. 2008). Thus, the lack of RBFOX and NOVA expression in the photoreceptor cells is consistent with the enrichment of their binding sites downstream from the exons with lower inclusion levels in photoreceptors compared to inner neurons (Figure 4A).

The PTBP proteins show the expected expression pattern with PTBP1 present in the nuclei of Muller glia cells, while PTBP2 (nPTB) is expressed in the neurons and photoreceptors (Figure 4B). The absence of PTBP1 from the retinal neurons and photoreceptors releases the splicing of alternative exons carrying PTBP binding sites within the upstream intron. These exons can then be regulated in a different manner in photoreceptors and inner neurons, explaining the enrichment of PTBP1 binding sites upstream of both up- and downregulated exons.

The ELAVL (Hu) proteins are expressed throughout the retina, with lower protein levels in the photoreceptors, consistent with the differences in ELAVL mRNA expression determined by RNA-Seq (Figure 4B). The pattern of ELAVL binding site enrichment that we observe in exons downregulated in photoreceptor cells is not consistent with data from one report showing

that the ELAVL1 protein acts as splicing repressor when bound to an alternative exon in the Fas gene (Izquierdo 2008).

The Khdrbs family of RNA binding proteins consists of the ubiquitously expressed KHDRBS1 (Sam68), and two orthologues, KHDRBS2 (Slm1) and KHDRBS3 (Slm2, T-STAR), which in the CNS are expressed in neurons (Stoss et al. 2004; Iijima et al. 2014; Ehrmann et al. 2013). Consistent with its ubiquitous expression, KHDRBS1 can be detected thought the retina with little variation in signal strength. In contrast, the KHDRBS2 and KHDRBS3 proteins were expressed only in the neurons of the inner retina, but not in photoreceptors. The KHRDBS3 protein expression is most likely suppressed posttranscriptionally as the KHDRBS3 RNA levels are uniform throughout the retina (Table 4). Accordingly, the 3'-UTR of KHDRBS3 contains conserved binding sites for microRNAs from the miR-96/miR-182/miR-183 cluster which is expressed in photoreceptors (Supplementary Figure 5) (Lumayag et al. 2013). The enrichment of KHDRBS binding sites in the downregulated exons is consistent with at least one previous report showing that KHDRBS3 binds to exonic splicing enhancers to activate exon inclusion (Stoss et al. 2001).

The Musashi proteins directly regulate splicing.

Msi binding site enrichment in the downstream intron is associated with exons whose inclusion level is increased in photoreceptor cells. The two Msi proteins are expressed throughout the retina and consistent with previous reports show mostly cytoplasmic localization in the inner neuronal layers (Figure 4A) (Nickerson et al. 2011; Susaki et al. 2009; Kaneko and Chiba 2009). As an adaptation to low light environment, the heterochromatin of mouse photoreceptors is packed in the center of the nucleus and the nucleoplasm pushed to the periphery (Solovei et al. 2009; Solovei et al. 2013). This morphology makes DNA staining unsuitable for identifying the boundaries of the nucleus. Thus, to determine if the Musashi proteins are present in the nuclei of photoreceptors, where they can regulate splicing, we

decorated the nuclear envelope with anti-Lamin antibody (Figure 5A and Supplementary figure 6). The Lamin staining of 4μm sections showed that both MSI1 (Figure 5) and MSI2 (Supplementary figure 6) are present in the nuclei of photoreceptor cells, where they are located in the periphery and are excluded from the heterochromatin core.

To generally validate whether the Musashi proteins can activate exon splicing directly we tested if the two Musashi proteins can promote inclusion of an alternative exon when bound downstream of it. For this purpose we used an alternative splicing reporter that has two lambda phage BoxB RNA hairpins engineered in the downstream intron (Heinicke et al. 2013). The loop of the BoxB hairpin is specifically bound by the lambda N-peptide. Consequently, proteins tagged with the lambda N-peptide will be tethered to the BoxB elements on the pre-mRNA. Cotransfection of the reporter with Musashi lambda-N fusions increased inclusion of the reporter exon (Figure 6 and Supplementary Figure 7A). The effect of Musashi on splicing is completely abolished in a reporter containing G to A point mutations in the two BoxB elements that disrupt binding of the lambda-N peptide. Thus, the Musashi proteins are capable of directly promoting exon inclusion when bound downstream of an alternative exon.

The Musashi proteins promote Ttc8 exon 2A inclusion in photoreceptors

To determine if the Musashi proteins directly regulate splicing in photoreceptors we turned to the photoreceptor specific exon 2A in the Ttc8 (Bbs8) gene. We previously mapped two 100nt sequence segments in the introns immediately adjacent to exon 2A that acted in concert to promote the splicing of this exon in photoreceptors (Murphy et al. 2015). Deletion mutagenesis showed that these segments contain multiple redundant cis-acting sequences (Murphy et al. 2015). The D4 segment located immediately downstream of exon 2A carries two clusters of Musashi binding sites, each containing three UAG motifs (Figure 7A). Within 320nt of the downstream intron immediately adjacent to exon 2A we find two more clusters containing three and four UAG motifs. A 350nt section of the intron immediately upstream of exon 2A

contains four Musashi binding sites, approximately the number of UAG triples that would be expected in random sequence of this size. To determine if the Musashi proteins can bind specifically to the D4 segment we used biotinylated RNA corresponding to this element to pull-down RNA binding proteins from retinal extracts. We also performed the pull-down with the other regulatory element, D3, and with segment D2, which is not required for splicing of exon 2A in photoreceptors. The binding was competed with non-biotinylated competitor RNA, either of the same sequence or a non-specific sequence of the same length. In this pulldown experiment the Musashi proteins bind specifically to segment D4, and their binding can be competed out by RNA of the same sequence and not by nonspecific competitor (Figure 7B). In contrast, segments D2 and D3, each of which contains a single UAG motif, had lower affinity for the Musashi proteins and the binding was completely blocked by a nonspecific competitor.

To determine how Msi1 binding downstream of exon 2A affects its inclusion levels in the retina we used a reporter minigene. The reporter, designed to produce GFP exon when the exon is skipped and RFP when the exon is included, was described previously (Murphy et al. 2015; Stoilov et al. 2008). We mutated all 15 Musashi binding sites in the downstream intron of the minigene (Figure 7A). We then co-transfected the wild type and mutant minigenes with Msi1 and Msi2 expression constructs in N2A cells. MSI1 and MSI2 potently promoted the inclusion of the wild type exon 2A but had no effect on the mutant minigene (Figure 7C and Supplementary figure 7A). To determine if the Msi binding sites are required for splicing of Ttc8 exon 2A in photoreceptor cells, we electroporated the wild type and mutant minigenes in the retina of neonate mice. We allowed the photoreceptors to develop and analyzed the splicing of the minigene transcripts in the retina by RT-PCR and immunofluorescence at postnatal days 16 and 20, respectively. As we have shown previously, the wild type Ttc8 exon 2A is included at high levels in the photoreceptors and is excluded from the mature transcripts in the inner neurons (Figure 7D and Supplementary figure 7B). In contrast, the inclusion level of exon 2A in the

transcripts of the mutant minigene, where the Musashi binding sites were disrupted, was reduced to approximately 38%.

Msi1 promotes the inclusion of photoreceptor specific exons

The enrichment of Musashi binding sites downstream of exons with elevated inclusion levels in photoreceptors suggests that multiple alternative exons should be regulated by the Musashi proteins in addition to Ttc8 exon 2A. To test this prediction, we analyzed the splicing in N2A cells of 11 exons with elevated inclusion levels in photoreceptors after expressing flag-tagged Msi1. Msi1 caused statistically significant increase (t-test p-value <0.01) in the inclusion levels of 7 exons located in the Ttc8, Cep290, Cc2d2a, Prom1, Cluap1, Impdh1, and Unc13b genes (Figure 8). Inclusion levels of five of these exons, including exon 2A of the endogenous Ttc8 gene, increased by at least 10% in response to Msi1 expression (Figure 8). The smaller amplitude of the effect of Msi1 transfection on the inclusion levels of the endogenous Ttc8 exon 2A compared to the minigene transcripts is due to the transfection efficiency, which was approximately 40% in these experiments. Among the exons coordinately regulated by the MSI1 are four “switch-like” exons in Ttc8, Cep290, Cc2d2a and Prom1. All four genes encode ubiquitously expressed proteins that are involved in ciliary biogenesis and function. Ttc8, Cep290, Cc2d2a and Prom1 are also required for the development and maintenance of the photoreceptor outer segments (Chang et al. 2006; Bachmann-Gagescu et al. 2011; Yang et al. 2008).

Discussion

The lack of comprehensive gene expression profiles of defined neuronal subtypes is a major obstacle to understanding how the neuronal diversity of the vertebrate CNS is established. To delineate the gene expression and alternative splicing programs of a single neuronal subtype we turned to the vertebrate retina. The high abundance of rod photoreceptors

in the mouse retina allowed us to isolate the characteristic features of their gene expression and alternative splicing programs by comparing the Aipl1 knockout model of retinal degeneration to wild type mice.

The splicing profile of photoreceptor cells is generally related to the spicing profiles of retinal and CNS neurons (Figure 2 and Supplementary figure 1). Alternative splicing in neurons is known to be regulated by SRRM4 and members of the PTBP, RBFOX, KHDRBS, NOVA and ELAVL families of RNA binding proteins (Q. Li, Lee, and Black 2007; Raj and Blencowe 2015; Iijima et al. 2014; Iijima et al. 2011; Ehrmann et al. 2013). Strikingly, photoreceptors lack RBFOX, NOVA, KHDRBS2 and KHDRBS3 protein expression, express lower amounts of ELAVL proteins and have markedly lower Srrm4 transcript levels. In light of this data, the switch from PTBP1 to PTBP2 expression during development emerges as a major determinant of the alternative splicing program that is shared between neurons and photoreceptor cells (Boutz et al. 2007; Makeyev et al. 2007).

To find photoreceptor specific splicing regulators we examined expression across the samples in our tissue panel of over 1000 candidate genes. We failed to identify candidates with an expression profile that correlates with the inclusion levels of the photoreceptor specific exons across the RNA-Seq samples in our panel. In the absence of a “master” regulator of splicing in photoreceptors, the characteristic splicing program of these cells can be determined by a unique combination of splicing factors with broader expression or through regulation of the activity of these factors by posttranslational modifications. Such combinatorial control of splicing is a well-established paradigm, but rarely has it been seen to produce the high level of cell type specificity we see for a subset of the differentially spliced exons we identify (Hertel 2008).

In support of the combinatorial mode of splicing regulation we show that MSI1 and MSI2 promote the splicing of exons with elevated inclusion levels in photoreceptors. The Musashi proteins are notable for their expression in stem cells, where they are involved in stem cell

maintenance and cell fate determination (Okano, Imai, and Okabe 2002; Fox et al. 2015; Nakamura et al. 1994). The best characterized function of Musashi is the regulation of mRNA stability and translation in the cytoplasm through binding to the 3'-UTR of the target transcripts (Fox et al. 2015). In the retina, the subcellular localization of the Musashi proteins varies during development and in mature neurons the two proteins are confined to the cytoplasm (Figure 4) (Nickerson et al. 2011). Here we show that in photoreceptor cells MSI1 and MSI2 are present not only in the cytoplasm but also in the nuclei, where they control alternative pre-mRNA splicing (Figure 5). Controlling the subcellular localization of the Musashi proteins provides an intriguing mechanism that can generate the characteristic splicing program of photoreceptors without requiring a photoreceptor specific RNA binding protein. Similar mechanisms that involve redistribution of RNA binding proteins between the nucleus and the cytoplasm have been shown to control alternative splicing in response to external stimuli (van der Houven van Oordt et al. 2000; Lee, Tang, and Black 2009; Daoud et al. 2002). The downregulation of neuronal splicing regulators is another characteristic of the combinatorial control mechanism that drives the alternative splicing program of photoreceptors. Consequently, exons whose inclusion depends on splicing factors like Rbfox and Nova are skipped in photoreceptor cells.

At present it is unclear how most of the alternative exons we identified affect protein function or to what degree alternative splicing shapes the properties of the photoreceptor cells. One exception is the 14nt exon 8 in the Arl6 (BBS3) gene, which has high inclusion levels in photoreceptors (Figure 1). ARL6, a Ras family GTP-binding protein, is part of a network of proteins involved in the development and maintenance of primary cilia (Figure 8C). The exon 8 containing isoform of ARL6 is required for normal vision in zebra fish (Pretorius et al. 2011; Pretorius et al. 2010). The vision phenotype of mice lacking Arl6 exon 8 has not been reported in detail, however gross histological examination and immunofluorescent staining of the retina show that the inner segments of photoreceptors are disorganized (Pretorius et al. 2010).

Several other components of the protein network that ARL6 is part of are also differentially spliced in photoreceptors. Four of these genes, Cep290, Cc2d2a, Ttc8 and Prom1 contain "switch-like" exons that produce isoforms highly specific to photoreceptors (Figure 8C and Figure 1B) (Riazuddin et al. 2010; Murphy et al. 2015). Strikingly, the splicing of these "switch-like" exons is coordinately regulated in development (Figure 3B) and their inclusion is promoted by MSI1. We are tempted to speculate that alternative splicing modifies the properties of these otherwise ubiquitously expressed proteins to enable the development of the outer segment membrane stacks by the photoreceptor cilia. Consistent with a role of MSI1 in controlling alternative splicing in photoreceptor morphogenesis, the photoreceptor outer segments of Msi1 knockout mice are short and fragmented (Susaki et al. 2009).

Further highlighting a potential role in photoreceptor differentiation, the photoreceptor splicing program is activated in the postmitotic progenitors, prior to the onset of outer segment development. A transcription factor cascade starting from Crx homeobox protein that is critical for photoreceptor morphogenesis is also activated during the same developmental time frame (Morrow et al. 2005; Swaroop, Kim, and Forrest 2010; Cepko 2014). Interestingly, alternative splicing in photoreceptors is not affected in the Crx knockout animals and in the Crx dominant negative mutant, which suppresses the upstream Otx2 transcription factor (Roger et al. 2014). Thus, the developmental switch to photoreceptor specific splicing is independent of the established transcriptional mechanism that activates the expression of photoreceptor specific genes.

In summary we demonstrate that photoreceptors express a characteristic splicing program that encompasses hundreds of alternative exons and affects the transcripts of multiple genes that are critical for vision.

Materials and methods

Clones and antibodies

To generate the flag-tagged Musashi 1 clone we amplified the coding sequence from mouse retinal cDNA using primers that introduced the flag tag and restriction sites for cloning (See Supplementary table 11 for primer sequences). The product was inserted into pCDNA3.1 vector linearized with BamH1 and Xho1.

The PKC-neg-40B-2xBoxB-EGFP splicing reporter and pIBX-C-FF-(B)-NLS-λN expression vector were described previously (Newman et al. 2006; Heinicke et al. 2013). PKC-neg-40B-2xBoxB (G1A)-EGFP was constructed by swapping the 2xBoxB cassette with the mutant 2xBoxB G1A via ClaI and XhoI (The first G in the loop of the BoxB hairpin (G1) is required for λN binding (Chattopadhyay et al. 1995).

The Bbs8 exon 2A minigene containing mutagenized Musashi 1 consensus binding motifs was created using Gibson Assembly (See Supplementary Table 11 for the oligonucleotide sequences).

Antibodies used in this work are listed in Supplementary table 8.

Mice

All procedures carried out on laboratory mice were approved by Institutional Animal Care and Use Committee at West Virginia University (WVU). Subretinal injection, time course analyses, and immunofluorescence of sections were performed on CD-1 mice (Charles River). Aipl1(-/-) mice were generated as described (Ramamurthy 2004).Toluidine blue staining in Figure 1 was performed on p65 C57bl/6j and p60 Aipl1(-/-) mice.

RNA-Seq library preparation and sequencing

Total RNA was isolated from wild type C57bl/6j and C57bl/6j:Aipl1 (-/-) retinas at postnatal day 50 using Tri-reagent (Sigma). rRNA subtracted RNA-Seq libraries were generated using 1µg of total RNA per replicate using RiboZero and TruSeq kits (Illumina) following manufacturer's instructions. Four replicates, each derived from different animal, were generated for each wild type and Aipl1(-/-) sample. The libraries were sequenced to a depth of 43 million reads (range 39 to 47 million reads) on Illumina Hi-Seq 15000. Library preparation was carried out by the WVU genomics core and the libraries were sequenced by the Marshall University genomics core. The reads produced by the RNA-Seq experiments are deposited at the NCBI SRA repository under accession number SRP068974.

Bioinformatics analysis

Reads from the retinal samples were mapped to the current mouse genome (GRCm38) using TopHat. Following the mapping, Cufflinks was used to carry out guided transcriptome assembly based on the ENSEMBL GRCm38 annotation (Supplementary data file 1 contains the updated annotation in GTF fromat). Additional RNA-Seq data sets for mouse tissues and retinal samples from genetically engineered mouse models were downloaded from the NCBI sequence read archive (Supplementary table 9) and aligned to the updated annotation.

Exon inclusion levels across all samples were calculated using rMATS version 3.08 (Shihao Shen et al. 2014). In light of the large data set that needed to be processed we modified rMATS to improve the speed of read pre-processing and counting. For this purpose we enabled rMATS software to read the binary BAM alignment format via samtools/pysam and to use multithreading (H. Li et al. 2009; “Pysam-Developers/pysam” 2016). We also added a basic capability to discover novel exons within annotated transcripts based on splice junction reads that are anchored on one end to a known exon (Supplementary figure 8). rMATS was also used to carry out differential splicing analysis of the wild type and Aipl1(-/-) retina samples. Differences in gene expression between the wild type and Aipl1(-/-) samples were identified

using featureCounts and edgeR (Robinson, McCarthy, and Smyth 2010; Liao, Smyth, and Shi 2014). Gene Ontology analysis was carried out using WebGestalt (J. Wang et al. 2013).

Motif enrichment analysis was carried out in R/Bioconductor using the PWMEnriched package (Stojnic and Diez 2015). Position weight matrices for RNA binding proteins were described previously (Ray et al. 2013). The matrices for RBFOX, PTBP, MBNL and MSI proteins were replaced with the matrices listed in Supplementary Table 10. Binding sites carrying 90% match to the scoring matrices were counted in the exons and in 200nt segments of the introns immediately adjacent to the exon. Binding site position for orthologues recognizing highly similar sequences, e.g. RBFOX1, 2 and 3 proteins, KHDRBS1, 2 and 3 proteins, etc, were pooled together. Binding sites whose positions on the transcript overlap by more than 50% were counted as a single site. Two single tailed hypergeometric tests were used to determine the significance of the binding site enrichment/depletion in each segment. The hypergeometric test p-values were then corrected for multiple testing using Benjamini-Hohberg's procedure. To assess if there is an enrichment of clustered binding sites, the binding sites for MSI, PTBP, ELAVL and NOVA proteins that were not located within a cluster were excluded from the analysis. Clusters were defined by two parameters: minimum number of binding sites necessary to form a cluster, ranging from 2 to 5; and the maximum spacing between them, ranging from 0nt to 30nt. The enrichment analysis was carried out for each pair of minimum binding site count and maximum spacing parameters.

RNA isolation and RT-PCR from retina

Mouse eyes were enucleated at post-natal day 16 and dissected under stereo microscope (Zeiss Stemi dv4) to isolate the retina. Retinal RNA was isolated with TRI reagent (Sigma) according to manufacturer’s guidelines. Reverse-transcription PCR reactions containing 0.1-0.5µg RNA were primed with Oligo dT and random hexamers to generate cDNA. Alternatively spliced regions were amplified using fluorescently labeled primers positioned in the

flanking exons (See Supplementary table 11 for primer sequences). The amplified products were separated by gel electrophoresis under denaturing conditions (urea/polyacrylamide gels) and imaged on a Typhoon 9410 imager (GE).

Retinal tissue sections and fluorescence imaging

Mouse eyes were enucleated at P20, punctured at the edge of the cornea with an 18-gauge needle, and incubated in 4% paraformaldehyde for 10 min. After removal of the cornea, the dissected eye was incubated in 4% paraformaldehyde for an additional 1 h with shaking. After three 5-min washes in PBS, the eyes were cryoprotected by shaking at 4°C overnight in PBS containing 20% sucrose. Eyes were then incubated for 1 h with shaking in a 1:1 mixture of optimal cutting temperature (OCT) (Tissue Tek) compound and 20% sucrose–PBS, during which time the lens was removed. Eye cups were then flash frozen in OCT compound and stored at -80°C. Retinal sections were cut to 4µm or 16µm (Leica CM1850) and mounted on Superfrost Plus (Fisher) slides and stored at -20°C. Slides were washed in PBS to remove excess OCT compound and mounted with Prolong Gold reagent containing DAPI (4-,6-diamidino-2-phenylindole) (Life Technologies). For immunofluorescence staining, slides were washed with PBS to remove excess OCT compound and blocked in PBS containing 10% FBS, 0.5% Triton X-100(Sigma), and $0.5x10^{-4}$% Sodium Azide. Slides were then washed once more with PBS before overnight incubation at 4°C with primary antibody. Primary antibodies were removed with three 15 minute washes in PBS containing 0.1% Triton X-100 prior to a 1 hour incubation at room temperature with secondary antibody. Following 3 additional washes for 20 minutes each in PBS containing 0.1% Triton X-100, slides were rinsed briefly in water and mounted. All antibodies for immunofluorescence were diluted in PBS containing 5% FBS, 0.5% Triton X-100 and $0.5x10^{-4}$% Sodium Azide.

The slides were imaged on Zeiss LSM 510 or 700 laser scanning confocal microscopes. Musashi, Lamin-B, and DAPI co-localization analysis was performed on 4µm sections using

ImageJ software to plot signal intensities spanning a 10μm line perpendicular to the border of nuclei in the ONL, n= 53. Signals from individual nuclei were normalized to the maximal signal for each channel. Each set of measurements were then centered relative to the maximal Lamin-B signal before calculating and plotting data.

Cell Line Transfections

Exponentially growing mouse neuroblastoma (N2A) cells were plated at $0.8x10^5$ cells per ml. Following 24 hours of incubation at 37°C cells were transiently transfected using a 2.5:1 ratio of Polyethylenimine to plasmid DNA mixture containing equal amounts of minigene reporter and expression vector. After 48 hours of incubation cells were washed twice with ice cold PBS. RNA was isolated with TRI reagent (Sigma) according to manufacturer's guidelines and cDNA was synthesized to analyze splice products as above.

293T cells were transfected using Mirus Transit 293 reagent with 150ng PKC-neg-40B-2xBoxB-EGFP or PKC-neg-40B-2xBoxB(G1A)-EGFP and 50ng pIBX-C-FF-(B)-NLS-λN (empty vector, Msi1 or Msi2) per well of a 24 well plate in triplicate. RNA and protein were isolated 48 hours later using Trizol reagent and RIPA buffer, respectively. RT-PCR of the mini-gene was carried out using primers in the flanking exons of the 40nt test exon with the reverse primer being FAM labeled.

Western Blotting

Transiently transfected N2A cells expressing wild type or mutagenized Bbs8 exon 2a splicing reporters along with N-terminally flag-tagged Msi1 expression vector or empty vector were washed twice in ice cold PBS and boiled at 95°C for 6 minutes in SDS buffer containing 1% 2-mercaptoethanol (Sigma). Lysates were stored at -80°C and resolved in 10% SDS-PAGE gel electrophoresis before being transferred to an Immobilon FL membrane (Millipore.) Membranes were blocked in Tris buffered saline solution containing 1% Tween-20 (sigma) and

0.25% bovine skin gelatin (Sigma). After blocking membranes were incubated with primary antibodies overnight at 4°C in the blocking solution. After removing the primary antibody and washing the membrane, the secondary antibodies were applied in the blocking solution for 1 hour at RT. Membranes were imaged on a Typhoon 9410 imager (GE) after removing the secondary antibodies and washing the membranes in PBS.

Subretinal Injection and Electroporation

Plasmid DNA was isolated at 4 to 6 µg/µl using a Qiagen Plasmid Plus Midi kit. DNA containing 0.1% fluorescein sodium was injected into the subretinal space of newborn CD-1 pups as described previously (Matsuda and Cepko 2004). Briefly, after anesthesia, an incision was made at the future eyelid with a 33-gauge needle under a dissecting microscope. The needle was used to make a pinhole puncture in the sclera away from the lens. A 0.5-µl volume of DNA was injected through the puncture into the subretinal space using a blunt-end syringe. Five pulses of 80 V at 50-ms duration with 950-ms intervals were then applied with tweezer-type electrodes (BTX model 520) (7-mm diameter).

RNA Pull-down

Template DNA was amplified using primers corresponding to intronic regions flanking BBS8 exon 2A (Supplementary Table 11) and purified through gel extraction (Zymo). RNA probes were synthesized with the Hi-Scribe T7 RNA Synthesis kit (NEB) using 0.5µg of template DNA. 100pmol of RNA probes were then biotinylated using the Pierce RNA 3' end biotinylation kit (Thermo Fisher) and purified according to manufacturer's instructions. Biotinylated RNA probes were re-suspended in 100µl of high salt buffer (0.5M NaCl, 10mM Hepes pH7.9). Approximately 0.4mg of streptavidin magnetic beads (NEB) were washed in high salt buffer and incubated with biotinylated probes on ice for 1-2 hours with occasional mixing. RNA-bead conjugates were then washed three times with wash buffer (0.1M KCl, 10mMHepes

pH 7.9, 0.1% Triton-X100). Washed beads were then incubated on ice with 100µg retinal extract and 6µg competitor RNA or water in binding buffer (0.1M KCl, 10mMHepes pH 7.9, 5µg/µl heparin (Sigma), 0.1% Triton-X100 and 20U RNAse Inhibitor (Santa Cruz Biotech)) for four hours with occasional mixing. Beads were then washed three times with wash buffer. Bound proteins were eluted in wash buffer containing 20ng RNAse A (Sigma). The Musashi proteins in the eluates were detected by western blotting using an antibody that reacts with both MSI1 and MSI2 (Supplementary table 8). All steps were carried out in low retention micro centrifuge tubes (Fisher).

Acknowledgments

We are grateful to Dr. Douglas Black (UCLA) for the kind gift of the Ptbp1, Ptbp2 and Rbfox antibodies. We thank Anand Swaroop for generously providing the Nrl knockout animal used in this study. We thank Dr. Lisa Salati (WVU) and Dr. Yi Xing (UCLA) for critical reading of the manuscript. We thank Dr. Rahul Kanadia (UCONN) for helpful suggestion on the immunofluorescence staining of retinal sections. Imaging experiments were performed in the West Virginia University Microscope Imaging Facility, which has been supported by the Mary Babb Randolph Cancer Center and NIH grants P20 RR016440, P30 GM103488, and P20 GM103434. This work was supported by National Institutes of Health grants R01EY017035 (VR), R01EY025536 (VR, PS) and R21 HG006892-01 (RC), West Virginia INBRE Genomics Pilot Grant (PS), West Virginia Lions, and Lions Club International Fund and by an internal grant from West Virginia University. Benjamin Cieply is supported by NIGMS fellowship F32GM109630.

Competing interests The authors declare that no competing interests exist.

References

Bachmann-Gagescu, Ruxandra, Ian G. Phelps, George Stearns, Brian A. Link, Susan E. Brockerhoff, Cecilia B. Moens, and Dan Doherty. 2011. “The Ciliopathy Gene cc2d2a Controls Zebrafish Photoreceptor Outer Segment Development through a Role in Rab8-Dependent Vesicle Trafficking.” *Human Molecular Genetics* 20 (20): 4041–55. doi:10.1093/hmg/ddr332.

Betel, Doron, Anjali Koppal, Phaedra Agius, Chris Sander, and Christina Leslie. 2010. “Comprehensive Modeling of microRNA Targets Predicts Functional Non-Conserved and Non-Canonical Sites.” *Genome Biology* 11 (8): R90. doi:10.1186/gb-2010-11-8-r90.

Boutz, Paul L, Peter Stoilov, Qin Li, Chia-Ho Lin, Geetanjali Chawla, Kristin Ostrow, Lily Shiue, Manuel Ares, and Douglas L Black. 2007. “A Post-Transcriptional Regulatory Switch in Polypyrimidine Tract-Binding Proteins Reprograms Alternative Splicing in Developing Neurons.” *Genes & Development* 21 (13): 1636–52. doi:10.1101/gad.1558107.

Cepko, Constance. 2014. “Cell Fate Determination of Photoreceptor Cells.” In *Vertebrate Photoreceptors*, edited by Takahisa Furukawa, James B. Hurley, and Satoru Kawamura, 217–44. Springer Japan. doi:10.1007/978-4-431-54880-5_9.

Chang, Bo, Hemant Khanna, Norman Hawes, David Jimeno, Shirley He, Concepcion Lillo, Sunil K. Parapuram, et al. 2006. “In-Frame Deletion in a Novel Centrosomal/ciliary Protein CEP290/NPHP6 Perturbs Its Interaction with RPGR and Results in Early-Onset Retinal Degeneration in the rd16 Mouse.” *Human Molecular Genetics* 15 (11): 1847–57. doi:10.1093/hmg/ddl107.

Chattopadhyay, S., S. C. Hung, A. C. Stuart, A. G. Palmer, J. Garcia-Mena, A. Das, and M. E. Gottesman. 1995. “Interaction between the Phage HK022 Nun Protein and the Nut RNA of Phage Lambda.” *Proceedings of the National Academy of Sciences* 92 (26): 12131–35. doi:10.1073/pnas.92.26.12131.

Daiger, S P, L S Sullivan, and S J Bowne. 2013. “Genes and Mutations Causing Retinitis Pigmentosa: Genes and Mutations Causing Retinitis Pigmentosa.” *Clinical Genetics* 84 (2): 132–41. doi:10.1111/cge.12203.

Daoud, Rosette, Gunter Mies, Agata Smialowska, Laszlo Olah, Konstantin-Alexander Hossmann, and Stefan Stamm. 2002. “Ischemia Induces a Translocation of the Splicing Factor tra2-Beta 1 and Changes Alternative Splicing Patterns in the Brain.” *J. Neurosci.* 22 (14): 5889–99. doi:20026571.

Ehrmann, Ingrid, Caroline Dalgliesh, Yilei Liu, Marina Danilenko, Moira Crosier, Lynn Overman, Helen M. Arthur, et al. 2013. “The Tissue-Specific RNA Binding Protein T-STAR Controls Regional Splicing Patterns of Neurexin Pre-mRNAs in the Brain.” *PLoS Genetics* 9 (4). doi:10.1371/journal.pgen.1003474.

Fox, Raymond G., Frederick D. Park, Claire S. Koechlein, Marcie Kritzik, and Tannishtha Reya. 2015. “Musashi Signaling in Stem Cells and Cancer.” *Annual Review of Cell and Developmental Biology* 31 (1): 249–67. doi:10.1146/annurev-cellbio-100814-125446.

Furukawa, Takahisa, Eric M. Morrow, Tiansen Li, Fred C. Davis, and Constance L. Cepko. 1999. “Retinopathy and Attenuated Circadian Entrainment in Crx-Deficient Mice.” *Nature Genetics* 23 (4): 466–70. doi:10.1038/70591.

Gargini, Cludia, Eva Terzibasi, Francesca Mazzoni, and Enrica Strettoi. 2007. “Retinal Organization in the Retinal Degeneration 10 (rd10) Mutant Mouse: A Morphological and ERG Study.” *The Journal of Comparative Neurology* 500 (2): 222–38. doi:10.1002/cne.21144.

Gehman, Lauren T, Peter Stoilov, Jamie Maguire, Andrey Damianov, Chia-Ho Lin, Lily Shiue, Manuel Ares, Istvan Mody, and Douglas L Black. 2011. “The Splicing Regulator Rbfox1 (A2BP1) Controls Neuronal Excitation in the Mammalian Brain.” *Nat Genet* 43 (7): 706–11. doi:10.1038/ng.841.

Gehman, L. T., P. Meera, P. Stoilov, L. Shiue, J. E. O'Brien, M. H. Meisler, M. Ares, T. S. Otis, and D. L. Black. 2012. "The Splicing Regulator Rbfox2 Is Required for Both Cerebellar Development and Mature Motor Function." *Genes & Development* 26 (5): 445–60. doi:10.1101/gad.182477.111.

Goers, Emily S., Jamie Purcell, Rodger B. Voelker, Devika P. Gates, and J. Andrew Berglund. 2010. "MBNL1 Binds GC Motifs Embedded in Pyrimidines to Regulate Alternative Splicing." *Nucleic Acids Research* 38 (7): 2467–84. doi:10.1093/nar/gkp1209.

Han, Areum, Peter Stoilov, Anthony J. Linares, Yu Zhou, Xiang-Dong Fu, and Douglas L. Black. 2014. "De Novo Prediction of PTBP1 Binding and Splicing Targets Reveals Unexpected Features of Its RNA Recognition and Function." *PLoS Computational Biology* 10 (1). doi:10.1371/journal.pcbi.1003442.

Heinicke, Laurie A., Behnam Nabet, Shihao Shen, Peng Jiang, Sebastiaan van Zalen, Benjamin Cieply, J. Eric Russell, Yi Xing, and Russ P. Carstens. 2013. "The RNA Binding Protein RBM38 (RNPC1) Regulates Splicing during Late Erythroid Differentiation." *PLoS ONE* 8 (10): e78031. doi:10.1371/journal.pone.0078031.

Hertel, Klemens J. 2008. "Combinatorial Control of Exon Recognition." *Journal of Biological Chemistry* 283 (3): 1211–15. doi:10.1074/jbc.R700035200.

Iijima, Takatoshi, Yoko Iijima, Harald Witte, and Peter Scheiffele. 2014. "Neuronal Cell Type–specific Alternative Splicing Is Regulated by the KH Domain Protein SLM1." *The Journal of Cell Biology* 204 (3): 331–42. doi:10.1083/jcb.201310136.

Iijima, Takatoshi, Karen Wu, Harald Witte, Yoko Hanno-Iijima, Timo Glatter, Stéphane Richard, and Peter Scheiffele. 2011. "SAM68 Regulates Neuronal Activity-Dependent Alternative Splicing of Neurexin-1." *Cell* 147 (7): 1601–14. doi:10.1016/j.cell.2011.11.028.

Irimia, Manuel, Robert J. Weatheritt, Jonathan D. Ellis, Neelroop N. Parikshak, Thomas Gonatopoulos-Pournatzis, Mariana Babor, Mathieu Quesnel-Vallières, et al. 2014. "A Highly

Conserved Program of Neuronal Microexons Is Misregulated in Autistic Brains." *Cell* 159 (7): 1511–23. doi:10.1016/j.cell.2014.11.035.

Izquierdo, José M. 2008. "Hu Antigen R (HuR) Functions as an Alternative Pre-mRNA Splicing Regulator of Fas Apoptosis-Promoting Receptor on Exon Definition." *Journal of Biological Chemistry* 283 (27): 19077–84. doi:10.1074/jbc.M800017200.

Jensen, Kirk B, B. Kate Dredge, Giovanni Stefani, Ru Zhong, Ronald J Buckanovich, Hirotaka J Okano, Yolanda Y. L Yang, and Robert B Darnell. 2000. "Nova-1 Regulates Neuron-Specific Alternative Splicing and Is Essential for Neuronal Viability." *Neuron* 25 (2): 359–71. doi:10.1016/S0896-6273(00)80900-9.

Johnson, Matthew B., Peter P. Wang, Kutay D. Atabay, Elisabeth A. Murphy, Ryan N. Doan, Jonathan L. Hecht, and Christopher A. Walsh. 2015. "Single-Cell Analysis Reveals Transcriptional Heterogeneity of Neural Progenitors in Human Cortex." *Nature Neuroscience* 18 (5): 637–46. doi:10.1038/nn.3980.

Kaneko, Jun, and Chikafumi Chiba. 2009. "Immunohistochemical Analysis of Musashi-1 Expression during Retinal Regeneration of Adult Newt." *Neuroscience Letters* 450 (3): 252–57. doi:10.1016/j.neulet.2008.11.031.

Kim, Kee K., Joseph Nam, Yoh-suke Mukouyama, and Sachiyo Kawamoto. 2013. "Rbfox3-Regulated Alternative Splicing of Numb Promotes Neuronal Differentiation during Development." *The Journal of Cell Biology* 200 (4): 443–58. doi:10.1083/jcb.201206146.

Kolandaivelu, Saravanan, Ratnesh K. Singh, and Visvanathan Ramamurthy. 2014. "AIPL1, A Protein Linked to Blindness, Is Essential for the Stability of Enzymes Mediating cGMP Metabolism in Cone Photoreceptor Cells." *Human Molecular Genetics* 23 (4): 1002–12. doi:10.1093/hmg/ddt496.

Lee, Ji-Ann, Zhen-Zhi Tang, and Douglas L. Black. 2009. "An Inducible Change in Fox-1/A2BP1 Splicing Modulates the Alternative Splicing of Downstream Neuronal Target Exons." *Genes & Development* 23 (19): 2284–93. doi:10.1101/gad.1837009.

Liao, Yang, Gordon K. Smyth, and Wei Shi. 2014. “featureCounts: An Efficient General Purpose Program for Assigning Sequence Reads to Genomic Features.” *Bioinformatics* 30 (7): 923–30. doi:10.1093/bioinformatics/btt656.

Licatalosi, Donny D., Aldo Mele, John J. Fak, Jernej Ule, Melis Kayikci, Sung Wook Chi, Tyson A. Clark, et al. 2008. “HITS-CLIP Yields Genome-Wide Insights into Brain Alternative RNA Processing.” *Nature* 456 (7221): 464–69. doi:10.1038/nature07488.

Li, Heng, Bob Handsaker, Alec Wysoker, Tim Fennell, Jue Ruan, Nils Homer, Gabor Marth, Goncalo Abecasis, and Richard Durbin. 2009. “The Sequence Alignment/Map Format and SAMtools.” *Bioinformatics* 25 (16): 2078–79. doi:10.1093/bioinformatics/btp352.

Li, Qin, Ji-Ann Lee, and Douglas L. Black. 2007. “Neuronal Regulation of Alternative Pre-mRNA Splicing.” *Nature Reviews Neuroscience* 8 (11): 819–31. doi:10.1038/nrn2237.

Li, Qin, Sika Zheng, Areum Han, Chia-Ho Lin, Peter Stoilov, Xiang-Dong Fu, and Douglas L Black. 2014. “The Splicing Regulator PTBP2 Controls a Program of Embryonic Splicing Required for Neuronal Maturation.” *eLife* 3 (January). doi:10.7554/eLife.01201.

Li, Yang I., Luis Sanchez-Pulido, Wilfried Haerty, and Chris P. Ponting. 2014. “RBFOX and PTBP1 Proteins Regulate the Alternative Splicing of Micro-Exons in Human Brain Transcripts.” *Genome Research*, December, gr.181990.114. doi:10.1101/gr.181990.114.

Lumayag, Stephen, Caroline E. Haldin, Nicola J. Corbett, Karl J. Wahlin, Colleen Cowan, Sanja Turturro, Peter E. Larsen, et al. 2013. “Inactivation of the microRNA-183/96/182 Cluster Results in Syndromic Retinal Degeneration.” *Proceedings of the National Academy of Sciences* 110 (6): E507–16. doi:10.1073/pnas.1212655110.

Macosko, Evan Z., Anindita Basu, Rahul Satija, James Nemesh, Karthik Shekhar, Melissa Goldman, Itay Tirosh, et al. 2015. “Highly Parallel Genome-Wide Expression Profiling of Individual Cells Using Nanoliter Droplets.” *Cell* 161 (5): 1202–14. doi:10.1016/j.cell.2015.05.002.

Makeyev, Eugene V., Jiangwen Zhang, Monica A. Carrasco, and Tom Maniatis. 2007. “The MicroRNA miR-124 Promotes Neuronal Differentiation by Triggering Brain-Specific Alternative Pre-mRNA Splicing.” *Molecular Cell* 27 (3): 435–48. doi:10.1016/j.molcel.2007.07.015.

Masland, Richard H. 2012. “The Neuronal Organization of the Retina.” *Neuron* 76 (2): 266–80. doi:10.1016/j.neuron.2012.10.002.

Matsuda, Takahiko, and Constance L. Cepko. 2004. “Electroporation and RNA Interference in the Rodent Retina in Vivo and in Vitro.” *Proceedings of the National Academy of Sciences* 101 (1): 16–22. doi:10.1073/pnas.2235688100.

Mears, Alan J., Mineo Kondo, Prabodha K. Swain, Yuichiro Takada, Ronald A. Bush, Thomas L. Saunders, Paul A. Sieving, and Anand Swaroop. 2001. “Nrl Is Required for Rod Photoreceptor Development.” *Nature Genetics* 29 (4): 447–52. doi:10.1038/ng774.

Morrow, Eric M., Takahisa Furukawa, Elio Raviola, and Constance L. Cepko. 2005. “Synaptogenesis and Outer Segment Formation Are Perturbed in the Neural Retina of Crx Mutant Mice.” *BMC Neuroscience* 6: 5. doi:10.1186/1471-2202-6-5.

Murphy, Daniel, Ratnesh Singh, Saravanan Kolandaivelu, Visvanathan Ramamurthy, and Peter Stoilov. 2015. “Alternative Splicing Shapes the Phenotype of a Mutation in BBS8 to Cause Nonsyndromic Retinitis Pigmentosa.” *Molecular and Cellular Biology*, March. doi:10.1128/MCB.00040-15.

Nakamura, Makoto, Hideyuki Okano, Julie A. Blendy, and Craig Montell. 1994. “Musashi, a Neural RNA-Binding Protein Required for Drosophila Adult External Sensory Organ Development.” *Neuron* 13 (1): 67–81. doi:10.1016/0896-6273(94)90460-X.

Newman, Emily A, Stephanie J Muh, Ruben H Hovhannisyan, Claude C Warzecha, Richard B Jones, Wallace L McKeehan, and Russ P Carstens. 2006. “Identification of RNA-Binding Proteins That Regulate FGFR2 Splicing through the Use of Sensitive and Specific Dual

Color Fluorescence Minigene Assays.” *RNA (New York, N.Y.)* 12 (6): 1129–41. doi:PMC1464843.

Nickerson, P. E. B., T. Myers, D. B. Clarke, and R. L. Chow. 2011. “Changes in Musashi-1 Subcellular Localization Correlate with Cell Cycle Exit during Postnatal Retinal Development.” *Experimental Eye Research* 92 (5): 344–52. doi:10.1016/j.exer.2011.02.002.

Ochrietor, Judith D., Tatiana P. Moroz, Leslie van Ekeris, Michael F. Clamp, Stephanie C. Jefferson, Ana C. deCarvalho, James M. Fadool, Graeme Wistow, Takashi Muramatsu, and Paul J. Linser. 2003. “Retina-Specific Expression of 5A11/Basigin-2, a Member of the Immunoglobulin Gene Superfamily.” *Investigative Ophthalmology & Visual Science* 44 (9): 4086–96. doi:10.1167/iovs.02-0995.

Okano, Hideyuki, Takao Imai, and Masataka Okabe. 2002. “Musashi: A Translational Regulator of Cell Fate.” *Journal of Cell Science* 115 (7): 1355–59.

Pretorius, Pamela R., Mohammed A. Aldahmesh, Fowzan S. Alkuraya, Val C. Sheffield, and Diane C. Slusarski. 2011. “Functional Analysis of BBS3 A89V That Results in Non-Syndromic Retinal Degeneration.” *Human Molecular Genetics* 20 (8): 1625–32. doi:10.1093/hmg/ddr039.

Pretorius, Pamela R., Lisa M. Baye, Darryl Y. Nishimura, Charles C. Searby, Kevin Bugge, Baoli Yang, Robert F. Mullins, Edwin M. Stone, Val C. Sheffield, and Diane C. Slusarski. 2010. “Identification and Functional Analysis of the Vision-Specific BBS3 (ARL6) Long Isoform.” *PLoS Genet* 6 (3): e1000884. doi:10.1371/journal.pgen.1000884.

“Pysam-Developers/pysam.” 2016. *GitHub*. Accessed January 20. https://github.com/pysam-developers/pysam.

Raj, Bushra, and Benjamin J. Blencowe. 2015. “Alternative Splicing in the Mammalian Nervous System: Recent Insights into Mechanisms and Functional Roles.” *Neuron* 87 (1): 14–27. doi:10.1016/j.neuron.2015.05.004.

Ramamurthy, Visvanathan, Gregory A. Niemi, Thomas A. Reh, and James B. Hurley. 2004. "Leber Congenital Amaurosis Linked to AIPL1: A Mouse Model Reveals Destabilization of cGMP Phosphodiesterase." *Proceedings of the National Academy of Sciences of the United States of America* 101 (38): 13897–902. doi:10.1073/pnas.0404197101.

Ray, Debashish, Hilal Kazan, Kate B. Cook, Matthew T. Weirauch, Hamed S. Najafabadi, Xiao Li, Serge Gueroussov, et al. 2013. "A Compendium of RNA-Binding Motifs for Decoding Gene Regulation." *Nature* 499 (7457): 172–77. doi:10.1038/nature12311.

Riazuddin, S. Amer, Muhammad Iqbal, Yue Wang, Tomohiro Masuda, Yuhng Chen, Sara Bowne, Lori S. Sullivan, et al. 2010. "A Splice-Site Mutation in a Retina-Specific Exon of BBS8 Causes Nonsyndromic Retinitis Pigmentosa." *American Journal of Human Genetics* 86 (5): 805–12. doi:10.1016/j.ajhg.2010.04.001.

Robinson, Mark D., Davis J. McCarthy, and Gordon K. Smyth. 2010. "edgeR: A Bioconductor Package for Differential Expression Analysis of Digital Gene Expression Data." *Bioinformatics* 26 (1): 139–40. doi:10.1093/bioinformatics/btp616.

Roger, Jerome E., Avinash Hiriyanna, Norimoto Gotoh, Hong Hao, Debbie F. Cheng, Rinki Ratnapriya, Marie-Audrey I. Kautzmann, Bo Chang, and Anand Swaroop. 2014. "OTX2 Loss Causes Rod Differentiation Defect in CRX-Associated Congenital Blindness." *The Journal of Clinical Investigation* 124 (2): 631–43. doi:10.1172/JCI72722.

Rotem, Assaf, Oren Ram, Noam Shoresh, Ralph A. Sperling, Michael Schnall-Levin, Huidan Zhang, Anindita Basu, Bradley E. Bernstein, and David A. Weitz. 2015. "High-Throughput Single-Cell Labeling (Hi-SCL) for RNA-Seq Using Drop-Based Microfluidics." *PLoS ONE* 10 (5): e0116328. doi:10.1371/journal.pone.0116328.

Shen, Shihao, Juw Won Park, Zhi-xiang Lu, Lan Lin, Michael D. Henry, Ying Nian Wu, Qing Zhou, and Yi Xing. 2014. "rMATS: Robust and Flexible Detection of Differential Alternative Splicing from Replicate RNA-Seq Data." *Proceedings of the National Academy of Sciences* 111 (51): E5593–5601. doi:10.1073/pnas.1419161111.

Shen, S., J. W. Park, J. Huang, K. A. Dittmar, Z.-x. Lu, Q. Zhou, R. P. Carstens, and Y. Xing. 2012. “MATS: A Bayesian Framework for Flexible Detection of Differential Alternative Splicing from RNA-Seq Data.” *Nucleic Acids Research* 40 (8): e61–e61. doi:10.1093/nar/gkr1291.

Shin, Jaehoon, Daniel A. Berg, Yunhua Zhu, Joseph Y. Shin, Juan Song, Michael A. Bonaguidi, Grigori Enikolopov, et al. 2015. “Single-Cell RNA-Seq with Waterfall Reveals Molecular Cascades Underlying Adult Neurogenesis.” *Cell Stem Cell* 17 (3): 360–72. doi:10.1016/j.stem.2015.07.013.

Siegert, Sandra, Erik Cabuy, Brigitte Gross Scherf, Hubertus Kohler, Satchidananda Panda, Yun-Zheng Le, Hans Jörg Fehling, Dimos Gaidatzis, Michael B. Stadler, and Botond Roska. 2012. “Transcriptional Code and Disease Map for Adult Retinal Cell Types.” *Nature Neuroscience* 15 (3): 487–95. doi:10.1038/nn.3032.

Solovei, Irina, Moritz Kreysing, Christian Lanctôt, Süleyman Kösem, Leo Peichl, Thomas Cremer, Jochen Guck, and Boris Joffe. 2009. “Nuclear Architecture of Rod Photoreceptor Cells Adapts to Vision in Mammalian Evolution.” *Cell* 137 (2): 356–68. doi:10.1016/j.cell.2009.01.052.

Solovei, Irina, Audrey S. Wang, Katharina Thanisch, Christine S. Schmidt, Stefan Krebs, Monika Zwerger, Tatiana V. Cohen, et al. 2013. “LBR and Lamin A/C Sequentially Tether Peripheral Heterochromatin and Inversely Regulate Differentiation.” *Cell* 152 (3): 584–98. doi:10.1016/j.cell.2013.01.009.

Stoilov, Peter, Chia-Ho Lin, Robert Damoiseaux, Julia Nikolic, and Douglas L Black. 2008. “A High-Throughput Screening Strategy Identifies Cardiotonic Steroids as Alternative Splicing Modulators.” *Proceedings of the National Academy of Sciences of the United States of America* 105 (32): 11218–23. doi:PMC2516208.

Stojnic, Robert, and Diego Diez. 2015. *PWMEnrich: PWM Enrichment Analysis. R Package Version 4.6.0*.

Stoss, Oliver, Tatyana Novoyatleva, Marieta Gencheva, Manuela Olbrich, Natalya Benderska, and Stefan Stamm. 2004. “p59fyn-Mediated Phosphorylation Regulates the Activity of the Tissue-Specific Splicing Factor rSLM-1.” *Molecular and Cellular Neuroscience* 27 (1): 8–21. doi:10.1016/j.mcn.2004.04.011.

Stoss, Oliver, Manuela Olbrich, Annette M. Hartmann, Harald König, John Memmott, Athena Andreadis, and Stefan Stamm. 2001. “The STAR/GSG Family Protein rSLM-2 Regulates the Selection of Alternative Splice Sites.” *Journal of Biological Chemistry* 276 (12): 8665–73. doi:10.1074/jbc.M006851200.

Susaki, Kanako, Jun Kaneko, Yuka Yamano, Kenta Nakamura, Wataru Inami, Taro Yoshikawa, Yoko Ozawa, et al. 2009. “Musashi-1, an RNA-Binding Protein, Is Indispensable for Survival of Photoreceptors.” *Experimental Eye Research* 88 (3): 347–55. doi:10.1016/j.exer.2008.06.019.

Swaroop, Anand, Douglas Kim, and Douglas Forrest. 2010. “Transcriptional Regulation of Photoreceptor Development and Homeostasis in the Mammalian Retina.” *Nature Reviews Neuroscience* 11 (8): 563–76. doi:10.1038/nrn2880.

van der Houven van Oordt, Willemien, Maria T. Diaz-Meco, Jose Lozano, Adrian R. Krainer, Jorge Moscat, and Javier F. Caceres. 2000. “The MKK3/6-p38-Signaling Cascade Alters the Subcellular Distribution of hnRNP A1 and Modulates Alternative Splicing Regulation.” *J. Cell Biol.* 149 (2): 307–16. doi:10.1083/jcb.149.2.307.

Wang, Eric T., Neal A.L. Cody, Sonali Jog, Michela Biancolella, Thomas T. Wang, Daniel J. Treacy, Shujun Luo, et al. 2012. “Transcriptome-Wide Regulation of Pre-mRNA Splicing and mRNA Localization by Muscleblind Proteins.” *Cell* 150 (4): 710–24. doi:10.1016/j.cell.2012.06.041.

Wang, Jing, Dexter Duncan, Zhiao Shi, and Bing Zhang. 2013. “WEB-Based GEne SeT AnaLysis Toolkit (WebGestalt): Update 2013.” *Nucleic Acids Research* 41 (W1): W77–83. doi:10.1093/nar/gkt439.

Weyn-Vanhentenryck, Sebastien M., Aldo Mele, Qinghong Yan, Shuying Sun, Natalie Farny, Zuo Zhang, Chenghai Xue, et al. 2014. “HITS-CLIP and Integrative Modeling Define the Rbfox Splicing-Regulatory Network Linked to Brain Development and Autism.” *Cell Reports*. Accessed March 21. doi:10.1016/j.celrep.2014.02.005.

Wu, Angela R., Norma F. Neff, Tomer Kalisky, Piero Dalerba, Barbara Treutlein, Michael E. Rothenberg, Francis M. Mburu, et al. 2014. “Quantitative Assessment of Single-Cell RNA-Sequencing Methods.” *Nature Methods* 11 (1): 41–46. doi:10.1038/nmeth.2694.

Yang, Zhenglin, Yali Chen, Concepcion Lillo, Jeremy Chien, Zhengya Yu, Michel Michaelides, Martin Klein, et al. 2008. “Mutant Prominin 1 Found in Patients with Macular Degeneration Disrupts Photoreceptor Disk Morphogenesis in Mice.” *The Journal of Clinical Investigation* 118 (8): 2908–16. doi:10.1172/JCI35891.

Zearfoss, N. Ruth, Laura M. Deveau, Carina C. Clingman, Eric Schmidt, Emily S. Johnson, Francesca Massi, and Sean P. Ryder. 2014. “A Conserved Three-Nucleotide Core Motif Defines Musashi RNA-Binding Specificity.” *Journal of Biological Chemistry*, November, jbc.M114.597112. doi:10.1074/jbc.M114.597112.

Zeisel, Amit, Ana B. Muñoz-Manchado, Simone Codeluppi, Peter Lönnerberg, Gioele La Manno, Anna Juréus, Sueli Marques, et al. 2015. “Cell Types in the Mouse Cortex and Hippocampus Revealed by Single-Cell RNA-Seq.” *Science* 347 (6226): 1138–42. doi:10.1126/science.aaa1934.

Zheng, Sika, and Douglas L. Black. 2013. “Alternative Pre-mRNA Splicing in Neurons: Growing up and Extending Its Reach.” *Trends in Genetics* 29 (8): 442–48. doi:10.1016/j.tig.2013.04.003.

Tables

Table 1. GO categories enriched in genes differentially expressed in wild type compared to Aipl1(-/-) retina.

Genes with higher expression in wild type retina

GO Term	*GO term ID*	*Fold enrichment*	*Adjusted p-value*
Biological Process			
visual perception	GO:0007601	9.43	1.13E-33
sensory perception of light stimulus	GO:0050953	9.43	1.13E-33
detection of light stimulus	GO:0009583	13.16	7.06E-17
phototransduction	GO:0007602	14.51	1.88E-15
photoreceptor cell differentiation	GO:0046530	9.48	2.84E-13
photoreceptor cell development	GO:0042461	10.69	2.11E-12
retina development in camera-type eye	GO:0060041	5.96	3.53E-12
detection of abiotic stimulus	GO:0009582	6.86	8.06E-12
eye photoreceptor cell differentiation	GO:0001754	9.84	4.52E-11
photoreceptor cell maintenance	GO:0045494	12.22	8.73E-10
Molecular Function			
3',5'-cyclic-nucleotide phosphodiesterase activity	GO:0004114	7.53	0.0016
cyclic-nucleotide phosphodiesterase activity	GO:0004112	7.23	0.0016
3',5'-cyclic-GMP phosphodiesterase activity	GO:0047555	10.43	0.0016
cyclic nucleotide-gated ion channel activity	GO:0043855	12.55	0.0018
intracellular cyclic nucleotide activated cation channel activity	GO:0005221	12.55	0.0018
Cellular Component			

cilium	GO:0005929	6.37	2.43E-33
nonmotile primary cilium	GO:0031513	9.35	7.01E-24
primary cilium	GO:0072372	8.29	1.56E-22
photoreceptor outer segment	GO:0001750	12.19	2.29E-19
cell projection	GO:0042995	2.08	1.03E-13
photoreceptor inner segment	GO:0001917	13.18	9.67E-13
cilium part	GO:0044441	6.4	2.36E-10
photoreceptor connecting cilium	GO:0032391	9.93	6.62E-07
photoreceptor outer segment membrane	GO:0042622	15.99	1.13E-06
BBSome	GO:0034464	19.58	1.48E-06

Genes with lower expression in wild type retina

GO Term	*GO term ID*	*Fold enrichment*	*Adjusted p-value*
Biological Process			
biological adhesion	GO:0022610	2.58	1.07E-75
cell adhesion	GO:0007155	2.59	1.07E-75
locomotion	GO:0040011	2.23	3.01E-58
Molecular Function			
substrate-specific channel activity	GO:0022838	2.83	3.15E-45
ion channel activity	GO:0005216	2.84	8.67E-45
channel activity	GO:0015267	2.76	4.05E-44
passive transmembrane transporter activity	GO:0022803	2.76	4.05E-44
ion gated channel activity	GO:0022839	3.03	4.24E-40
transmembrane transporter activity	GO:0022857	2.09	4.24E-40

gated channel activity	GO:0022836	3.03	4.24E-40
substrate-specific transmembrane transporter activity	GO:0022891	2.14	2.83E-39
Cellular Component			
neuron projection	GO:0043005	2.38	9.01E-59
synapse	GO:0045202	2.62	1.62E-54
extracellular matrix	GO:0031012	2.99	9.06E-54
cell junction	GO:0030054	2.35	3.35E-52

Table 2. GO terms enriched in genes with exons differentially spliced in wild type retina compared to retina from Aipl1(-/-) animals

GO Term	GO term ID	Fold enrichment	Adjusted p-value
Biological Process			
cellular component organization or biogenesis at cellular level	GO:0071841	1.6	3.00E-04
cellular component organization at cellular level	GO:0071842	1.61	3.00E-04
nervous system development	GO:0007399	1.96	4.00E-04
cellular component organization	GO:0016043	1.5	4.00E-04
cellular component organization or biogenesis	GO:0071840	1.49	4.00E-04
single-organism process	GO:0044699	1.35	7.00E-04
neuron differentiation	GO:0030182	2.22	7.00E-04
cellular process	GO:0009987	1.16	1.40E-03
cell projection organization	GO:0030030	2.09	2.60E-03
neuron development	GO:0048666	2.25	2.60E-03
generation of neurons	GO:0048699	2.05	2.60E-03

neuron projection development	GO:0031175	2.33	3.30E-03
regulation of cellular process	GO:0050794	1.27	3.30E-03
cell communication	GO:0007154	1.42	3.30E-03
cell development	GO:0048468	1.81	3.30E-03
neurogenesis	GO:0022008	1.97	3.30E-03
cellular component morphogenesis	GO:0032989	2.05	3.30E-03
biological regulation	GO:0065007	1.24	3.40E-03
cell morphogenesis	GO:0000902	2.07	3.90E-03
cell-cell signaling	GO:0007267	2.14	6.00E-03
regulation of biological process	GO:0050789	1.24	6.00E-03
organelle organization	GO:0006996	1.56	6.90E-03
Molecular Function			
binding	GO:0005488	1.25	1.54E-08
protein binding	GO:0005515	1.32	4.00E-04
cytoskeletal protein binding	GO:0008092	2.2	1.90E-03
Cellular Component			
intracellular	GO:0005622	1.24	1.44E-09
cell part	GO:0044464	1.18	5.95E-08
cell	GO:0005623	1.18	5.95E-08
intracellular part	GO:0044424	1.22	8.83E-08
cytoplasm	GO:0005737	1.28	3.71E-06
organelle	GO:0043226	1.21	8.11E-05
intracellular organelle	GO:0043229	1.21	1.00E-04
cell projection	GO:0042995	1.79	3.00E-04
synapse	GO:0045202	2.17	1.10E-03

non-membrane-bounded organelle	GO:0043228	1.48	1.10E-03
intracellular non-membrane-bounded organelle	GO:0043232	1.48	1.10E-03
microtubule	GO:0005874	2.71	1.40E-03
clathrin coat of coated pit	GO:0030132	13.37	1.80E-03
cytoskeleton	GO:0005856	1.61	1.80E-03
membrane-bounded organelle	GO:0043227	1.18	3.40E-03
intracellular membrane-bounded organelle	GO:0043231	1.17	8.00E-03
nucleus	GO:0005634	1.26	9.00E-03

Table 3: Binding site enrichment in the regulated exons and 200nt of the adjacent introns. Locations with significant enrichment/depletion (FDR corrected p-value < 0.01) are shown in bold typeface.

RNA binding protein	Upregulated exons					
	Upstream intron		Exon		Downstream intron	
	Fold enrichment	FDR	Fold enrichment	FDR	Fold enrichment	FDR
A1CF	1.13	3.08E-01	1.42	7.72E-01	1.14	4.88E-01
EIF2S1	1.17	3.08E-01	1.71	4.96E-02	1.06	9.77E-01
ELAVL1/2/3	1.14	1.60E-01	***0.73***	***6.10E-04***	1.08	6.31E-01
KHDRBS1/2/3	1.14	8.25E-01	1.87	4.68E-01	0.79	3.56E-01
LIN28	0.60	7.47E-02	0.79	6.97E-01	0.85	5.86E-01
MEX3A/B/C/D	1.31	3.44E-01	2.41	6.68E-01	0.82	6.16E-01
MSI1/2	0.90	3.08E-01	1.13	9.14E-01	***1.29***	***3.32E-07***
NOVA1/2	1.12	1.20E-01	1.09	1.64E-01	0.96	5.79E-02
PCBP1/2/3	***1.34***	***2.68E-03***	0.76	3.49E-01	1.09	3.67E-01
PTBP1/2/3	***1.11***	***1.42E-03***	0.98	7.72E-01	1.07	9.79E-02
RBFOX1/2/3	1.81	1.47E-01	2.14	5.84E-02	1.22	9.81E-01
RBM41	1.23	1.72E-01	1.42	7.88E-01	0.73	1.17E-01

SRSF2	0.84	4.54E-01	0.90	9.62E-01	0.87	6.16E-01
SRSF9	0.75	1.20E-01	0.96	9.14E-01	0.97	7.93E-01

RNA binding protein	Downregulated exons					
	Upstream intron		Exon		Downstream intron	
	Fold enrichment	FDR	Fold enrichment	FDR	Fold enrichment	FDR
A1CF	0.86	4.91E-01	***2.39***	***4.65E-03***	1.26	2.56E-01
EIF2S1	0.91	5.24E-01	1.08	3.99E-01	***2.46***	***7.10E-05***
ELAVL1/2/3	1.00	5.24E-01	***1.82***	***9.84E-05***	1.30	3.88E-02
KHDRBS1/2/3	2.31	1.25E-02	***2.37***	***4.38E-03***	0.79	3.02E-01
LIN28	1.29	3.20E-01	***0.55***	***4.38E-03***	0.66	2.56E-01
MEX3A/B/C/D	0.82	5.70E-01	***4.57***	***4.38E-03***	0.57	2.98E-01
MSI1/2	0.88	2.14E-01	***1.45***	***9.29E-07***	0.93	3.06E-01
NOVA1/2	1.06	2.77E-01	0.99	5.80E-01	***1.25***	***3.21E-04***
PCBP1/2/3	0.87	3.48E-01	0.77	1.24E-01	1.03	4.45E-01
PTBP1/2/3	1.03	3.02E-02	0.93	3.64E-01	1.05	1.00E-02
RBFOX1/2/3	1.40	3.20E-01	0.90	5.30E-01	***4.18***	***5.43E-07***
RBM41	0.75	3.48E-01	***2.45***	***4.38E-03***	1.14	3.26E-01
SRSF2	0.76	3.86E-01	***0.40***	***1.01E-05***	0.64	2.48E-01
SRSF9	0.80	2.05E-01	***0.75***	***6.47E-03***	0.73	7.99E-02

Table 4. Expression level difference of RNA binding protein in wild type retina compared to retina from Aipl1(-/-) mice. Significant differences in gene expression are shown in bold typeface.

Entrez GeneID	*Symbol*	*Log(2) Fold Change WT/AIPL1(-/-)*	*FDR*
15568	**Elavl1**	**-0.56**	**6.113E-3**
15569	**Elavl2**	**-1.21**	**1.226E-7**
15571	**Elavl3**	**-1.51**	**1.762E-16**
15572	**Elavl4**	**-1.23**	**1.796E-11**
20218	Khdrbs1	-0.16	5.493E-1
170771	**Khdrbs2**	**-1.33**	**5.649E-16**
13992	Khdrbs3	0.47	1.224E-2
17690	**Msi1**	**0.50**	**9.849E-3**
76626	Msi2	0.36	6.597E-2

664883	**Nova1**	**-1.69**	**3.542E-10**
384569	**Nova2**	**-2.02**	**1.272E-14**
19205	**Ptbp1**	**-0.49**	**8.269E-4**
56195	Ptbp2	-0.34	1.634E-1
230257	Ptbp3	-0.24	2.717E-1
268859	**Rbfox1**	**-1.32**	**1.798E-16**
93686	**Rbfox2**	**-1.21**	**3.027E-15**
52897	**Rbfox3**	**-1.20**	**1.954E-10**
51796	Srrm1	0.16	6.699E-1
75956	Srrm2	-0.21	5.651E-1
58212	Srrm3	-0.26	2.886E-1
68955	**Srrm4**	**-1.35**	**3.802E-6**

Figure legends

Figure 1. Identification of differentially spliced exons in photoreceptors. (A) Retinal sections from wild type (left) and Aipl1(-/-) mice stained with toluidine blue at postnatal day 50. Low magnification images show the overall retinal structure near the site of the optic nerve (top). Red rectangles indicate the position of the magnified images shown below. Below, high magnification images show the layered retinal structure. The Aipl1(-/-) animals lack layers formed by the photoreceptor cells: outer nuclear layer (ONL), inner segment (IS) and outer segment (OS). The retinal pigmented epithelium (RPE), the inner nuclear layer (INL) and ganglion cell layer (GCL) are intact in the Aipl1(-/-) animals. **(B)** Experimental approach for identifying transcripts differentially expressed in photoreceptors. The retina transcriptome is an aggregate of the transcriptomes of multiple cell types. Approximately 40-60% of the cells in the neural retina are photoreceptors. Due to the abundance of photoreceptors in the retina, their loss produces changes in the retinal transcriptome that are readily detectable. **(C)** RT-PCR analysis of the inclusion levels of exons identified in the RNA-Seq analysis in retina from wild type, Aipl1(-/-) and Nrl(-/-) mice. The exons include the previously described photoreceptor specific exon 2A in the Ttc8 gene and retina enriched exon 6 in the Arl6 gene. The bands corresponding to the exon skipped and exon included mRNA isoforms are labeled with '+' and '-', respectively. The relative exon inclusion and standard error of three independent replicates are shown below each lane.

Figure 2. The photoreceptors express a splicing program that is distinct from the splicing profiles of CNS or other retinal neurons. Heatmap showing the relative inclusion levels of exons differentially spliced between the retina of wild type and Aipl(-/-) animals across a panel of mouse tissues. Unsupervised hierarchical clustering places retinal samples from Aipl1(-/-) mice along with the CNS samples, while the wild type retina samples form a separate cluster.

Microexons with length of 30nt or less are annotated on the right. The red bar on the left shows a cluster of photoreceptor specific exons with “switch like” splicing pattern.

Figure 3. The photoreceptor splicing program is executed in the postmitotic progenitors independent of Crx. (A) Heatmap showing the inclusion of exon differentially spliced in photoreceptors across retinal samples from wild type mice and genetically engineered mouse models. Unsupervised hierarchical clustering groups the sample in two major clusters. One cluster groups samples from retinas that lack photoreceptors (RD10, Aipl1(-/-)) with wild type retina at postnatal day 2 (P2). The second cluster contains wild type retina samples from postnatal days 50 (P50) and 21 (P21) along with samples from mice carrying a dominant negative mutation in the Crx gene (Crx-DN) and knockout animals lacking the Crx or Nrl genes. Microexons with length of 30nt or less are annotated on the right. **(B)** RT-PCR analysis of the splicing of four photoreceptor specific exons in the developing retina between postnatal days 0 and 16. The bands corresponding to the exon skipped and exon included mRNA isoforms are labeled with ‘+’ and ‘-’, respectively. Key landmarks in eye development between postnatal days 0 and 16 are indicated with arrows below the gel images.

Figure 4. Enriched motifs for RNA binding proteins in exons differentially spliced in photoreceptors and expression of neuronal splicing regulators in the retina. (A) Diagram showing the position and enrichment of RNA binding protein motifs in proximity to the exons that are differentially spliced in photoreceptors. Sites enriched/depleted in the upregulated exons are shown on top in green and sites enriched/depleted in downregulated exons are shown below the exon diagram in red. Stacked ovals indicate clusters of binding sites. Pale colors indicate depletion of the motif. The fold enrichment and false discovery rate corrected p-values are shown next to each site. Clustered motifs are also labeled with the minimum number of motifs per cluster and the maximum spacing between the motifs in the cluster. **(B)** Immunofluorescence (IF) staining of retinal sections with antibodies against RBFOX, NOVA1,

ELAVL, PTBP1, PTBP2, MSI1, MSI2, KHDRBS1, KHDRBS2 and KHDRBS3. IF signal is shown in grayscale and DAPI staining of the nuclear DNA is in blue. DAPI staining, shown for half of each section, indicates the position of the outer nuclear (ONL), inner nuclear (INL) and ganglion cell (GCL) layers.

Figure 5. Musashi 1 is present in the nuclei of photoreceptor cells. (A) Immunofluorescence staining of the outer nuclear layer on 4μm retinal sections. The nuclear envelope is stained with Lamin-B antibody (red). MSI1 staining is shown in gray. The nuclear DNA is stained with DAPI (blue). **(B)** Quantification of the Lamin-B, Msi1 and DAPI signal in the nuclei of photoreceptor cells. Lamin-B, Msi1 and DAPI fluorescence intensities were measured along a line perpendicular to the nuclear envelope (inset). The intensities measured on 54 nuclei were normalized and aligned to the peak of the Lamin-B staining.

Figure 6. Binding of Musashi 1 downstream of an alternative exon promotes its inclusion. (A) Diagram of the BoxB minigenes. In the wild type minigene two BoxB hairpins are positioned in the intron downstream of an alternative exon. In the G1A minigene a G to A mutation in the BoxB hairpins prevents binding of the λN peptide to the RNA. **(B)** RT-PCR analysis of the splicing of the wild type and G1A minigenes after co-transfection with empty vector (EV) or vector expressing Msi1- λN fusion (left). The exon included and exon skipped isoforms are indicated with '+' and '-', respectively. Relative exon inclusion levels with standard error are shown below each lane. On the right, western blot shows the expression levels of the Msi1- λN protein as detected by the anti-Msi1 and anti-Flag antibodies. GAPDH and Lamin-B are used as loading controls.

Figure 7. Musashi proteins bind downstream of Ttc8 exon 2A and promote its inclusion in photoreceptor cells. (A) Diagram of Ttc8 exon 2A and the adjacent introns. Musashi binding sites in the introns are shown with tick marks above the intron. Clusters of Musashi binding sites in the downstream intron are labeled with numbers. Binding sites in the downstream intron that

were mutated to create the Ttc8-dMsi minigene are shown in red. The sequence mutated in the Ttc8-dMsi minigene is shown below the diagram with the mutated bases in red. **(B)** Pull-down of Musashi proteins from retinal extracts. Three biotinylated probes corresponding to segments D2, D3, and D4 were used to pull down RNA binding proteins from retinal extracts. The binding was competed with the competitor RNA as indicated above. The Musashi proteins were then detected by western blot using an antibody that recognizes both Msi1 and Msi2. **(C)** RT-PCR analysis of the wild type and mutant Ttc8 exon 2A minigene transcripts after co-transfection with construct expressing flag-tagged Msi1 protein. The exon included and exon skipped isoforms are indicated with '+' and '-', respectively. Relative exon inclusion levels with standard error are shown below each lane. On the right western blot shows the expression levels of the Msi1- flag protein as detected by the anti-Msi1 and anti-Flag antibodies. GAPDH and Lamin-B are used as loading controls. **(D)** RT-PCR analysis and fluorescence imaging of the splicing of the Ttc8 minigene transcripts in the retina. Mouse retinas were electroporated with each minigene at postnatal day 0 and the splicing was analyzed by RT-PCR at postnatal day 16 and by fluorescence imaging at postnatal day 20. Relative exon inclusion levels with standard error are shown below each lane. The minigene is designed to produce GFP when the alternative exon is skipped or RFP when the exon is included. The wild type minigene is shown on the right. High RFP and low GFP expression in the photoreceptors indicates that the exon is included in the mature transcripts from the minigene. The inner neurons, marked with yellow arrows, express almost exclusively GFP, an indication that the exon is skipped. Reduced RFP expression and increased GFP levels in the mutant minigene indicate that the exon is mostly skipped in photoreceptors, in agreement with the RT-PCR analysis.

Figure 8. Musashi 1 promotes the inclusion of photoreceptor specific exons. (A) RT-PCR analysis of the inclusion levels of 11 exons with elevated inclusion levels in photoreceptors in N2A cell transfected with flag-tagged Msi1 expression construct. The exon included and exon

skipped isoforms are indicated with '+' and '-' respectively. On the right, western blot shows the expression of the flag-tagged Msi1 protein. **(B)** Chart showing the quantification of the inclusion levels of seven exons affected by the Msi1 protein. **(C)** Diagram showing a protein interaction network enriched in photoreceptor specific isoforms. The network is centered on Cep290 and the BBSome. Genes containing "switch-like" exons are shown in dark red or green. Red and green colors indicate inclusion and skipping in photoreceptors, respectively. Genes containing exons differentially spliced in photoreceptors are shown in pale red or green.

Figure 1

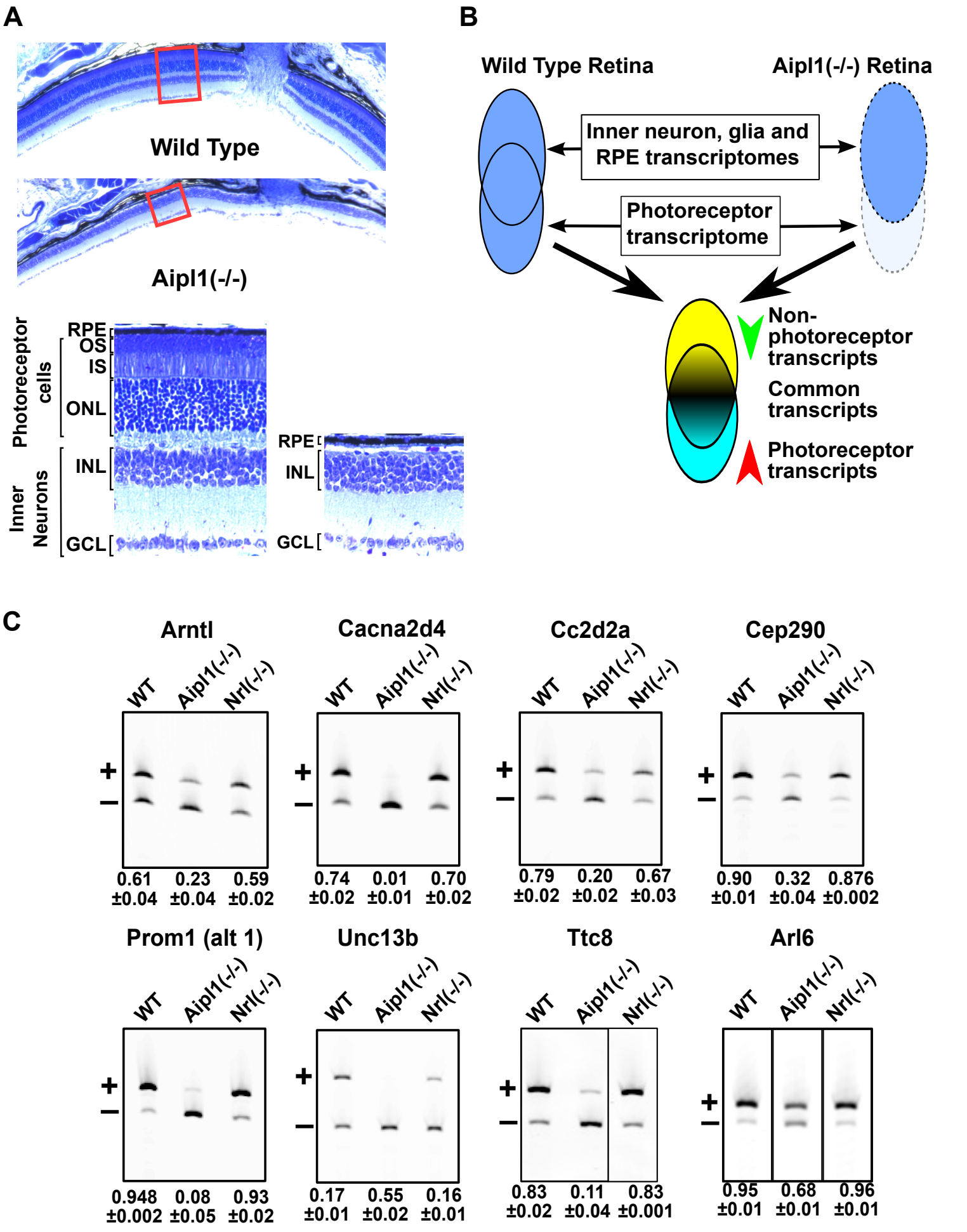
A
Wild Type
Aipl1(-/-)
Photoreceptor cells
RPE
OS
IS
ONL
Inner Neurons
INL
GCL
RPE
INL
GCL
B
Wild Type Retina
Aipl1(-/-) Retina
Inner neuron, glia and RPE transcriptomes
Photoreceptor transcriptome
Non-photoreceptor transcripts
Common transcripts
Photoreceptor transcripts
C
Arntl
Cacna2d4
Cc2d2a
Cep290
WT
Aipl1(-/-)
Nrl(-/-)
+
−
0.61 ±0.04
0.23 ±0.04
0.59 ±0.02
0.74 ±0.02
0.01 ±0.01
0.70 ±0.02
0.79 ±0.02
0.20 ±0.02
0.67 ±0.03
0.90 ±0.01
0.32 ±0.04
0.876 ±0.002
Prom1 (alt 1)
Unc13b
Ttc8
Arl6
0.948 ±0.002
0.08 ±0.05
0.93 ±0.02
0.17 ±0.01
0.55 ±0.02
0.16 ±0.01
0.83 ±0.02
0.11 ±0.04
0.83 ±0.001
0.95 ±0.01
0.68 ±0.01
0.96 ±0.01

Figure 2

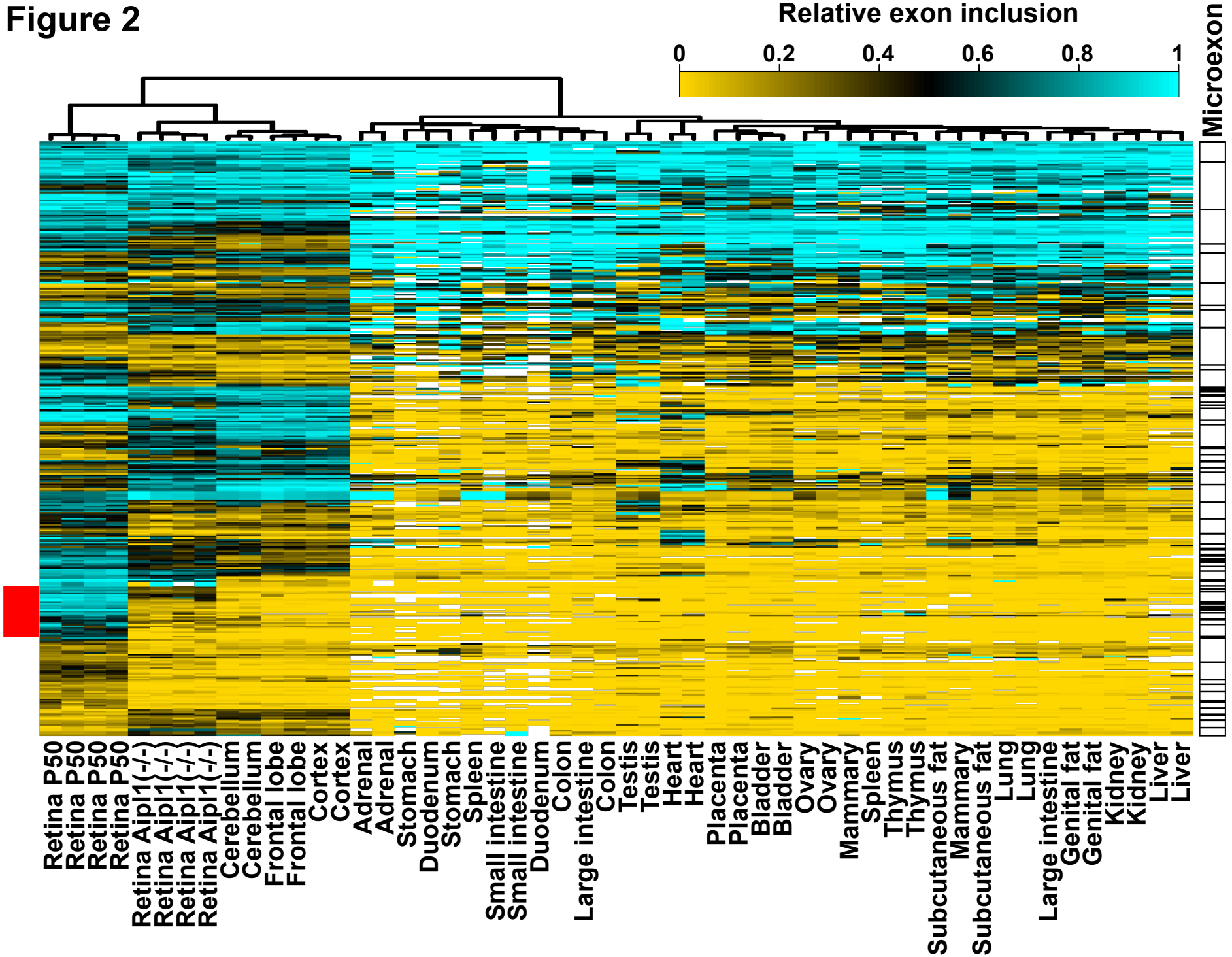
Relative exon inclusion
0
0.2
0.4
0.6
0.8
1
Microexon
Retina P50
Retina P50
Retina P50
Retina P50
Retina Aipl1(-/-)
Retina Aipl1(-/-)
Retina Aipl1(-/-)
Retina Aipl1(-/-)
Cerebellum
Cerebellum
Frontal lobe
Frontal lobe
Cortex
Cortex
Adrenal
Adrenal
Stomach
Duodenum
Stomach
Spleen
Small intestine
Small intestine
Duodenum
Colon
Large intestine
Colon
Testis
Testis
Heart
Heart
Placenta
Placenta
Bladder
Bladder
Ovary
Ovary
Mammary
Spleen
Thymus
Thymus
Subcutaneous fat
Mammary
Subcutaneous fat
Lung
Lung
Large intestine
Genital fat
Genital fat
Kidney
Kidney
Liver
Liver

Figure 3

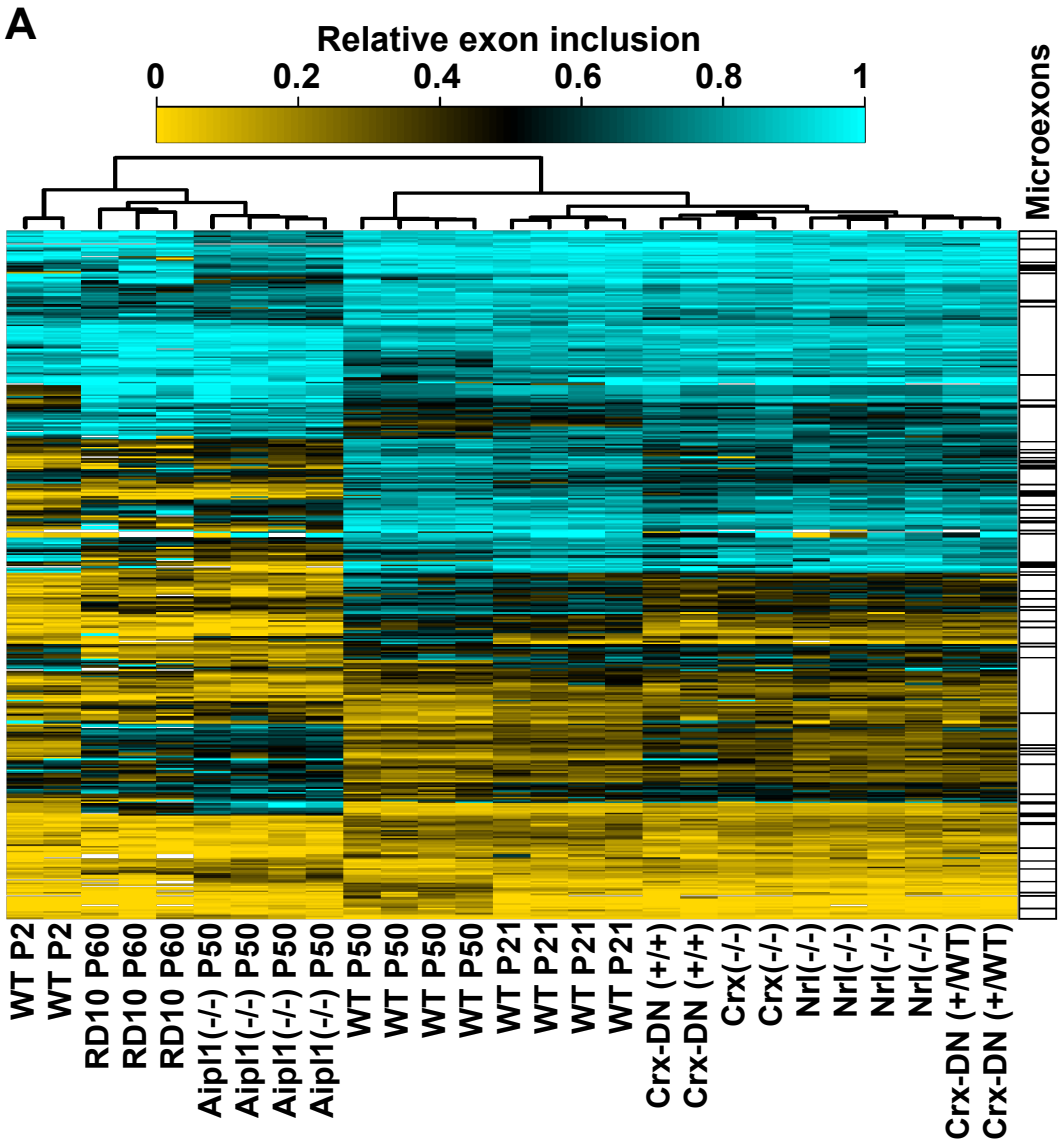
A
Relative exon inclusion
0
0.2
0.4
0.6
0.8
1
Microexons
WT P2
WT P2
RD10 P60
RD10 P60
RD10 P60
Aipl1(-/-) P50
Aipl1(-/-) P50
Aipl1(-/-) P50
Aipl1(-/-) P50
WT P50
WT P50
WT P50
WT P50
WT P21
WT P21
WT P21
WT P21
Crx-DN (+/+)
Crx-DN (+/+)
Crx(-/-)
Crx(-/-)
Nrl(-/-)
Nrl(-/-)
Nrl(-/-)
Nrl(-/-)
Crx-DN (+/WT)
Crx-DN (+/WT)

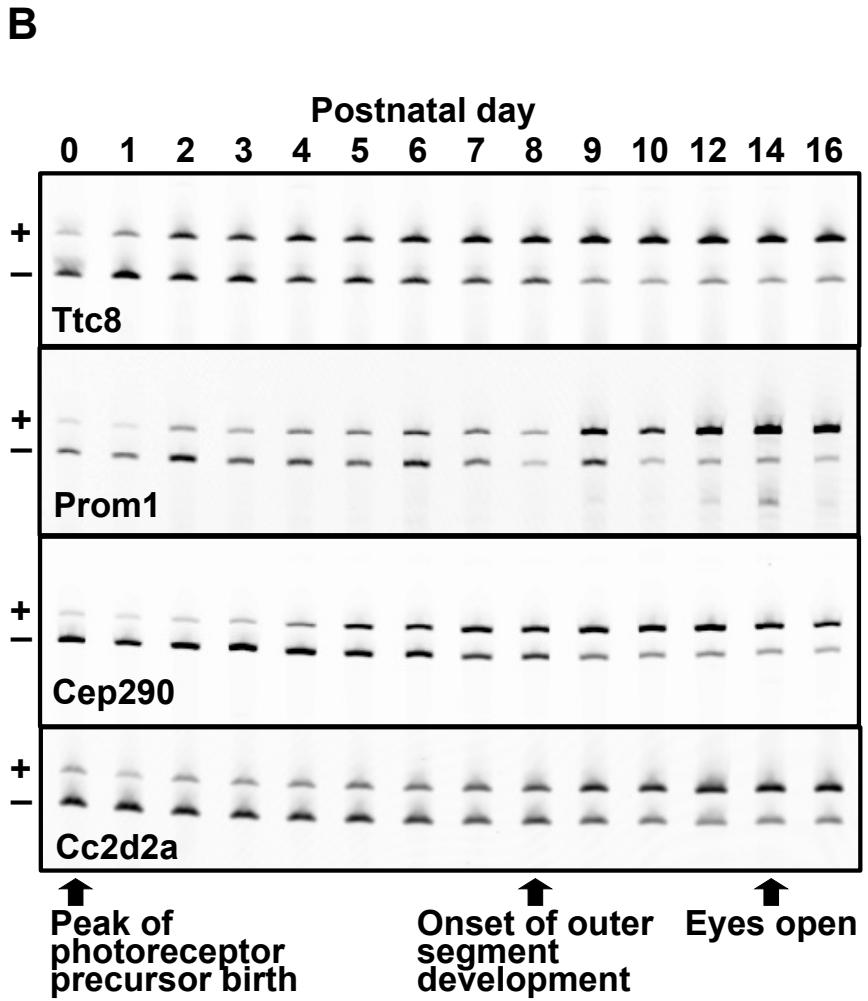
B
Postnatal day
0 1 2 3 4 5 6 7 8 9 10 12 14 16
+
–
Ttc8
+
–
Prom1
+
–
Cep290
+
–
Cc2d2a
Peak of photoreceptor precursor birth
Onset of outer segment development
Eyes open

Figure 4

A

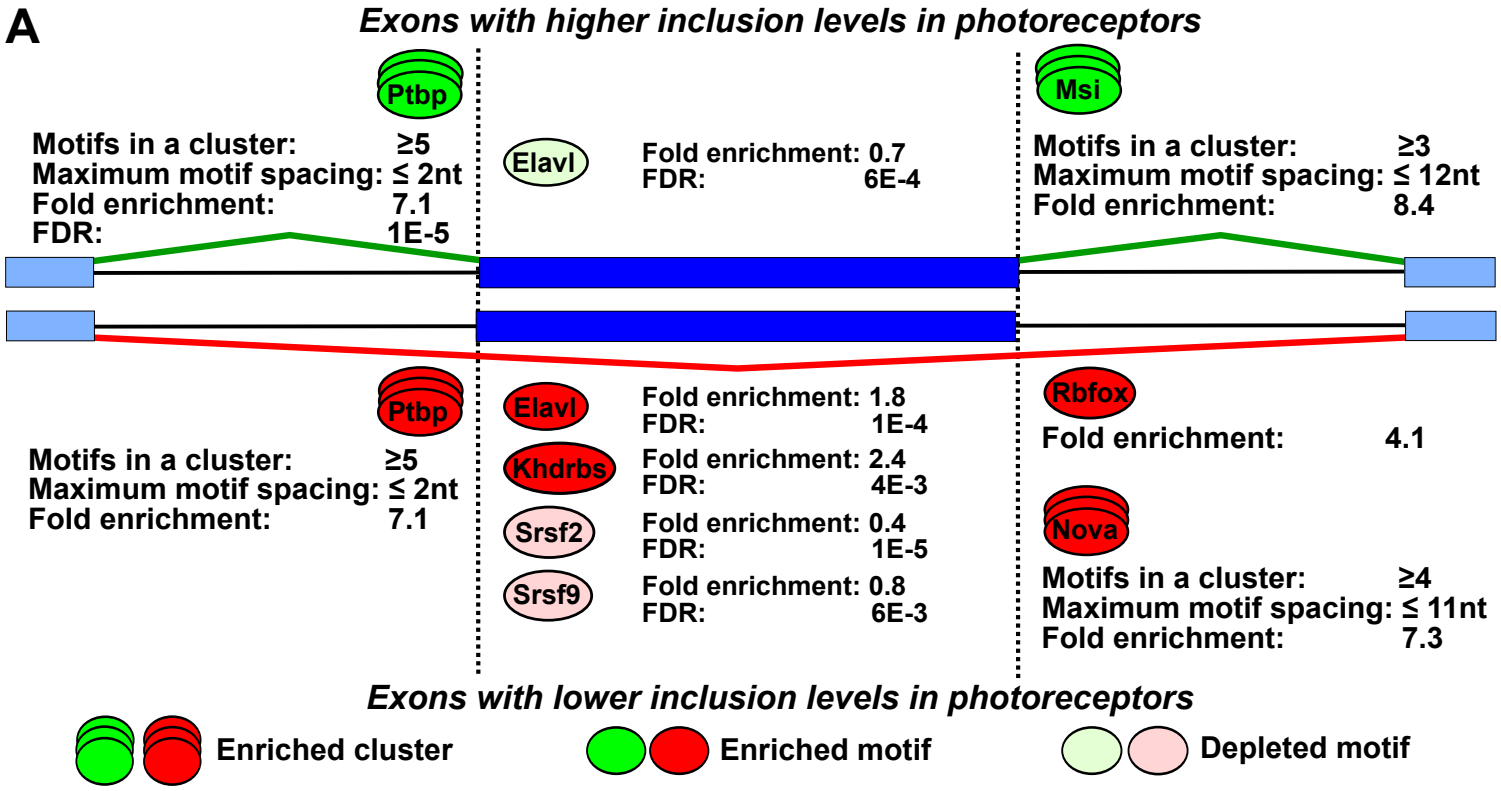
Exons with higher inclusion levels in photoreceptors
Ptbp
Motifs in a cluster: ≥5
Maximum motif spacing: ≤ 2nt
Fold enrichment: 7.1
FDR: 1E-5
Elavl
Fold enrichment: 0.7
FDR: 6E-4
Msi
Motifs in a cluster: ≥3
Maximum motif spacing: ≤ 12nt
Fold enrichment: 8.4
Ptbp
Motifs in a cluster: ≥5
Maximum motif spacing: ≤ 2nt
Fold enrichment: 7.1
Elavl
Fold enrichment: 1.8
FDR: 1E-4
Khdrbs
Fold enrichment: 2.4
FDR: 4E-3
Srsf2
Fold enrichment: 0.4
FDR: 1E-5
Srsf9
Fold enrichment: 0.8
FDR: 6E-3
Rbfox
Fold enrichment: 4.1
Nova
Motifs in a cluster: ≥4
Maximum motif spacing: ≤ 11nt
Fold enrichment: 7.3
Exons with lower inclusion levels in photoreceptors
Enriched cluster
Enriched motif
Depleted motif

B

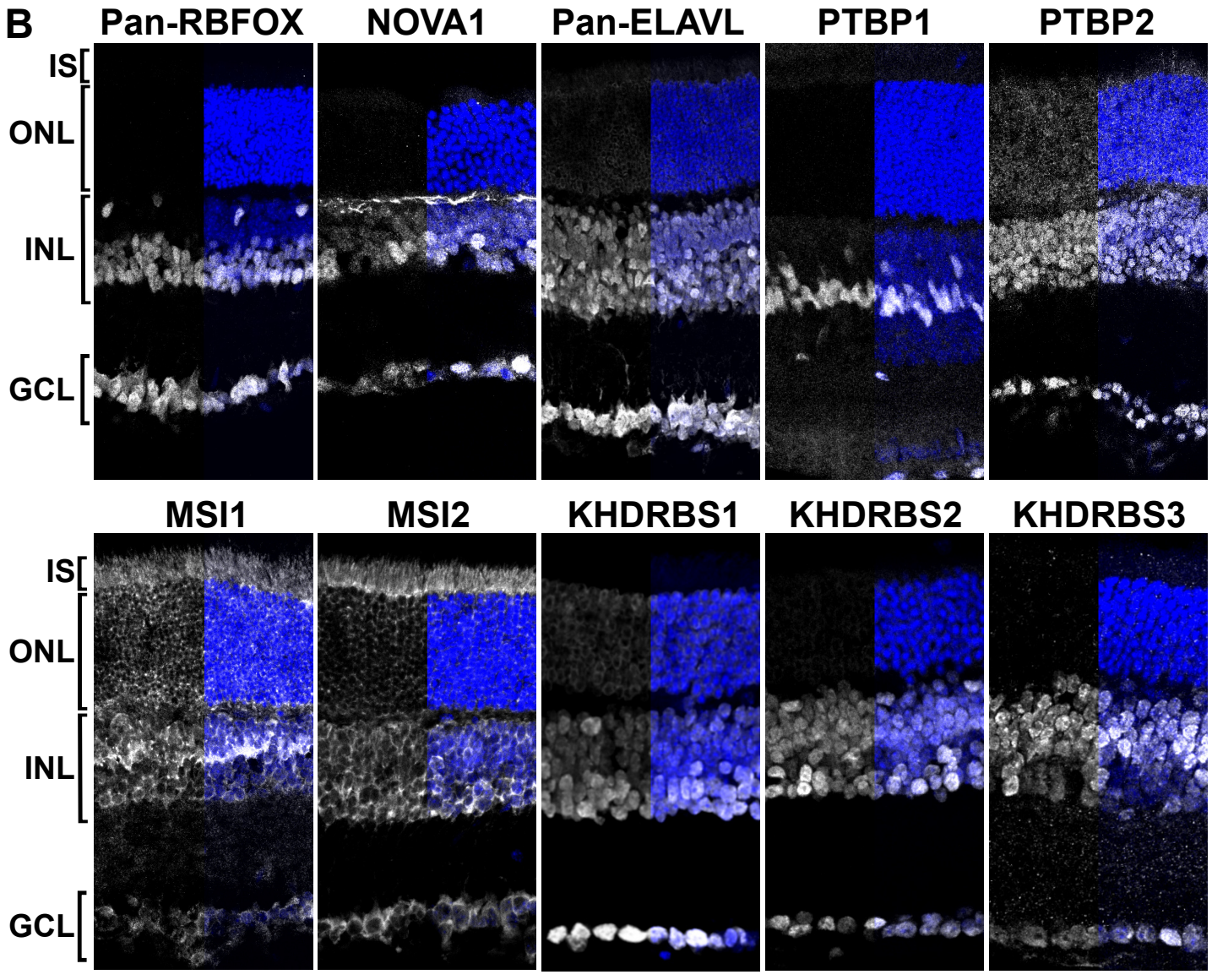
Pan-RBFOX
NOVA1
Pan-ELAVL
PTBP1
PTBP2
IS
ONL
INL
GCL
MSI1
MSI2
KHDRBS1
KHDRBS2
KHDRBS3
IS
ONL
INL
GCL

Figure 5

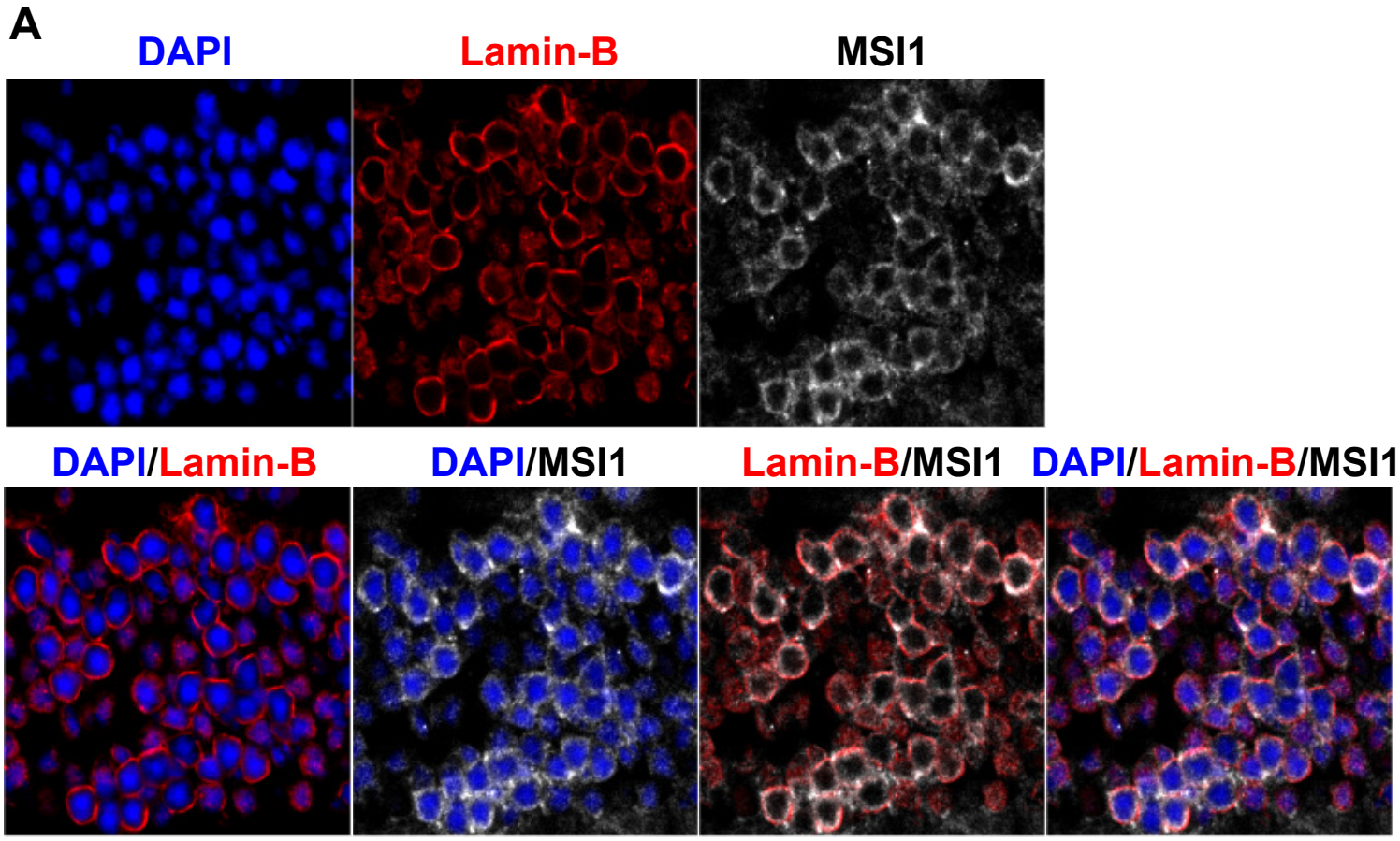
A
DAPI
Lamin-B
MSI1
DAPI/Lamin-B
DAPI/MSI1
Lamin-B/MSI1
DAPI/Lamin-B/MSI1

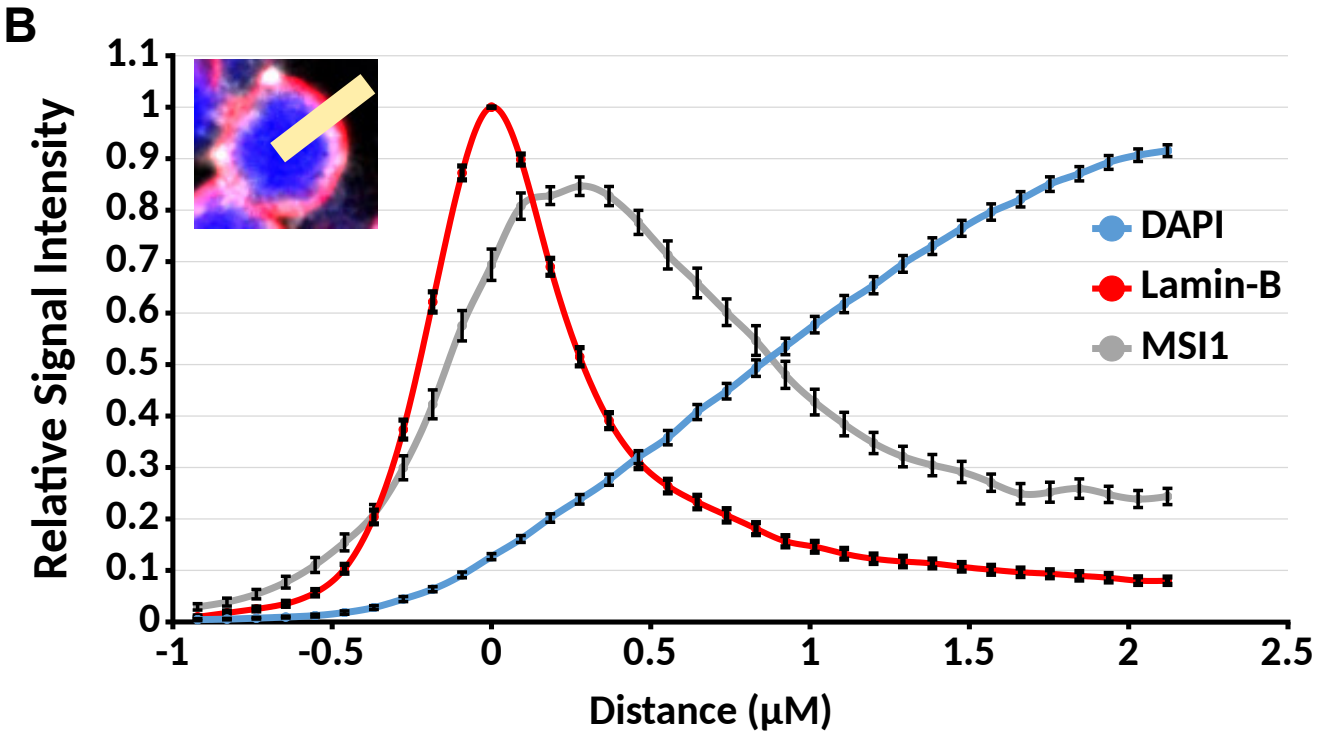
B
Relative Signal Intensity
1.1
1
0.9
0.8
0.7
0.6
0.5
0.4
0.3
0.2
0.1
0
-1
-0.5
0
0.5
1
1.5
2
2.5
Distance (µM)
DAPI
Lamin-B
MSI1

Figure 6

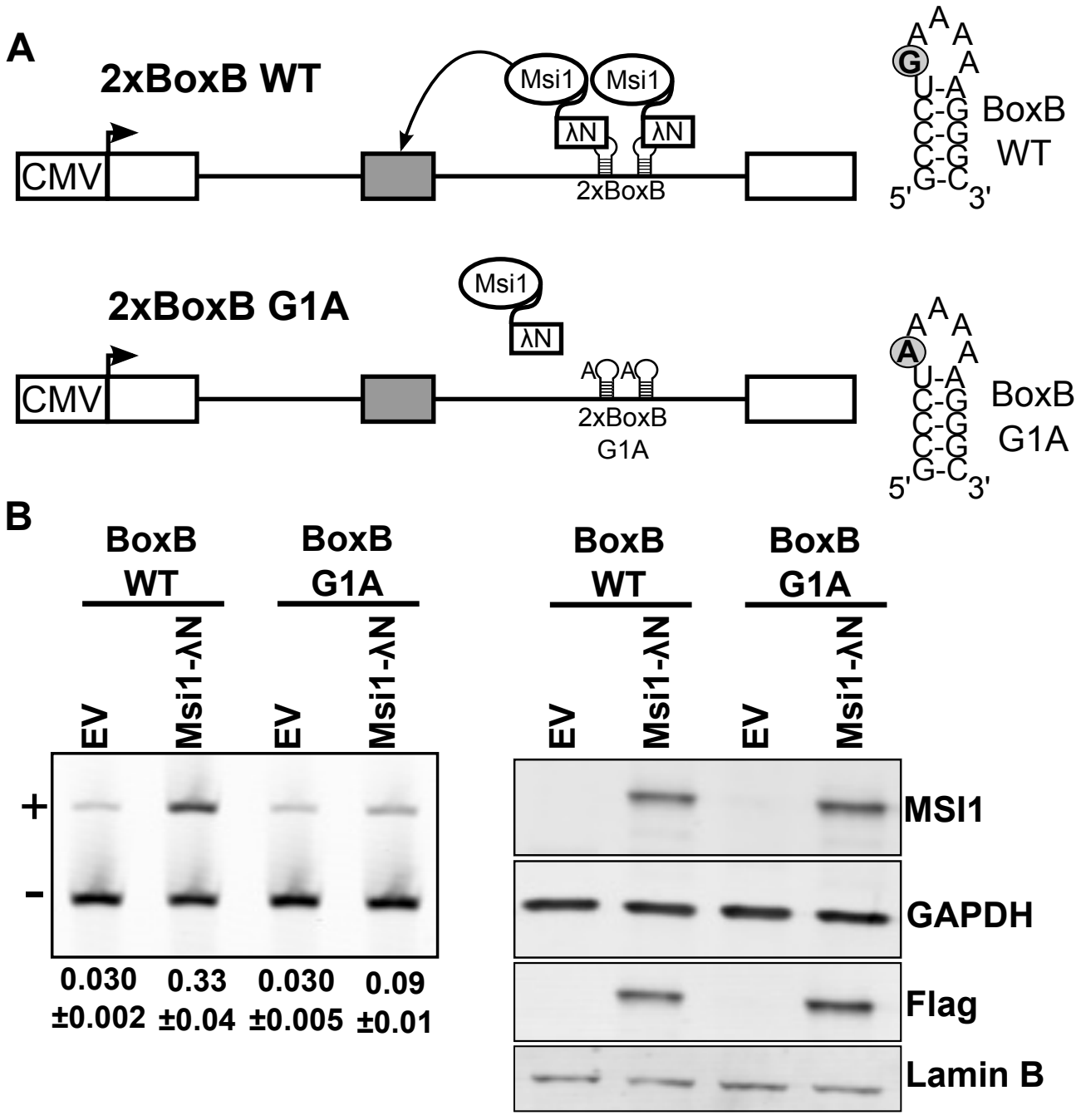
A
2xBoxB WT
Msi1
Msi1
λN
λN
CMV
2xBoxB
BoxB WT
5'
3'
2xBoxB G1A
Msi1
λN
A A
CMV
2xBoxB G1A
BoxB G1A
B
BoxB WT
BoxB G1A
BoxB WT
BoxB G1A
EV
Msi1-λN
EV
Msi1-λN
EV
Msi1-λN
EV
Msi1-λN
+
-
0.030 ±0.002
0.33 ±0.04
0.030 ±0.005
0.09 ±0.01
MSI1
GAPDH
Flag
Lamin B

Figure 7

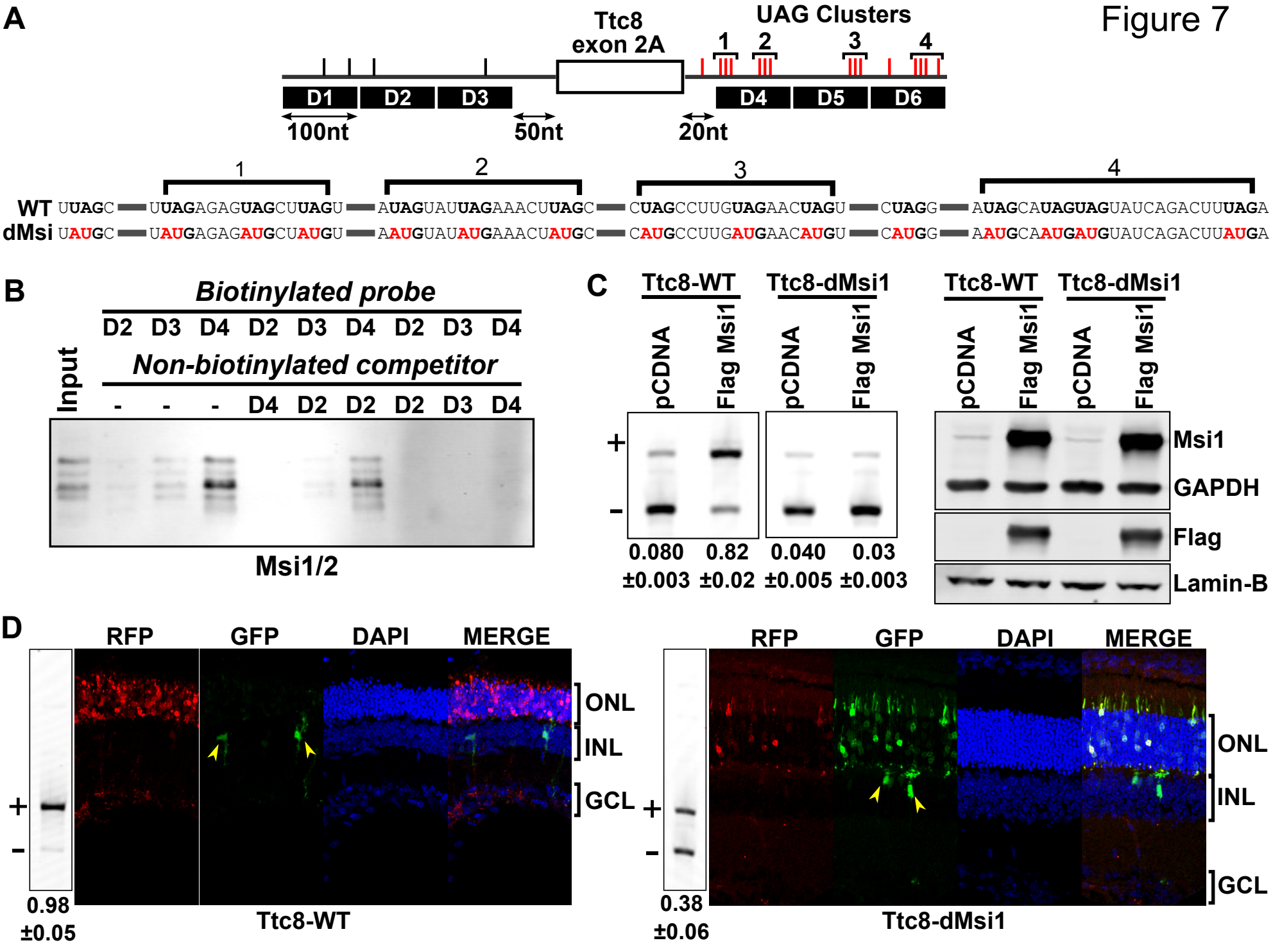
A
Ttc8
exon 2A
UAG Clusters
1
2
3
4
D1
D2
D3
D4
D5
D6
100nt
50nt
20nt
WT UUAGC UUAGAGAGUAGCUUAGU AUAGUAUUAGAAACUUAGC CUAGCCUUGUAGAACUAGU CUAGG AUAGCAUAGUAGUAUCAGACUUUAGA
dMsi UAUGC UAUGAGAGAUGCUAUGU AAUGUAUAUGAAACUAUGC CAUGCCUUGAUGAACAUGU CAUGG AAUGCAAUGAUGUAUCAGACUUAUGA
B
Biotinylated probe
D2 D3 D4 D2 D3 D4 D2 D3 D4
Non-biotinylated competitor
Input
- - - D4 D2 D2 D2 D3 D4
Msi1/2
C
Ttc8-WT
Ttc8-dMsi1
pCDNA
Flag Msi1
+
-
0.080 ±0.003
0.82 ±0.02
0.040 ±0.005
0.03 ±0.003
Msi1
GAPDH
Flag
Lamin-B
D
RFP
GFP
DAPI
MERGE
ONL
INL
GCL
0.98 ±0.05
Ttc8-WT
0.38 ±0.06
Ttc8-dMsi1

Figure 8

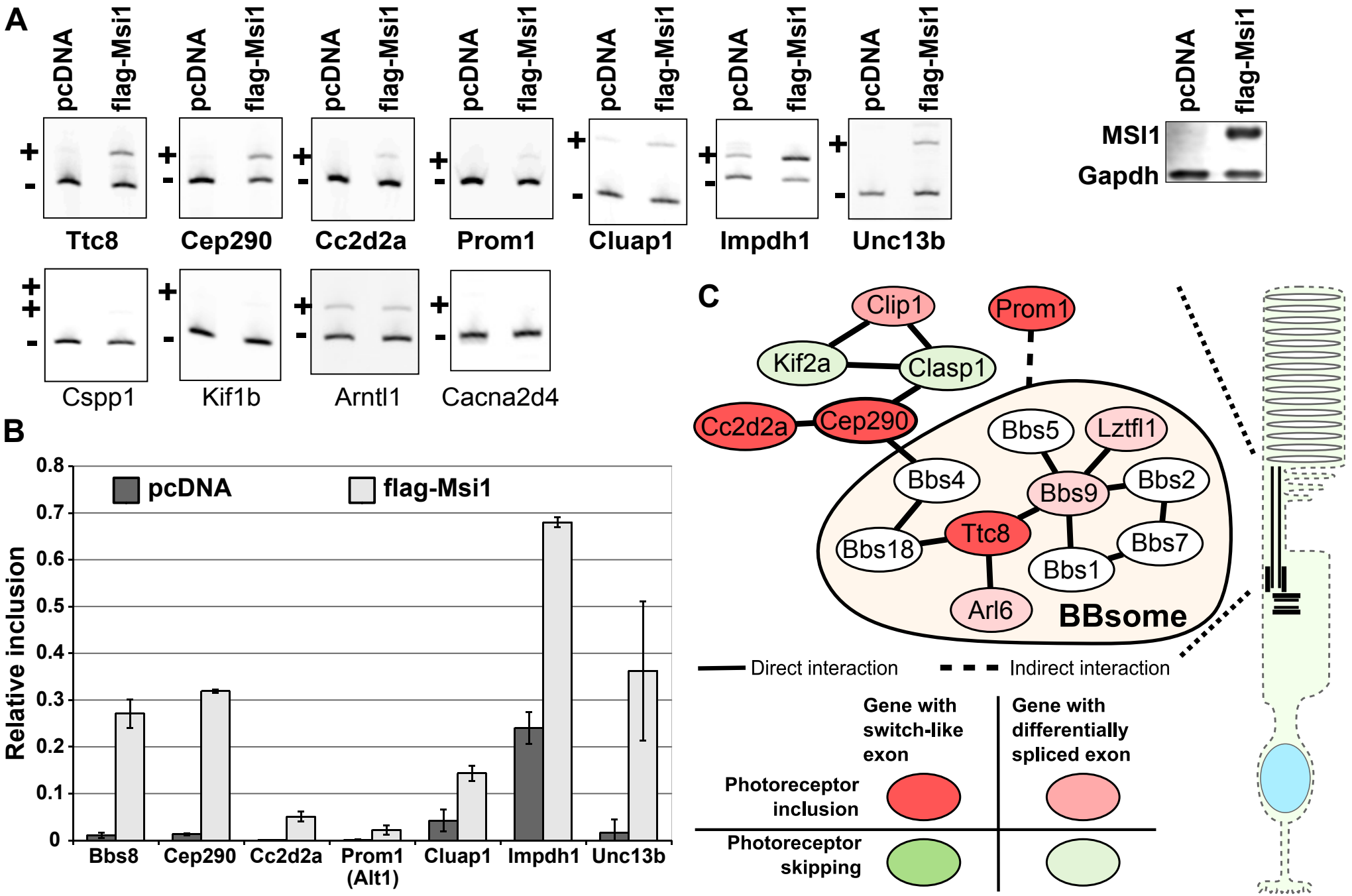
A
pcDNA
flag-Msi1
Ttc8
Cep290
Cc2d2a
Prom1
Cluap1
Impdh1
Unc13b
Cspp1
Kif1b
Arntl1
Cacna2d4
MSI1
Gapdh
B
Relative inclusion
0.8
0.7
0.6
0.5
0.4
0.3
0.2
0.1
0
pcDNA
flag-Msi1
Bbs8
Cep290
Cc2d2a
Prom1 (Alt1)
Cluap1
Impdh1
Unc13b
C
Clip1
Prom1
Kif2a
Clasp1
Cc2d2a
Cep290
Bbs5
Lztfl1
Bbs4
Bbs9
Bbs2
Ttc8
Bbs18
Bbs7
Bbs1
Arl6
BBsome
Direct interaction
Indirect interaction
Gene with switch-like exon
Gene with differentially spliced exon
Photoreceptor inclusion
Photoreceptor skipping

Supplementary Material

Chapter 5 Supplementary tables are available electronically.

Supplementary figure legends

Supplementary figure 1. Retinal neurons express a characteristic splicing program that is related to the splicing program of CNS neurons. (A) Heat map showing unsupervised hierarchical clustering of a panel of mouse tissues based on the inclusion levels of 8539 alternative exons. Microexons of 30nt or less in length are annotated on the right. Retinal samples form an independent cluster which is related to the cluster formed by the samples from the central nervous system and show frequent use of microexons. **(B)** Unsupervised hierarchical clustering of tissue samples based on the inclusion levels of 483 microexons shows elevated microexon use in neuronal tissues. A subset of the microexons marked with a red box on the left of the heat map are specifically included in retinal transcripts.

Supplementary figure 2. RT-PCR analysis of the inclusion levels of exons differentially spliced between wild type and Aipl1(-/-) retina. The bands corresponding to the exon skipped and exon included mRNA isoforms are labeled with '+' and '-', respectively. The relative exon inclusion and standard error of three independent replicates are shown below each lane.

Supplementary figure 3. Enrichment of Msi, Ptbp and Nova binding site motifs in clusters adjacent to exons upregulated in photoreceptors. Clusters with minimum size of 2, 3, 4 or 5 motifs were tested for each protein. The spacing between the motifs in a cluster was varied from 0 to 30nt (x - axis). Enrichment upstream or downstream of the exons is plotted with circles and triangles, respectively. Statistically enriched clusters are represented by filled markers using red or blue colors for positions upstream or downstream of the exon, respectively.

Supplementary figure 4. Enrichment of Msi, Ptbp and Nova binding site motifs in clusters adjacent to exons downregulated in photoreceptors. Clusters with minimum size of 2, 3, 4 or 5 motifs were tested for each protein. The spacing between the motifs in a cluster was varied from 0 to 30nt (x - axis). Enrichment upstream or downstream of the exons is plotted with circles

and triangles, respectively. Statistically enriched clusters are represented by filled markers using red or blue colors for positions upstream or downstream of the exon, respectively.

Supplementary figure 5. Khdrbs3 is targeted by micro-RNAs from the mir-96/182/183 cluster. (A) Predicted binding sites for retinal micro-RNAs in the 3'-UTR of Khdrb3. Binding sites conserved between mouse and human are shown in bold typeface. **(B)** Alignment of the retina specific micro-RNAs to the predicted binding sites. Seed sequences conserved between mouse and human are underlined. Each alignment is accompanied with mirSVR score representing the predicted efficiency of the target site (lower score means higher efficiency) and PhastCons sequence conservation score (Betel et al. 2010)

Supplementary figure 6. Musashi 2 is present in the nuclei of photoreceptor cells. Immunofluorescence staining of the outer nuclear layer on 4µm retinal sections. The nuclear envelope is stained with Lamin-B antibody (red). Msi2 staining is shown in gray. The nuclear DNA is stained with DAPI (blue).

Supplementary figure 7. Binding of the Musashi proteins downstream of an alternative exon promotes its inclusion. (A) RT-PCR analysis of the splicing of the wild type and G1A minigenes after co-transfection with empty vector or vectors expressing Msi1- λN and Msi2- λN fusions (top). The exon included and exon skipped isoforms are indicated with '+' and '-', respectively. Relative exon inclusion levels with standard error are shown below each lane. Below, western blot shows the expression levels of the Msi1- λN and Msi2- λN proteins. GAPDH and Lamin-B are used as loading controls. **(B)** RT-PCR analysis of the wild type and mutant Ttc8 exon 2A minigene transcripts after co-transfection with construct expressing flag-tagged Msi1 and Msi2 proteins. The exon included and exon skipped isoforms are indicated with '+' and '-', respectively. Relative exon inclusion levels with standard error are shown below each lane.

Below, western blot shows the expression levels of the Msi1 and Msi2 proteins. Lamin-B is used as loading control.

Supplementary figure 8. New exon discovery. Junction reads that map on one end of an exon in annotated transcripts are used to identify novel exons. A novel exon is defined by two sets of junction reads of at least 10 reads per set, one anchored on the left and a second one anchored on the right to a known exon, that map within a predefined distance (300nt) from each other.

Supplementary figure 9. Musashi proteins are present in the nuclei of photoreceptor cells in the Nrl (-/-) retina. Immunofluorescence staining of the outer nuclear layer on 6µm retinal sections. The nuclear envelope is stained with Lamin-B antibody (red). Msi1 and Msi2 staining are shown in gray. The nuclear DNA is stained with DAPI (blue).

Supplementary Figure 1

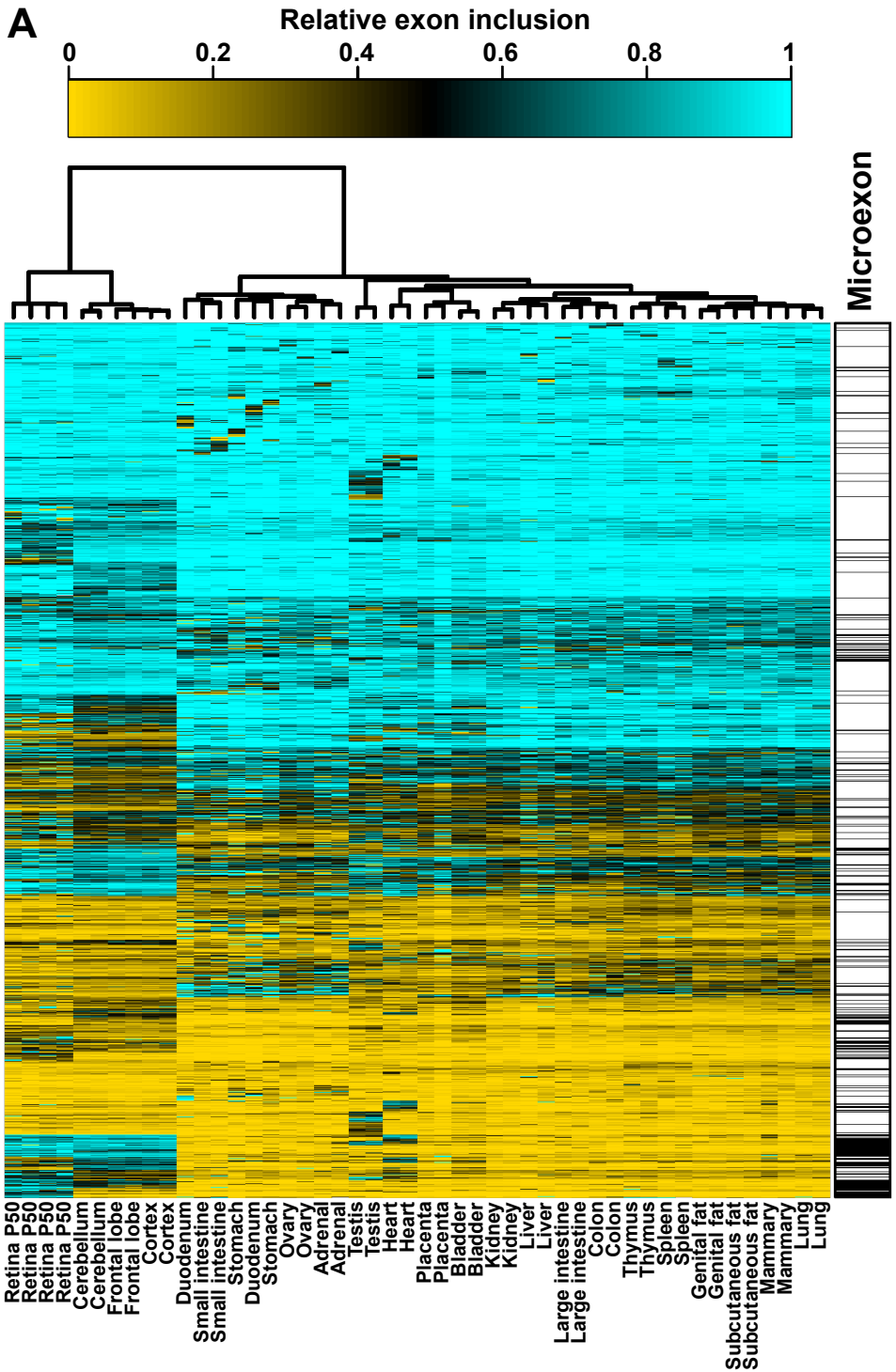

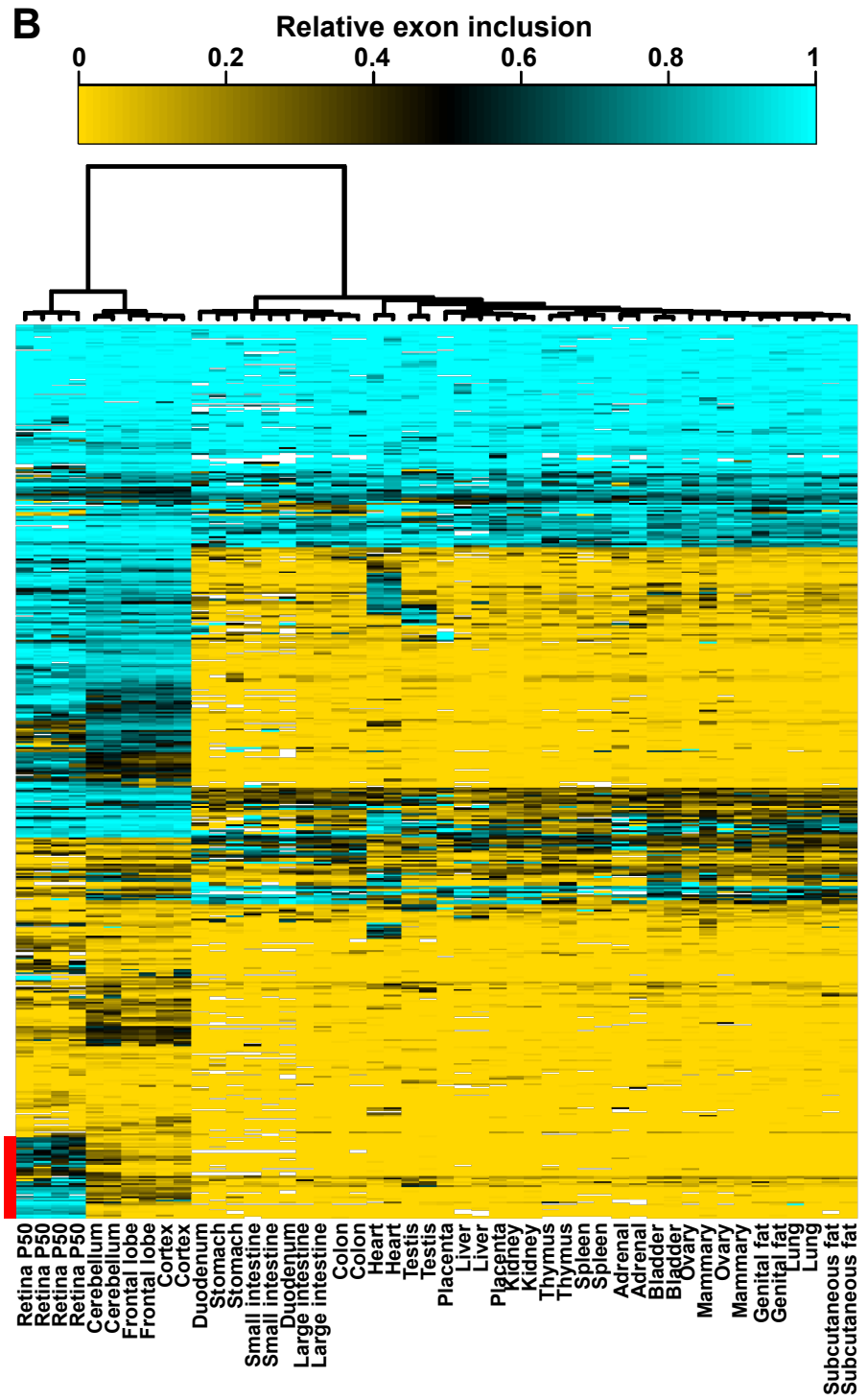

Supplementary Figure 2

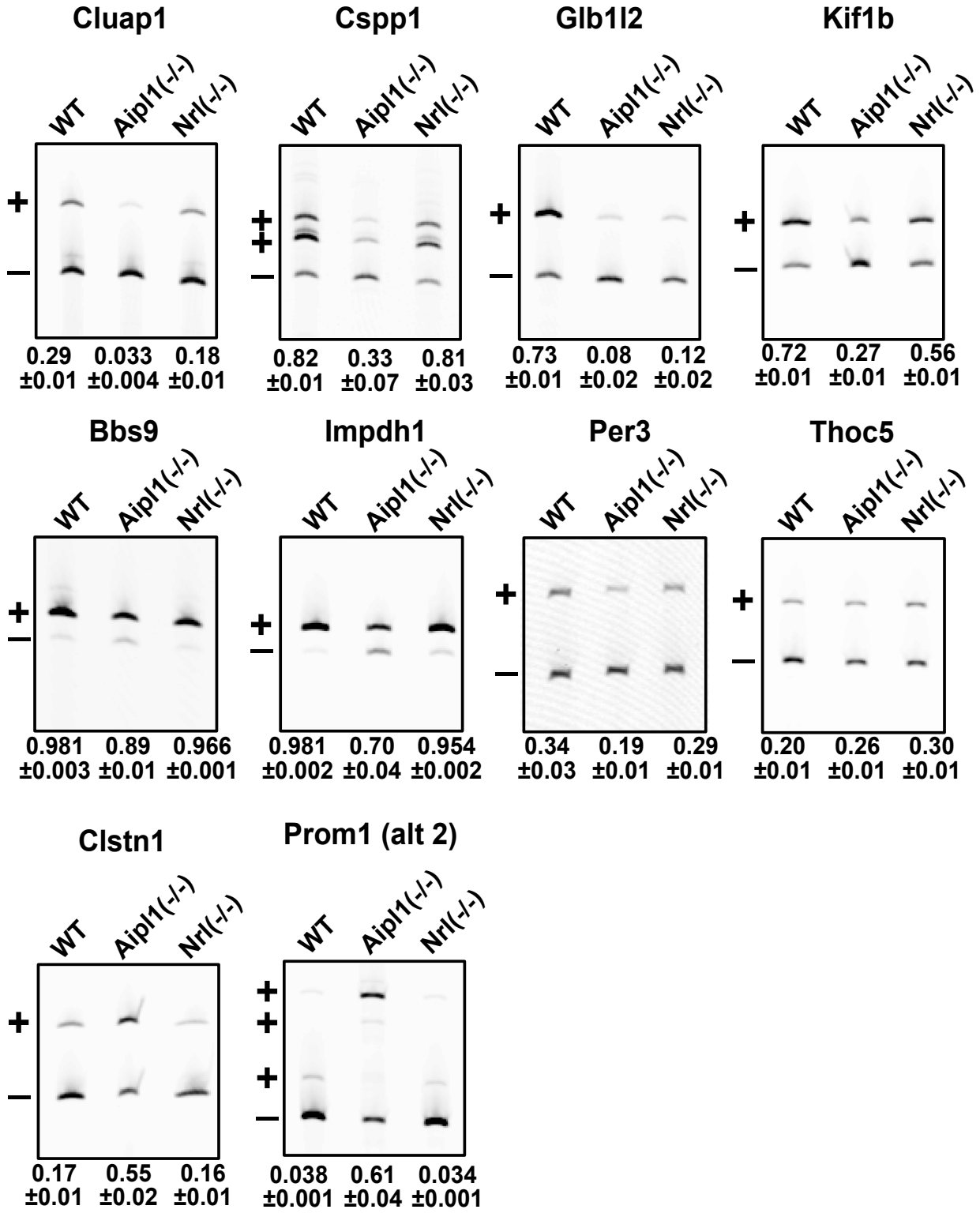

Supplementary Figure 3

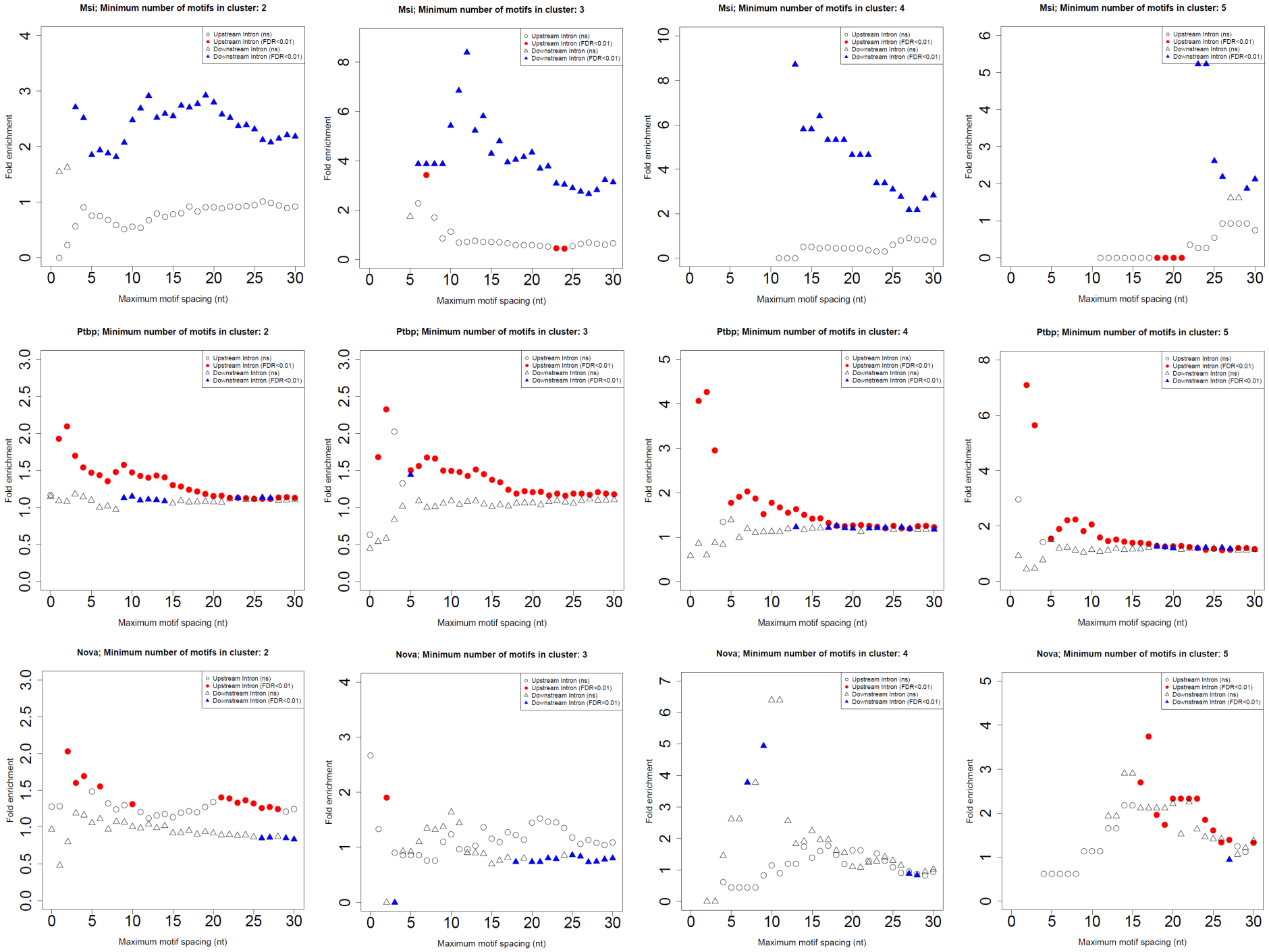

Supplementary Figure 4

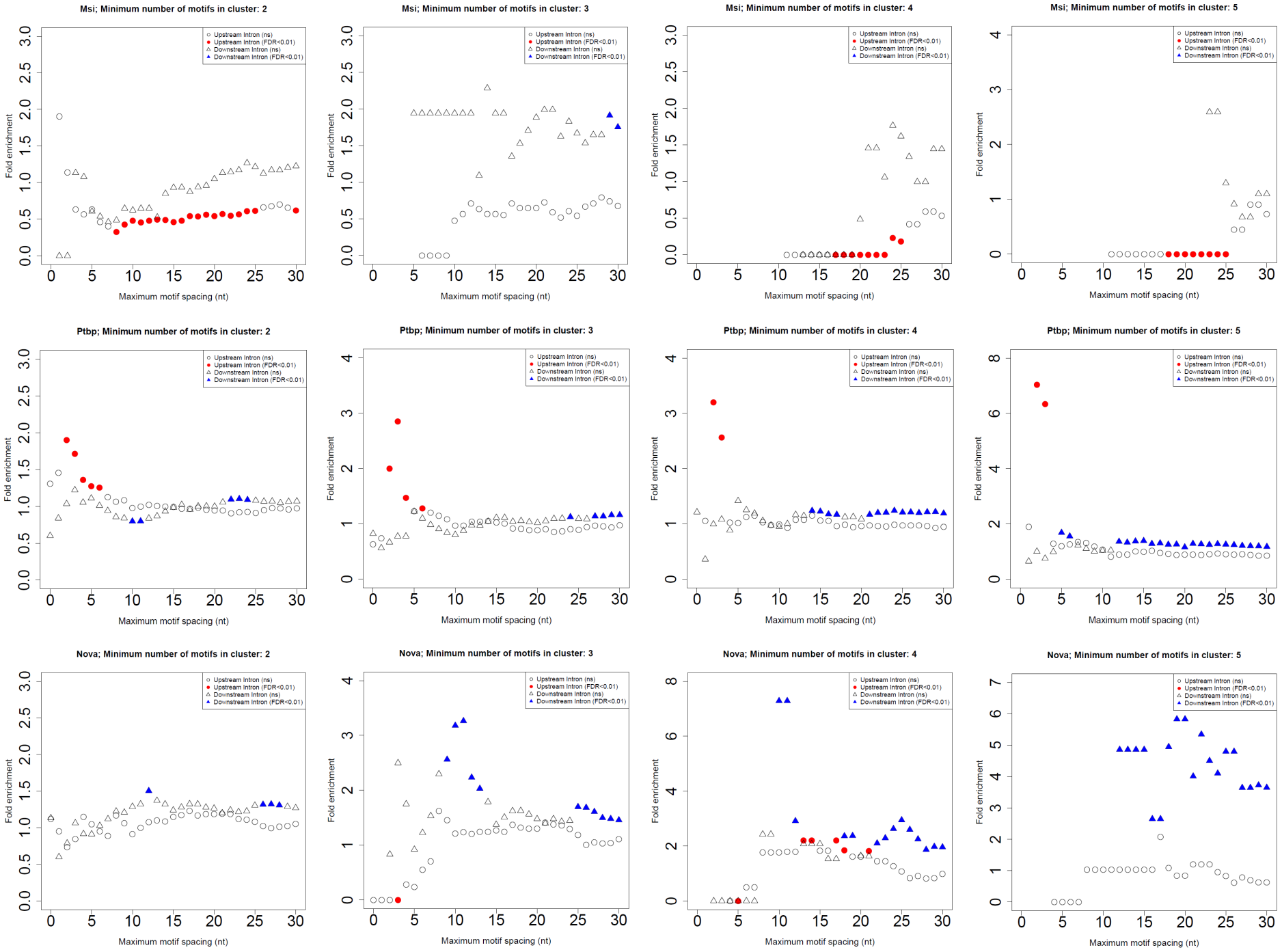

Supplementary figure 5

(A)

NM_010158 Mouse Khdrbs3 3'UTR

```
1    UUGUACUGUCUGAUGUUGUGAAAUAGCCAAUCUCCACCGUCCUGUAUACU 50

51   GUUCAAAGUAAUUUUUUUUCUAUGACCAAUCCCUUUUUAAAUAAAUCAAAA 100

101 UGCUUAAAAUCUGAAUGGAUGGAACUUAAAGCCACUUUGUUGAAGCAUCC 150

151 ACUUGACAGGGAGAAGAAGGACAUGUAAAAUUUUGUUAUUUGCAGUCUGU 200

201 AUAUGAAAACUAGGUUAUGAAAAGGAAAAAAAUAACUUUGAUUAACUAGU 250

251 GUUAAACAAAAAGAUAGGUUUACUAAAUAUGUUAAUCCAUUCUUUAACAU 300

301 AAGUCUCACCUUUCAUCUUAAAGGUUUCCAUAGAAUUUAGUUAUUUUAUC 350

                                                    miR-96
                                                   miR-182
351 UUUCAGCCAUAUGCUAGUUUUUUUUUUUCUUUCUUUCUUUCUUGCCAACU 400

401 UGCGUAAAAAGGGAGCCGAUUACAAGUGCAGACAAUGUGGUAUUCUUUUG 450

451 UAACUGAGUCCUGAAAUGUUCUGUAGUGUUAGGCAAAGUCUCCUCUUGCU 500

501 UGAUACUAAAUAAACUUUUGAAAGAAAUUUUGUGUGUGUGAGCUAACGAU 550

551 UUCAUGUUUUUUUUUUUUUCUAUUUAAAAAGUUCUUCAUAAAUAGCUGUA 600

601 AACAGGGAAAGGGCUCCUCUAACAGCGCUUGUCAUAAAAGGGUCACACUA 650

                                                        miR-183
651 AAUAUUGUACAGCUUCCUUUAAAAGUGGUAUAAAAUUAAACGUGCCAUGG 700

701 UAUACUCACCAUAGGUUCAGAUGCGGUCUAAAGAGUCCACACGGUAUCAA 750

751 GCUACUCACUCAGGUGGCACGUUAAACCCAUGCAAACCAAAUCUGACUUU 800

801 AAAAACUGGUUCUAAAAUAACUACUGGCUUUUCUGAAAAGGAUGUGAUCA 850

851 GAUUUCAUCUUGUCGAGCGUUUUUUCACUAGUGCAACUUUGGAUUUUUUA 900

901 UGAGACUUUUGGUACCUUAAUGAACACCUCGCUCCAUGCUGGAAGCAUAA 950

951 ACAGAGAGCUUUUAAAGACAUUCUGACUUGCCUAAUUGAGGUCGCACUCG 1000

1001 CCAAGGCUGAGGAUGUGUAAGCCUUAAACGGUCUUCAUUUUCAAAGGUAA 1050

1051 AUAAACGAAAUAAGAUUUUAAUCUCACUUAAUUUAUCUUAAUAUAUAACU 1100
```

1101 AAUAAAGCCAGGGAGAUUACAACUUAGCCGGUUUCAUUAUCCAUUCUAGA 1150

1151 AAGGUUUUAAGAUCACCUAAAUUCUCAUUUUAAAAAGUUUAAUUUGUUUU 1200

1201 AGUCAUCUAAAAAGCCUUAGUCUAGCCAGUUUAAUUGGGGCCAAUUCUUC 1250

1251 CCUGUUAAACAACUGUAAAACCUCAUAACUAGUCGUGUGUAAUACAUCUU 1300

1301 UUGGUUAAUAAUUGAGGGCAUUCUUAAAAGUGACAAGGGUUUAAUAAAGU 1350

1351 UAUUUGUUAAUCAUUUGGCUUAAGUUUUAAUGGUAGAUUAUGUAAAAUGU 1400

1401 UUAUCUUUAGUUUCGGAGGGGGGCUCCUUAUAUUUAUUUUGAGUAAACAG 1450

1451 AUUUCUUCUUUUGUUAGGAAAUGUCGACCACCUUGGACUGUCAGAGAGCU 1500

1501 CCAAGUGACUUAGAGCAGACAAAG 1524

(B)

miR-182
Mouse
mirSVR score: -0.8830
PhastCons score:0.7999

```
     3' gccacacucAAGAUGGUAACGGUUu 5' mmu-miR-182
                 |||| :| |||||||
 376:5' uuucuuucuUUCUUUC-UUGCCAAc 3' Khdrbs3
```

Human
mirSVR score: -1.0912
PhastCons score:0.8312

```
     3' ucaCACUCAAGAUGGUAACGGUUu 5' hsa-miR-182
           ||   ||:| |: |||||||
 373:5' cuaGUUUUUUUUUCUCUUGCCAAc 3' KHDRBS3
```

miR-96
Mouse
mirSVR score: -0.1050
PhastCons score:0.7999

```
     3' ucguuuuuacacgaucACGGUUu 5' mmu-miR-96
                        ||||||
 377:5' uucuuucuuucuuucuUGCCAAc 3' Khdrbs3
```

Human
mirSVR score: -0.2023
PhastCons score:0.8312

```
     3' ucguuuuuacacgaucACGGUUu 5' hsa-miR-96
                        ||||||
 374:5' uaguuuuuuuuucucuUGCCAAc 3' KHDRBS3
```

```
miR-183
Mouse
mirSVR score:   -0.7699
PhastCons score:0.7820

     3' ucacUUAAGAUGGUCACGGUAu 5' mmu-miR-183
           ||||  ||  |||||||
 680:5' auaaAAUUAAAC--GUGCCAUg 3' Khdrbs3
```

Supplementary Figure 6

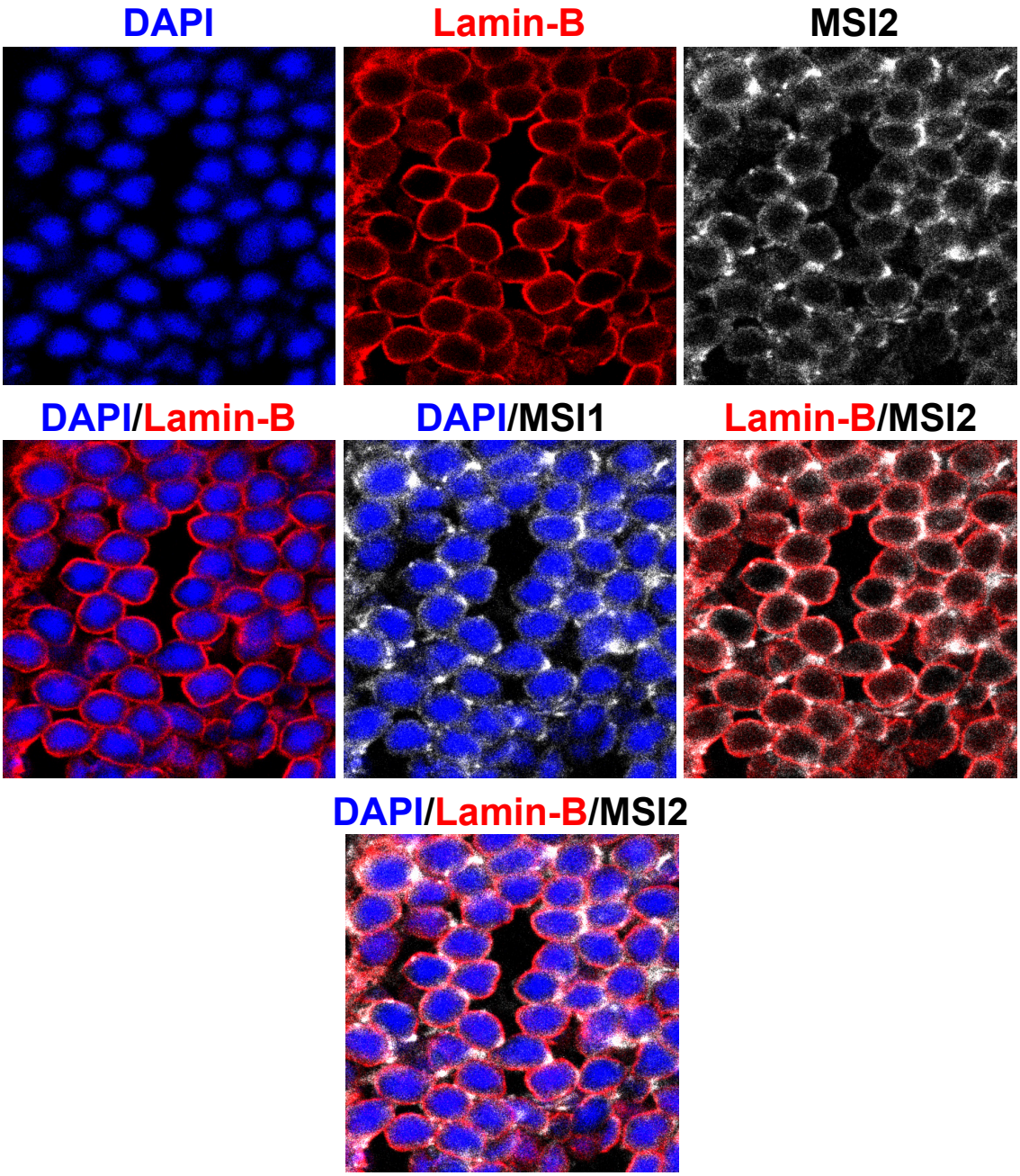

Supplementary Figure 7

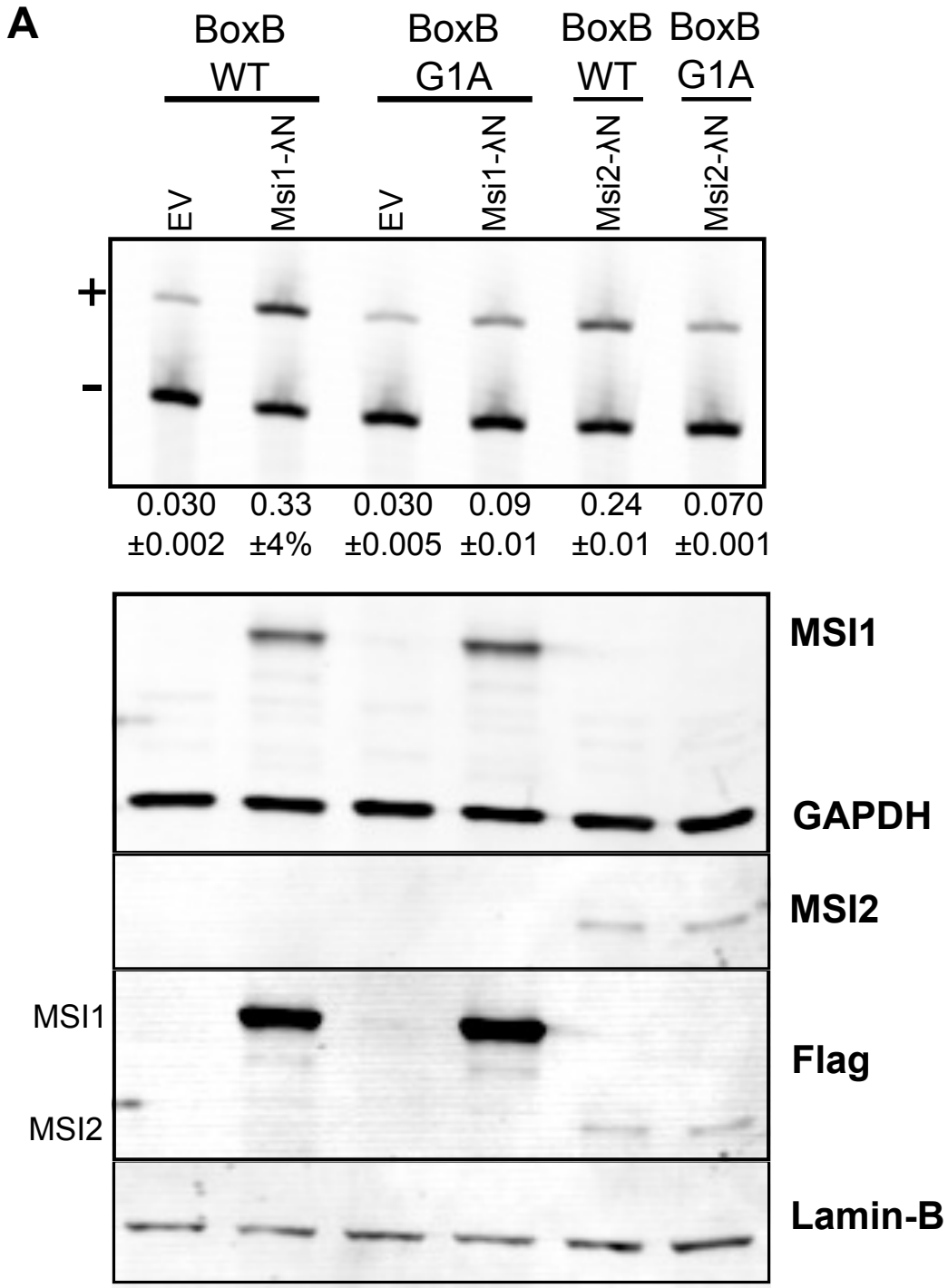

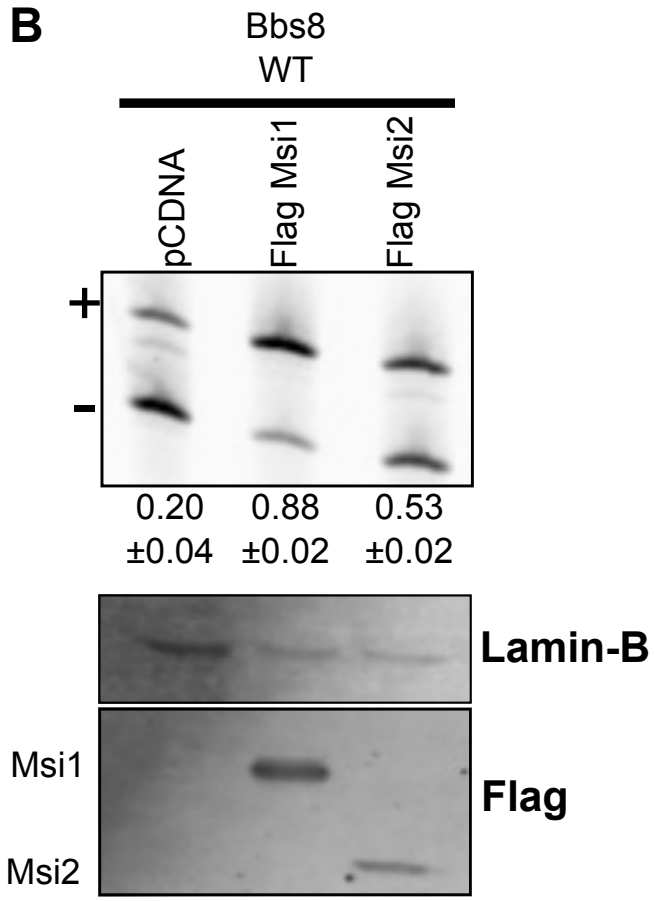

Supplementary Figure 8

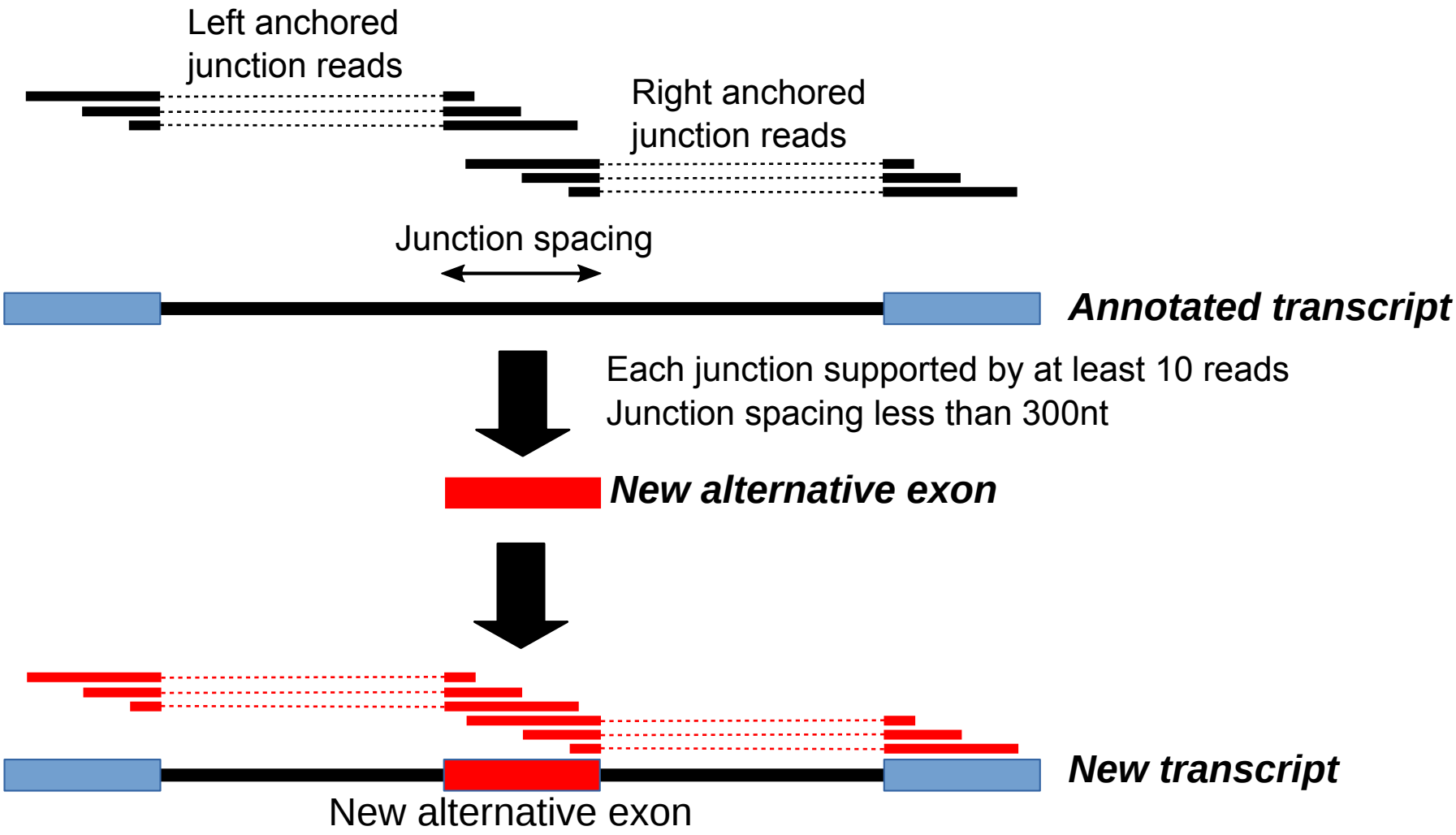

Supplementary Figure 9

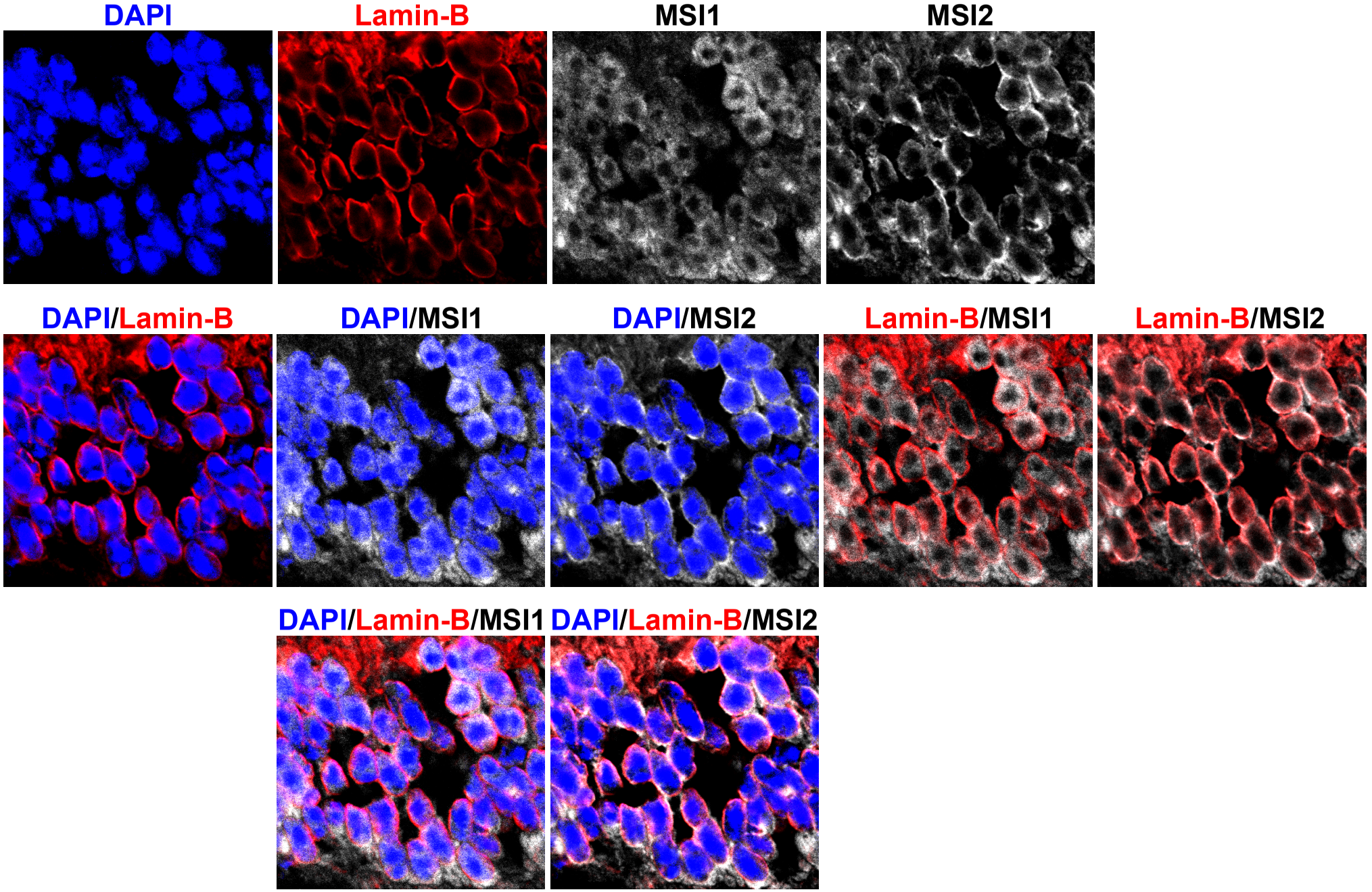

Chapter 6. Summary

Complex tissues and cell types require a vast number of functionally distinct proteins in order to develop and function. Alternative splicing of pre-mRNA is a fundamental mechanism for expanding the coding capacity of the genome to meet this requirement. This is especially apparent in the myriad of cell types that comprise the vertebrate nervous system, a tissue which utilizes alternative splicing to a higher degree than others. Despite well characterized roles for alternative splicing in the majority of cellular functions, the degree to which cell type specific splicing shapes cellular identity in complex tissues is difficult to determine. The well-defined morphology and fewer cell types make the retina an attractive model to study alternative splicing in neurons. The focus of my dissertation was to characterize the unique regulation of alternative splicing in retinal photoreceptor cells.

Using in vivo subretinal injection and electroporation, I was able to analyze the splicing of minigenes and BAC constructs within the native retinal tissue (Chapter 2). In combination with Dr Stoilov's two-color fluorescent reporter, this technique allowed me to visually demonstrate a splicing switch between photoreceptor cells and other retinal neurons (Chapter 3). I created minigenes with various deletions and substitutions in order to map the sequence elements which regulated the photoreceptor specific splicing of BBS8 exon 2a. Through these studies I was able to identify the mechanism which restricted the phenotype of a mutation in BBS8 to the retina (Chapter 4).

With the assistance of Dr. Stoilov, I was able to identify a photoreceptor specific splicing program by comparing a wild type retina with a mouse model lacking photoreceptor cells (Chapter 5). Various approaches including bioinformatics, minigene splicing assays, and RNA immunoprecipitations were used to demonstrate a role for Musashi proteins in activation of photoreceptor specific splicing. Analysis of splicing over a time course showed that this splicing program is activated prior to the development of the photoreceptor outer segment. The

presence of photoreceptor specific exons in multiple genes required for biogenesis and maintenance of primary cilia suggest that this splicing program may play a role in shaping the unique structure of photoreceptor cells.

While this work has established a foundation for the regulation of alternative splicing in photoreceptors, many questions yet remain. Our data suggests a combinatorial mechanism for the regulation of photoreceptor specific splicing, and further analysis will be needed in order to identify the additional regulators. Likewise, functional analysis of photoreceptor specific protein isoforms will be necessary to elucidate the role of this splicing program in vision. These studies will inform on potential disease mechanisms and increase our understanding of the molecular machinery within primary cilia of sensory neurons.

Appendix

Tables.

Appendix Table 1. Proteins identified by mass spectrometry in bands cut from D3.

Identified Proteins (81)	Accession Number	Molecular Weight	70kD SpC	50kD SpC
Non-POU domain-containing octamer-binding protein OS=Mus musculus GN=Nono PE=1 SV=3	sp|Q99K48|NONO_MOUSE	55 kDa	87	21
Heterogeneous nuclear ribonucleoprotein L OS=Mus musculus GN=Hnrnpl PE=1 SV=2	sp|Q8R081|HNRPL_MOUSE	64 kDa	67	18
Poly(U)-binding-splicing factor PUF60 OS=Mus musculus GN=Puf60 PE=2 SV=2	sp|Q3UEB3|PUF60_MOUSE	60 kDa	45	0
Paraspeckle component 1 OS=Mus musculus GN=Pspc1 PE=1 SV=1	sp|Q8R326|PSPC1_MOUSE	59 kDa	44	4
Heterogeneous nuclear ribonucleoprotein K OS=Mus musculus GN=Hnrnpk PE=1 SV=1	sp|P61979|HNRPK_MOUSE	51 kDa	27	2
Splicing factor, proline- and glutamine-rich OS=Mus musculus GN=Sfpq PE=1 SV=1	sp|Q8VIJ6|SFPQ_MOUSE	75 kDa	26	20
RNA-binding protein FUS OS=Mus musculus GN=Fus PE=2 SV=1	sp|P56959|FUS_MOUSE	53 kDa	23	0
KH domain-containing, RNA-binding, signal transduction-associated protein 1 OS=Mus musculus GN=Khdrbs1 PE=1 SV=2	sp|Q60749|KHDR1_MOUSE	48 kDa	18	4
Far upstream element-binding protein 1 OS=Mus musculus GN=Fubp1 PE=1 SV=1	sp|Q91WJ8|FUBP1_MOUSE	69 kDa	17	13
Far upstream element-binding protein 2 OS=Mus musculus GN=Khsrp PE=1 SV=2	sp|Q3U0V1|FUBP2_MOUSE	77 kDa	15	6
Serine/threonine-protein phosphatase 2A 65 kDa regulatory subunit A alpha isoform OS=Mus musculus GN=Ppp2r1a PE=1 SV=3	sp|Q76MZ3|2AAA_MOUSE	65 kDa	14	0
Myelin expression factor 2 OS=Mus musculus GN=Myef2 PE=1 SV=1	sp|Q8C854|MYEF2_MOUSE	63 kDa	14	0
Splicing factor 3B subunit 3 OS=Mus musculus GN=Sf3b3 PE=2 SV=1	sp|Q921M3|SF3B3_MOUSE	136 kDa	12	0
Histone deacetylase 1 OS=Mus musculus GN=Hdac1 PE=1 SV=1	sp|O09106|HDAC1_MOUSE	55 kDa	9	0

General transcription factor 3C polypeptide 5 OS=Mus musculus GN=Gtf3c5 PE=2 SV=2	sp|Q8R2T8|TF3C5_MOUSE	61 kDa	6	0
Kelch-like protein 3 OS=Mus musculus GN=Klhl3 PE=1 SV=2	sp|E0CZ16|KLHL3_MOUSE	65 kDa	5	0
Heterogeneous nuclear ribonucleoprotein M OS=Mus musculus GN=Hnrnpm PE=1 SV=3	sp|Q9D0E1|HNRPM_MOUSE	78 kDa	5	0
Heterogeneous nuclear ribonucleoproteins A2/B1 OS=Mus musculus GN=Hnrnpa2b1 PE=1 SV=2	sp|O88569|ROA2_MOUSE	37 kDa	4	6
Tubulin alpha-1B chain OS=Mus musculus GN=Tuba1b PE=1 SV=2	sp|P05213|TBA1B_MOUSE (+2)	50 kDa	4	10
26S proteasome non-ATPase regulatory subunit 3 OS=Mus musculus GN=Psmd3 PE=1 SV=3	sp|P14685|PSMD3_MOUSE	61 kDa	4	0
Splicing factor 3A subunit 2 OS=Mus musculus GN=Sf3a2 PE=1 SV=2	sp|Q62203|SF3A2_MOUSE	50 kDa	4	0
Retinoblastoma-binding protein 5 OS=Mus musculus GN=Rbbp5 PE=1 SV=2	sp|Q8BX09|RBBP5_MOUSE	59 kDa	4	0
Nuclear receptor coactivator 5 OS=Mus musculus GN=Ncoa5 PE=1 SV=1	sp|Q91W39|NCOA5_MOUSE	65 kDa	4	0
Dihydropyrimidinase-related protein 4 OS=Mus musculus GN=Dpysl4 PE=1 SV=1	sp|O35098|DPYL4_MOUSE	62 kDa	3	0
Microtubule-associated protein 1B OS=Mus musculus GN=Map1b PE=1 SV=2	sp|P14873|MAP1B_MOUSE	270 kDa	3	0
T-complex protein 1 subunit epsilon OS=Mus musculus GN=Cct5 PE=1 SV=1	sp|P80316|TCPE_MOUSE	60 kDa	3	0
Tubulin beta-5 chain OS=Mus musculus GN=Tubb5 PE=1 SV=1	sp|P99024|TBB5_MOUSE	50 kDa	3	13
Interleukin enhancer-binding factor 3 OS=Mus musculus GN=Ilf3 PE=1 SV=2	sp|Q9Z1X4|ILF3_MOUSE	96 kDa	3	0
T-complex protein 1 subunit alpha OS=Mus musculus GN=Tcp1 PE=1 SV=3	sp|P11983|TCPA_MOUSE	60 kDa	2	0
T-complex protein 1 subunit theta OS=Mus musculus GN=Cct8 PE=1 SV=3	sp|P42932|TCPQ_MOUSE	60 kDa	2	0
Dihydropyrimidinase-related protein 1 OS=Mus musculus GN=Crmp1 PE=1 SV=1	sp|P97427|DPYL1_MOUSE	62 kDa	2	0
Protein FAM98A OS=Mus musculus GN=Fam98a PE=2 SV=1	sp|Q3TJZ6|FA98A_MOUSE	55 kDa	2	0

Probable ATP-dependent RNA helicase DDX17 OS=Mus musculus GN=Ddx17 PE=1 SV=1	sp|Q501J6|DDX17_MOUSE (+1)	72 kDa	2	0
T-complex protein 1 subunit zeta-2 OS=Mus musculus GN=Cct6b PE=2 SV=4	sp|Q61390|TCPW_MOUSE	58 kDa	2	0
Dihydropyrimidinase-related protein 3 OS=Mus musculus GN=Dpysl3 PE=1 SV=1	sp|Q62188|DPYL3_MOUSE	62 kDa	2	0
Heterogeneous nuclear ribonucleoprotein U OS=Mus musculus GN=Hnrnpu PE=1 SV=1	sp|Q8VEK3|HNRPU_MOUSE	88 kDa	2	0
H/ACA ribonucleoprotein complex subunit 4 OS=Mus musculus GN=Dkc1 PE=1 SV=4	sp|Q9ESX5|DKC1_MOUSE	57 kDa	2	0
MAGUK p55 subfamily member 2 OS=Mus musculus GN=Mpp2 PE=1 SV=1	sp|Q9WV34|MPP2_MOUSE	62 kDa	2	0
Treacle protein OS=Mus musculus GN=Tcof1 PE=1 SV=1	sp|O08784|TCOF_MOUSE	135 kDa	0	2
Heterogeneous nuclear ribonucleoprotein H OS=Mus musculus GN=Hnrnph1 PE=1 SV=3	sp|O35737|HNRH1_MOUSE	49 kDa	0	14
ATP-dependent RNA helicase A OS=Mus musculus GN=Dhx9 PE=1 SV=2	sp|O70133|DHX9_MOUSE	149 kDa	0	2
Glutamine synthetase OS=Mus musculus GN=Glul PE=1 SV=6	sp|P15105|GLNA_MOUSE	42 kDa	0	11
Heterogeneous nuclear ribonucleoprotein A1 OS=Mus musculus GN=Hnrnpa1 PE=1 SV=2	sp|P49312|ROA1_MOUSE	34 kDa	0	8
Nucleolysin TIA-1 OS=Mus musculus GN=Tia1 PE=1 SV=1	sp|P52912|TIA1_MOUSE	43 kDa	0	26
Poly(rC)-binding protein 4 OS=Mus musculus GN=Pcbp4 PE=2 SV=1	sp|P57724|PCBP4_MOUSE	41 kDa	0	2
Actin, cytoplasmic 1 OS=Mus musculus GN=Actb PE=1 SV=1	sp|P60710|ACTB_MOUSE	42 kDa	0	50
Alpha-centractin OS=Mus musculus GN=Actr1a PE=2 SV=1	sp|P61164|ACTZ_MOUSE	43 kDa	0	3
26S protease regulatory subunit 8 OS=Mus musculus GN=Psmc5 PE=1 SV=1	sp|P62196|PRS8_MOUSE	46 kDa	0	7
Nucleolysin TIAR OS=Mus musculus GN=Tial1 PE=1 SV=1	sp|P70318|TIAR_MOUSE	43 kDa	0	22
Heterogeneous nuclear ribonucleoprotein H2 OS=Mus musculus GN=Hnrnph2 PE=2 SV=1	sp|P70333|HNRH2_MOUSE	49 kDa	0	8
RISC-loading complex subunit TARBP2 OS=Mus musculus GN=Tarbp2 PE=1 SV=2	sp|P97473|TRBP2_MOUSE	39 kDa	0	5

Creatine kinase B-type OS=Mus musculus GN=Ckb PE=1 SV=1	sp|Q04447|KCRB_MOUSE	43 kDa	0	10
WD repeat-containing protein 18 OS=Mus musculus GN=Wdr18 PE=1 SV=1	sp|Q4VBE8|WDR18_MOUSE	47 kDa	0	4
Heterogeneous nuclear ribonucleoprotein D0 OS=Mus musculus GN=Hnrnpd PE=1 SV=2	sp|Q60668|HNRPD_MOUSE	38 kDa	0	56
Poly(rC)-binding protein 2 OS=Mus musculus GN=Pcbp2 PE=1 SV=1	sp|Q61990|PCBP2_MOUSE	38 kDa	0	3
Protein FAM98B OS=Mus musculus GN=Fam98b PE=2 SV=1	sp|Q80VD1|FA98B_MOUSE	45 kDa	0	7
Elongation factor Tu, mitochondrial OS=Mus musculus GN=Tufm PE=1 SV=1	sp|Q8BFR5|EFTU_MOUSE	50 kDa	0	2
Heterogeneous nuclear ribonucleoprotein A3 OS=Mus musculus GN=Hnrnpa3 PE=1 SV=1	sp|Q8BG05|ROA3_MOUSE	40 kDa	0	3
RNA binding protein fox-1 homolog 2 OS=Mus musculus GN=Rbfox2 PE=1 SV=2	sp|Q8BP71|RFOX2_MOUSE (+1)	47 kDa	0	2
G-rich sequence factor 1 OS=Mus musculus GN=Grsf1 PE=1 SV=2	sp|Q8C5Q4|GRSF1_MOUSE	53 kDa	0	6
Polyadenylate-binding protein 2 OS=Mus musculus GN=Pabpn1 PE=2 SV=3	sp|Q8CCS6|PABP2_MOUSE	32 kDa	0	13
Zinc finger protein 385A OS=Mus musculus GN=Znf385a PE=1 SV=2	sp|Q8VD12|Z385A_MOUSE	40 kDa	0	31
Eukaryotic initiation factor 4A-III OS=Mus musculus GN=Eif4a3 PE=2 SV=3	sp|Q91VC3|IF4A3_MOUSE	47 kDa	0	9
Ribonuclease inhibitor OS=Mus musculus GN=Rnh1 PE=1 SV=1	sp|Q91VI7|RINI_MOUSE	50 kDa	0	4
RNA binding motif protein, X-linked-like-1 OS=Mus musculus GN=Rbmxl1 PE=1 SV=1	sp|Q91VM5|RMXL1_MOUSE	42 kDa	0	29
Spermatid perinuclear RNA-binding protein OS=Mus musculus GN=Strbp PE=1 SV=1	sp|Q91WM1|STRBP_MOUSE	74 kDa	0	2
TAR DNA-binding protein 43 OS=Mus musculus GN=Tardbp PE=1 SV=1	sp|Q921F2|TADBP_MOUSE	45 kDa	0	18
26S proteasome non-ATPase regulatory subunit 6 OS=Mus musculus GN=Psmd6 PE=1 SV=1	sp|Q99JI4|PSMD6_MOUSE	46 kDa	0	5
Cleavage stimulation factor subunit 1 OS=Mus musculus GN=Cstf1 PE=2 SV=1	sp|Q99LC2|CSTF1_MOUSE	48 kDa	0	7
Interleukin enhancer-binding factor 2 OS=Mus musculus GN=Ilf2 PE=1 SV=1	sp|Q9CXY6|ILF2_MOUSE	43 kDa	0	26

RNA 3'-terminal phosphate cyclase OS=Mus musculus GN=RtcA PE=2 SV=2	sp|Q9D7H3|RTCA_MOUSE	39 kDa	0	6
Transcription initiation factor TFIID subunit 8 OS=Mus musculus GN=Taf8 PE=2 SV=1	sp|Q9EQH4|TAF8_MOUSE	34 kDa	0	2
DAZ-associated protein 1 OS=Mus musculus GN=Dazap1 PE=2 SV=2	sp|Q9JII5|DAZP1_MOUSE	43 kDa	0	26
LanC-like protein 2 OS=Mus musculus GN=Lancl2 PE=1 SV=1	sp|Q9JJK2|LANC2_MOUSE	51 kDa	0	3
Muscleblind-like protein 1 OS=Mus musculus GN=Mbnl1 PE=1 SV=1	sp|Q9JKP5|MBNL1_MOUSE	37 kDa	0	3
Photoreceptor specific nuclear receptor OS=Mus musculus GN=Nr2e3 PE=1 SV=1	sp|Q9QXZ7|NR2E3_MOUSE	43 kDa	0	4
KH domain-containing, RNA-binding, signal transduction-associated protein 3 OS=Mus musculus GN=Khdrbs3 PE=1 SV=1	sp|Q9R226|KHDR3_MOUSE	39 kDa	0	6
RNA-binding motif protein, X chromosome OS=Mus musculus GN=Rbmx PE=1 SV=1	sp|Q9WV02|RBMX_MOUSE	42 kDa	0	26
Succinyl-CoA ligase [ADP-forming] subunit beta, mitochondrial OS=Mus musculus GN=Sucla2 PE=1 SV=2	sp|Q9Z2I9|SUCB1_MOUSE	50 kDa	0	4
Actin-like protein 6A OS=Mus musculus GN=Actl6a PE=1 SV=2	sp|Q9Z2N8|ACL6A_MOUSE	47 kDa	0	3
Heterogeneous nuclear ribonucleoprotein F OS=Mus musculus GN=Hnrnpf PE=1 SV=3	sp|Q9Z2X1|HNRPF_MOUSE	46 kDa	0	9

Appendix Table 2. Proteins identified by mass spectrometry of D4 probe eluate.

Identified Proteins (332)	**Accession Number**	**MW**	**SpC**	**SAF**	**NSAF**	**SUM SAF**
Heterogeneous nuclear ribonucleoproteins A2/B1 OS=Mus musculus GN=Hnrnpa2b1 PE=1 SV=2	sp|O88569|ROA2_MOUSE	37	272	7.351351351	7.56 %	97.27929014
Heterogeneous nuclear ribonucleoprotein A1 OS=Mus musculus GN=Hnrnpa1 PE=1 SV=2	sp|P49312|ROA1_MOUSE	34	155	4.558823529	4.69 %	
Splicing factor 3B subunit 3 OS=Mus musculus GN=Sf3b3 PE=2 SV=1	sp|Q921M3|SF3B3_MOUSE	136	137	1.007352941	1.04 %	
ATP-dependent RNA helicase A OS=Mus musculus GN=Dhx9 PE=1 SV=2	sp|O70133|DHX9_MOUSE	149	128	0.859060403	0.88 %	

Pre-mRNA-processing-splicing factor 8 OS=Mus musculus GN=Prpf8 PE=1 SV=2	sp|Q99PV0|PRP8_MOUSE	274	102	0.372262774	0.38 %	
Heterogeneous nuclear ribonucleoprotein A3 OS=Mus musculus GN=Hnrnpa3 PE=1 SV=1	sp|Q8BG05|ROA3_MOUSE	40	99	2.475	2.54 %	
Poly(rC)-binding protein 3 OS=Mus musculus GN=Pcbp3 PE=2 SV=3	sp|P57722|PCBP3_MOUSE	39	84	2.153846154	2.21 %	
Heat shock cognate 71 kDa protein OS=Mus musculus GN=Hspa8 PE=1 SV=1	sp|P63017|HSP7C_MOUSE	71	84	1.183098592	1.22 %	
Microtubule-associated protein 1B OS=Mus musculus GN=Map1b PE=1 SV=2	sp|P14873|MAP1B_MOUSE	270	82	0.303703704	0.31 %	
U5 small nuclear ribonucleoprotein 200 kDa helicase OS=Mus musculus GN=Snrnp200 PE=1 SV=1	sp|Q6P4T2|U520_MOUSE	245	74	0.302040816	0.31 %	
Poly(rC)-binding protein 2 OS=Mus musculus GN=Pcbp2 PE=1 SV=1	sp|Q61990|PCBP2_MOUSE	38	59	1.552631579	1.60 %	
Tubulin beta-5 chain OS=Mus musculus GN=Tubb5 PE=1 SV=1	sp|P99024|TBB5_MOUSE	50	55	1.1	1.13 %	
Muscleblind-like protein 1 OS=Mus musculus GN=Mbnl1 PE=1 SV=1	sp|Q9JKP5|MBNL1_MOUSE	37	52	1.405405405	1.44 %	
Muscleblind-like protein 2 OS=Mus musculus GN=Mbnl2 PE=2 SV=2	sp|Q8C181|MBNL2_MOUSE	40	48	1.2	1.23 %	
Desmoplakin OS=Mus musculus GN=Dsp PE=1 SV=1	sp|E9Q557|DESP_MOUSE	333	43	0.129129129	0.13 %	
Cold shock domain-containing protein E1 OS=Mus musculus GN=Csde1 PE=2 SV=1	sp|Q91W50|CSDE1_MOUSE	89	43	0.483146067	0.50 %	
DAZ-associated protein 1 OS=Mus musculus GN=Dazap1 PE=2 SV=2	sp|Q9JII5|DAZP1_MOUSE	43	42	0.976744186	1.00 %	
Actin, cytoplasmic 1 OS=Mus musculus GN=Actb PE=1 SV=1	sp|P60710|ACTB_MOUSE (+1)	42	41	0.976190476	1.00 %	
Far upstream element-binding protein 2 OS=Mus musculus GN=Khsrp PE=1 SV=2	sp|Q3U0V1|FUBP2_MOUSE	77	41	0.532467532	0.55 %	
Junction plakoglobin OS=Mus musculus GN=Jup PE=1 SV=3	sp|Q02257|PLAK_MOUSE	82	40	0.487804878	0.50 %	
Poly(rC)-binding protein 1 OS=Mus musculus GN=Pcbp1 PE=1 SV=1	sp|P60335|PCBP1_MOUSE	37	38	1.027027027	1.06 %	
Poly(U)-binding-splicing factor PUF60 OS=Mus musculus GN=Puf60 PE=2 SV=2	sp|Q3UEB3|PUF60_MOUSE	60	37	0.616666667	0.63 %	
Tubulin beta-4B chain OS=Mus musculus GN=Tubb4b PE=1 SV=1	sp|P68372|TBB4B_MOUSE	50	36	0.72	0.74 %	
Tubulin beta-2A chain OS=Mus musculus GN=Tubb2a PE=1 SV=1	sp|Q7TMM9|TBB2A_MOUSE	50	36	0.72	0.74 %	

Heterogeneous nuclear ribonucleoprotein U-like protein 1 OS=Mus musculus GN=Hnrnpul1 PE=1 SV=1	sp|Q8VDM6|HNRL1_MOUSE	96	36	0.375	0.39 %	
Heterogeneous nuclear ribonucleoprotein H OS=Mus musculus GN=Hnrnph1 PE=1 SV=3	sp|O35737|HNRH1_MOUSE	49	35	0.714285714	0.73 %	
Tubulin alpha-1B chain OS=Mus musculus GN=Tuba1b PE=1 SV=2	sp|P05213|TBA1B_MOUSE (+2)	50	35	0.7	0.72 %	
TAR DNA-binding protein 43 OS=Mus musculus GN=Tardbp PE=1 SV=1	sp|Q921F2|TADBP_MOUSE	45	35	0.777777778	0.80 %	
RING finger protein unkempt homolog OS=Mus musculus GN=Unk PE=2 SV=1	sp|Q8BL48|UNK_MOUSE	88	34	0.386363636	0.40 %	
Eukaryotic initiation factor 4A-III OS=Mus musculus GN=Eif4a3 PE=2 SV=3	sp|Q91VC3|IF4A3_MOUSE	47	34	0.723404255	0.74 %	
Elongation factor 2 OS=Mus musculus GN=Eef2 PE=1 SV=2	sp|P58252|EF2_MOUSE	95	32	0.336842105	0.35 %	
Polypyrimidine tract-binding protein 2 OS=Mus musculus GN=Ptbp2 PE=1 SV=2	sp|Q91Z31|PTBP2_MOUSE	57	31	0.543859649	0.56 %	
Heterogeneous nuclear ribonucleoprotein A/B OS=Mus musculus GN=Hnrnpab PE=1 SV=1	sp|Q99020|ROAA_MOUSE	31	31	1	1.03 %	
Heterogeneous nuclear ribonucleoprotein D0 OS=Mus musculus GN=Hnrnpd PE=1 SV=2	sp|Q60668|HNRPD_MOUSE	38	30	0.789473684	0.81 %	
Tubulin beta-4A chain OS=Mus musculus GN=Tubb4a PE=1 SV=3	sp|Q9D6F9|TBB4A_MOUSE	50	28	0.56	0.58 %	
116 kDa U5 small nuclear ribonucleoprotein component OS=Mus musculus GN=Eftud2 PE=2 SV=1	sp|O08810|U5S1_MOUSE	109	26	0.23853211	0.25 %	
RNA-binding protein Musashi homolog 1 OS=Mus musculus GN=Msi1 PE=1 SV=1	sp|Q61474|MSI1H_MOUSE	39	25	0.641025641	0.66 %	
Heterogeneous nuclear ribonucleoprotein U OS=Mus musculus GN=Hnrnpu PE=1 SV=1	sp|Q8VEK3|HNRPU_MOUSE	88	25	0.284090909	0.29 %	
Far upstream element-binding protein 1 OS=Mus musculus GN=Fubp1 PE=1 SV=1	sp|Q91WJ8|FUBP1_MOUSE	69	25	0.362318841	0.37 %	
Spliceosome RNA helicase Ddx39b OS=Mus musculus GN=Ddx39b PE=1 SV=1	sp|Q9Z1N5|DX39B_MOUSE	49	25	0.510204082	0.52 %	
Heterogeneous nuclear ribonucleoprotein H2 OS=Mus musculus GN=Hnrnph2 PE=2 SV=1	sp|P70333|HNRH2_MOUSE	49	24	0.489795918	0.50 %	

Serine/arginine-rich splicing factor 1 OS=Mus musculus GN=Srsf1 PE=1 SV=3	sp|Q6PDM2|SRSF1_MOUSE	28	24	0.857142857	0.88 %	
Heterogeneous nuclear ribonucleoprotein U-like protein 2 OS=Mus musculus GN=Hnrnpul2 PE=1 SV=2	sp|Q00PI9|HNRL2_MOUSE	85	21	0.247058824	0.25 %	
Interleukin enhancer-binding factor 3 OS=Mus musculus GN=Ilf3 PE=1 SV=2	sp|Q9Z1X4|ILF3_MOUSE	96	21	0.21875	0.22 %	
Transcriptional activator protein Pur-beta OS=Mus musculus GN=Purb PE=1 SV=3	sp|O35295|PURB_MOUSE	34	20	0.588235294	0.60 %	
Programmed cell death protein 6 OS=Mus musculus GN=Pdcd6 PE=1 SV=2	sp|P12815|PDCD6_MOUSE	22	20	0.909090909	0.93 %	
Vimentin OS=Mus musculus GN=Vim PE=1 SV=3	sp|P20152|VIME_MOUSE	54	20	0.370370 37	0.38 %	
14-3-3 protein epsilon OS=Mus musculus GN=Ywhae PE=1 SV=1	sp|P62259|1433E_MOUSE	29	20	0.689655172	0.71 %	
WD40 repeat-containing protein SMU1 OS=Mus musculus GN=Smu1 PE=2 SV=2	sp|Q3UKJ7|SMU1_MOUSE	58	20	0.344827586	0.35 %	
14-3-3 protein zeta/delta OS=Mus musculus GN=Ywhaz PE=1 SV=1	sp|P63101|1433Z_MOUSE	28	19	0.678571429	0.70 %	
Keratin, type I cytoskeletal 14 OS=Mus musculus GN=Krt14 PE=1 SV=2	sp|Q61781|K1C14_MOUSE	53	19	0.358490566	0.37 %	
Interphotoreceptor matrix proteoglycan 1 OS=Mus musculus GN=Impg1 PE=1 SV=1	sp|Q8R1W8|IMPG1_MOUSE	89	19	0.213483146	0.22 %	
Heterogeneous nuclear ribonucleoprotein M OS=Mus musculus GN=Hnrnpm PE=1 SV=3	sp|Q9D0E1|HNRPM_MOUSE	78	19	0.243589744	0.25 %	
Interferon-inducible double-stranded RNA-dependent protein kinase activator A OS=Mus musculus GN=Prkra PE=1 SV=1	sp|Q9WTX2|PRKRA_MOUSE	34	19	0.558823529	0.57 %	
Heat shock protein HSP 90-alpha OS=Mus musculus GN=Hsp90aa1 PE=1 SV=4	sp|P07901|HS90A_MOUSE	85	18	0.211764706	0.22 %	
Heat shock 70 kDa protein 1B OS=Mus musculus GN=Hspa1b PE=1 SV=3	sp|P17879|HS71B_MOUSE (+1)	70	18	0.257142857	0.26 %	
Transcriptional activator protein Pur-alpha OS=Mus musculus GN=Pura PE=1 SV=1	sp|P42669|PURA_MOUSE	35	18	0.514285714	0.53 %	
14-3-3 protein gamma OS=Mus musculus GN=Ywhag PE=1 SV=2	sp|P61982|1433G_MOUSE	28	18	0.642857143	0.66 %	

GTP-binding nuclear protein Ran OS=Mus musculus GN=Ran PE=1 SV=3	sp|P62827|RAN_MOUSE	24	18	0.75	0.77 %	
High mobility group protein B1 OS=Mus musculus GN=Hmgb1 PE=1 SV=2	sp|P63158|HMGB1_MOUSE	25	18	0.72	0.74 %	
G-rich sequence factor 1 OS=Mus musculus GN=Grsf1 PE=1 SV=2	sp|Q8C5Q4|GRSF1_MOUSE	53	18	0.339622642	0.35 %	
Polyubiquitin-B OS=Mus musculus GN=Ubb PE=2 SV=1	sp|P0CG49|UBB_MOUSE (+3)	34	17	0.5	0.51 %	
Guanine nucleotide-binding protein G(t) subunit alpha-1 OS=Mus musculus GN=Gnat1 PE=1 SV=3	sp|P20612|GNAT1_MOUSE	40	17	0.425	0.44 %	
RNA-binding protein Musashi homolog 2 OS=Mus musculus GN=Msi2 PE=1 SV=1	sp|Q920Q6|MSI2H_MOUSE	37	17	0.459459459	0.47 %	
Serine/threonine-protein phosphatase 2A 65 kDa regulatory subunit A alpha isoform OS=Mus musculus GN=Ppp2r1a PE=1 SV=3	sp|Q76MZ3|2AAA_MOUSE	65	16	0.246153846	0.25 %	
Spermatid perinuclear RNA-binding protein OS=Mus musculus GN=Strbp PE=1 SV=1	sp|Q91WM1|STRBP_MOUSE	74	16	0.216216216	0.22 %	
Serine-threonine kinase receptor-associated protein OS=Mus musculus GN=Strap PE=1 SV=2	sp|Q9Z1Z2|STRAP_MOUSE	38	16	0.421052632	0.43 %	
Putative pre-mRNA-splicing factor ATP-dependent RNA helicase DHX15 OS=Mus musculus GN=Dhx15 PE=1 SV=2	sp|O35286|DHX15_MOUSE	91	15	0.164835165	0.17 %	
Protein mago nashi homolog OS=Mus musculus GN=Magoh PE=2 SV=1	sp|P61327|MGN_MOUSE	17	15	0.882352941	0.91 %	
14-3-3 protein theta OS=Mus musculus GN=Ywhaq PE=1 SV=1	sp|P68254|1433T_MOUSE	28	15	0.535714286	0.55 %	
Importin subunit beta-1 OS=Mus musculus GN=Kpnb1 PE=1 SV=2	sp|P70168|IMB1_MOUSE	97	15	0.154639175	0.16 %	
ELAV-like protein 1 OS=Mus musculus GN=Elavl1 PE=1 SV=2	sp|P70372|ELAV1_MOUSE	36	15	0.416666667	0.43 %	
Probable ATP-dependent RNA helicase DDX5 OS=Mus musculus GN=Ddx5 PE=1 SV=2	sp|Q61656|DDX5_MOUSE	69	15	0.217391304	0.22 %	
Myelin expression factor 2 OS=Mus musculus GN=Myef2 PE=1 SV=1	sp|Q8C854|MYEF2_MOUSE	63	15	0.238095238	0.24 %	
Reticulon-4 OS=Mus musculus GN=Rtn4 PE=1 SV=2	sp|Q99P72|RTN4_MOUSE	127	15	0.118110236	0.12 %	
RNA 3'-terminal phosphate cyclase OS=Mus musculus GN=RtcA PE=2 SV=2	sp|Q9D7H3|RTCA_MOUSE	39	15	0.384615385	0.40 %	

Cap-specific mRNA (nucleoside-2'-O-)-methyltransferase 1 OS=Mus musculus GN=Cmtr1 PE=1 SV=1	sp|Q9DBC3|CMTR1_MOUSE	96	15	0.15625	0.16 %	
CUGBP Elav-like family member 2 OS=Mus musculus GN=Celf2 PE=1 SV=1	sp|Q9Z0H4|CELF2_MOUSE	54	15	0.277777778	0.29 %	
Hemoglobin subunit beta-1 OS=Mus musculus GN=Hbb-b1 PE=1 SV=2	sp|P02088|HBB1_MOUSE	16	14	0.875	0.90 %	
PHD finger-like domain-containing protein 5A OS=Mus musculus GN=Phf5a PE=1 SV=1	sp|P83870|PHF5A_MOUSE	12	14	1.166666667	1.20 %	
ATP-dependent RNA helicase DDX1 OS=Mus musculus GN=Ddx1 PE=1 SV=1	sp|Q91VR5|DDX1_MOUSE	83	14	0.168674699	0.17 %	
Serine/arginine-rich splicing factor 9 OS=Mus musculus GN=Srsf9 PE=1 SV=1	sp|Q9D0B0|SRSF9_MOUSE	26	14	0.538461538	0.55 %	
Heterogeneous nuclear ribonucleoprotein F OS=Mus musculus GN=Hnrnpf PE=1 SV=3	sp|Q9Z2X1|HNRPF_MOUSE	46	14	0.304347826	0.31 %	
Cleavage and polyadenylation specificity factor subunit 2 OS=Mus musculus GN=Cpsf2 PE=1 SV=1	sp|O35218|CPSF2_MOUSE	88	13	0.147727273	0.15 %	
Guanine nucleotide-binding protein G(I)/G(S)/G(T) subunit beta-1 OS=Mus musculus GN=Gnb1 PE=1 SV=3	sp|P62874|GBB1_MOUSE	37	13	0.351351351	0.36 %	
14-3-3 protein eta OS=Mus musculus GN=Ywhah PE=1 SV=2	sp|P68510|1433F_MOUSE	28	13	0.464285714	0.48 %	
Nucleolysin TIAR OS=Mus musculus GN=Tial1 PE=1 SV=1	sp|P70318|TIAR_MOUSE	43	13	0.302325581	0.31 %	
Enhancer of rudimentary homolog OS=Mus musculus GN=Erh PE=1 SV=1	sp|P84089|ERH_MOUSE	12	13	1.083333333	1.11 %	
Splicing factor, proline- and glutamine-rich OS=Mus musculus GN=Sfpq PE=1 SV=1	sp|Q8VIJ6|SFPQ_MOUSE	75	13	0.173333333	0.18 %	
Heterogeneous nuclear ribonucleoprotein L-like OS=Mus musculus GN=Hnrnpll PE=1 SV=3	sp|Q921F4|HNRLL_MOUSE	64	13	0.203125	0.21 %	
14-3-3 protein beta/alpha OS=Mus musculus GN=Ywhab PE=1 SV=3	sp|Q9CQV8|1433B_MOUSE	28	13	0.464285714	0.48 %	
Syntaxin-binding protein 1 OS=Mus musculus GN=Stxbp1 PE=1 SV=2	sp|O08599|STXB1_MOUSE	68	12	0.176470588	0.18 %	
Heat shock protein HSP 90-beta OS=Mus musculus GN=Hsp90ab1 PE=1 SV=3	sp|P11499|HS90B_MOUSE	83	12	0.144578313	0.15 %	
Glutamine synthetase OS=Mus musculus GN=Glul PE=1 SV=6	sp|P15105|GLNA_MOUSE	42	12	0.285714286	0.29 %	

S-arrestin OS=Mus musculus GN=Sag PE=1 SV=1	sp|P20443|ARRS_MOUSE	45	12	0.266666667	0.27 %	
Putative E3 ubiquitin-protein ligase UNKL OS=Mus musculus GN=Unkl PE=2 SV=2	sp|Q5FWH2|UNKL_MOUSE	80	12	0.15	0.15 %	
Non-POU domain-containing octamer-binding protein OS=Mus musculus GN=Nono PE=1 SV=3	sp|Q99K48|NONO_MOUSE	55	12	0.218181818	0.22 %	
RNA-binding protein 8A OS=Mus musculus GN=Rbm8a PE=1 SV=3	sp|Q9CWZ3|RBM8A_MOUSE	20	12	0.6	0.62 %	
Zinc finger RNA-binding protein OS=Mus musculus GN=Zfr PE=1 SV=2	sp|O88532|ZFR_MOUSE	117	11	0.094017094	0.10 %	
Spectrin alpha chain, non-erythrocytic 1 OS=Mus musculus GN=Sptan1 PE=1 SV=4	sp|P16546|SPTN1_MOUSE	285	11	0.038596491	0.04 %	
Protein argonaute-2 OS=Mus musculus GN=Ago2 PE=1 SV=3	sp|Q8CJG0|AGO2_MOUSE	97	11	0.113402062	0.12 %	
Heterogeneous nuclear ribonucleoprotein L OS=Mus musculus GN=Hnrnpl PE=1 SV=2	sp|Q8R081|HNRPL_MOUSE	64	11	0.171875	0.18 %	
Cell cycle and apoptosis regulator protein 2 OS=Mus musculus GN=Ccar2 PE=1 SV=2	sp|Q8VDP4|CCAR2_MOUSE	103	11	0.106796117	0.11 %	
Protein syndesmos OS=Mus musculus GN=Nudt16l1 PE=1 SV=2	sp|Q8VHN8|SDOS_MOUSE	23	11	0.478260087	0.49 %	
UPF0568 protein C14orf166 homolog OS=Mus musculus PE=2 SV=1	sp|Q9CQE8|CN166_MOUSE	28	11	0.392857143	0.40 %	
Interleukin enhancer-binding factor 2 OS=Mus musculus GN=Ilf2 PE=1 SV=1	sp|Q9CXY6|ILF2_MOUSE	43	11	0.255813953	0.26 %	
Target of rapamycin complex subunit LST8 OS=Mus musculus GN=Mlst8 PE=1 SV=1	sp|Q9DCJ1|LST8_MOUSE	36	11	0.305555556	0.31 %	
Regulator of nonsense transcripts 1 OS=Mus musculus GN=Upf1 PE=1 SV=2	sp|Q9EPU0|RENT1_MOUSE	124	11	0.088709677	0.09 %	
Triosephosphate isomerase OS=Mus musculus GN=Tpi1 PE=1 SV=4	sp|P17751|TPIS_MOUSE	32	10	0.3125	0.32 %	
Rod cGMP-specific 3',5'-cyclic phosphodiesterase subunit alpha OS=Mus musculus GN=Pde6a PE=2 SV=3	sp|P27664|PDE6A_MOUSE	100	10	0.1	0.10 %	
High mobility group protein B2 OS=Mus musculus GN=Hmgb2 PE=1 SV=3	sp|P30681|HMGB2_MOUSE	24	10	0.416666667	0.43 %	
Guanine nucleotide-binding protein subunit beta-2-like 1 OS=Mus musculus GN=Gnb2l1 PE=1 SV=3	sp|P68040|GBLP_MOUSE	35	10	0.285714286	0.29 %	

Histone-binding protein RBBP4 OS=Mus musculus GN=Rbbp4 PE=1 SV=5	sp|Q60972|RBBP4_MOUSE	48	10	0.208333333	0.21 %	
Serine/arginine-rich splicing factor 2 OS=Mus musculus GN=Srsf2 PE=1 SV=4	sp|Q62093|SRSF2_MOUSE	25	10	0.4	0.41 %	
Transcription intermediary factor 1-beta OS=Mus musculus GN=Trim28 PE=1 SV=3	sp|Q62318|TIF1B_MOUSE	89	10	0.112359551	0.12 %	
Eukaryotic translation initiation factor 2 subunit 1 OS=Mus musculus GN=Eif2s1 PE=1 SV=3	sp|Q6ZWX6|IF2A_MOUSE	36	10	0.277777778	0.29 %	
WD repeat-containing protein 82 OS=Mus musculus GN=Wdr82 PE=1 SV=1	sp|Q8BFQ4|WDR82_MOUSE	35	10	0.285714286	0.29 %	
Transportin-1 OS=Mus musculus GN=Tnpo1 PE=1 SV=2	sp|Q8BFY9|TNPO1_MOUSE	102	10	0.098039216	0.10 %	
Splicing factor 3B subunit 5 OS=Mus musculus GN=Sf3b5 PE=2 SV=1	sp|Q923D4|SF3B5_MOUSE	10	10	1	1.03 %	
Cleavage stimulation factor subunit 1 OS=Mus musculus GN=Cstf1 PE=2 SV=1	sp|Q99LC2|CSTF1_MOUSE	48	10	0.208333333	0.21 %	
Cleavage and polyadenylation specificity factor subunit 3 OS=Mus musculus GN=Cpsf3 PE=1 SV=2	sp|Q9QXK7|CPSF3_MOUSE	78	10	0.128205128	0.13 %	
Nucleolysin TIA-1 OS=Mus musculus GN=Tia1 PE=1 SV=1	sp|P52912|TIA1_MOUSE	43	9	0.209302326	0.22 %	
Transcription elongation factor B polypeptide 2 OS=Mus musculus GN=Tceb2 PE=1 SV=1	sp|P62869|ELOB_MOUSE	13	9	0.692307692	0.71 %	
Apolipoprotein A-I OS=Mus musculus GN=Apoa1 PE=1 SV=2	sp|Q00623|APOA1_MOUSE	31	9	0.290322581	0.30 %	
Nucleophosmin OS=Mus musculus GN=Npm1 PE=1 SV=1	sp|Q61937|NPM_MOUSE	33	9	0.272727273	0.28 %	
ATP-dependent RNA helicase DDX3X OS=Mus musculus GN=Ddx3x PE=1 SV=3	sp|Q62167|DDX3X_MOUSE	73	9	0.123287671	0.13 %	
Interphotoreceptor matrix proteoglycan 2 OS=Mus musculus GN=Impg2 PE=1 SV=1	sp|Q80XH2|IMPG2_MOUSE	138	9	0.065217391	0.07 %	
RNA binding motif protein, X-linked-like-1 OS=Mus musculus GN=Rbmxl1 PE=1 SV=1	sp|Q91VM5|RMXL1_MOUSE	42	9	0.214285714	0.22 %	
Protein arginine N-methyltransferase 1 OS=Mus musculus GN=Prmt1 PE=1 SV=1	sp|Q9JIF0|ANM1_MOUSE	42	9	0.214285714	0.22 %	
Squamous cell carcinoma antigen recognized by T-cells 3 OS=Mus musculus GN=Sart3 PE=1 SV=1	sp|Q9JLI8|SART3_MOUSE	110	9	0.081818182	0.08 %	

Hemoglobin subunit alpha OS=Mus musculus GN=Hba PE=1 SV=2	sp|P01942|HBA_MOUSE	15	8	0.533333333	0.55 %	
Transitional endoplasmic reticulum ATPase OS=Mus musculus GN=Vcp PE=1 SV=4	sp|Q01853|TERA_MOUSE	89	8	0.08988764	0.09 %	
Keratin, type II cytoskeletal 2 oral OS=Mus musculus GN=Krt76 PE=2 SV=1	sp|Q3UV17|K22O_MOUSE	63	8	0.126984127	0.13 %	
U1 small nuclear ribonucleoprotein A OS=Mus musculus GN=Snrpa PE=2 SV=3	sp|Q62189|SNRPA_MOUSE	32	8	0.25	0.26 %	
PEST proteolytic signal-containing nuclear protein OS=Mus musculus GN=Pcnp PE=1 SV=1	sp|Q6P8I4|PCNP_MOUSE	19	8	0.421052632	0.43 %	
Sodium/potassium-transporting ATPase subunit alpha-3 OS=Mus musculus GN=Atp1a3 PE=1 SV=1	sp|Q6PIC6|AT1A3_MOUSE	112	8	0.071428571	0.07 %	
Zinc finger matrin-type protein 4 OS=Mus musculus GN=Zmat4 PE=2 SV=1	sp|Q8BZ94|ZMAT4_MOUSE	26	8	0.307692308	0.32 %	
Polyadenylate-binding protein 2 OS=Mus musculus GN=Pabpn1 PE=2 SV=3	sp|Q8CCS6|PABP2_MOUSE	32	8	0.25	0.26 %	
UDP-N-acetylglucosamine--peptide N-acetylglucosaminyltransferase 110 kDa subunit OS=Mus musculus GN=Ogt PE=1 SV=2	sp|Q8CGY8|OGT1_MOUSE	117	8	0.068376068	0.07 %	
Splicing factor 3B subunit 1 OS=Mus musculus GN=Sf3b1 PE=1 SV=1	sp|Q99NB9|SF3B1_MOUSE	146	8	0.054794521	0.06 %	
Cleavage and polyadenylation specificity factor subunit 5 OS=Mus musculus GN=Nudt21 PE=1 SV=1	sp|Q9CQF3|CPSF5_MOUSE	26	8	0.307692308	0.32 %	
Microfibrillar-associated protein 1 OS=Mus musculus GN=Mfap1 PE=1 SV=1	sp|Q9CQU1|MFAP1_MOUSE	52	8	0.153846154	0.16 %	
Dihydropyrimidinase-related protein 2 OS=Mus musculus GN=Dpysl2 PE=1 SV=2	sp|O08553|DPYL2_MOUSE	62	7	0.112903226	0.12 %	
AP-1 complex subunit beta-1 OS=Mus musculus GN=Ap1b1 PE=2 SV=2	sp|O35643|AP1B1_MOUSE	104	7	0.067307692	0.07 %	
Putative RNA-binding protein 3 OS=Mus musculus GN=Rbm3 PE=2 SV=1	sp|O89086|RBM3_MOUSE	17	7	0.411764706	0.42 %	
L-lactate dehydrogenase A chain OS=Mus musculus GN=Ldha PE=1 SV=3	sp|P06151|LDHA_MOUSE	36	7	0.194444444	0.20 %	
Alpha-crystallin A chain OS=Mus musculus GN=Cryaa PE=2 SV=1	sp|P24622|CRYAA_MOUSE	22	7	0.318181818	0.33 %	

Ezrin OS=Mus musculus GN=Ezr PE=1 SV=3	sp|P26040|EZRI_MOUSE	69	7	0.101449275	0.10 %	
Peroxiredoxin-1 OS=Mus musculus GN=Prdx1 PE=1 SV=1	sp|P35700|PRDX1_MOUSE	22	7	0.318181818	0.33 %	
RuvB-like 1 OS=Mus musculus GN=Ruvbl1 PE=1 SV=1	sp|P60122|RUVB1_MOUSE	50	7	0.14	0.14 %	
Serine/threonine-protein phosphatase 2A catalytic subunit alpha isoform OS=Mus musculus GN=Ppp2ca PE=1 SV=1	sp|P63330|PP2AA_MOUSE	36	7	0.194444444	0.20 %	
DNA damage-binding protein 1 OS=Mus musculus GN=Ddb1 PE=1 SV=2	sp|Q3U1J4|DDB1_MOUSE	127	7	0.055111811	0.06 %	
TNF receptor-associated factor 3 OS=Mus musculus GN=Traf3 PE=1 SV=2	sp|Q60803|TRAF3_MOUSE	64	7	0.109375	0.11 %	
Guanine nucleotide-binding protein G(T) subunit gamma-T1 OS=Mus musculus GN=Gngt1 PE=1 SV=3	sp|Q61012|GBG1_MOUSE	9	7	0.777777778	0.80 %	
Host cell factor 1 OS=Mus musculus GN=Hcfc1 PE=1 SV=2	sp|Q61191|HCFC1_MOUSE	210	7	0.033333333	0.03 %	
Sperm flagellar protein 2 OS=Mus musculus GN=Spef2 PE=2 SV=2	sp|Q8C9J3|SPEF2_MOUSE	199	7	0.035175879	0.04 %	
Paraspeckle component 1 OS=Mus musculus GN=Pspc1 PE=1 SV=1	sp|Q8R326|PSPC1_MOUSE	59	7	0.118644068	0.12 %	
Zinc finger CCHC domain-containing protein 8 OS=Mus musculus GN=Zcchc8 PE=2 SV=3	sp|Q9CYA6|ZCHC8_MOUSE	78	7	0.089744359	0.09 %	
RuvB-like 2 OS=Mus musculus GN=Ruvbl2 PE=2 SV=3	sp|Q9WTM5|RUVB2_MOUSE	51	7	0.137254902	0.14 %	
Eukaryotic translation initiation factor 4H OS=Mus musculus GN=Eif4h PE=1 SV=3	sp|Q9WUK2|IF4H_MOUSE	27	7	0.259259259	0.27 %	
Retinoschisin OS=Mus musculus GN=Rs1 PE=1 SV=1	sp|Q9Z1L4|XLRS1_MOUSE	26	7	0.269230769	0.28 %	
Kelch-like protein 3 OS=Mus musculus GN=Klhl3 PE=1 SV=2	sp|E0CZ16|KLHL3_MOUSE	65	6	0.092307692	0.09 %	
Hexokinase-2 OS=Mus musculus GN=Hk2 PE=2 SV=1	sp|O08528|HXK2_MOUSE	103	6	0.058252427	0.06 %	
Serum albumin OS=Mus musculus GN=Alb PE=1 SV=3	sp|P07724|ALBU_MOUSE	69	6	0.086956522	0.09 %	
Nucleolin OS=Mus musculus GN=Ncl PE=1 SV=2	sp|P09405|NUCL_MOUSE	77	6	0.077922078	0.08 %	
60S acidic ribosomal protein P0 OS=Mus musculus GN=Rplp0 PE=1 SV=3	sp|P14869|RLA0_MOUSE	34	6	0.176470588	0.18 %	
Lysozyme C-1 OS=Mus musculus GN=Lyz1 PE=1 SV=1	sp|P17897|LYZ1_MOUSE	17	6	0.352941176	0.36 %	

CUGBP Elav-like family member 1 OS=Mus musculus GN=Celf1 PE=1 SV=2	sp|P28659|CELF1_MOUSE	52	6	0.115384615	0.12 %	
RNA-binding protein FUS OS=Mus musculus GN=Fus PE=2 SV=1	sp|P56959|FUS_MOUSE	53	6	0.113207547	0.12 %	
Dihydropyrimidinase-related protein 3 OS=Mus musculus GN=Dpysl3 PE=1 SV=1	sp|Q62188|DPYL3_MOUSE	62	6	0.096774194	0.10 %	
Cleavage stimulation factor subunit 2 OS=Mus musculus GN=Cstf2 PE=1 SV=2	sp|Q8BIQ5|CSTF2_MOUSE	61	6	0.098360656	0.10 %	
Aryl-hydrocarbon-interacting protein-like 1 OS=Mus musculus GN=Aipl1 PE=2 SV=2	sp|Q924K1|AIPL1_MOUSE	38	6	0.157894737	0.16 %	
Superkiller viralicidic activity 2-like 2 OS=Mus musculus GN=Skiv2l2 PE=1 SV=1	sp|Q9CZU3|SK2L2_MOUSE	118	6	0.050847458	0.05 %	
Phenylalanine--tRNA ligase beta subunit OS=Mus musculus GN=Farsb PE=2 SV=2	sp|Q9WUA2|SYFB_MOUSE	66	6	0.090909091	0.09 %	
Phospholipid hydroperoxide glutathione peroxidase, mitochondrial OS=Mus musculus GN=Gpx4 PE=1 SV=4	sp|O70325|GPX41_MOUSE (+1)	22	5	0.227272727	0.23 %	
C-terminal-binding protein 1 OS=Mus musculus GN=Ctbp1 PE=1 SV=2	sp|O88712|CTBP1_MOUSE	48	5	0.104166667	0.11 %	
Elongation factor 1-alpha 1 OS=Mus musculus GN=Eef1a1 PE=1 SV=3	sp|P10126|EF1A1_MOUSE	50	5	0.1	0.10 %	
Histone H2B type 1-F/J/L OS=Mus musculus GN=Hist1h2bf PE=1 SV=2	sp|P10853|H2B1F_MOUSE (+8)	14	5	0.357142857	0.37 %	
DNA-(apurinic or apyrimidinic site) lyase OS=Mus musculus GN=Apex1 PE=1 SV=2	sp|P28352|APEX1_MOUSE	35	5	0.142857143	0.15 %	
F-actin-capping protein subunit beta OS=Mus musculus GN=Capzb PE=1 SV=3	sp|P47757|CAPZB_MOUSE	31	5	0.161290323	0.17 %	
Pyruvate kinase PKM OS=Mus musculus GN=Pkm PE=1 SV=4	sp|P52480|KPYM_MOUSE	58	5	0.086206897	0.09 %	
Calmodulin OS=Mus musculus GN=Calm1 PE=1 SV=2	sp|P62204|CALM_MOUSE	17	5	0.294117647	0.30 %	
Transcription elongation factor B polypeptide 1 OS=Mus musculus GN=Tceb1 PE=1 SV=1	sp|P83940|ELOC_MOUSE	12	5	0.416666667	0.43 %	
Dihydropyrimidinase-related protein 1 OS=Mus musculus GN=Crmp1 PE=1 SV=1	sp|P97427|DPYL1_MOUSE	62	5	0.080645161	0.08 %	
Constitutive coactivator of PPAR-gamma-like protein 1 OS=Mus musculus GN=FAM120A PE=1 SV=2	sp|Q6A0A9|F120A_MOUSE	122	5	0.040983607	0.04 %	

Staphylococcal nuclease domain-containing protein 1 OS=Mus musculus GN=Snd1 PE=1 SV=1	sp|Q78PY7|SND1_MOUSE	102	5	0.049019608	0.05 %	
HIV Tat-specific factor 1 homolog OS=Mus musculus GN=Htatsf1 PE=1 SV=1	sp|Q8BGC0|HTSF1_MOUSE	86	5	0.058139535	0.06 %	
Integrator complex subunit 4 OS=Mus musculus GN=Ints4 PE=1 SV=1	sp|Q8CIM8|INT4_MOUSE	108	5	0.046296296	0.05 %	
Protein argonaute-1 OS=Mus musculus GN=Ago1 PE=1 SV=2	sp|Q8CJG1|AGO1_MOUSE	97	5	0.051546392	0.05 %	
Transmembrane emp24 domain-containing protein 9 OS=Mus musculus GN=Tmed9 PE=1 SV=2	sp|Q99KF1|TMED9_MOUSE	27	5	0.185185185	0.19 %	
Cleavage stimulation factor subunit 3 OS=Mus musculus GN=Cstf3 PE=1 SV=1	sp|Q99LI7|CSTF3_MOUSE	83	5	0.060240964	0.06 %	
Elongation factor 1-gamma OS=Mus musculus GN=Eef1g PE=1 SV=3	sp|Q9D8N0|EF1G_MOUSE	50	5	0.1	0.10 %	
WD repeat-containing protein 61 OS=Mus musculus GN=Wdr61 PE=2 SV=1	sp|Q9ERF3|WDR61_MOUSE	34	5	0.147058824	0.15 %	
General transcription factor II-I OS=Mus musculus GN=Gtf2i PE=1 SV=3	sp|Q9ESZ8|GTF2I_MOUSE	112	5	0.044642857	0.05 %	
Profilin-2 OS=Mus musculus GN=Pfn2 PE=1 SV=3	sp|Q9JJV2|PROF2_MOUSE	15	5	0.333333333	0.34 %	
Treacle protein OS=Mus musculus GN=Tcof1 PE=1 SV=1	sp|O08784|TCOF_MOUSE	135	4	0.029629630	0.03 %	
DNA-directed RNA polymerase I subunit RPA1 OS=Mus musculus GN=Polr1a PE=1 SV=2	sp|O35134|RPA1_MOUSE	194	4	0.020618557	0.02 %	
Elongation factor 1-beta OS=Mus musculus GN=Eef1b PE=1 SV=5	sp|O70251|EF1B_MOUSE	25	4	0.16	0.16 %	
Fructose-bisphosphate aldolase A OS=Mus musculus GN=Aldoa PE=1 SV=2	sp|P05064|ALDOA_MOUSE	39	4	0.102564103	0.11 %	
40S ribosomal protein SA OS=Mus musculus GN=Rpsa PE=1 SV=4	sp|P14206|RSSA_MOUSE	33	4	0.121212121	0.12 %	
Glyceraldehyde-3-phosphate dehydrogenase OS=Mus musculus GN=Gapdh PE=1 SV=2	sp|P16858|G3P_MOUSE	36	4	0.111111111	0.11 %	
Hexokinase-1 OS=Mus musculus GN=Hk1 PE=1 SV=3	sp|P17710|HXK1_MOUSE	108	4	0.037037037	0.04 %	
AP-1 complex subunit gamma-1 OS=Mus musculus GN=Ap1g1 PE=1 SV=3	sp|P22892|AP1G1_MOUSE	91	4	0.043956044	0.05 %	
Poly(rC)-binding protein 4 OS=Mus musculus GN=Pcbp4 PE=2 SV=1	sp|P57724|PCBP4_MOUSE	41	4	0.097560976	0.10 %	

Cold-inducible RNA-binding protein OS=Mus musculus GN=Cirbp PE=1 SV=1	sp|P60824|CIRBP_MOUSE	19	4	0.210526316	0.22 %	
Small ubiquitin-related modifier 2 OS=Mus musculus GN=Sumo2 PE=1 SV=1	sp|P61957|SUMO2_MOUSE	11	4	0.363636364	0.37 %	
40S ribosomal protein S12 OS=Mus musculus GN=Rps12 PE=1 SV=2	sp|P63323|RS12_MOUSE	15	4	0.266666667	0.27 %	
Plakophilin-1 OS=Mus musculus GN=Pkp1 PE=2 SV=1	sp|P97350|PKP1_MOUSE	81	4	0.049382716	0.05 %	
Heat shock protein beta-6 OS=Mus musculus GN=Hspb6 PE=2 SV=1	sp|Q5EBG6|HSPB6_MOUSE	18	4	0.222222222	0.23 %	
Growth factor receptor-bound protein 2 OS=Mus musculus GN=Grb2 PE=1 SV=1	sp|Q60631|GRB2_MOUSE	25	4	0.16	0.16 %	
Clathrin heavy chain 1 OS=Mus musculus GN=Cltc PE=1 SV=3	sp|Q68FD5|CLH1_MOUSE	192	4	0.020833333	0.02 %	
Cleavage stimulation factor subunit 2 tau variant OS=Mus musculus GN=Cstf2t PE=1 SV=2	sp|Q8C7E9|CSTFT_MOUSE	66	4	0.060606061	0.06 %	
Transcription elongation factor A protein-like 5 OS=Mus musculus GN=Tceal5 PE=1 SV=1	sp|Q8CCT4|TCAL5_MOUSE	22	4	0.181818182	0.19 %	
Translation machinery-associated protein 7 OS=Mus musculus GN=Tma7 PE=2 SV=1	sp|Q8K003|TMA7_MOUSE	7	4	0.571428571	0.59 %	
Histone chaperone ASF1A OS=Mus musculus GN=Asf1a PE=2 SV=1	sp|Q9CQE6|ASF1A_MOUSE	23	4	0.173913043	0.18 %	
Protein PBDC1 OS=Mus musculus GN=Pbdc1 PE=2 SV=1	sp|Q9D0B6|PBDC1_MOUSE	22	4	0.181818182	0.19 %	
Peptidyl-prolyl cis-trans isomerase H OS=Mus musculus GN=Ppih PE=2 SV=1	sp|Q9D868|PPIH_MOUSE	20	4	0.2	0.21 %	
Coiled-coil domain-containing protein 97 OS=Mus musculus GN=Ccdc97 PE=1 SV=1	sp|Q9DBT3|CCD97_MOUSE	39	4	0.102564103	0.11 %	
AMP deaminase 2 OS=Mus musculus GN=Ampd2 PE=1 SV=1	sp|Q9DBT5|AMPD2_MOUSE	92	4	0.043478261	0.04 %	
Transmembrane emp24 domain-containing protein 2 OS=Mus musculus GN=Tmed2 PE=1 SV=1	sp|Q9R0Q3|TMED2_MOUSE	23	4	0.173913043	0.18 %	
Scaffold attachment factor B1 OS=Mus musculus GN=Safb PE=1 SV=2	sp|D3YXK2|SAFB1_MOUSE	105	3	0.028571429	0.03 %	
Histone deacetylase 1 OS=Mus musculus GN=Hdac1 PE=1 SV=1	sp|O09106|HDAC1_MOUSE	55	3	0.054545455	0.06 %	
Dolichyl-diphosphooligosaccharide--protein glycosyltransferase 48 kDa	sp|O54734|OST48_MOUSE	49	3	0.06122449	0.06 %	

subunit OS=Mus musculus GN=Ddost PE=1 SV=2						
Retinal rod rhodopsin-sensitive cGMP 3',5'-cyclic phosphodiesterase subunit delta OS=Mus musculus GN=Pde6d PE=1 SV=1	sp|O55057|PDE6D_MOUSE	17	3	0.176470588	0.18 %	
Protein lin-7 homolog C OS=Mus musculus GN=Lin7c PE=1 SV=2	sp|O88952|LIN7C_MOUSE	22	3	0.136363636	0.14 %	
Annexin A2 OS=Mus musculus GN=Anxa2 PE=1 SV=2	sp|P07356|ANXA2_MOUSE	39	3	0.076923077	0.08 %	
Thioredoxin OS=Mus musculus GN=Txn PE=1 SV=3	sp|P10639|THIO_MOUSE	12	3	0.25	0.26 %	
Microtubule-associated protein 4 OS=Mus musculus GN=Map4 PE=1 SV=3	sp|P27546|MAP4_MOUSE	117	3	0.025641026	0.03 %	
Dynamin-1 OS=Mus musculus GN=Dnm1 PE=1 SV=2	sp|P39053|DYN1_MOUSE	98	3	0.030612245	0.03 %	
ATP synthase subunit beta, mitochondrial OS=Mus musculus GN=Atp5b PE=1 SV=2	sp|P56480|ATPB_MOUSE	56	3	0.053571429	0.06 %	
Synaptosomal-associated protein 25 OS=Mus musculus GN=Snap25 PE=1 SV=1	sp|P60879|SNP25_MOUSE	23	3	0.130434783	0.13 %	
Histone H4 OS=Mus musculus GN=Hist1h4a PE=1 SV=2	sp|P62806|H4_MOUSE	11	3	0.272727273	0.28 %	
Vesicle-associated membrane protein 3 OS=Mus musculus GN=Vamp3 PE=1 SV=1	sp|P63024|VAMP3_MOUSE (+1)	11	3	0.272727273	0.28 %	
Dynein light chain 1, cytoplasmic OS=Mus musculus GN=Dynll1 PE=1 SV=1	sp|P63168|DYL1_MOUSE	10	3	0.3	0.31 %	
Thioredoxin-like protein 4A OS=Mus musculus GN=Txnl4a PE=2 SV=1	sp|P83877|TXN4A_MOUSE	17	3	0.176470588	0.18 %	
Serine/arginine-rich splicing factor 3 OS=Mus musculus GN=Srsf3 PE=1 SV=1	sp|P84104|SRSF3_MOUSE	19	3	0.157894737	0.16 %	
RISC-loading complex subunit TARBP2 OS=Mus musculus GN=Tarbp2 PE=1 SV=2	sp|P97473|TRBP2_MOUSE	39	3	0.076923077	0.08 %	
Peroxiredoxin-2 OS=Mus musculus GN=Prdx2 PE=1 SV=3	sp|Q61171|PRDX2_MOUSE	22	3	0.136363636	0.14 %	
Desmoglein-1-alpha OS=Mus musculus GN=Dsg1a PE=2 SV=2	sp|Q61495|DSG1A_MOUSE (+2)	115	3	0.026086957	0.03 %	
Serum paraoxonase/arylesterase 2 OS=Mus musculus GN=Pon2 PE=1 SV=2	sp|Q62086|PON2_MOUSE	40	3	0.075	0.08 %	
Calcium/calmodulin-dependent protein kinase type II subunit delta	sp|Q6PHZ2|KCC2D_MOUSE	56	3	0.053571429	0.06 %	

OS=Mus musculus GN=Camk2d PE=1 SV=1						
DNA-directed RNA polymerases I, II, and III subunit RPABC1 OS=Mus musculus GN=Polr2e PE=2 SV=1	sp|Q80UW8|RPAB1_MOUSE	25	3	0.12	0.12 %	
Protein FAM98B OS=Mus musculus GN=Fam98b PE=2 SV=1	sp|Q80VD1|FA98B_MOUSE	45	3	0.066666667	0.07 %	
Complexin-4 OS=Mus musculus GN=Cplx4 PE=1 SV=2	sp|Q80WM3|CPLX4_MOUSE	18	3	0.166666667	0.17 %	
ATP-dependent RNA helicase DDX42 OS=Mus musculus GN=Ddx42 PE=1 SV=3	sp|Q810A7|DDX42_MOUSE	102	3	0.029411765	0.03 %	
Parkinson disease 7 domain-containing protein 1 OS=Mus musculus GN=Pddc1 PE=1 SV=1	sp|Q8BFQ8|PDDC1_MOUSE	23	3	0.130434783	0.13 %	
Zinc finger CCCH domain-containing protein 14 OS=Mus musculus GN=Zc3h14 PE=1 SV=1	sp|Q8BJ05|ZC3HE_MOUSE	82	3	0.036585366	0.04 %	
Importin-5 OS=Mus musculus GN=Ipo5 PE=1 SV=3	sp|Q8BKC5|IPO5_MOUSE	124	3	0.024193548	0.02 %	
Gephyrin OS=Mus musculus GN=Gphn PE=1 SV=2	sp|Q8BUV3|GEPH_MOUSE	83	3	0.036144578	0.04 %	
Peptidylprolyl isomerase domain and WD repeat-containing protein 1 OS=Mus musculus GN=Ppwd1 PE=2 SV=2	sp|Q8CEC6|PPWD1_MOUSE	73	3	0.041095589	0.04 %	
Transmembrane emp24 domain-containing protein 4 OS=Mus musculus GN=Tmed4 PE=2 SV=1	sp|Q8R1V4|TMED4_MOUSE	26	3	0.115384615	0.12 %	
Vigilin OS=Mus musculus GN=Hdlbp PE=1 SV=1	sp|Q8VDJ3|VIGLN_MOUSE	142	3	0.021126761	0.02 %	
Telomeric repeat-binding factor 2-interacting protein 1 OS=Mus musculus GN=Terf2ip PE=1 SV=1	sp|Q91VL8|TE2IP_MOUSE	43	3	0.069767442	0.07 %	
Brain acid soluble protein 1 OS=Mus musculus GN=Basp1 PE=1 SV=3	sp|Q91XV3|BASP1_MOUSE	22	3	0.136363636	0.14 %	
Double-stranded RNA-specific editase 1 OS=Mus musculus GN=Adarb1 PE=1 SV=1	sp|Q91ZS8|RED1_MOUSE	78	3	0.038461538	0.04 %	
tRNA-splicing ligase RtcB homolog OS=Mus musculus GN=Rtcb PE=2 SV=1	sp|Q99LF4|RTCB_MOUSE	55	3	0.054545455	0.06 %	
CD2 antigen cytoplasmic tail-binding protein 2 OS=Mus musculus GN=Cd2bp2 PE=1 SV=1	sp|Q9CWK3|CD2B2_MOUSE	38	3	0.078947368	0.08 %	
NHP2-like protein 1 OS=Mus musculus GN=Nhp2l1 PE=1 SV=4	sp|Q9D0T1|NH2L1_MOUSE	14	3	0.214285714	0.22 %	
Vacuolar protein sorting-associated protein 28 homolog OS=Mus musculus GN=Vps28 PE=2 SV=1	sp|Q9D1C8|VPS28_MOUSE	25	3	0.12	0.12 %	

Peptidyl-prolyl cis-trans isomerase-like 3 OS=Mus musculus GN=Ppil3 PE=2 SV=1	sp|Q9D6L8|PPIL3_MOUSE	18	3	0.166666667	0.17 %	
Vesicular integral-membrane protein VIP36 OS=Mus musculus GN=Lman2 PE=2 SV=2	sp|Q9DBH5|LMAN2_MOUSE	40	3	0.075	0.08 %	
C-Myc-binding protein OS=Mus musculus GN=Mycbp PE=2 SV=5	sp|Q9EQS3|MYCBP_MOUSE	12	3	0.25	0.26 %	
Zinc finger protein 346 OS=Mus musculus GN=Znf346 PE=1 SV=1	sp|Q9R0B7|ZN346_MOUSE	33	3	0.090909091	0.09 %	
Acyl-protein thioesterase 2 OS=Mus musculus GN=Lypla2 PE=1 SV=1	sp|Q9WTL7|LYPA2_MOUSE	25	3	0.12	0.12 %	
Protein FAM50A OS=Mus musculus GN=Fam50a PE=2 SV=1	sp|Q9WV03|FA50A_MOUSE	40	3	0.075	0.08 %	
THO complex subunit 4 OS=Mus musculus GN=Alyref PE=1 SV=3	sp|O08583|THOC4_MOUSE	27	2	0.074074074	0.08 %	
Dihydropyrimidinase-related protein 4 OS=Mus musculus GN=Dpysl4 PE=1 SV=1	sp|O35098|DPYL4_MOUSE	62	2	0.032258065	0.03 %	
Importin subunit alpha-3 OS=Mus musculus GN=Kpna4 PE=1 SV=1	sp|O35343|IMA3_MOUSE (+1)	58	2	0.034482759	0.04 %	
High mobility group protein B3 OS=Mus musculus GN=Hmgb3 PE=2 SV=3	sp|O54879|HMGB3_MOUSE	23	2	0.086956522	0.09 %	
Synaptogyrin-1 OS=Mus musculus GN=Syngr1 PE=1 SV=2	sp|O55100|SNG1_MOUSE	26	2	0.076923077	0.08 %	
Eukaryotic translation initiation factor 6 OS=Mus musculus GN=Eif6 PE=1 SV=2	sp|O55135|IF6_MOUSE	27	2	0.074074074	0.08 %	
Cytoplasmic dynein 1 intermediate chain 2 OS=Mus musculus GN=Dync1i2 PE=1 SV=1	sp|O88487|DC1I2_MOUSE	68	2	0.029411765	0.03 %	
Neurofilament medium polypeptide OS=Mus musculus GN=Nefm PE=1 SV=4	sp|P08553|NFM_MOUSE	96	2	0.020833333	0.02 %	
4F2 cell-surface antigen heavy chain OS=Mus musculus GN=Slc3a2 PE=1 SV=1	sp|P10852|4F2_MOUSE	58	2	0.034482759	0.04 %	
Activated RNA polymerase II transcriptional coactivator p15 OS=Mus musculus GN=Sub1 PE=1 SV=3	sp|P11031|TCP4_MOUSE	14	2	0.142857143	0.15 %	
T-complex protein 1 subunit alpha OS=Mus musculus GN=Tcp1 PE=1 SV=3	sp|P11983|TCPA_MOUSE	60	2	0.033333333	0.03 %	
cAMP-dependent protein kinase type II-alpha regulatory subunit OS=Mus musculus GN=Prkar2a PE=1 SV=2	sp|P12367|KAP2_MOUSE	45	2	0.044444444	0.05 %	

ATP-dependent 6-phosphofructokinase, liver type OS=Mus musculus GN=Pfkl PE=1 SV=4	sp|P12382|PFKAL_MOUSE	85	2	0.023529412	0.02%	
Rhodopsin OS=Mus musculus GN=Rho PE=1 SV=2	sp|P15409|OPSD_MOUSE	39	2	0.051282051	0.05%	
AP-2 complex subunit alpha-2 OS=Mus musculus GN=Ap2a2 PE=1 SV=2	sp|P17427|AP2A2_MOUSE	104	2	0.019230769	0.02%	
Alpha-crystallin B chain OS=Mus musculus GN=Cryab PE=1 SV=2	sp|P23927|CRYAB_MOUSE	20	2	0.1	0.10%	
Polyadenylate-binding protein 1 OS=Mus musculus GN=Pabpc1 PE=1 SV=2	sp|P29341|PABP1_MOUSE	71	2	0.028169014	0.03%	
Recoverin OS=Mus musculus GN=Rcvrn PE=2 SV=2	sp|P34057|RECO_MOUSE	23	2	0.086956522	0.09%	
Neuronal membrane glycoprotein M6-a OS=Mus musculus GN=Gpm6a PE=1 SV=1	sp|P35802|GPM6A_MOUSE	31	2	0.064516129	0.07%	
Neuronal membrane glycoprotein M6-b OS=Mus musculus GN=Gpm6b PE=1 SV=2	sp|P35803|GPM6B_MOUSE	36	2	0.055555556	0.06%	
T-complex protein 1 subunit theta OS=Mus musculus GN=Cct8 PE=1 SV=3	sp|P42932|TCPQ_MOUSE	60	2	0.033333333	0.03%	
Cyclin-dependent kinase inhibitor 1B OS=Mus musculus GN=Cdkn1b PE=1 SV=2	sp|P46414|CDN1B_MOUSE	22	2	0.090909091	0.09%	
Vesicle-fusing ATPase OS=Mus musculus GN=Nsf PE=1 SV=2	sp|P46460|NSF_MOUSE	83	2	0.024096386	0.02%	
F-actin-capping protein subunit alpha-1 OS=Mus musculus GN=Capza1 PE=1 SV=4	sp|P47753|CAZA1_MOUSE	33	2	0.060606061	0.06%	
Heat shock 70 kDa protein 4L OS=Mus musculus GN=Hspa4l PE=1 SV=2	sp|P48722|HS74L_MOUSE	94	2	0.021276596	0.02%	
V-type proton ATPase catalytic subunit A OS=Mus musculus GN=Atp6v1a PE=1 SV=2	sp|P50516|VATA_MOUSE	68	2	0.029411765	0.03%	
Probable ATP-dependent RNA helicase DDX6 OS=Mus musculus GN=Ddx6 PE=1 SV=1	sp|P54823|DDX6_MOUSE	54	2	0.037037037	0.04%	
DDB1- and CUL4-associated factor 7 OS=Mus musculus GN=Dcaf7 PE=2 SV=1	sp|P61963|DCAF7_MOUSE	39	2	0.051282051	0.05%	
Heterogeneous nuclear ribonucleoprotein K OS=Mus musculus GN=Hnrnpk PE=1 SV=1	sp|P61979|HNRPK_MOUSE	51	2	0.039215686	0.04%	
Beta-crystallin B2 OS=Mus musculus GN=Crybb2 PE=1 SV=2	sp|P62696|CRBB2_MOUSE	23	2	0.086956522	0.09%	

DNA-directed RNA polymerase I subunit RPA2 OS=Mus musculus GN=Polr1b PE=2 SV=2	sp|P70700|RPA2_MOUSE	128	2	0.015625	0.02 %	
AP-2 complex subunit mu OS=Mus musculus GN=Ap2m1 PE=1 SV=1	sp|P84091|AP2M1_MOUSE	50	2	0.04	0.04 %	
60S acidic ribosomal protein P2 OS=Mus musculus GN=Rplp2 PE=1 SV=3	sp|P99027|RLA2_MOUSE	12	2	0.166666667	0.17 %	
Apoptosis regulator BAX OS=Mus musculus GN=Bax PE=1 SV=1	sp|Q07813|BAX_MOUSE	21	2	0.095238095	0.10 %	
ELAV-like protein 2 OS=Mus musculus GN=Elavl2 PE=2 SV=1	sp|Q60899|ELAV2_MOUSE	40	2	0.05	0.05 %	
Methylosome subunit pICln OS=Mus musculus GN=Clns1a PE=2 SV=1	sp|Q61189|ICLN_MOUSE	26	2	0.076923077	0.08 %	
Translin OS=Mus musculus GN=Tsn PE=1 SV=1	sp|Q62348|TSN_MOUSE	26	2	0.076923077	0.08 %	
Transferrin receptor protein 1 OS=Mus musculus GN=Tfrc PE=1 SV=1	sp|Q62351|TFR1_MOUSE	86	2	0.023255814	0.02 %	
Synapsin-2 OS=Mus musculus GN=Syn2 PE=1 SV=2	sp|Q64332|SYN2_MOUSE	63	2	0.031746032	0.03 %	
U5 small nuclear ribonucleoprotein 40 kDa protein OS=Mus musculus GN=Snrnp40 PE=2 SV=1	sp|Q6PE01|SNR40_MOUSE	39	2	0.051282051	0.05 %	
Nuclear ubiquitous casein and cyclin-dependent kinase substrate 1 OS=Mus musculus GN=Nucks1 PE=1 SV=1	sp|Q80XU3|NUCKS_MOUSE	26	2	0.076923077	0.08 %	
PITH domain-containing protein 1 OS=Mus musculus GN=Pithd1 PE=2 SV=1	sp|Q8BWR2|PITH1_MOUSE	24	2	0.083333333	0.09 %	
Unconventional myosin-IXa OS=Mus musculus GN=Myo9a PE=2 SV=2	sp|Q8C170|MYO9A_MOUSE	292	2	0.006849315	0.01 %	
RNA-binding protein 4 OS=Mus musculus GN=Rbm4 PE=1 SV=1	sp|Q8C7Q4|RBM4_MOUSE (+1)	40	2	0.05	0.05 %	
BAG family molecular chaperone regulator 5 OS=Mus musculus GN=Bag5 PE=1 SV=1	sp|Q8CI32|BAG5_MOUSE	51	2	0.039215686	0.04 %	
Zinc finger protein 385A OS=Mus musculus GN=Znf385a PE=1 SV=2	sp|Q8VD12|Z385A_MOUSE	40	2	0.05	0.05 %	
Protein FAM3C OS=Mus musculus GN=Fam3c PE=1 SV=1	sp|Q91VU0|FAM3C_MOUSE	25	2	0.08	0.08 %	
Dolichyl-diphosphooligosaccharide--protein glycosyltransferase subunit 1 OS=Mus musculus GN=Rpn1 PE=1 SV=1	sp|Q91YQ5|RPN1_MOUSE	69	2	0.028985507	0.03 %	
Protein dpy-30 homolog OS=Mus musculus GN=Dpy30 PE=1 SV=1	sp|Q99LT0|DPY30_MOUSE	11	2	0.181818182	0.19 %	

Serrate RNA effector molecule homolog OS=Mus musculus GN=Srrt PE=1 SV=1	sp|Q99MR6|SRRT_MOUSE	100	2	0.02	0.02 %	
Transcription initiation factor IIA subunit 1 OS=Mus musculus GN=Gtf2a1 PE=2 SV=2	sp|Q99PM3|TF2AA_MOUSE	42	2	0.047619048	0.05 %	
40S ribosomal protein S21 OS=Mus musculus GN=Rps21 PE=2 SV=1	sp|Q9CQR2|RS21_MOUSE	9	2	0.222222222	0.23 %	
Chromatin target of PRMT1 protein OS=Mus musculus GN=Chtop PE=1 SV=2	sp|Q9CY57|CHTOP_MOUSE	27	2	0.074074074	0.08 %	
mRNA cap guanine-N7 methyltransferase OS=Mus musculus GN=Rnmt PE=1 SV=1	sp|Q9D0L8|MCES_MOUSE	53	2	0.037735849	0.04 %	
Protein LSM12 homolog OS=Mus musculus GN=Lsm12 PE=1 SV=1	sp|Q9D0R8|LSM12_MOUSE	22	2	0.090909091	0.09 %	
WD repeat-containing protein 89 OS=Mus musculus GN=Wdr89 PE=2 SV=1	sp|Q9D0R9|WDR89_MOUSE	42	2	0.047619048	0.05 %	
Peptidyl-prolyl cis-trans isomerase-like 1 OS=Mus musculus GN=Ppil1 PE=2 SV=1	sp|Q9D0W5|PPIL1_MOUSE	18	2	0.111111111	0.11 %	
Transmembrane emp24 domain-containing protein 10 OS=Mus musculus GN=Tmed10 PE=2 SV=1	sp|Q9D1D4|TMEDA_MOUSE	25	2	0.08	0.08 %	
Splicing factor 3A subunit 3 OS=Mus musculus GN=Sf3a3 PE=2 SV=2	sp|Q9D554|SF3A3_MOUSE	59	2	0.033898305	0.03 %	
Ubiquitin-like protein 5 OS=Mus musculus GN=Ubl5 PE=1 SV=1	sp|Q9EPV8|UBL5_MOUSE	9	2	0.222222222	0.23 %	
LanC-like protein 2 OS=Mus musculus GN=Lancl2 PE=1 SV=1	sp|Q9JJK2|LANC2_MOUSE	51	2	0.039215686	0.04 %	
Microtubule-associated protein 1A OS=Mus musculus GN=Map1a PE=1 SV=2	sp|Q9QYR6|MAP1A_MOUSE	300	2	0.006666667	0.01 %	
Destrin OS=Mus musculus GN=Dstn PE=1 SV=3	sp|Q9R0P5|DEST_MOUSE	19	2	0.105263158	0.11 %	
Septin-6 OS=Mus musculus GN=Sept6 PE=1 SV=4	sp|Q9R1T4|SEPT6_MOUSE	50	2	0.04	0.04 %	
Band 4.1-like protein 3 OS=Mus musculus GN=Epb41l3 PE=1 SV=1	sp|Q9WV92|E41L3_MOUSE	103	2	0.019417476	0.02 %	
Mitotic checkpoint protein BUB3 OS=Mus musculus GN=Bub3 PE=2 SV=2	sp|Q9WVA3|BUB3_MOUSE	37	2	0.054054054	0.06 %	
Actin-like protein 6A OS=Mus musculus GN=Actl6a PE=1 SV=2	sp|Q9Z2N8|ACL6A_MOUSE	47	2	0.042553191	0.04 %	

Figure legends.

Figure 1. Mass spectrometry analysis of RNA immunoprecipitation from retinal extracts. See Chapter 5 Figure 7 B. **(A)** Silver stained gel loaded with protein eluate from RNA immunoprecipitation using the indicated biotinylated probes. Black arrows indicate bands of approximately 70kd and 50kd which were cut from lane D3 and analyzed by mass spectrometry along with the entire eluate from lane D4. **(B).** Western blot analysis confirms binding of Musashi and hnRNPA1 proteins to probe D4.

Figure 1.

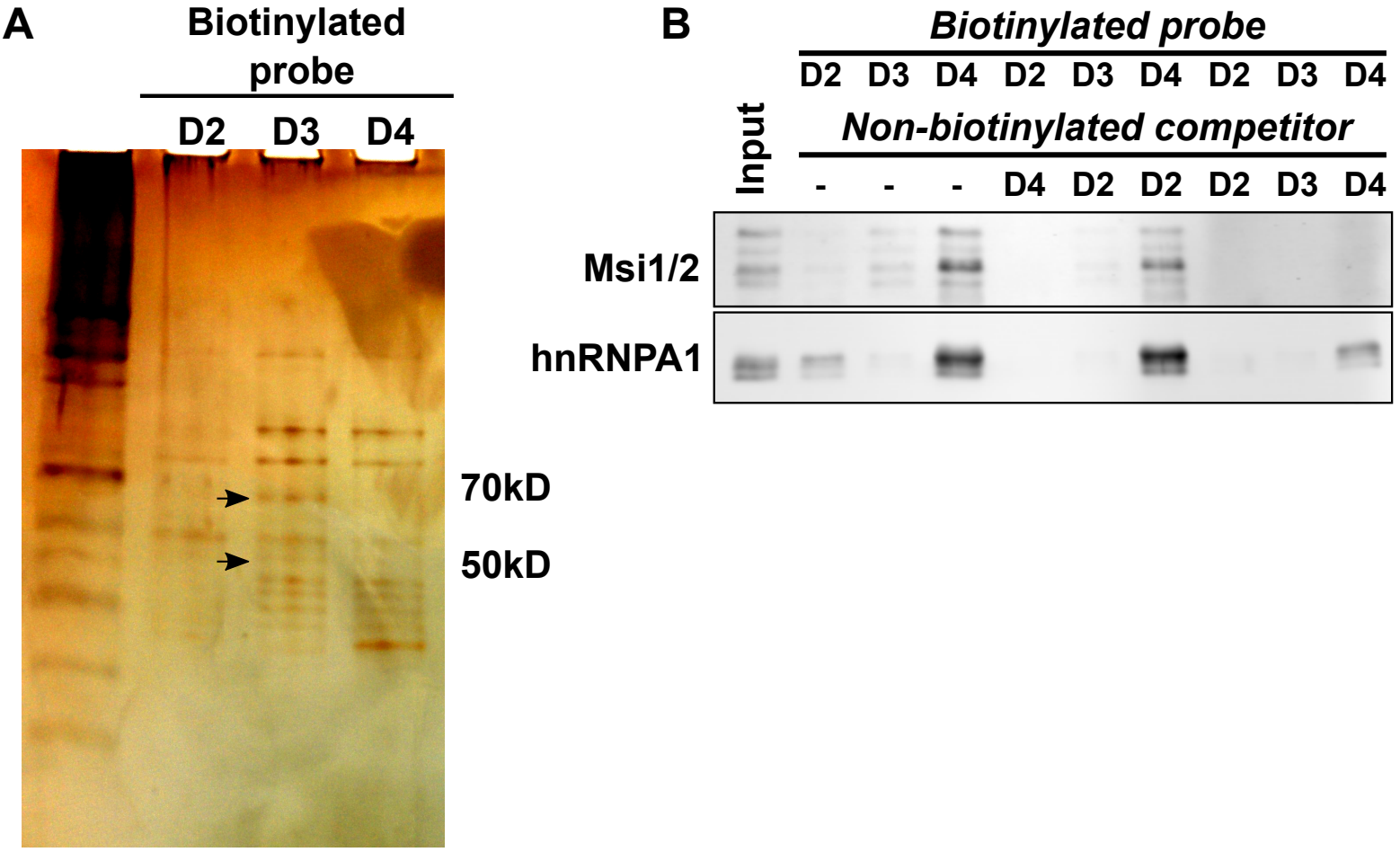
A
Biotinylated probe
D2
D3
D4
70kD
50kD
B
Biotinylated probe
D2 D3 D4 D2 D3 D4 D2 D3 D4
Input
Non-biotinylated competitor
- - - D4 D2 D2 D2 D3 D4
Msi1/2
hnRNPA1